STUDIA
UNIVERSITATIS BABEŞ-BOLYAI

CHEMIA

1-2

1991

CLUJ-NAPOCA

ANUL XXXVI 1991

STUDIA
UNIVERSITATIS BABEŞ-BOLYAI

CHEMIA
1—2

Redacţia: 3400 CLUJ-NAPOCA, str. M. Kogălniceanu, 1 ● Telefon 11 61 01

SUMAR — CONTENTS — SOMMAIRE — INHALT

F. MÁNOK, CS. VÁRHELYI, I. TIMSA, Á. DARADICS, Polarographic Behaviour of some Isothiocyanato-Complexes of Chromium (III) 3
CS. VÁRHELYI, I. GĂNESCU, Neue Komplexsalze der Halogeno-Cyano-Säuren des Platins (IV) ● New Complex Salts of the Halogeno-Cyano Acid s of Platinum (IV) 8
CS. VÁRHELYI, F. MAKKAY, E. KAZINCZY, E. BODIS, On the Dioximine Complexes of Transition Metals. LXXXIV. Part. Study on the formation of rhodium (III)—chelates with aliphatic oximes 15
CS. VÁRHELYI, J. ZSAKO, M. MÁTHÉ, E. GRUNWALD, On the Dioximine Complexes of Transition Metals. LXXXV. New isothiocyanato-amine-bis-dimethylglyoximato-cobalt (III) nonelectrolytes 22
I. SIMINICEANU, C. PETRILA, A. POP, Modelling of the Overall Methane-Steam Reforming Process 28
F. MAKKAY, CS. VÁRHELYI, M. FORRO, New Cobalt (III)-Amine Perchlorates and the Gravimetric Determination of the ClO_4^-—Ion 36
F. MAKKAY, CS. VÁRHELYI, E. KIS, New Tetraacido-Mercury (II) — Derivatives and the Gravimetric Determination of Mercury with Cobalt (III)-Amines 41
E. HOPÎRTEAN, F. KORMOS, Complexometric Titrations with Tungsten Electrode . . . 48
S. MAGER, I. GROSU, M. HORN, Aromatic Solvent Induced Shifts (ASIS) in ^{1}H-NMR Spectroscopy of some 2,5-Substituted 1,3-Dioxanes 53

SIMPOZION — SYMPOZIUM — SYMPOSION

„20 Years of high Education in Chemical Engineering in Cluj-Napoca" (L. LITERAT) . 59
O. GOGU, N. ZIMAN, A. LATIA, Binders for Grinding-Stones with High Hardness 61
AL. SZEP, M. D. BUCEVSCHI, GH. MIHĂILĂ, Modelling of the Precipitate Calcium Carbonate Obtention Process 64
I. SIMINICEANU, Carbon Dioxide Absorption into Promoted Potash Solutions I. Enhancement Factor Determining 71
S. INVĂŞCANU, C. V. ZĂNOAGĂ, Medium's *rH*—A Possible Criterion for the Interpretation and Characterization of Corrosion Processes 78
TSAKIRIS, C., MARIA, G., IGNĂTESCU, G., MANOLIU, D., BOERU, R., NATU, N., POP, G., BOZGA, G., MUNTEAN, O., Steady State Simulation of a Methanol to Hydrocarbons Conversion Experimental Plant 86

PINCOVSCHI, E., REHNER, H., UNTEA, I., LATSOS, TH., L'Absorption des gas en Régime nonstationnaire 96
PINCOVSCHI, E., REHNER, H., UNTEA, I., LATSOS, TH., L'Absorption Statique des polluantes polaires en utilisant des tamis moleculaires NaX 100
GH. IORDACHE, GH. MENCINICOPSCHI, GH. ENE, T. SIMA, Rheologic Constants of certain Biologic Materials. 104
M. ANDRECUȚ, I. BURDA, C. ANDRECUȚ, Monte-Carlo Simulation of Short-Range Order in Monoatomic Amorphous Semiconductors 109
I. SIMINICEANU, C. PETRILA, Modelling and Simulation of the Urea Synthesis Process at Equilibrium 114
S. OPREA, E. DUMITRIU, V. HULEA, A. MAREȘ, I. RUSU, The Study of the Transalkylation Reaction Between Trimethylbenzene and Phenol. 123
I. BALASANIAN, The Application of the Fluidized Bed Model at the $(NH_4)_2SO_4$ Drying . 133
I. ROȘCA, N. FOCA, D. SUTIMAN, Possibilities of Recovery of Waste Vanadium Catalyst 138
O. FLOAREA, M. MIHAI, Romanian Research in Filtration 143
M. GEOGESCU, A. PURI, Der Einfluss von Plastifikatoren auf die Eigenschaften der Zementpasten ● The Effects of the Plasticizer Admixtures on the Properties of Cement-Pastes 148
I. TEOREANU, N. ANGELESCU, Neue Generationen feuerfester Beton — Additivierter Beton mit geringem Tonerdezement-Gehalt. Erhärtungsmechanismen ● New Generations of Fire-Proof Concretes. Effects of Admixtures upon their Hardening 154
V. KASZTL, I. MARINESCU, Technology and Line for Complex Processing of Plants . . 167

Recenzii — Book Reviews — Comptes rendus — Buchbesprechungen

Proceedings of the Sixth International Symposium on Instrumental Planar Chromatography (S. GOCAN) 172

STUDIA UNIV. BABEŞ-BOLYAI, CHEMIA, XXXVI, 1—2, 1991

POLAROGRAPHIC BEHAVIOUR OF SOME ISOTHIOCYANATO-COMPLEXES OF CHROMIUM (III)

FERENC MÁNOK*, CSABA VÁRHELYI*, ILDIKÓ TIMSA* and ÁGNES DARADICS*

Received: 20. Ian. 1990

ABSTRACT. The polarographic behaviour of $K_3[Cr(NCS)_6]$ and some of their substitution products with mono- and diamines: $[Cr(NCS)_4(Am)_2]^-$ (Am = NH_3, aniline, p-toluidine, benzylamine), cis- and trans- $[Cr(en)_2(NCS)_2]NCS$ and $[Cr(en)_3](NCS)_3$ was studied in a wide *pH* range, especially from analytical point of view.

Introduction. The hydrated chromium(III)-ion: $[Cr(H_2O)_6]^{3+}$ is reduced stepwise at the dropping mercury electrode to produce a polarogram with two well defined waves. In neutral supporting electrolytes (KCl, NH_4ClO_4, etc.) in the presence of gelatine as maximum suppressor, the half-wave potentials are -0.91 *V* and -1.4 *V* (vs. SCE), respectively.

The first wave corresponds to the reduction of Cr(III) to Cr(II) and the second to the reduction of Cr(II) to the metal. In a neutral unbuffered solution, the height of the second wave is significantly greater than twice the first, because of the hydrogen ion coreduction, which contributes to the second diffusion current [1].

The chromium(III)-ion has complexing properties especially towards O- and S- donors. The N-donors react with this transition metal ion mainly in anhydrous media. The formation of $K_3[Cr(NCS)_6]$ is an exception. This acido-complex can participate in a series of substitution reactions with NH_3, primary and tertiary aliphatic and heterocyclic mono- and diamines. The monoamines substitute only 2—3 co-ordinated NCS groups. The reaction with aliphatic diamines (ethylenediamine, 1,2- and 1,3-propanediamine) leads to the stepwise substitution of all six NCS^--groups [2].

From polarographic point of view the Reinecke-salt ($K[Cr(NCS)_4(NH_3)_2]$) was studied in neutral supporting electrolytes (KCl, NH_4ClO_4) [3, 4]. This compound was also used for the amperometric determination of some alkaloides (codeine, strichnine, cinchonine, etc.) [5].

Results and discussions. In this preliminary paper the reduction of eight isothiocynyto-chromium (III)-complexes at the dropping mercury electrode was studied at various *pH*-values.

* *University Babeş-Bolyai, Dept. of Chemical Technology, 3400 Cluj-Napoca, Romania*

Some typical polarograms are presented in Figs. 1—2.
The numerical data are summarized in Table 1.
The polarograms of all the studied complexes generally present two waves, corresponding to the reduction steps:

$$Cr(III) + e \rightarrow Cr(II) \quad (I)$$

$$Cr(II) + 2e \rightarrow Cr(O) \quad (II)$$

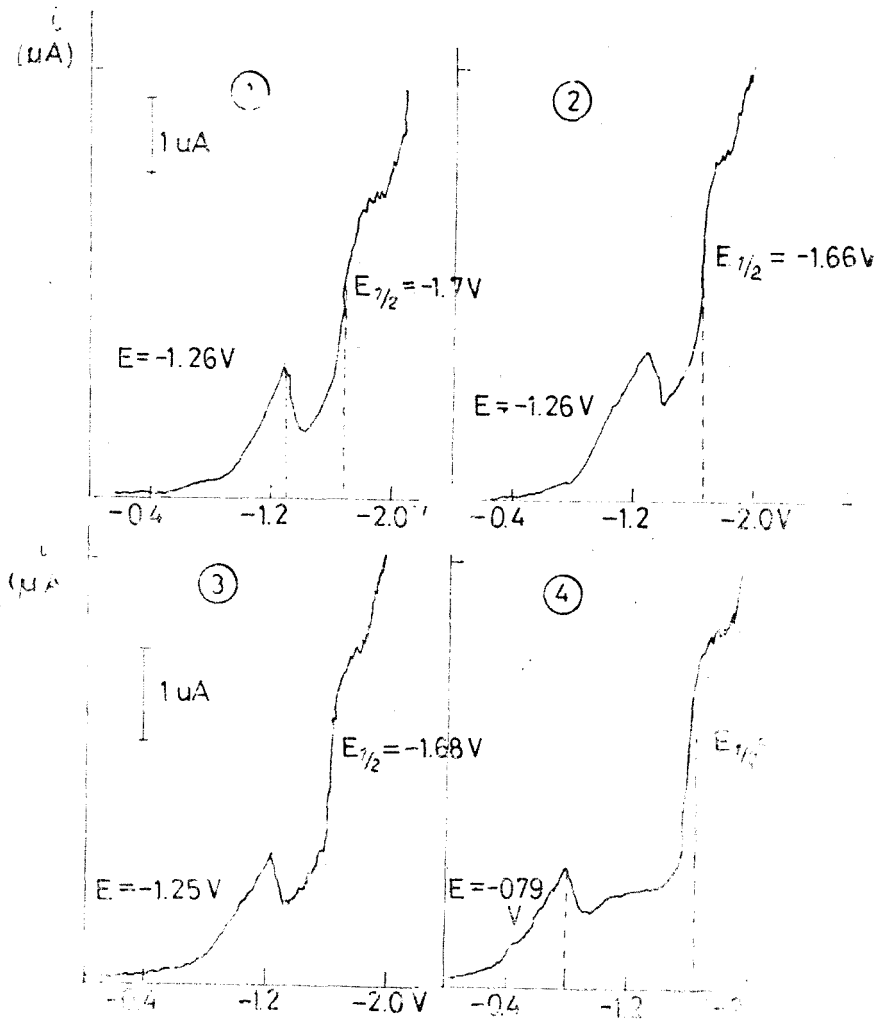

Fig. 1.

1. Polarogram of cis-$[Cr(en)_2(NCS)_2]NCS$, (pH = 7.96)
2. Polarogram of trans-$[Cr(en)_2(NCS)_2]\cdot NCS$, ($p$H = 8.36)
3. Polarogram of $[Cr(en)_3](NCS)_3$, (pH = 7.96)
4. Polarogram of $K_3[Cr(NCS)_6]$, (pH = 7.24)

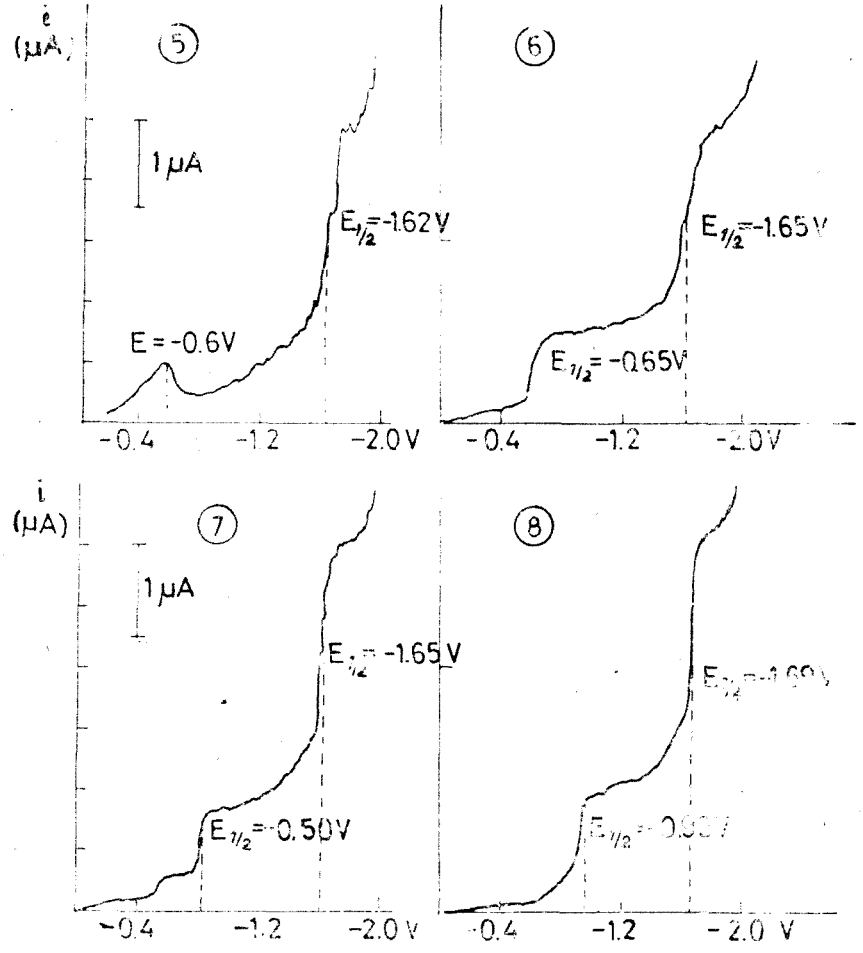

Fig. 2.

5. Polarogram of $NH_4[Cr(NCS)_4(NH_3)_2]$ ($pH = 6.80$)
6. Polarogram of $NH_4[Cr(NCS)_4(aniline)_2]$ ($pH = 3.29$)
7. Polarogram of p-tol. $H \cdot [Cr(NCS)_4(p\text{-toluidine})_2]$ ($pH = 11.98$)
8. Polarogram of $NH_4[Cr(NCS)_4(benzylamine)_2]$ ($pH = 7.96$)

Generally, the first wave is accopmanied with a sharp maximum, which cannot be suppressed by addition of gelatine. The height of this maximum increases with the concentration of the complex, up to a well defined concentration value. This phenomenon shows the adsorption character of the wave. The half-wave potential values of the first waves and the peak potentials of the maxima, respectively, lay between -0.6 and -1.0 V (vs. SCE) depending on the composition of the inner co-ordination sphere of the chromium (III)

Table 1

Polarographic data on some thiocyanato-chromium (III)-complexes

Compound	*p*H	$E^1/_2$(A) *volt*	$E^1/_2$(B) *volt*
cis-$[Cr(en)_2(NCS)_2]NCS$	4.10	−1.07*	−1.70
	7.96	−1.20*	−1.68
	9.91	−1.20*	−1.70
trans-$[Cr(en)_2(NCS)_2]\cdot NCS$	3.29	−0.95	−1.66
	8.36	−1.20*	−1.70
$K_3[Cr(NCS)_6]$	4.10	−0,76*	−1.65
	7.24	−0.77*	−1.65
	9.91	−0,78*	−1.65
	11.98	−0.79*	−1.69
$[Cr(en)_3](NCS)_3$	3.29	−0.95*	−1.57
	7.96	−1.20*	−1.68
	11.20**	−1.05**	−1.60
$NH_4[Cr(NCS)_4(NH_3)_2]$	4.10	−0.6−0.8**	−1.55
	6.80	−0.60−0.80**	−1.60
	8.36	−0.60−0.80**	−1.65
	9.91	−0.70−0.90**	−1.67
	11.98	−0.70−0.90**	−1.67
$NH_4[Cr(NCS)_4(aniline)_2]$	3.29	−0.65	−1.50
	8.36	−0.65*	−1.60
	11.98	−0.70	−1.65
p-tol.H.$[Cr(NCS)_4(p\text{-tol.})_2]$	3.29	−0.60	−1.50
	8.36	−0.55	−1.50
	11.98	−0.50	−1.60
		−0.80	
$NH_4[Cr(NCS)_4(benzylamine)_2]$	3.29	−0.93	−1.50
	7.96	−0.93	−1.69
	11.98	−0.95	−1.70

complex. (number of the NCS^--goups, nature of the amine ligands). With increasing *pH* values, these $E_{1/2}$ values are shifted towards more negative potentials.

The height of the second wave is grater than twice the first (In the case of $NH_4[Cr(NCS)_4(p\text{ toluidine})_2]$ six fold higher in acidic medium), especially at lower *pH* values.

This means, that the reduction of Cr(II) is accompanied with the catalytic reduction of the hydrogen ions. The catalytic activity is probably due to the formation of Cr(O). This phenomenon is analogous with that observed in the case of the polarographic reduction of the hydrated chromium(III) ion [6,7].

The half wave potential values of the second waves are situated between −1.60−1.70 *V* (vs. SCE), showing that the reduction of the chromium(III) complexes (I. step) is followed irresepctive of the nature and composition of the inner co-ordination sphere, by the total decomposition of the complexes.

* — peak of a maximum; ** — undefined adsorption wave

e.g.

$$[Cr(NCS)_6]^{3-} + e + 6H_2O \rightarrow [Cr(H_2O)_6]^{2+} + 6NCS^-$$

$$[Cr(en)_2(NCS)_2]^+ + e + 6H_2O \rightarrow [Cr(H_2O)_6]^{2+} + 2NCS^- + 2en^0$$

$$[Cr(NCS)_4(aniline)_2]^- + e + 6H_2O \rightarrow [Cr(H_2O)_6]^{2+} + 4NCS^- + 2\ aniline^0$$

The half-wave potentials of the second waves are independent of the *pH* in a wide range of $[H^+]$, as in the case of the $[Cr(H_2O)_6]^{2+}$ ion. This phenomenon supports the above mentioned mechanism.

The second waves are generally well formed at defined *pH*-values and their height varies linearly with the concentration of the complex (e.g. with $K_3[Cr(NCS)_6]$ at $pH = 7.24$, with $NH_4[Cr(NCS)_4(benzylamine)_2]$ at $pH = 3.29$) in a large concentration range: $10^{-3} - 10^{-5}$ *mole/L*.

The $K_3[Cr(NCS)_6]$ (aqueous solution) and the $NH_4[Cr(NCS)_4(amine)_2]$ (dil. methanol: 1 : 2) can be used for the amperometric determination of various heterocyclic N-bases, alkyl-aryl-phosphines and alkaloides (chinine, scopolamine, nicotine, etc.), which form slightly soluble salts with these isothiocyanato-chromium(III) complexes in the presence of hydrochloric acid.

$(Amine.H)_3[Cr(NCS)_6]$ and $Amine.H.[Cr(NCS)_4(amine)_2]$, respectively). The titrations can be carried out at -1.2 -1.4 *V* (vs. SCE). The titration curves have an *L*-shape. Accuracy $\pm 0.3-0.5\%$. The method is not specific and selective.

Experimental. The $NH_4[Cr(NCS)_4(amine)_2]$ type complexes were obtained from anhydrous $K_3[Cr(NCS)_6]$ [8] and the corresponding amines by melting [9]. The $[Cr(en)_2(NCS)_2]NCS$ and $[Cr(en)_3](NCS)_3$ derivatives are formed in an analogous way from the mentioned starting material and anhydrous ethylenediamine [10, 11].

The polarograms were taken with a RADELKIS OH-120 type polarograph using a conventional polarographic cell with a saturated calomel reference electrode, connected to the cell by means of an agar-agar bridge (1 *M* KNO_3). The oxygen was eliminated from the solutions with purified methane. The polarograms were taken in Britton Robinson's buffer solutions. The constant ionic strenght of 0.5 *M* was ensured with sodium perchlorate.

REFERENCES

1. I. M. Kolthoff, J. J. Lingane, *Polarography*, Interscience Publ., New-York–London, 1952, Vol. **II**, p. 453, 612.
2. F. Hein, *Chemische Koordinationslehre*, S. Hirzel Verlag, Leipzig, 1954, p. 514, 518.
3. M. Cihakova, J. Zyka, *Ceskoslov. Farmac.*, **5**, 572 (1956).
4. N. Maki, Y. Shimura, R. Tsuchida, *Bull. Chem. Soc. Japan*, **31**, 413 (1958).
5. T. C. Ichniowski, A. Clifford, *J. Inorg. Nuclear Chem.*, **22**, 133 (1962).
6. M. Demassieux, J. Heyrovsky, *J. chim. phys.*, **26**, 219 (1929).
7. J. J. Lingane, R. L. Pecsok, *J. Amer. Chem. Soc.*, **71**, 425 (1949).
8. J. Roessler, *Ann. d. Chem. und Pharm.*, **141**, 189 (1867).
9. Cs. Várhelyi, I. Gănescu, *Monatsh.*, **98**, 472 (1967).
10. J. E. House, J. C. Bailar jr., *J. Amer. Chem. Soc.*, **91**, 68 (1969).
11. P. Pfeiffer, *Ber. dtsch. chem. Ges.*, **37**, 4277 (1964).

STUDIA UNIV. BABEŞ-BOLYAI, CHEMIA, XXXVI, 1—2, 1991

NEUE KOMPLEZSALZE DER HALOGENO-CYANO-SÄUREN DES PLATINS (IV)

CSABA VÁRHELYI* und ION GANESCU**

Eingegangen am 20. Ian. 1990

ABSTRACT. New complex salts of the Halogeno-cyano Acids of Platinum (IV) A number of 15 new ammonium salts of the type (amine.H)$_2$ [Pt(CN)$_4$X$_2$] and 30 new cobalt-(III) — and chromium (III)-amine derivatives of the H$_2$[Pt(CN)$_4$X$_2$] acids (X = Cl, Br, I) were obtained by double decomposition reactions. Some metal — and ammonium salts were characterized by electronic and IR spectra.

Einleitung. Das Cyanid-Ion mit ausgeprägten nukleophilen Eigenschaften kann, Halogene-, Pseudohalogene-, verschiedene ein- und zweizähnige neutrale Liganden in klassischen Komplexen und Chelaten der Übergangsmetalle austaschen [1]. Im Falle der Platin-komplexe ist diese Substitutionsreaktion auch von Redoxprozessen (Pt(IV) → Pt(II)) begleitet [2—4]. Die Reaktion der Alkalicyanide mit Hexaacido-platinaten (IV) führt zur Bildung von M$_2$[Pt(CN)$_4$] (z.B. im Falle der K$_2$[PtCl$_6$], K$_2$[PtBr$_6$], PtI$_4$, K$_2$[PtI$_6$], usw.). Ist diese Substitutionsreaktion von keinen Redoxvorgängen begleitet, können auch gemischte Pt(IV) — Derivate ([Pt(CN)$_2$X$_4$]$^{2-}$, [Pt(CN)$_3$X$_3$]$^{2-}$, [Pt(CN)$_5$X]$^{2-}$, usw.) erhalten werden.

Die Tetracyano-Platinum (II)-Säure: H$_2$[Pt(CN)$_4$], und ihre Alkalisalze können leicht zu Derivate des Platin(IV) oxydiert werden. Zu diesem Zweck wurden verschiedene Oxydationsmittel, wie z.B. H$_2$O$_2$, JCN, (NCS)$_2$, verwendet. [5]. Wenn die Oxydation mit freien Halogenen ausgeführt ist, entstehen gemischte Halogene-cyano-säuren: H$_2$[Pt(CN$_4$X$_2$], mit X = Cl, Br, I. Fluorocyano-säuren der obigen Reihe wurden noch nicht erwähnt [6, 7]. Das [Pt(CN$_4$(H$_2$O)X]$^-$ — Ion tritt bei dieser Reaktion als Zwischenprodukt auf [8].

Die Reaktionen verlaufen mit Farbänderung und deshalb sind diese Redox- und Ligandaustauschreaktionen für spektrophctometrische kinetische Untersuchungen sehr geeignet. So wurden, z.B., die Hydrolysen — und andere Ligandaustauschreaktionen der [Pt(CN)$_4$X$_2$]$^{2-}$ und [Pt(CN)$_4$(N$_3$)X]$^{2-}$ (X = Cl, Br, NCS, NCSe, NO$_2$, usw) auf diesem wege verfolgt [9—13].

Ergebnisse und Diskussionen. Wir haben die Oxydation des K$_2$[Pt(CN)$_4$]-Salzes in wässrigen Lösungen bei Wasserbadtemperatur mit überschüssigem Halogenen (gasförmiges Chlor, flüssiges Brom, alkoholische Iodlösung) durchgeführt. Durch Eindampfen dieser Lösungen scheiden sich: K$_2$[Pt(CN)$_4$Cl$_2$) .

* *Universität Babeş—Bolyai, Fakultät für Chemische Technologie, 3400 Cluj-Napoca, Rumanien*
** *Universität Craiova, Fakultät der Naturwiss, 1100 Craiova, Rumänien*

$\cdot 2H_2O$ (farblose Krist.); $K_2[Pt(CN)_4Br_2] \cdot 2H_2O$ (hellgelbe, trigonale Krist.); $K_2[Pt(CN)_4I_2]$ (dünne, braun-violette Plättchen), aus.

Die wässrigen Lösungen dieser Salze geben eine Reihe von Fällungsreaktionene mit Kationen von verschiedeneni Typ: Amine, Sschwermetalle, Metal (III)-amine. Diese chemischen Eigenschaften der Halogeno-cyano-säuren wurden nur wenig untersucht.

Wir haben beobachtet, daß die aliphatischen — und aromatischen Amine für solche Fällungsreaktionen nur wenig geeignet sind. Die Salze der heterocyclischen Amine, und insbesonders der Alkaloide mit HY (Y = Cl, Br, I, HSO_4, ClO_4) geben schöne kristalline Fällungen mit den Halogenocyano-säuren. Die Löslichkeit dieser Komplexsalze ist viel geringer, als diejenige der analogen Derivate der $H_2[Pt(CN)_4]$, und deshalb haben sie auch eine analytische Bedeutung. Eine Reihe von neuen Ammoniumsalze sind in Tabelle 1 charakterisiert.

Tabelle 1

Neue Amoniumsalze der $H_2[Pt(CN)_4X_2]$ — Säuren

No.	Formel	Mol. Gew. ber.	Charakteristik		Analyse Ber.	Gef.
1.	(α, α'-Dipyridyl.H)$_2$.A	684,4	gelbbraune mikrokrist. Masse	C	42,11	42,01
				H	2,65	2,50
				N	16,36	16,25
2.	(α, α'-Dipyridyl·H)$_2$·B	773,3	braune mikrokrist. Masse	C	37,27	37,20
				H	2,35	2,30
				N	14,48	14,40
3.	(α, α'-Dipyridyl·H)$_2$·C	864,3	unregelmässige, kleine braune Krist.	C	33,23	33,09
				H	2,09	1,99
				N	12,91	12,65
4.	(o-Phenanthrolin·H)$_2$·A	736,1	gelbbraune mikrokrist. Masse	C	45,68	45,50
				H	2,46	2,29
				N	15,21	15,17
5.	(o-Phenanthrolin·H)$_2$·B	825	braune mikrokrist. Masse	C	40,76	40,60
				H	2,20	2,15
				N	13,58	13,41
6.	(o-Phenanthrolin·H)$_2$·C	919	dunkelbraune mikrokrist. Masse	C	36,59	36,41
				H	1,97	1,91
				N	12,19	12,02
7.	(o-Oxy-Chinolein·H)$_2$A	660,4	goldgelbe, dünne Plättchen	C	40,01	39,88
				H	2,42	2,30
				N	12,72	12,66
8.	(o-Oxy-Chinolein·H)$_2$·B	749,2	goldgelbe hexagonale Platten	C	35,26	35,11
				H	2,15	2,00
				N	11,21	11,07
9.	(o-Oxy-Chinolein·H)·C	843,2	gelbbraune unregelmäss. Plättchen	C	31,33	31,17
				H	1,91	1,76
				N	9,96	9,80
10.	(Pyramidon·H)$_2$·A	834,7	gelbbraune unregelmäss. Plättchen	C	43,17	43,00
				H	4,35	4,20
				N	16,77	16,70
11.	(Pyramidon·H)$_2$·B	923,5	braune mikrokryst. Masse	C	39,01	38,74
				H	3,93	3,80
				N	15,16	15,02

(continuare tabelle 1)

No.	Formel	Mol. Gew. ber.	Charakteristik		Analyse Ber.	Gef.
12.	(Pyramidon·H)$_2$·C	1017,5	dunkelbraune mikrokryst. Masse	C	35,41	35,18
				H	3,57	3,31
				N	13,69	13,33
13.	(Benzimidazol·H)$_2$A	608,3	gelbbraune rechtanguläre Prismen	C	35,54	35,10
				H	2,32	2,19
				N	18,41	18,23
14.	(Benzimidazol·H)$_2$·B	697,2	braune mikrokrist. Masse	C	31,00	31,20
				H	2,02	1,80
				N	16,06	16,20
15.	(Piperazin.H)$_2$·C	792	braune, lange Nadeln	C	27,32	27,10
				N	13,69	13,93

Die Kobalt(III)- und Chrom(III)-amin-Basen von Monoacido-pentammin $[Co(NH_3)_5X]^2$, $[Cr(NH_3)_5X]^{2+}$), bzw. Diacido-tetramin — Typ ($[M((Am)_4X_2]^+$ $[M(Diox.H)_2(Am_2]^+$) geben schöne, charakteristische kristalline Fällungen mit diesen zweibasischen Platin(IV)-Söuren. Die leicht erhaltbare Co(III)- und Cr(III)-amin-Basen können auch zur gravimetrischen Bestimmung des Platins, nach Überführung in $H_2[Pt(CN)_4X_2]$, verwendet werden.

Die erhaltenen neuen Komplexsalze sind in den Tabellen 2—4 charakterisiert.

Tabelle 2

Metall (III)-amin-Salze der $H_2[Pt(CN)_4Cl_2]$ — Säure

No.	Formel	Mol. Gew. ber.	Charakteristik		Analyse Ber.	Gef.
16.	trans-$[Co(en)_2Br_2]$·A·H_2O	1065,8	gelbbraune mikrokrist. Masse	Pt	18,30	18,42
				Co	11,05	10,93
				N	15,76	15,60
				H_2O	1,75	1,14
17.	trans-$[Co(pn)_2Cl_2]$·A	926,2	grüne Nadeln	Pt	21,06	20,92
				Co	12,73	12,88
				N	18,13	18,31
18.	trans-$[Co(en)_2Cl_2]$·A·H_2O	888,1	grüne rhomb. Plättchen	Pt	21,96	21,90
				Co	13,27	13,60
				H_2O	1,89	1,87
19.	trans-$[Cr(en)_2(NCS)_2]$·A	946,7	gelbbraune mikrokrist. Masse	Pt	20,60	20,51
				N	23,65	23,53
20.	$[Co(Pyridin)_4Cl_2]_2$·A·H_2O	1280,1	grüne unregelmässige mässige Prismen	Pt	15,23	15,48
				Co	9,20	9,27
				N	13,12	13,06
21.	$[Co(DH)_2(Pyridin)_2]_2$·A	1268,4	schimmernde,braune rhomb. Plättchen	Pt	15,38	15,42
				Co	9,29	9,17
				N	17,65	17,82

(Fortsetzung Tabelle 2)

No.	Formel	Mol Gew. ber.	Charakteristik		Analyse Ber.	Gef.
22.	$[Co(DH)_2(m\text{-Toluidin})_2]_2 \cdot A$	1376,6	gelbbraune, kleine Prismen	Pt	14,17	14,30
				Co	8,56	8,77
				N	16,27	16,19
23.	$[Co(DH)_2(p\text{-Phenetidin})]_2 \cdot A$	1496,6	braune, lange Prismen	Pt	13,03	13,30
				Co	7,88	7,70
				N	14,96	14,81
24.	$[Co(DH)_2(p\text{-Toluidin})_2]_2 \cdot A$	1376,6	braune rhomb. Plättchen	Pt	14,17	14,29
				Co	8,56	8,80
				N	16,27	16,19
25.	$[Co(DH)_2(m\text{-Amino-Phenol})_2]_2 \cdot A$	1384,5	braune trigonale Prismen	Pt	14,09	13,95
				Co	8,51	8,64
				N	16,17	16,26

A = $[Pt(CN)_4Cl_2]^{--}$. en = Äthylendiamin, *pn* = 1,2-Diamino-propan, DH = deprotoniertes Dimethylglyoxim

Tabelle 3

Metall (III)-amin-Salze der $H_2[Pt(CN)_4Br_2]$ — Säure

No.	Formel	Mol. Gew. ber.	Charakteristik		Analyse Ber.	Gef.
26.	trans-$[Co(pn)_2(NCS)_2]_2B$	1105,7	rotbraune rechtianguläre Platten	Pt	17,64	17,83
				Co	10,66	10,50
				N	20,25	20,19
27.	trans-$[Co(en)_2Cl_2]_2 \cdot B \cdot H_2O$	977	grüne Dendryte	Pt	19,96	19,83
				Co	12,06	12,30
				H_2O	1,84	1,90
28.	trans-$[Cr(en)_2(NCS)_2]_2 \cdot B$	1035,5	rotbraune, kleine unregelmäss. Prismen	Pt	18,84	18,77
				N	21,62	21,50
29.	trans-$[Co(en)_2Br_2]_2 \cdot B \cdot H_2O$	1154,7	glänzende, grüne lange Nadeln	Pt	16,89	16,80
				Co	10,20	10,47
				H_2O	1,70	1,90
30.	trans-$[Co(pn)_2Cl_2]_2 \cdot B \cdot H_2O$	1033,1	gelbgrüne, rhomb. Plättchen	Pt	18,88	19,08
				Co	11,40	11,23
				N	16,26	16,09
				H_2O	1,77	1,90
31.	$[Co(Pyridin)_4Cl_2]_2 \cdot B \cdot H_2O$	1369	kleine, grüne unregelmäss. Krist.	Pt	14,25	14,00
				Co	8,61	9,85
				N	12,27	12,00
32.	$[Co(DH)_2(Pyridin)_2]_2 \cdot B$	1357.3	gelbbraune Dendryte	Pt	14,37	14,70
				Co	8,68	8,59
				N	16,50	16,24
33.	$[Co(DH)_2(m\text{-Toluidin})_2]_2 \cdot B$	1465,4	rotbraune Nadeln	Pt	13,31	13,20
				Co	8,04	8,24
				N	15,28	15,02
34.	$[Co(DH)_2(p\text{-Phenetidin})_2]_2 \cdot B$	1585,5	braune, kurze Prismen	Pt	12,30	12,69
				Co	7,43	7,35
				N	14,12	14,01
35.	$[Co(DH)_2(m\text{-Amino-Phenol})_2]_2 \cdot B$	1473,4	rotbraune mikrokrist. Masse	Pt	13,24	13,54
				Co	8,00	7,96
				N	15,20	15,02

B = $Pt(CN)_4Br_2]^{2-}$

Tabelle 4

Metall (III)-amin-Salze der $H_2[Pt(CN)_4I_2]$ — Säure

No.	Formel	Mol. Gew. ber.	Charakteristik		Analyse Ber.	Gef.
36.	trans-$[Co(en)_2Br_2]_2 \cdot C \cdot H_2O$	1248,7	grüne, glänzende Dendryte	Pt	15,62	15,49
				Co	9,43	9,80
				N	13,45	13,33
37.	trans-$[Co(en)_2Cl_2]_2 \cdot C \cdot H_2O$	1071	grüne, rechtanguläre Prismen	Pt	18,21	18,70
				Co	11,00	10,92
				N	15,68	15,35
				H_2O	1,70	1,90
38.	trans-$[Co(pn)_2Cl_2]_2 \cdot C$	1109,1	unregelmässige, dicke Platten	Pt	17,59	17,38
				Co	10,62	10,80
				N	15,14	15,08
39.	trans-$[Cr(en)_2(NCS)_2]_2 \cdot C$	1129,6	rotbraune, mikrokrist. Masse	Pt	17,27	17,49
				N	19,82	19,76
40.	$[Co(Pyridin)_4Cl_2]_2 \cdot C \cdot H_2O$	1463	gelbrüne, kleine unregelmäss. Krist.	Pt	13,33	13,26
				Co	8,05	8,20
				N	11,48	11,58
41.	trans-$[Co(pn)_2(NCS)_2]_2 \cdot C$	1200	rotbraune, dicke unregelmäss. Platten	Pt	16,26	16,39
				Co	9,83	9,77
				N	18,67	18,38
42.	$[Co(DH)_2(Pyridin)_2]_2 \cdot C$	1441,3	gelbbraune Dendryte	Pt	13,53	13,20
				Co	8,18	8,40
				N	15,54	15,84
43.	$[Co(DH)_2(m\text{-}Toluidin)_2]_2 \cdot C$	1559,4	gelbbraune Sternchen	Pt	12,51	12,30
				Co	7,56	7,76
				N	14,36	14,08
44.	$[Co(DH)_2(p\text{-}Phenetidin)_2]_2 \cdot C$	1679,5	braune Platten	Pt	11,61	11,40
				Co	7,02	6,68
				N	13,33	13,59
45.	$[Co(DH)_2(m\text{-}Amino\text{-}Phenol)_2]_2 \cdot C$	1567,4	dünne, braune rhomb. Platten	Pt	12,45	12,10
				Co	7,52	7,81
				N	14,29	14,09

$C = [Pt(CN)_4I_2]^{2-}$

Die Analysendaten bestätigen daß in allen untersuchten Fällen nur normale Salze der zweibasischen Pt(IV)-Säuren entstehen. Die meisten neuen Komplexsalze sind sehr schwer löslich im Wasser und lösen sich in einigen polaren organischen Lösungsmitteln, wie Aceton, Dimethylformamid, Dimethylsulphoxid, usw.

In den IR Spektren einiger Metall- und Ammoniumsalze (K, Pyridin) tritt eine sehr scharfe Bande um 2130—2155 cm^{-1} auf, die der $\nu C{\equiv}N$ — Valenzschwingungsfrequenz der komplexgebundenen CN — Gruppe zuzuordnen ist. Diese Frequenzen erscheinen bei den freien, nicht koordinierten CN — Liganden, wie z.B. im Falle des KCN, bei 2080 cm^{-1}. Die Verschiebung der $\nu C{\equiv}N$ — Valenzschwingungsfrequenzen nach höheren Wellenzahlen ist im Einklang mit der Resonanz-

theorie (:C=N:$^-$ Struktur CN^- in KCN und $Pt^+ = C = N:^{-\cdot\cdot}$ Struktur für die in Cyano-komplexen gebundenen CN^- [14—16].

Die νPt—C — Schwingungsfrequenzen erscheinen bei 490—510 cm^{-1}. Diese *IR* — Daten bestätigen daß die Pt—CN Bindung durch das Kohlenstoff-atom verwirklicht ist.

Das Aufstreten der δPt—C=N und δC—Pt—C Deformations-schwingungsfrequenzen ist in fernem *IR* — Bereiche 240—330 cm^{-1}, bzw. um 100 cm^{-1} zu erwarten. [17—18].

Die elektronischen Spektren der $K_2[Pt(CN)_4X_2]$ wurden in wässrigen Lösungen aufgenommen (siehe Abb. 1.)

Die Spektraldaten der obigen Verbindungen sind in der Tabelle 5 zusammengestellt.

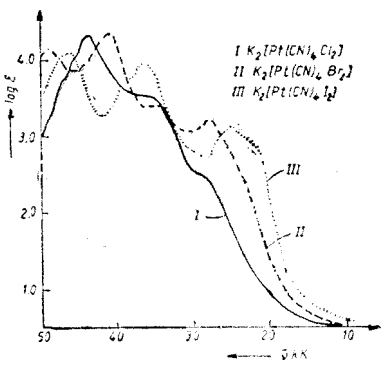

A b b. 1. Elektronische Spektren der $K_2[Pt(CN)_4X_2]$-Komplexe
I. — $K_2[Pt(CN)_4Cl_2]$
II. — $K_2[Pt(CN)_4Br_2]$
III. — $K_2[Pt(CN)_4I_2]$

Tabelle 5

Elektronische Spektral Data der $K_2[Pt(CN)_4X_2]$ — Komplexen

Verbindung	Absorptionsbande (*k*K)			
	A	B	C	D
$K_2[Pt(CN)_4Cl_2]$	29—32*i*	—	37—39	44,6
$K_2[Pt(CN)_4Br_2]$	29,2	33,5—35	38*i*	41,5 45
$K_2[Pt(CN)_4I_2]$	24,6	36,4	38*i*	41,5*i* 46,5

i = Inflexionspunkt

Die gemischten Cyanokomplexe haben nur eine Absorptionsbande im sichtbaren Bereiche des Spektrums, um 24—30 *kK*, welche einem Kristallfeldübergänge zuzuordnen ist. Diese Bande ist in er Reihe

$$X\text{: } Cl < Br < I$$

nach niedrigeren Wellenzahlen verschoben.
Die Absorptionsbanden im *UV* — Bereiche gehören zu Ladungsüberführungs übergänge.

Experimenteller Teil — $K_2[Pt(CN)_4Cl_2]$ —, $K_2[Pt(CN)_4Br_2]$ — und $K_2[Pt(CN)_4I_2]$ — Lösungen

4,5 g $K_2[PtCl_4] \cdot 2H_2O$ (10 mMol) werden auf dem Wasserbade in 200 ml Wasser mit 2,8 g NaCN behandelt. Nach 30—40 Min. Erwärmen entfärbt siel die rotbraune Lösung. Dann wird das $[Pt(CN_4)]^{2-}$ — Komplex durch Einleiten von Chlor oxidiert. Die Lösung wird hellgelb gefärbt. Das überschüssige Chlor wird durch 30—40 Min. Erwärmen entfernt. Dann wird die Lösung auf 200 ml Volumen aufgefüllt, filtriert und zur doppelten Umsetzungsreaktionen verwendet. 20 ml Lösung enthält 1 mMol $K_2[Pt(CN)_4Cl_2]$. Die analogerweise entstehende $K_2[Pt(CN)_4Br_2]$ — Lösung ist gel-

borange und die $K_2[Pt(CN)_4I_2]$ hellbraun gefärbt. Die (amin. H)$_2$ $[Pt(CN)_4X_2]$ und die Kobalt (III) —, bzw. Chrom(III)-amin-Derivate der $H_2[Pt(CN)_4X_2]$ — Säuren wurden nach in vorhergehenden Arbeiten beschriebenen Methoden erhalten [19, 20].

Analyse. Das Platin wurde mikrogravimetrisch als metallisches Pt, Kobalt komplexometrisch, C, H und N gazvolumetrisch bestimmt.

LITERATUR

1. M. T. Beck, Pure & Appl. Chem., **59,** 703 (1987).
2. J. Haidlen, R. Fresenius, Liebigs Ann. Chem., **43,** 136 (1842).
3. R. J. Triswell, A. J. Greenaway, J. Chem. Soc., **32,** 252 (1877).
4. A. Chugaev, Z. anorg. Chem., **46,** 152 (1905).
5. R. Osso, V. J. Rund, J. Coord. Chem., **8,** 169 (1978).
6. H. Terrey, J. Chem. Soc., **1928,** 204.
7. T. Wilm, Ber. dtsch. chem. Ges., **21,** 1453 (1888).
8. W. Roy Mason, Inorg. Chem., **10,** 1914 (1971).
9. W. Roy Mason, Inorg. Chem., **8,** 1756 (1969). **9,** 1528 (1970).
10. L. D. Swihart, W. Roy Mason, Inorg. Chem., **9,** 1749 (1970).
11. P. J. C. Vuik, A. Pol, Inorg. Chim. Acta, **34,** 129 (1979).
12. E. Ch. Skinner, M. M. Jones, J. Amer. Chem. Soc., **91,** 1984, 4405 (1969).
13. A. V. Babkov, M. N. Kuznetsova, Koord. Khim., **6,** 1593 (1980).
14. E. F. Harrington, W. Kynaston, J. Chem. Soc., **1955,** 3555.
15. W. P. Griffith, G. Wilkinson, J. Chem. Soc., **1959,** 2757.
16. M. F. El-Sayed, R. K. Sheline, J. Inorg. Nuclear Chem., **6,** 187 (1958).
17. C. V. Pistorius, Z. physik. Chem., **23,** 197 (1960).
18. D. M. Sweeny, J. Nakagawa, S. Mizushima, J. V. Quagliano, J. Amer. Chem. Soc., **78,** 889 (1956).
19. Cs. Várhelyi, I. Gănescu, Stud. Univ. Babeş-Bolyai, Chem., **31,** (2), 26 (1986).
20. Cs. Várhelyi, I. Gănescu, Stud. Univ. Babeş-Bolyai, Chem., **34,** (1), 70 (1989).

STUDIA UNIV. BABEŞ-BOLYAI, CHEMIA, XXXVI, 1—2, 1991

ON THE DIOXIMINE COMPLEXES OF TRANSITION METALS. LXXXIV. Part. Study on the formation of rhodium(III)—chelates with aliphatic oximes

CSABA VÁRHELYI*, FERENC MAKKAY*, ENIKŐ KAZINCZY* and EUGEN BÓDIS**

Received 28.03.1990

ABSTRACT. The composition of some rhodium (III)-chelates with aliphatic α-dioxjmes (dimethylglyoxime, methyl-isopropyl-dione dioxime) (Rh : L = 1 : 2) and α-keto-oximes (diacetylmonoxime, methyl-isopropyl-dione monoxime) (*R* : *L* = = 1 : 3) were determined by the continuous variation method. The electronic spectra of these compounds and those of some $[Rh(Diox.H)_2X_2]$ (X = Cl, Br, I, N_3, NO_2) derivatives were recorded and discussed. Some complexes can be used for the spectrophotometric determination of rhodium.

Introduction. The rhodium forms (in various oxidation states) coloured classical complexes and chelates with O-, S- and especially with N—donor ligands. The structure and stability of these derivatives are unknown in any cases. The electronic spectral data show that these compounds can be considered as sensitive analytical reaction products, but their selectivity is generally not sufficient. E.g. the well-known spectrophotometric method for Rh(III) with SnX_2 (X = Cl, Br, I) is interfered by a series of transition metals (Ag, Hg, Au), platin metals and non metals (Se, Te) [1].

The Rh(III) salts can be oxidized with NaClO, $NaBiO_3$, $Na_2S_2O_8$, to Rh(V) derivatives coloured in violet, blue, dark brown, with unknown structure [2]. One can also mention the catalytic action of Rh(III) upon the oxidation of Mn(II) to MnO_4^- [3], and Cu(II) to Cu(III) ($[Cu(IO_6)_2]^{7-}$ and $[Cu(TeO_6)_2]^{7-}$, respectively, of redbrown colour). These reactions were also proposed for the spectrophotometric determination of the above mentioned metal [4]. The interference of other accompanying metals was not studied.

From the sulphur containing organic ligands, some thioalcohols [5, 6], thioacids [7], substituted thioureas [8, 9], and thiazole derivatives [10, 11], have been recommended for this purpose.

The nitrogen donor ligands also present high affinity for the formation of different type complexes with rhodium(III) (e.g. some heterocyclic amines (imidazole, triazole, tetrazole derivatives [12, 13]), aminopolycarboxylic acids [14, 15], azo-dyes [16—21]). These soluble derivatives were also used for the spectrophotometric determination of this metal. However these methods are, generally, not specific from analytical point of view.

Various oximes form chelates with rhodium(III). α-Nitroso-β-naphtol [22, 23] and thiophen-2-aldoxime [24] have been proposed for the gravimetric determination of Rh(III). The majority of chelates with oxime derivatives are soluble in water or in organic solvents and for this reason are useful in the

* *University Babeş—Bolyai, Dept. of Chemical Technology, 3400 Cluj-Napoca, Romania*
** *Institute of Chemistry, 3400 Cluj-Napoca, Romania*

analysis of this platin metal (e.g. phenantrenchinone monoxime [25], 1,4-naphtochinone monoxime [26, 27], α-benzylmonoxime [28, 29, 30], α-furylmonoxime and α-dioxime [31]).

For the aliphatic oxime derivatives has been shown only a few attention from this point of view.

In the present paper we studied the formation and optical properties of some rhodium(III)-complexes with aliphatic monoximes (diacetylmonoxime, methyl-isopropyl-dione monoxime) and dioximes (glyoxime, dimethylglyoxime, methyl-isopropyl-dione dioxime), which might be used for analytical purposes.

Results and Discussion. As compared to the analogous cobalt(III) complexes, the formation rate of Rh(III) derivatives is 100—1000 times slower and for this reason it is necessary to warm the aqueous solutions of the reagents (45—60 minutes on a sand bath). The oximino-chelates of Rh(III) are stable in aqueous solutions in a wide *pH* range, their colour varies from light to dark yellow (yellow-brown) as function of the nature of the chelating agent and the anions present (the latter in the case of anionic chelates).

The electronic spectra of the ketoxime-$RhCl_3$-systems (5 : 1) and those of the dioxime-$RhCl_3$ (5 : 1) ones in a wide *pH* range are presented in Fig. 1—4.

The spectral data are shown in a Table 1.

In the case of the α-dioximino-chelates, the absorption bands of $RhCl_3$ at 22 and 29 *kK* disappear and in the visible part of the spectrum, only a single band or inflexion appears at 24—28 *kK*, the position of which is influenced in some extent by the nature of the monodentate ligand (ligand : halogen or pseudohalogen). The ultraviolet part of the spectra of the $[Rh(Diox.H)_2X_2]^-$ complexes shows an analogy with that of the $[Co(Diox.H)_2X_2]^-$ ones. This phenomenon pleads for an analogous trans-octahedral geometric structure [32—33].

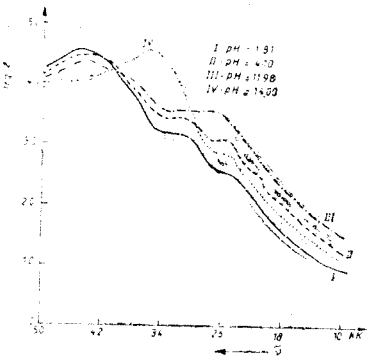

Fig. 1. Electronic spectra of the$RhCl_3$-diacetylmoxime mixture (1 : 5) at various *pH*-values

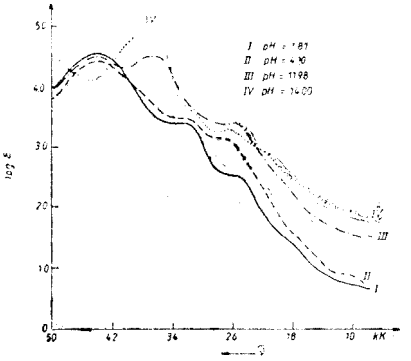

Fig. 2. Electronic spectra of the $RhCl_3$-methyl-isopropyl-dione monoxime mixture (1 : 5) at various *pH*-values

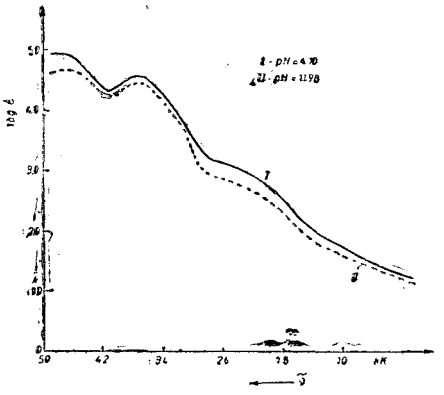

F i g. 3. Electronic spectra of the $RhCl_3$-dimethylglyoxime mixture (1 : 5) at various *pH*-values

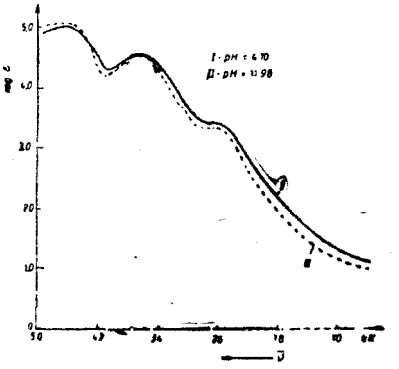

F i g. 4. Electronic spectra of the $RhCl_3$-methyl-isopropyl-dione dioxime mixture (1 : 5) at various *pH*-values

Table 1

Electronic spectral data on some Rh(III)-oxime systems at various pH — values

Oxime	$\tilde{\nu}_1$ log ε_1	$\tilde{\nu}_2$ log ε_2	$\tilde{\nu}_3$ log ε_3
diacetylmonoxime			
pH = 1.81	$25-27_i$	31—33	44.5
	2.6	3.25	4.63
pH = 4.10	$25-26_i$	31—33	44.5
	3.1	3.5	4.5
pH = 11.98	$26-29_i$	36	44
	3.55	4,48	4.3
pH = 14.00	$25-30_i$	36.5	49
	2.95	4,58	4.2
methyl-isopropyl-dione monoxime			
pH = 1.81	25.5—26.5	31—33	43.5
	2.7	3.3	4.57
pH = 4.10	$26-28_i$	31—33	43.5
	3.3	3.5	4.48
pH = 11.98	$25-28_i$	35	43
	3.4	4.5	4.48
pH = 14.0	$25-27_i$	35.5	49
	3.3	4.9	4.38
dimethylglyoxime	$24-28_i$	35—37	48
pH = 4.1	3.7	4.7	5.1
methyl-isopropyl-dione dioxime	25—27.5	35—37	46—48
	3.5	4.6	5.0
pH = 4.1			
glyoxime	24—28	36—38	46—48
pH = 4.1	2.7	4.0	4.5

Wave number in *kK*; *i* — inflexion

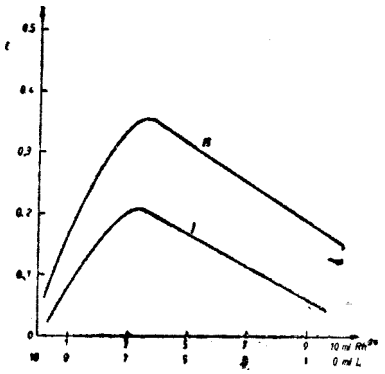

Fig. 5. Job's curves for the $RhCl_3$-glyoxime (I) and $RhCl_3$-dimethyl-glyoxime (II) system al pH- $xH = 4.1$

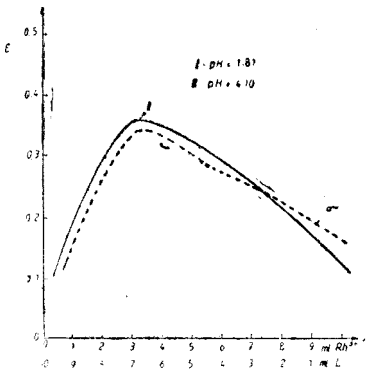

Fig. 6. Job's curve for the $RhCl_3$-methyl-isopropyl-dione dioxime system at pH 1.81 and 4.1

The UV band at 40—41 kK appears in the spectra of all complexes of the types $[Co(Diox.H)_2(Am)X]$, $[Co(Diox.H)_2(Am)_2]X$ and $H[Co(Diox.H)_2X_2]$ and can be attributted to the $Co(Diox.H)_2$ coplanar moiety [34]. In the case of the $H[Rh(Diox.H)_2X_2]$ derivatives this band is shifted towards lower frequency values: 35—37 kK. By substitution of the central cobalt atom with rhodium with a greater atomic number, appears a hypsochromic effect.

In the spectra of the Rh(III)-ketoxime systems the band at 35—37 kK is absent and a new band is observed at 31—33 kK, which pleads probably for an other geometric (assymetric) structure. In the spectra of the majority of chelates with dioximes and ketoximes, the band at approx. 48 kK can be attributed to a charge transfer with the participation of the oxime ligands [35].

The composition of the rhodium(III)-oxime complexes was established by means of the continuous variation method (Job's method).

The $RhCl_3$-glyoxime, $RhCl_3$-dimethyglyoxime and $RhCl_3$-propoxime systems ($pH = 1.81$, 4.10) show the formation of $Rh : Diox.H_2 = 1 : 2$ complexes (Fig. 5—6).

The known $H[Rh(DH)_2Cl_2]$ and $H[Rh(DH)_2Br_2]$ studied by x-ray and $I.R.$ spectral measurements have a trans geometric structure stabilized by strong intramolecular O—H..O hydrogen bridges [36]. The monodendate X ligands are situated in trans position.

In the visible region the electronic spectra of these complexes are influenced in a certain extent by the nature of the X-ligand.

The electronic spectra of some $[Rh(DH)_2X_2]^-$ and $[Rh(Propox.H)_2X_2]^-$ complexes (X = Cl, Br, N_3, NO_2) are presented in Fig. 7—8.

These derivatives are easily formed from the components in aqueous solution by warming. With the exception of irridium, the other platin metals, which form sparingly soluble $M(Diox.H)_2$ (M = Pd, Pt) type complexes, don't inter-

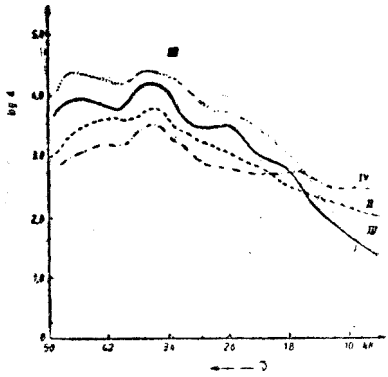

Fig. 7. Electronic spectra of: I. $H[Rh(DH)_2(N_3)_2]$; II. $H[Rh(DH)_2I_2]$; III. $H[Rh(DH)_2Br_2]$ IV. $Na[Rh(DH)_2(NO_2)_2]$

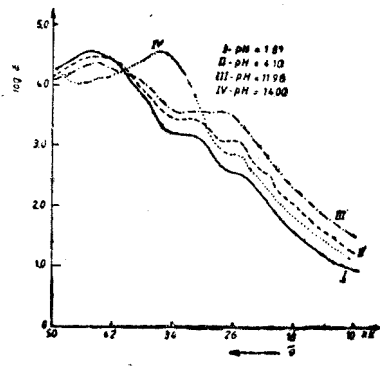

Fig. 8. Electronic spectra of: I. $H[Rh(Propox.H)_2Br_2]$; II. $H[Rh(Propox\cdot H)_2(NO_2)_2]$; III. $H[Rh(Propox\cdot H)_2I_2]$

fere the spectrophotometric determination of rhodium in $[Rh(Diox.H)_2X_2]^-$ form. The brown coloured iodine derivative: $[Rh(Diox.H)_2I_2]^-$ seems to be most suitable for this purpose. The interference of Ru and Os was not studied. The presence of Cu and Co is to be avoided, since they form also brown coloured soluble compounds with these chelating agents. The Lambert-Beer's law is followed in a wide concentration range ($5 \times 10^{-5} - 10^{-3}$ *mole* Rh/*l*). The sensitivity of these colour reactions is, however, not very significant ($\varepsilon = 500 - 2000$ in the visible region).

From the α-keto-oximes, diacetylmonoxime and methyl-isopropyl-dionemonoxime were used for the above mentioned purpose. The electronic spectra of the $RhCl_3$-keto-oxime systems at various *pH*-values are presented in Fig. 1 and 2.

The Job's curves of these systems taken at 440 and 480 *nm*, at various *pH* values (1.81,4.10) are shown in Fig. 9 and 10.

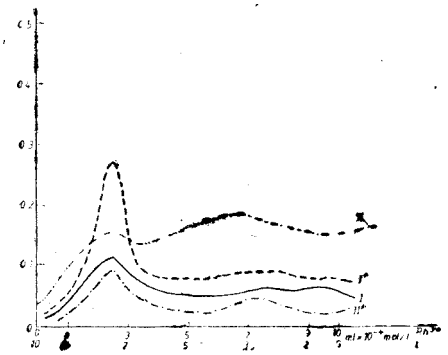

Fig. 9. Job's curves for the $RhCl_3$-diacetylmonoxime system at *pH* 1.81 (I, I') and *pH* 4.1 (II, II') by 440 and 480 *nm*

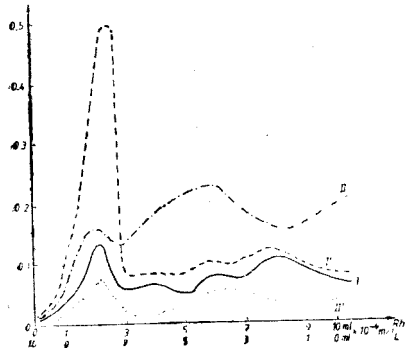

Fig. 10. Job's curves for the $RhCl_3$-methyl-isopropyl-dione monoxime system at *pH* 1.81 (I, I') and *pH* 4.1 (II, II') by 440 and 480 *nm*

Unlike the Rh-dioxime-systems, in this case the optical measurements show the formation of Rh : keto-oxime = 1 : 3 complexes, analogously with the Co(III) and Rh(III) derivatives with α-nitroso-β-naphtol, where the keto-modification participates in the formation of nonelectrolytic type chelates:

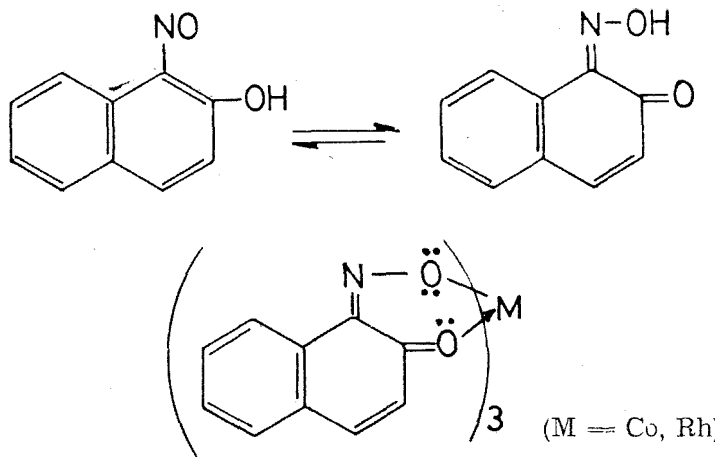

(M = Co, Rh)

The *UV* spectral data present also important deviations from those of the α dioximine derivatives (Table 1).

The light yellow colour of these chelates (log ε = 2.8—3.5 in a wave number range of 25—28 *kK*), can be used also for the above mentioned analytical purpose. The yellow solutions obey the Lambert-Beer's law in a concentration range of $5 \times 10^{-5} - 10^{-3}$ *mole/l* Rh, as in the case of dioximine derivatives.

Experimental. With the exception of dimethylglyoxime (p.a.), the reagens were prepared and recrystallized in our laboratory from water or alcohol, respectively.

The electronic spectra were recorded in aqueous Britton-Robinson buffer solutions (*pH* = 1.81, 4.11, 11.98) and in KOH 0.1 *N*. The $RhCl_3$-oxime (1 : 5) mixtures were heated in 10 *ml* buffer solution on a sand bath during 45—60 minutes, cooled, adjusted to 25 *ml* with water and the absorbance measured with a Specord spectrophotometer. Concentration: 10^{-3} *mole/l* $RhCl_3$ in the visible region and 5×10^{-5} *mole/l* in the ultraviolet part.

$RhCl_3$-oxime izomolar solutions:

0, 1, 2, 3, ... 10 *ml* 10^{-2} *mole/l* $RhCl_3$ +

10, 9, 8, ... 0 *ml* 10^{-2} *mole/l* oxime in dil.ethanol

(1 : 2) in 10 *ml* Britton-Robinson solution were kept on a sand bath during 45 minutes, cooled, adjusted to 25 *ml* and the extinction measured at 440 (480 *nm*, respectively) with a FEK colorimeter (USSR).

Observation: At higher *pH* values and Rh/oxime > 1 ratios a turbulence appears in the studied solutions ($Rh(OH)_3$), which affects the measurements.

REFERENCES

1. E. B. Sandell: *Colorimetric Determination of Traces of Metals*, 3rd Ed., Interscience Publ., New-York, London, 1959.
2. G. H. Ayres, F. Young, Anal. Chem., **24,** 165 (1952).
3. R. P. Mirozova, K. B. Yatsimirskii, I. T. Egorova, Zhur. analit. Khim., **25,** 1954 (1970).
4. V. E. Kalinina, V. M. Lyakushina, A. E. Rybina, Zhur. anal. Khim., **33,** 125 (1978)
5. A. K. Singh, M. Katyal, R. P. Singh, Indian J. Chem., Sect. A. **19,** 712 (1980).
6. A. L. J. Rao, U. Gupta, B. K. Puri, Analyst (London), **111,** 1401 (1986).
7. B. Morelli, Analyst (London), **108,** 959 (1983).
8. S. C. Shome, M. Mazumdar, M. K. Chakrabarti, J. Indian Chem. Soc., **54,** 225 (1977).
9. Yu. J. Usatenko, N. R. Meshcheryankova, V. P. Pedab, Zhur. analit. Khim., **34,** 1211 (1979).
10. D. E. Ryan, Analyst, (London), **75,** 557 (1950); **76,** 731 (1951).
11. G. G. Goroshko, Yu. M. Dedkov, A. N. Ermakov. Zhur. analit. Khim., **33,** 1114 (1978).
12. C. F. Pereira, J. Gah Gomez, Mikrochim. Acta II. **1985,** 357.
13. D. N. Purohit, A. M. Golwalker, J. S. N. Rodriguez, Ann. Chim. (Roma), **74,** 869 (1984).
14. M. R. Patil, B. C. Halder, J. Indian Chem. Soc., **56,** 576 (1979).
15. Y. M. Issa, F. M. Issa, Z. analyt. Chem., **276,** 72 (1975).
16. M. Duchkova, L. Cermakova, M. Malat, Chem. Listy, **71,** 535 (1977).
17. J. Sabartova, M. Hermanova, M. Malat, L. Cermakova, Chem. Zvesti, **34** 111 (1980).
18. Yu. M. Dedkov, A. N. Ermakov, N. V. Korsakova, Zavodskaya Labor., **50,** 8 (1984)
19. G. G. Goroshko, Yu. M. Dedkov, A. N. Ermakov, N. V. Korsakova, Zavodskaya Labor., **50,** 11 (1984).
20. V. M. Ivanov, J. V. Troyanovskii, N. T. Yatsimirskaya, Zhur. anal. Khim. **41,** 1085 (1986).
21. Y. Shijo, K. Nakaji, T. Shimizu, Analyst (London), **113,** 519 (1988).
22. K. Watanabe, Nippon Kagaku Zasshi, **77,** 547 (1947).
23. F. A. Beamish, Talanta, **13,** 773 (1966).
24. N. Gupta, D. N. Patkar, J. Indian Chem. Soc., **56,** 839 (1979); Anal. Abstr. **39,** 4B 168.
25. A. Wasey, R. K. Bansal, M. Satake, B. K. Puri, Bull. Chem. Soc. Japan, **56,** 3603 (1983); Anal. Abstr. **46,** 9B, 162.
26. K. Shrawah, S. K. Sindhwani, Bull. Soc. chim. France **5,** 737 (1986).
27. K. Shrawah, S. K. Sindhwani, Bull. Chem. Soc. Japan, **58,** 3560 (1985).
28. V. M. Savostina, O. A. Sopigun, T. V. Chebrikova, Zhur. analit. Khim., **37,** 285 (1982).
29. P. K. Paria, S. K. Majumdar, Indian J. Chem., Sect. A., **15,** 157 (1977); Anal. Abstr. **34,** 2B 122 .
30. P. K. Paria, S. K. Majumdar, J. Indian Chem. Soc., **53,** 846 (1976); Anal. Abstr. **34,** 5B 179.
31. V. M. Savostina, A. Shpigun, T. V. Chebrikova, Vestn. Moskovskogo Univ. Khim. **22,** 482 (1981); Anal. Abstr. **42,** 4B 205.
32. G. P. Syrzova, T. S. Bolgar, Zuhr, neorg. Khim., **14,** 242 (1969); **16,** 2478 (1971).
33. G. P. Syrzova, T. S. Bolgar, Zhur. neorg. Khim., **17,** 3015 (1972); **18,** 2156 (1973); **19,** 1573 (1974).
34. A. V. Ablov, M. P. Filippov, Zhur, neorg. Khim., **3,** 1565 (1958); **4,** 2204 (1959).
35. R. D. Gillard, J. A. Osborn, G. Wilkinson, J. Chem. Soc., **1965,** 1951.
36. V. M. Peshkova, V. M. Savastina, E. K. Ivanova, ,,Oksimi", Izdat. ,,Nauka", Moscova, **1977,** 86.

STUDIA UNIV. BABEŞ-BOLYAI, CHEMIA, XXXVI, 1—2, 1991

ON THE DIOXIMINE COMPLEXES OF TRANSITION METALS LXXXV.* New isothiocyanato-amine-bis-dimethylglyoximato cobalt(III) non-electrolytes

CSABA VÁRHELYI, JÁNOS ZSAKÓ, MÁRTA MÁTÉ and ERNEST GRÜNWALD

Received: 10.05.1990

ABSTRACT. A number of 23 new isothiocyanato mixed chelates of cobalt (III) of the type $[Co(DH)_2(NCS)(Am)]$ (DH_2 — dimethylglyoxime, *Am* — primary aromatic or tertiary heterocyclic amine and phosphine) were obtained by substitution reactions from $K[Co(DH)_2(NCS)_2]$ and the corresponding *Am* ligands in aqueous-alcoholic ammonium acetate buffer solutions. The new products were characterized by chemical methods, electrical conductivity and thermal measurements and *IR* spectra. Force constants are calculated in a rough approximation and discussed in terms of electronic effects.

Introduction. The first thiocyanato-complex acid of cobalt(III) with α-dioximes, the hydrogen-dithiocyanato-bis-dimethyl-glyoximato-cobaltat(III) : $H[Co(DH)_2(NCS)_2]$ was obtained by Ablov et al. [1]. Other mixed chelates of this type: $H[Co(DH)_2(NCS)X]$ (X = Cl, Br, I, NO_2) were described also by these authors [2—4].

The NCS—group has a greater trans-effect as the halide and NO_2^- — ions and therefore in aqueous solutions these mixed thiocyanato- derivatives undergo an aquation process resulting always the thiocyanato-aquo-nonelectrolyte: $[Co(DH)_2(H_2O)(NCS)]$.

Our kinetic measurements show the $H[Co(DH)_2(NCS)_2]$ acid to undergo an aquation reaction, but the rate constants are with 3—4 orders of magnitude less than those of the mixed halogenothiocyanato derivatives at the same temperature and even the formation of $[Co(DH)_2(H_2O)(NCS)]$ leads to an equilibrium [5].

Nonelectrolytic chelates of this type with amine ligands instead of water molecules in the inner coordination sphere were obtained first by Chugaev [6] by the oxidation of a mixture of $Co(NO_3)_2$, dimethylglyoxime and amine, followed by addition of NH_4NCS. The formation of $[Co(DH)_2(NCS)(amine)]$ as relatively stable intermediate was reported as the result of the partial deamination reaction:

$$[Co(DH)_2(amine)_2]NCS = [Co(DH)_2(NCS)(amine)] + amine$$

occuring in the solid state under dynamic temperature conditions and evidenced by means of thermogravimetry [7,8]. The above mentioned procedures do not lead to pure products.

Results and discussion. We observed the substitution reaction of $[Co(DH)_2(NCS)_2]^-$ in ammonium acetate buffer solution with various aromatic primary amines and tertiary heterocyclic amines and phosphines to yield the above mentioned nonelectrolytes in a pure state.

$$K[Co(DH)_2(NCS)_2] + amine = [Co(DH)_2(NCS)(amine)] + KCNS.$$

* *University Babeş—Bolyai, Dept. of Chemical Technology, 3400 Cluj-Napoca, Romania*

The very weak bases (nitro anilines, sulphanylic acids, etc. with $pK_b = 14 - 16$) are not suitable for this purpose.

In the present paper 23 new compounds were obtained by means of the above reaction. They are indicated and characterized in Table 1.

Table 1

New $[Co(DH)_2(NCS)(am)]$ type epomplexes

No.	Formula	Mol. Wt. calcd.	Yield (%)	Appearance		Analysis (%) Calcd.	Found
1.	[Co(DH)$_2$(NCS)(aniline)]	440.3	80	yellow-brown prisms	Co	13.38	13.14
					S	7.28	7.10
2.	[Co(DH)$_2$(NCS)(p-toluidine)]	454.3	75	brown rhomb. prisms	Co	12.97	13.16
					S	7.05	6.98
3.	[Co(DH)$_2$(NCS)(m-toluidine)]	454.3	70	brown hexagonale plates	Co	12.97	13.05
					S	7.05	7.17
4.	[Co(DH)$_2$(NCS)(N-diethyl-aniline)]	496.4	50	orange needles	Co	11.87	12.15
					S	6.46	6.20
5.	[Co(DH)$_2$(NCS)(m-xylidine)]	468.4	85	light brown short prisms	Co	12.58	12.25
					S	6.84	6.65
6.	[Co(DH)$_2$(NCS)(o-ethylaniline)]	468.4	75	yellow-brown needles	Co	12,58	12.88
					S	6.84	7.10
7.	[Co(DH)$_2$(NCS)(p-ethylaniline)]	468.4	80	brown prisms	Co	12.58	12.50
8.	[Co(DH)$_2$(NCS)(m-Cl-aniline)]	474.8	85	brown dendrytes	Co	12.41	12.33
					S	6.75	6.60
9.	[Co(DH)$_2$(NCS)(m-Br-aniline)]	519.2	70	light brown dendrytes	Co	11.35	11.42
					S	6.24	6.17
10.	[Co(DH)$_2$(NCS)(o-dianisidine)]	591.5	45	brown cryst. crops	Co	9.96	10.20
					S	5.42	5.23
11.	[Co(DH)$_2$(NCS)(2,4-dimethoxy-aniline)]	499.4	45	red-brown irreg. plates	Co	11.80	11.52
					S	6.42	6.26
12.	[Co(DH)$_2$(NCS)(triethyl-amine)]	448.4	40	brown rhomb. prisms	Co	13.45	13.75
					S	7.15	7.27
13.	[Co(DH)$_2$(NCS)(pyridine)]	426.3	55	dark yellow	Co	13.82	13.45
					S	7.52	7.97
14.	[Co(DH)$_2$(NCS)(β-picoline)]	440.3	90	sparkling, gold-yellow hexag. plates	Co	13.38	13.32
					S	7.28	7.47
15.	[Co(DH)$_2$(NCS)(γ-picoline)]	440.3	85	sparkling brown octahedral cryst.	Co	13.38	13.52
					S	7.28	7.05
16.	[Co(DH)$_2$(NCS)(3,5-lutidine)]	454.4	90	sparkling rhomb. prisms	Co	12.97	12.55
					S	7.05	7.06
17.	[Co(DH)$_2$(NCS)(3,4-lutidine)]	454.4	90	brown dendrytes	Co	12,97	13.00
					S	7.05	7.11
18.	[Co(DH)$_2$(NCS)(imidazole)]	415.3	75	sparkling dark yellow plates	Co	14.19	14.51
					S	7.72	8.13
19.	[Co(DH)$_2$(NCS)(2-aminothiazole)]	448.6	40	dark brown cryst. crops	Co	13.13	12.90
					S	14.30	13.87
20.	[Co(DH)$_2$(NCS)(Bu_3P)]	549.5	35	dark yellow cryst. crops	Co	10.73	10.66
					S	5.84	5.55
21.	[Co(DH)$_2$(NCS)($Et_2Ph.P$)]	513.4	60	dark yellow rhomb. prisms	Co	11.48	11.51
					S	6.24	6.35
22.	[Co(DH)$_2$(NCS)(Ph_2EtP)]	561.5	70	irregular crops	Co	10.50	10.58
					S	5.71	5.92
23.	[Co(DH)$_2$(NCS)(Et_2(p-tolyl-phosphine)]	527.4	65	gold-yellow irreg. sparkling plates	Co	11.17	10.91
					S	6.08	6.33

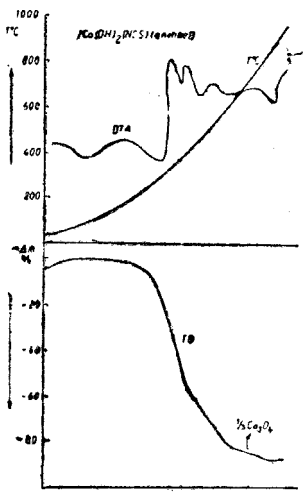

Fig. 1.

These complexes are, generally, sparingly soluble in water, more soluble in methanol and ethanol. They dissolve easily in dimethylformamide, dimethyl sulfoxid, THF or acetone.

The electrical conductance measurements show that at $20 \pm 0.1\,^{\circ}C$ their molar conductivity at a dilution of $V = 1000$ *l/mole* or $V = 2000$ *l/mole* is $3 - 10$ ohm^{-1} cm^2 $mole^{-1}$, in agreement with the nonelectrolytic character of the products.

Thermogravimetric measurements performed on some $[Co(DH)_2(NCS)(amine)]$ derivatives cannot evidence the formation of any stoechiometrical intermediary decomposition products. The nonelectrolytes are stable up to $200-240\,^{\circ}C$ as function of the nature of the amine ligand. The aromatic amine derivatives have a lower thermal stability. The final product of the pyrolysis at $850-900\,^{\circ}C$ is Co_3O_4, which transfoms up to $1000\,^{\circ}C$ into CoO (strong endotherm peak on the DTA curve). The decomposition of the complexes between $250-550\,^{\circ}C$ takes place in static air atmosphere in some consecutive and simultaneous elimination and oxidation processes marked by 2—4 exothermal peaks on the DTA curves. A typical derivatogram is presented in Fig. 1.

The infrared spectra of these compounds present broad weak bands at $2280-2320$ cm^{-1} (valence vibration of O—H) and $1680-1720$ cm^{-1} (O—H..O deformation vibrations) due, according to Nakahara [9—10], to the intramolecular hydrogen bridges O—H...O in the $Co(DH)_2$ grouping. The presence of these weak bands in the spectra of the above mentioned chelates suggests a planar configuration of the $Co(DH)_2$ grouping and a trans geometric configuration of the NCS and amine ligands.

The N—H stretching frequencies of the co-ordinated primary amines appear at $3200-3250$ and $3030-3080$ cm^{-1} (*s*), shifted towards lower frequency values as compared to the free, non co-ordinated amines (3500, 3300 cm^{-1}) showing a strong covalent character of the Co—N(amine) bonds.

The stretching vibration C=N (oxime) appears at $1530-1545$ cm^{-1} (*s*). In the free non co-ordinated dimethylglyoxime these vibrations are situated at $1620-1630$ cm^{-1}. The very strong bands at $1080-1090$ and $1230-1240$ cm^{-1} belong to the stretching vibrations N—O, the first to the non ionised, the second one to the ionised N—OH group of the mentioned chelating agent. The position of these bands indicates strong Co—N(oxime) covalent bonds.

The ν_{NC}, ν_{CS} and δ_{NCS} frequencies of the free NCS^- ion appear also in NCS—complexes, but they are shifted due to the formation of M—N or M—S σ bonds as well as of M ligand π bonds. The position of these bands is a function of the thiocyanato — or isothiocyanato character of the complex. As shown also by means of HMO calculations [11], the bond order of the NC bond is lower in the case of M—NCS and it is higher with M—SCN type complexes. Reversely, the C—S bond order is higher in the former, and it is lower in the

latter case. These conclusions are in perfect agreement with literature data [12—16], indicating the ν_{NC} frequency to be less than 2100 cm^{-1} in the case of the existence of M—N bonds, and higher than 2100 cm^{-1} if there are M—S bonds. The ν_{CS} frequency is comprized between 860 and 780 cm^{-1} in the former and between 720 and 690 cm^{-1} in the latter case.

In our previous papers [11, 17], a rough, diatomic approach was used to calculate force constants for the N—C and C—S stretching vibrations of $M_3[Cr(NCS)_6]$ and $M[Cr(NCS)_4(amine)_2]$ type complexes.

In the present paper the same approximation is used to work up the *IR* spectral data obtained and presented in Table 2.

Table 2

IR absorption bands of the co-ordinated NCS -ion of $[Co(DH)_2(NCS)(amine)]$ type complexes and force constants of the N—C and C—S bonds

amine	pK_b	$\tilde{\nu}$, cm^{-1}			$f_{NC} \cdot 10^{-6}$, *dyne/cm*	$f_{CS} \cdot 10^{-6}$, dyne/*cm*
		ν_{NC}	ν_{CS}	δ_{NCS}		
N-diethylaniline	7.44	2120	830	520	10.650	1.219
p-toluidine	8.92	2120	825	518	10.554	1.197
m-xylidine	9.26	2125	840	520	10.638	1.243
o-ethylaniline	9.54	2125	795	518	10.638	1.114
2-4-dimethoxy-aniline	9.65*	2127	818	522	10.728	1.185
3-Br-aniline	10.77	2122	795	518	10.716	1.122
mean value					10.654	1.180
imidazole	6*	2130	825	521	10.547	1.188
γ-picoline	7.89	2120	820	516	10.518	1.179
3.5-lutidine	8*	2112	788	520	10.475	1.092
β-picoline	8.32	2110	810	518	10.419	1.151
mean value					10.490	1.152

In this Table the wave numbers of the ν_{CN}, ν_{NS} and δ_{NCS} vibrations are presented for 10 complexes of the $[Co(DH)_2(NCS)(amine)]$ type. In the approach used both ν_{NC} and ν_{CS} vibrations are considered as being the vibrations of a „diatomic" molecule A—B and C—D, respectively, with A : $Co(DH)_2(amine)N$, B : CS, C : $Co(DH)_2(amine)NC$ and D : S. The frequency of these vibrations is presumed to obey the formula of diatomic molecules:

$$\nu = \frac{1}{2\pi}\sqrt{\frac{f}{\mu}} \tag{1}$$

leading to

$$f_{NC} = 4\pi^2 c^2 \tilde{\nu}_{NC}^2 \mu_{AB} \quad \text{and} \quad f_{CS} = 4\pi^2 c^2 \tilde{\nu}_{CS}^2 \mu_{CD} \tag{2}$$

where f_{NC} and f_{CS} stand for the force constants of the valence vibrations, c for the velocity of light, $\tilde{\nu}_{NC}$ and $\tilde{\nu}_{CS}$ for the wave numbers of the valence vibrations bands and μ_{AB} and μ_{CD} stand for the reduced masses

$$\mu_{AB} = \frac{M_A M_B}{M_A + M_B}, \quad \mu_{CD} = \frac{M_C M_D}{M_C + M_D}$$

The force constants calculated on the above mentioned way are presented in the same Table 2.

Table 3

Coefficients a and b of Eq. (4) and correlation coefficients r

amines	f_{NC}			f_{CS}		
	a	b	r	a	b	r
without π orbitals	10.406	0.027	0.464	1.462	−0.030	0.638
π donors	10.809	−0.042	0.799	1.322	−0.022	0.545

In Table 2 the compounds studied are given in two groups. The first group contains amine ligands having no π type orbitals available for the central Co atom. The second group amine ligands have a π donor character and as observed in our previous paper [17], they entail a shift of f_{NC} towards lower values. The same thing is observed also with the complexes studied as seen on the basis of the mean values presented in Table 2. Since the formation of the retrodative metal to NCS π bonds reduces the π bond order of both N—C and C—S bonds [11], a similar effect may be expected also with the force constants f_{CS}. Inspection of Table 2 shows the mean f_{CS} value to be less indeed with the second group amine ligands as compared to the first group ones.

It is worth mentioning that f_{NC} values of the complexes studied are a little higher, and f_{CS} values are lower as compared to the force constants obtained earlier for Cr(III) complexes [11, 17].

Concerning the influence of the nucleophilic character of the ligand an almost linear variation of the force constant with pK_b of the amine was reported earlier [17]. The

$$f = a + bpK_b \tag{4}$$

type relation was found with negative b parameter as expected on the base of electronic effects.

By using a linear regression, the parameters a and b of equation (4), as well as the correlation coefficients have been calculated. Results are presented in Table 3., by using pK_b values indicated in Table 2. These data were taken from the literature [18], values with star were evaluated by taking into account electronic effects.

As seen from this table, coefficient b is negative, as expected, excepting with f_{NC} for amines without π orbitals. Correlation coefficients are not good at all and it is the worse even in this anomalous case with $b > 0$. Therefore,

the validity of a linear law as given by equation (4) cannot be considered to be proved, but anyhow it is quite clear that with increasing base strength of the amine increase both f_{NC} nd f_{CS} force constants, irrespective of the existence of π type orbitals on the coordinated ligand atom.

Experimental. **K[Co(DH)$_2$(NCS)$_2$]** solution·25*g* cobalt(II) acetate ($Co(CH_3-COO)_2 \cdot 4H_2O$) (0.1 *mole*) in 200 *ml* water were treated with 23.2 *g* finely pulverized dimethylglyoxime (0.2 *mole*) in 600 *ml* methanol. The mixture is oxidized by bubbling air through it for 4—5 *hours*. Then 0.25 *moles* KCNS (25 *g*) in 100 *ml* water were added drop by drop under continuous stirring. The oxidation was continued for 2—3 *hours*. After filtration the dark brown solution is used for substitution reactions. **[Co(DH)$_2$(NCS)(amine)]**. 10 *mmoles* of $K[Co(DH)_2(NCS)_2]$ in 100 *ml* dil. methanol (1 : 4) were treated on a water bath with 15 *mmoles* amine or phosphine, respectively, in 25—100 *ml* alcohol. After 30—45 minutes warming, the dark brown solution is cooled and the separated yellow brown up to red brown crystalline product (as function of the nature of the Am component) is filtered off, washed with ice cooled water and dried on air.

Analysis. Cobalt was determined complexometrically by using murexide as indicator. Organic ligands were destroyed by heating with conc. H_2SO_4 and several crystals of KNO_3. After dilution with water, the solution was neutralized with sodium acetate and ammonia.

Sulphur was determined gravimetrically as $BaSO_4$ after destroying of the samples (200—300 *mg*) with a mixture of 10—15 *ml* conc. HNO_3 and 15—25 drops of bromine.

The infrared spectra were recorded in KBr pellets using an UR 20 spectrophotometer (Carl Zeiss Jena).

The thermal measurements were carried out with a MOM Derivatograph (Budapest) in static air. Sample weight 100 *mg*, heating rate 10°/*min*.

REFERENCES

1. A. V. Ablov, G. P. Syrzova, Zhur. obshchei Khim., **20**, 2053 (1955).
2. A. V. Ablov, N. M. Samush, Zhur. neorg. Khim., **3**, 1818 (1958).
3. A. V. Ablov, N. M. Samush, M. S. Popov, Doklady Akad. Nauk SSSR, **106**, 665 (1956).
4. A. V. Ablov, N. M. Samush, Zhur. neorg. Khim., **4**, 1753 (1959).
5. Z. Finta, Cs. Várhelyi, J. Zsakó, J. inorg. nucl. Chem., **32**, 3013 (1970).
6. L. A. Chugaev, Ber. dtsch. chem. Ges., **40**, 3498 (1907).
7. J. Zsakó, Cs. Várhelyi, E. Kékedy, Anal. Univ. Bucureşti, **14**, (2), 15 (1965).
8. J. Zsakó, Cs. Várhelyi, E. Kékedy, J. inorg. nucl. Chem., **28**, 2637 (1966).
9. A. Nakahara, Bull. chem. soc. Japan, **28**, 473 (1955).
10. A. Nakahara, J. Fujita, R. Tsuchida, Bull. chem. soc. Japan, **29**, 296 (1956).
11. J. Zsakó, Cs. Várhelyi, M. Máté, Stud. Univ. Babeş-Bolyai, Chem., 1989 (2) 74.
12. J. Fujita, K. Nakamoto, M. Kobayashi, J. Amer. Chem. Soc., **78**, 3295 (1956).
13. M. Chamberlain, J. C. Bailar, J. Amer. Chem. Soc., **81**, 6412 (1959).
14. J. Lewis, R. S. Nyholm, P. W. Smith, J. Chem. Soc., 4590 (1961).
15. A. Turco, L. Pecil, J. Chem. Soc., 3008 (1962).
16. A. Sabastini, J. Bertini, Inorg. Chem., **4**, 959, 1665 (1965); **5**, 1025 (1966).
17. J. Zsakó, Cs. Várhelyi, I. Gănescu, M. Máté, Rev. Roumaine Chim. 37, 187 (1992).
18. Landolt-Börnstein, *Zahlenwerte und Fuktionen aus Physik, Chemie, Astronomie, Geophysik*, Technik, II. Band, 7 Teil, Elektrische Eigenschaften II. Springer Verlag, Berlin—Göttingen—Heidelberg, 1970, p. 898—917.

STUDIA UNIV. BABEŞ-BOLYAI, CHEMIA, XXXVI, 1—2, 1991

MODELLING OF THE OVERALL METHANE-STEAM REFORMING PROCESS

ILIE SIMINICEANU*, CORNELIU PETRILĂ*, ALEXANDRU POP*

Received: 26.03.1991

ABSTRACT. A mathematical model for the overall methane-steam reforming process, in an ammonia plant, is established. The model correlates the specific heat consumption (q), the temperature (T_1) and the methone conversion (α_1) in the primary reformer, as well as the conversion (α_2) and the temperature (T_2) in the secondary reformer as function of the imput parametres: steam/carbon ratio (R_1); steam/carbon ratio (R_2); airtemperature (T); methane steam mixture temperature (T_{01}); primary reformer pressure (P_1). The influence of R_1 and T_1 variations is analysed quantatively by a computer, at $R_2 = 1.33$; $T_{01} = 797\ K$; $T = 730\ K$; $P_1 = 3.0\ MP_a$. The optimal conditions (R_1, T_1), at which the specific heat consumption has a minimal value, can be stated by this method. New data show the possibility to diminish R_1 from the present 3.5—4.0 values to 3.0 without essential influence on the final methane conversion (α_2), and on other output variables of the process.

Estimates to ensure food for the world's population — which, by the end of this millenium is thought to outnumber 6 billions — show that the consumption of mineral fertilizers ($N + P_2O + K_2O$) will have to increase with cca 80 million tons of active substance [1]. Possibly, nitrates will amount to 50% of this quantity. In the near future too, *synthesis of ammonia* will be the only industrial way to fix the *atmospheric* nitrogen, and the most effective source of hydrogen needed in this synthesis will lie further in the catalysis of natural gas with water vapours [2], also known as *reforming*. Over 99% of such ammonia installation input energy consists of *natural gas* of which one third is consumed as fuel in the primary reforming oven and for the generation of steam, while two thirds — as raw material [3].

The possibility to reduce the natural gas — raw material consumption by analysis and synthesis of the global technologic process to fabricate ammonia was studied elsewhere [4]. In the present paper, an attempt is made to investigate the possibility to diminish the natural gas-fuel consumption by decreasing the steam-carbon ratio at the input of the primary reformer, and also the consequences of this upon the out-turn of the global reforming process. To this end, a mathematical model is established, which correlates the specific heat consumption in the primary reformer, the specific natural gas consumption in the radiation area and the concentration of untransformed methane at the output of the secondary reformer as function of the initial steam/carbon molar ratio. The model is tested by comparing the calculated values with those measured in an industrial installation. Then, the influence of the diminution of steam/carbon ratio,from 4.0—2.0, upon the above parameters is analysed on a computer.

* *Politechnical Institute Jassy, Dept. of Chemical Engineering, 6600 Iaşi, Romania*

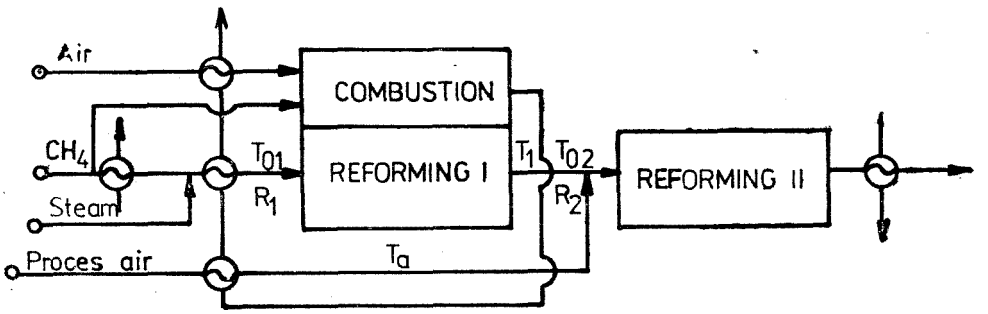

Fig. 1. The bloc diagram of the global technological process of reforming the natural gas.

1. The Mathematical Model. The natural gas reforming global process consists in three distinctive chemical processes (primary reforming, the process of combustion, secondary reforming) as well as in a range of heat exchange processes, connected conformably to the block scheme in Fig. 1.

Let the primary reforming process be described by Eqs. (1) and (2), the secondary reforming process by Eqs. (1)—(3) and the combustion by Eq. (4):

$$CH_4 + H_2O = CO + 3H_2 \tag{1}$$

$$CO + H_2O = CO_2 + H_2 \tag{2}$$

$$1/2O_2 + H_2 = H_2O \tag{3}$$

$$CH_4 + 2O_2 = CO_2 + 2H_2O \tag{4}$$

The mathematical model for the primary reforming relies on the experimentally verified hypothesis [5] that the process develops conformably to a heat transfer macrocinetic model, and the chemical transformations in Eqs. (1) and (2) practically reach equilibrium. Whence the primary reforming process is described by Eqs. (5)—(8):

$$K_{p1} - \frac{(\alpha_1 - \beta_1)(3\alpha_1 + \beta_1)^3 \cdot p^2}{(1 - \alpha_1)(R_1 - \alpha_1 - \beta_1)(1 + R + 2\alpha_1)^2} = 0 \tag{5}$$

$$K_{p2} - \frac{\beta_1(3\alpha_1 + \beta_1)}{(\alpha_1 - \beta_1)(R_1 - \beta_1 - \alpha_1)} = 0 \tag{6}$$

$$\lg K_{p1} = -9861{,}11/T - 11{,}87 - 2{,}0585 \cdot 10^{-3} \cdot T + 0{,}1779 \cdot 10^{-6} \cdot T^2 + 8{,}3432 \lg T \tag{7}$$

$$\lg K_{p2} = 2217{,}18/T - 3{,}27467 + 0{,}3524 \cdot 10^{-3} \cdot T - 0{,}0507 \cdot 10^{-6} \cdot T^2 + 0{,}2969 \lg T \tag{8}$$

Making the thermic balance for the primary reformer one obtains Eq. (9), which allows to calculate the heat specific consumption ($q \cdot J/mol\ H_2$) as function of the transformation degrees α_1, β_1 and the parameters R_1, T_{01}, T_1:

$$q = 1{,}045/\alpha_1[41\,100\alpha_1 - 10\,320\beta_1 + (32{,}5\alpha_1 + 0{,}522\beta_1 + 3{,}422 + 7{,}219\ R_1) \cdot T_1 - (17{,}93\alpha_1 - 4{,}13\beta_1 - 8{,}922 - 1{,}187R_1) \cdot 10^{-3} \cdot T_1^2 + (2{,}85\alpha_1 - 1{,}336\beta_1 - 1{,}388 + 0{,}089\ R_1) \cdot 10^{-6} \cdot T_1^3 - (3{,}422 + 7{,}219\ R_1) \cdot T_{01} - (8{,}922 - 1{,}187R_1 \cdot 10^{-3} \cdot T_{01}^2 + (1{,}388 - 0{,}089\ R_1) \cdot 10^{-6} \cdot T_{01}^3 \tag{9}$$

On the basis of the mass and heat transfer in the combustion process, equations for the combustive methane gas were set up as function of the parameter in the reforming process (T_{01}, T_1, R_1, P_1) and those in the burning process: initial temperature of the air and the combustion gas, temperature of the burning gases that leave the radiation area of the oven, and the air excess coefficient. These conditions were presented elsewhere [6].

The secondary reforming process is adiabated-autotherm. The heat discharge in Eq.(3) increases the temperature of the mass reaction to over 1273 K, and thus the equilibrium of the reaction mass is shifted rightwards, the methane transformation degree being enhanced. The mathematical model of this process covers the thermodynamic equilibrium Eqs.(7), (8) and (10), (11), and also those of the thermal balance (13) and (14):

$$K_{p_1} - \frac{(\dot{X}^0_{CO} - \dot{X}_{CO}\beta_2/\alpha_1 + \alpha_2 - \beta_2)(\dot{X}^0_{H_2} + \dot{X}^0_{CO}\beta_2/\alpha_2 - 2\dot{X}^0_{O_2} + 3\alpha_2 + \beta_2) \cdot P^2}{(1-\alpha_2)(\dot{X}^0_{H_2O} - X^0_{CO}\beta_2/\alpha_2 + 2\dot{X}^0_{O_2} - \alpha_2 - \beta_2)(S + 2\alpha_2)^2} = 0 \quad (10)$$

$$K_{p2} - \frac{(\dot{X}^0_{CO_2} + \dot{X}^0_{CO} \cdot \beta/\alpha_2 + \beta_2)(X^0_{H_2} + X^0_{CO}\beta_2/\alpha_2 - 2\dot{X}^0_{C_2} + I3\alpha_2 + \beta_2)}{(\dot{X}^0_{CO} + \alpha_2 - \beta_2 - \dot{X}^0_{CO}\beta_2/\alpha_2)(X_{H_2O} - X^0_{CO}\beta_2/\alpha_2 + 2\dot{X}^0_{O_2} - \alpha_2 - \beta_2)} = 0 \quad (11)$$

$$S = 1 + \dot{X}^0_{CO} + \dot{X}^0_{CO_2} + \dot{X}^0_{H_2} + \dot{X}^0_{H_2O} + \dot{X}^0_{N_2} \quad (12$$

$$[A - 0{,}291\dot{x}^0_{O_2} + 3{,}256\alpha_2 + 1{,}162\beta_2(1 + \dot{x}^0_{CO_2}\dot{x}^0_{H_2O}) \cdot 10^{-6} \cdot T^3 + [B + 3{,}443\dot{x}^0_{O_2} -$$
$$- 18{,}838\alpha_2 + 3{,}225\beta_2(1 + \dot{x}^0_{CO}/\alpha_2) \cdot 10^{-3} \cdot T^2 + [C \quad 12{,}22\ \dot{x}^0_{O_2} + 33{,}156\alpha_2 +$$
$$+ 1{,}18\beta_2(1 + \dot{x}^0_{CO}/\alpha_2) \cdot T + 40\,124{,}32\alpha_2 - 10\,455{,}484\beta_2(1 + \dot{x}^0_{CO}\ \alpha_2) -$$
$$- 112\,252{,}487\,\dot{x}^0_{CO} = A \cdot 10^{-}_{6} \cdot T^3_{02} + B \cdot 10^{-3} \cdot T \quad + C \cdot T_2 \quad (13)$$

$$A = -1{,}388 - 0{,}114\dot{x}^0_{H_2O} - 0{,}153\ \dot{x}_{CO} - 0{,}825\ \dot{x}^0_{CO_2} + 0{,}093\ \dot{x}^{0\,\pi}_{H_2} - 0{,}115\ \dot{x}^0_{N_2} -$$
$$- 0{,}269\ x^0_{O_2}$$

$$B = 8{,}922 + 1{,}641\ \dot{x}^0_{H_2O} + 1{,}045\ \dot{x}^0_{CO} + 4{,}266\ \dot{x}^0_{CO_2} + 0{,}033\ \dot{x}^0_{H_2} + 0{,}909\ \dot{x}^0_{N_2} +$$
$$+ 1{,}495\ \dot{x}^0_{O_2}$$

$$C = 3{,}422 + 6{,}89\,\dot{x}^0_{H_2O} + 6{,}25\ \dot{x}^0_{CO} + 6{,}85\ \dot{x}^0_{CO_2} + 6{,}88\ \dot{x}^0_{H_2} + 6{,}30\ \dot{x}^0_{N_2} + 6{,}13\,\dot{x}^0_{O_2} \quad (14)$$

Molar ratios x_i, at the input in the secondary reformer, are correlated in function of α_1, β_1, R_1 and R_2 by relations (15), established on the basis of the balance of the process of the air with the gas resulted in the primary reformer.

$$\dot{x}^0_{CO} = \frac{\alpha_1 - \beta_1}{1 - \alpha_1} \qquad \dot{x}_{H_2O} = \frac{R_1 - \alpha_1 - \beta_1}{1 - \alpha_1} \qquad \dot{x}_{CO_2} = \frac{\beta_1}{1 - \alpha_1}$$

$$\dot{x}^0_{H_2} = \frac{3\alpha_1 + \beta_1}{1 - \alpha_1} \qquad \dot{x}^0_{N_2} = \frac{0{,}79\ R_2}{1 - \alpha_1} \qquad \dot{x}^0_{O_2} = \frac{0{,}21R_2}{1 - \alpha_1} \quad (15)$$

The temperature at the input in the secondary reformer (T_{02}) is calculated from the thermic balance of the same process of mixing:

$$T_{02} = \frac{C_1 T_1 + Ca\, Ta}{C_1 + Ca} \tag{16}$$

where:

$$C_a = R_2(0{,}79\, C_{pN^2} + 0{,}21\, C_{pO_2}) \tag{17}$$

$$C_1 = (1 - \alpha_1)C_{p\mathrm{CH_4}} + (R_1 - \alpha_1 - \beta_1)C_{p\mathrm{H_2O}} + (\alpha_1 - \beta_1)C_{p\mathrm{CO}} + \beta_1 C_{p\mathrm{CO_2}} + (3\alpha_1 + \beta_1)C_{p\mathrm{H_2}} \tag{18}$$

The molar caloric capacities of the components are dependent on temperature by relations of the form:

$$C_{pi} = a_i + b_i \cdot T + c_i \cdot T^2 \tag{19}$$

the values of coefficients a, b, c being tabulated in the reference temperature [7, 8].

The molar fraction of methane remained untransformed after the I-st and II reforming stages, sa compared to the ,,dry'' gas, is determined by Eqs. (20) and (21), respectively:

$$(x_{\mathrm{CH_4}})_1 = \frac{1 - \alpha_1}{1 + 23\alpha_1 + \beta_1} \tag{20}$$

$$(x_{\mathrm{CH_4}})_2 = \frac{(1 - \alpha_1)(1 - \alpha_2)}{1 + 3\alpha_1 + \beta_1 + 0{,}37R_2 + (1 - \alpha_1)(3\alpha_2 + \beta_2 + \beta_2/\alpha_2)} \tag{21}$$

The system of Eqs. (5)—(21) allows to determine the magnitudes α_1, β_1 α_2, β_2, q, T_2, $(x_{\mathrm{CH_4}})_2$, $(x_{\mathrm{CH_4}})_1$ as function of the parameters R_1, R_2, P_1, T_1 and T_a. In order to compare the system (5)—(21), the measured values found on an industrial installation and those calculated in the same circumstances were compared. Thus, it was found that the transformation degrees α_1 and δ_1 calculated by relation (5)—(8) are greater than the real ones. This deviation from the equilibrium was introduced in the calculation program by a correction of the temperature at the output of the primary reformer: $T_i = T_1 - \Delta T$: Trials showed that $\Delta T = 18\ K$ at $P_1 = 3.0\ MP_a$. The pressure loss between the two reformers was also taken into account. Measurements showed $P_1 - P_2 = 0.1\ MP_a$ Based on these corrections the system (5)—(21) was tested by simulation of an industrial installation, comparing the calculated values of the final concentration $(x_{\mathrm{CH_4}})_2$, with the measured ones. The calculated values are with at most 1.3% smaller than the measured ones. This deviation shows that the transformations in the secondary reformer do not reach equilibrium, also. However, the precision of the model can be considered as satisfactory for the object of this paper.

2. **Results.** The system (5) (21) was solved by the Newton Raphson method, programed in BASIC on a microsystem FELIX M 18. The values obtained for $R_1 = 2.0—4.0$ and $T_1 = 1050—1200\ K$, at $R_2 = 1.33$; $T_{01} = 797\ K$; $T_a = 730\ K$ and $P_1 = 3.0\ MP_a$ are given in Tables 1—4.

Table 1

The influence of ratio R_1, at $T_1 = 1050$ K

R_1	2,0	2,5	3,0	3,5	4,0
α_1	0,4143	0,4693	0,5189	0,5640	0,6051
β_1	0,2225	0,2665	0,3075	0,3458	0,3819
$q \cdot 10^{-4}$ *J/mol*	8,5043	8,3664	8,6451	8,7342	8,8304
$100 \cdot (X_{CH_4})_1$	23,7498	19,419	16,7930	14,3508	12,3491
α_2	0,7630	0,8159	0,8631	0,9022	0,9317
β_2	0,0711	0,0811	0,0870	0,0879	0,0836
T_2	1150,20	1155,95	1163,22	1173,32	1184,66
$100 \cdot (X_{CH_4})_2$	3,1574	2,1417	1,4033	0,8896	0,5539

Table 2

The influence of ratio R_1, at $T_1 = 1100$ K

R_1	2,0	2,5	3,0	3,5	4,0
α_1	0,5240	0,5964	0,6406	0,6879	0,7293
β_1	0,2198	0,2673	0,3113	0,3521	0,3903
$q \cdot 10^{-4} J/mol$	8,4178	8,4012	8,5842	8,6920	8,8097
$100 \cdot (X_{CH_4})_1$	17.0474	13,640	11,1145	9,1339	7,5636
α_2	0,9811	0,9641	0,9645	0,9744	0,9865
β_2	0,0333	0,0262	0,0176	0,0070	0,0027
T_2	1218,07	1240,63	1265,97	1288,33	1305,55
$100 \cdot (X_{CH_4})_2$	1,2363	0,5798	0,2665	0,1330	0,0747

Table 3

The influence of ratio R_1, at $T_1 = 1150$ K

R_1	2,0	2,5	3,0	3,5	4,0
α_1	0,6413	0,7065	0,7506	0,8030	0,8384
β_1	0,2052	0,2545	0,3002	0,3424	0,3812
$q \cdot 10^{-4} J/mol$	8,3566	0,4532	8,5744	8,7122	8,8654
$100 \cdot (X_{CH_4})_1$	11,4622	8,6917	6,7161	5,2511	4,1465
α_2	0,9733	0,9887	0,9937	0,9956	0,9964
β_2	0,0030	0,0255	0,0491	0,0720	0,0936
T_2	1336,19	1379,20	1407,74	1424,36	1432,48
$100 \cdot (X_{CH_4})_2$	0,2048	0,0690	0,0316	0,0180	0,0119

Table 4

The influence of ratio R, at $T_1 = 1200$ K

R_1	2,0	2,5	3,0	3,5	4,0
α_1	0,7540	0,8140	0,8585	0,8915	0,9161
β_1	0,1842	0,2542	0,2805	0,3229	0,3615
$q \cdot 10^{-4} J/mol$	8,3391	8,4721	8,6340	0,8164	9,0141
$100 \cdot (X_{CH_4})_1$	7,1505	5,075	3,6670	2,7117	2,3969
α_2	0,9954	0,9974	0,9979	0,9981	0,9980
$-\beta_2$	0,0241	0,0479	0,0707	0,0915	0,1099
T_2	1493,10	1526,79	1540,21	1541,70	1536,29
$100 \cdot (X_{CH_4})_2$	0,0242	0,0102	0,0059	0,0042	0,0033

The obtained data allow to analyse the influence of parameters R_1 and T_1 on magnitudes: α_1, δ_1, α_2, δ_2, q, T_2, $(x\ \ )_1$, $(x\ \ )_2$. Of these, the specific heat consumption in the primary reformer (q) and the final transformation degree of methane (α_2) can be considered as basic output of the reforming global process. δ is less important, as it stands for of the secondary reaction (2). The obtained data show at high temperatures ($T_1 > 1150\ K$) the reverse of this reaction ($\delta_2 > 0$). The temperature value in both reforming stages is limited, mechanically. Before 1980, the tubes of the primary reformer were made of only steel HK — 40 (25 Cr — 20 Ni), with an inside diameter of 0.1 m and a thickness of 0.018 m. These tubes were guaranteed for a term of 10 years, at a pressure of 3.0 MP and maximum temperature of 1227 K [9]. The use of tubes made of higher standard steels (25 Cr—35 Ni), with a smaller dilatation coefficient will allow the maximum temperature increase up to 1225 K [9]. This means that T_1 can be enhanced from 1083 K to about 1123 K, and T_2 from 1269 to about 1300 K.

The $q - R_1 - T_1$ dependence (Fig. 2) shows the existence of a minimum in the specific heat consumption at T_1, which increases as the steam excess decreases. The geometrical locus of the pairs $R_1 - T_1$ — which give the minimum q — is shown under the form of the curve in Fig. 3. In the conditions studied ($P_1 = 3.0\ MPa$; $T = 730\ K$; $T_{01} = 797\ K$; $R_2 = 1.33$, at $R_1 = 3.5$), q becomes minimum when $T_1 = 1100\ K$. In order to reduce the R_1 ratio at 3.0, the temperature in the reformer must be increased to 1125 K. This temperature can be attained by replacing the conventional pipes with those made of special steel. The further reduction of R_1 would necessitate even higher temperatures.

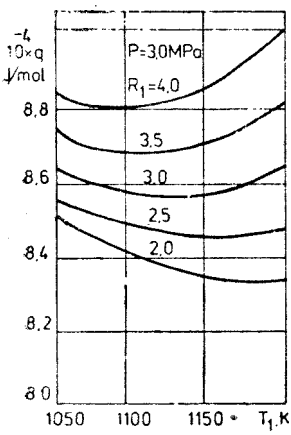

Fig. 2. Influence of ratio R_1 and temperature T_1 on the specific heat consumption, at $P = 3.0 MPa$.

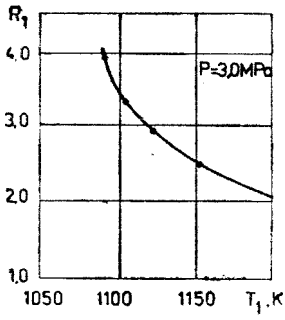

Fig. 3. Curve of the minimum specific consumption, at $P = 3.0\ MPa$.

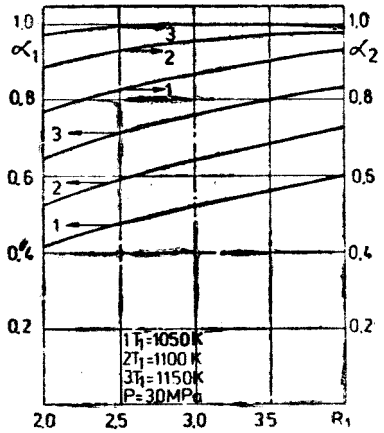

Fig. 4. Dependency of the transformation degrees α_1 and α_2 on the ratio R_1 at varied temperatures: 1. $T_1 = 1050\ K$; 2. $T_1 = 1100\ K$; 3. $T_1 = 1150\ K$

The transformation degrees α_1 and α_2 are strongly influenced by parameters R_1 and T_1 (Fig. 4). At $T_1 = 1100\ K$, for instance, by reducing R_1 from 4.0 to 3.0, α_1 decreases from 0.7293 to 0.6406 and α_2 — from 0.9865 to 0.9645. Practically, α_2 has to be greater than 0.95 so as the actionless content (CH_4 + + Ar) should increase not too much in the synthesis cycle.

From this viewpoint, too, data show that the reduction of ratio R_1 can be possible only down to 3.0.

Conclusions. The here advanced mathematical model allows to analyse the influence of the main technological parameters (P_1, T_{01}, T, T_1, R_1, R_2) on the output of the global reforming process (q, α_1, α_2, T_2, x_{CH_4}).

The data obtained on computer and given in this paper refer to the in fluence of reducing the steam/carbon ration on the basic output of the process: the specific heat/fuel consumption and the final degree of methane transformation. Thus, optimal $R_1 - T_1$ pairs are found, where the energy specific consumption is minimum.

In the conditions under investigation ($R_2 = 1.33$; $T_{01} = 797\ K$; $T_a = 730\ K$; $P_1 = 3.0\ MPa$), the ratio R_1 can be diminished from (the present) 3.5—4.0 to 3.0. The decrease of R_1 below 3.0 would necessitate too high T_1 temperatures, whence the untransformed methane content would increase, which has a negative influence on the synthesis cycle.

It is to be expected that reduction of R_1 also affects the output of other processes that follow the reforming: the carbon oxide conversion, the methaning. Hence the need to work out a more complex model in view of investigating the effects of the diminution of steam/carbon ratio on the entire ammonia producing installation.

SYMBOLS

A, B, C — magnitudes defined by Eq. (14);

C_a, C_{11} — the caloric capacity of air and of the mixture in the main reformer, defined by Eqs. (17) and (18);

C_{pi} — the molar caloric capacity of component i;

K_{p1}, K_{p2} — the equilibrium constants of reactions (1) and (2), respectively;

P_1, P_2 — working pressures in the primary and secondary reformers, respectively;

q — specific heat consumption in the primary reformer ($J/mol\ H_2$);

R_1 — the steam/carbon molar ratio at the input in the primary reformer;

R_2 — the process air/carbon molar ratio;

S — magnitude defined by Eq. (12);

T_1, T_2 — final temperatures in the primary and secondary reformers, respectively;

T_{01}, T_{02} — temperatures at the input in the primary and secondary reformers, respectively;

T_a — temperature of the process air;

$\dot{x}_i^0$ — initial molar rations ($\dot{x}_i^0 = n_i^0/n_{CH_4}$);

x_{CH_4} — the molar fraction of methone, related to the „dry" gas;

α_1, α_2 — the methane degree of transformation (η_{CH_4}) in the primary and secondary reformers, respectively;

β_1, β_2 — the $\eta_{CH} \cdot \eta_{CH}$ product in the primary and secondary reformers, respectively.

REFERENCES

1. * * *, *Hrană pentru şase miliarde*, Ed. Politică, Bucureşti, 1986.
2. I. Siminiceanu, *Sinteza industrială a amoniacului la* **75** *ani*, Al IV-lea Simpozion naţional de inginerie a proceselor chimice, Piatra Neamţ, 1988.
3. G. D. Honti, *Energy Conservation in the Nitrogen Industry*, Brit. Sulphur Corp. Symp., London, 1981, Paper 1.
4. I. Siminiceanu, Rev. chim., 1989, **40**, 2, p. 125.
5. I. Siminiceanu, Teză de doctorat, I. P. Iaşi, 1980.
6. I. Siminiceanu, C. Calistru, Rev. chim., 1979, **30**, 1, p. 45.
7. C. Calistru, ş.a., *Tehnologia îngrăşămintelor minerale*, vol. **I**, Ed. Tehn., Bucureşti, 1984.
8. I. Siminiceanu, C. Petrilă, D. Jianu, Rev. chim., 1987, **38**, 1, p. 39.
9. C. M. Schillmoller, Rydrocarbon Processing, 1986, 9, p. 63.

STUDIA UNIV. BABEŞ-BOLYAI, CHEMIA, XXXVI, 1—2, 1991

NEW COBALT(III)-AMINE PERCHLORATES AND THE GRAVIMETRIC DETERMINATION OF THE ClO_4^--ION

FERENC MAKKAY*, CSABA VÁRHELYI* and MELINDA FORRÓ*

Received: 15.04 1991

ABSTRACT. Eleven diacido-tetramine cobalt (III) perchlorates of the types: $[Co(en)_2X_2]ClO_4$, $[Co(pyridine)_4Cl_2]ClO_4$ and $[Co(Diox.H)_2(amine)_2]ClO_4$ (X = = Cl, Br, $1/2C_2O_4$; Diox. H_2 = dimethylglyoxime, heptoxime) were obtained and characterized by i.r. spectral and derivatographic measurements. The obtained binary salts were proved for the gravimetric determination of the perchlorate ion. The best results were obtained by using trans-$[Co(en)_2Cl_2]ClO_4$ for this purpose.

Introduction. The perchlorate ion with a thermochemical ion radius of about 2.5Å forms a series of sparingly soluble salts with monovlaent metals (K^+, Rb^+, Cs^+), voluminous N-bases (nitrone [1], antipyrine derivatives [2]), with phosphonium — and arsonium salts (tetraphenyl-derivatives [3, 4]) has also been proposed for the gravimetric determination of this oxoanion. The perchlorates of various organic dyes: methylene blue [5], brilliant green [6], neutral red [7], variamine blue [8, 9], etc. are silghtly soluble in water and readily soluble in some organic solvents (benzene, nitrobenzene, $CHCl_3$, CCl_4). These salts were recomanded for the spectrophotometric determination of ClO_4^-.

The perchloric acid and the alkaline perchlorates have been used for the separation of cobalt (III)— and chromium (III) — amine bases of various types. It was observed, that the hexamine- and monoacido-pentamine type bases form $[Co(amine)_6](ClO_4)_3$, $[Cr(amine)_6](ClO_4)_3$, $[Co(amine)_5X](ClO_4)_2$ etc. type perchlorates with a considerable solubility in water ($1 - 5.10^{-3}$ *mole/l*). The diacido- tetramine type derivatives in this class present a much lower solubility in neutral or acidic aqueous solutions ($10^{-5} - 10^{-4}$ *mole/l*). Their solubility is influenced by the composition of the inner co-ordination sphere of the complex. The hydrophile ligands (H_2O, OH, SO_3, NO_2, CO_3 etc.) increase the solubility of the above mentioned binary salts.

Results and discussions. We have obtained a series of perchlorates of the diacido-tetramine-cobalt(III) type by double decomposition reactions, using $[Co(en)_2X_2]^+$ (X = Cl, Br, $1/2C_2O_4$), $[Co(pyridine)_4Cl_2]^+$ and various $[Co(Diox,-H)_2(amine)_2]^+$ type bases for this purpose (diox.H_2 = dimethylglyoxime: DH_2, heptox.H_2: 1,2 cycloheptane dione dioxime (heptoxime).

The obtained perchlorates are characterized in Table 1.

* *University Babeş—Bolyai, Dept. of Chemical Technology, 3400 Cluj-Napoca, Romania*

Table 1

$[Co(amine)_4X_2]ClO_4$ and $[Co(Diox.H)_2(amine)_2]ClO_4$ type perchlorates

Formula	mol. wt. calcd.	Yield (%)	Appearance		Analysis (%) calcd.	found	Ref.
trans-$[Co(en)_2Cl_2]ClO_4$	349.515	90	sparkling, green plates	Co	16.87	17.10	15
trans-$[Co(en)_2Br_2]ClO_4$	438.433	98	green prisms	Co	13.45	13.10	15
$[Co(en)_2(C_2O_4)]ClO_4$	366.603	95	irregular red cryst.	Co	16.08	15.86	15
$[Co(pyridine)_4Cl_2]ClO_4$	545.723	98	green irreg. cryst.	Co	10.80	10.70	15
$[Co(DH)_2(NH_3)_2]ClO_4$	422.7	90	yellow prisms	Co	13.94	13.86	12
$[Co(DH)_2(aniline)_2]\cdot ClO_4$	574.6	96	brown spears	Co	10.28	10.05	12
$[Co(DH)_2(pyridine)_2]\cdot ClO_4$	546.8	90	brown prisms	Co	10.78	10.65	12
$[Co(Heptox.H)_2(\beta\text{-picoline})_2]ClO_4$	654.9	95	brown prisms	Co	9.00	9.10	*
				N	12.83	12.72	
$[Co(Heptox.H)_2(3,4\text{-lutidine})_2]ClO_4$	682.9	94	yellow-brown needles	Co	8.63	8.77	*
				N	12.31	12.19	
$[Co(Heptox.H)_2(3,5\text{-lutidine})_2]ClO_4$	682.9	95	yellow-brown needles	Co	8.63	8.45	*
				N	12.31	12.60	
$[Co(Heptox.H)_2(benzylamine)_2]ClO_4$	682.9	88	brown needles	Co	8.63	8.55	*
				N	12.31	12.75	

Co detn. complexometrically, N as N_2 gazvolumetrically;
* — unpublished, new compound
„DH" = $C_4H_6N_2O_2$; „Heptox. H" — $C_4H_{11}N_2O_2$

These salts are unitary, crystalline products, which can be rapidly filtered off, washed and dried.

The $[Co(en)_2X_2]ClO_4$ are very slightly soluble in water and insoluble in alcohol. The solubility of the $[Co(Diox.H)_2(amine)_2]ClO_4$ derivatives increases with increasing alcohol concentration in function of the nature of the monodentate amine ligand.

The characteristic i.r. frequencies of the perchlorate appear in all cases approximately at the same wave number values as in the case of the $KClO_4$ (see Table 2).

Table 2

Infrared spectral data on some cobalt (III)-amine perchlorates

Vibration	I.	II.	III.	IV.	V.
$\nu_1(Cl-O)$	935 *m*	940 *m*	938 *m*	930—40 *m*	930—40 *m*
$\delta_2(O-Cl-O)$	460 *m*	471 *m*	470 *m*	470 *m*	470 *m*
$\nu_3(Cl-O)$	1080—1170 *vs*	1060—1140 *vs*	1050—1150 *vs*	1060—1135 *vs*	1060—1140 *vs*
$\delta_4(O-Cl-O)$	630 *vs*	620—	630 *vs*	620—	620—
$\delta_4(OClO)$		640 *vs*		640 *vs*	640 *vs*

I. — $KClO_4$; II. — trans-$[Co(en)_2Cl_2]ClO_4$; III. — trans-$[Co(en)_2Br_2]ClO_4$; IV. — $[Co(DH)_2(aniline)_2]ClO_4$; V. — $[Co(Heptox.H)_2(3,4\text{-lutidine})_2]ClO_4$

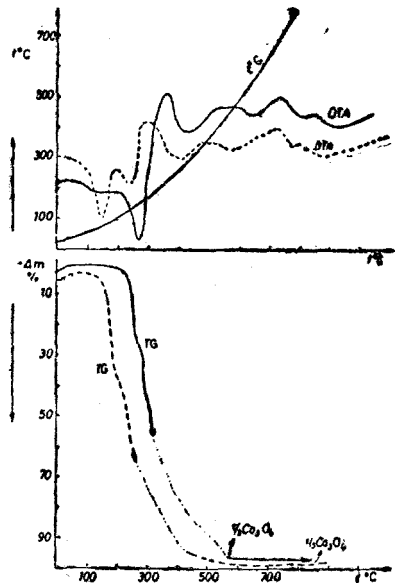

Fig. 1. *TG* and *DTA* curves of
— trans-$[Co(en)_2Cl_2]ClO_4$
---- trans-$[Co(en)_2Br_2]ClO_4$

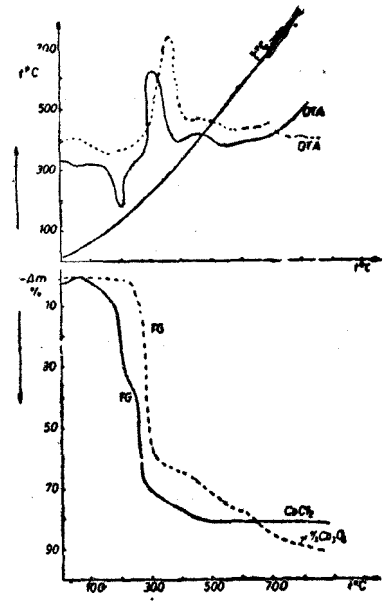

Fig. 2. *TG* and *DTA* curves of
— $[Co(pyridine)_4Cl_2]ClO_4$
---- $[Co(DH)_2(aniline)_2]ClO_4$

This phenomenon excludes the formation of perchlorato-complexes with $Co-ClO_4$-bonding [10].

The thermal stability of the perchlorates was studied by means of derivatographic measurements. Some TG and DTA curves are presented in Fig. 1. and 2.

As shown, the cobalt(III)-amine perchlorates studied are anhydrous salts. The thermograms don't present weight loss up to 120—240°C in function of the composition of the cation. At higher temperatures (150—290°C) the total decomposition of the complexes can be observed. This complicated process with endo- and strong exothermic peaks on the DTA curves takes place in some simultaneous and successive processes (e.g. partial deamination, dehydration, decomposition, oxidation with ClO_4^- and air etc.) with eliberation of amine, water, free halogen, NO, N_2, CO, CO_2, etc. in nonstoechiometric ratios.

These processes occur suddenly, generally, with explosion. One cannot observe inflexion points or horizontal parts on the *TG* curves corresponding to a stoechiometric partial deamination process. e.g.

$[Co(DH)_2(amine)_2]ClO_4 = [Co(DH)_2(Amine)(ClO_4)] +$ amine as in the case of Cl^-, Br^-, I^-, NCS^-, $NCSe^-$ salts of this class [11—14].

From gravimetric analytical point of view is important the thermal stability of the slightly soluble perchlorates up to 130—200°C, which make possible the drying of the filtered and washed precipitates at 105—120°C. The thermal stability of the $[Co(pyridine)_4Cl_2]ClO_4$ is lower, and for this reason the above mentioned perchlorate can be dried only by room temperature.

Because of the explosive character of the thermal decomposition the residue by 800—900°C is much less than the stoechiometric amount of Co_3O_4 calculated.

Gravimetric determination of perchlorate with cobalt(III)-amines. The neutral or acidic perchlorate samples were treated with an excess of cobalt(III)-amine salts (in aqueous or dil. alcoholic solutions). The precipitates formed were filtered off, washed and dried. From the diacido-tetramine-Co(III)-complexes trans-$[Co(en)_2Cl_2]Cl$, trans-$[Co(en)_2Br_2]Br$, $[Co(en)_2(C_2O_4)]Cl$, and $[Co(DH)_2(amine)_2]Cl$ (amine = NH_3, pyridine, aniline) were used for this purpose. The gravimetrical factor's values vary between 0.1730 (for $[Co(DH)_2(aniline)_2]ClO_4$) and 0,28456 (for $[Co(en)_2Cl_2]ClO_4$). The experimental results also were statistically estimated. (See Table 3).

Table 3

Analytical and statistical data on the gravimetric determination of perchlorate with cobalt(III)-amine salts

Experimental conditions		Precipitating agents for ClO_4^-				
		I	II	III	IV	V
Conc. of ClO_4^- (*mg*/50 *ml* sol.)		50—150	50—150	50—150	50—150	50—150
Working temperature °C		20—25	20—25	20—25	20—25	20—25
Washing solution 3×5—10 *ml*		40% alcohol	40% alcoho	40% alcohol	water	water
Drying temperature °C		120—140	105—1101	120—130	25—40	120
Gravimetric factor		0.28456	0.22685	0.2713	0.1823	0.1730
Digression		±0.20%	—0.50— —2.0%	—1.0— —2.0%	—0.50— —1.0%	—3.0— —5.0%
Statistical data	Ag	0.10046	0.10046	0.10046	0.10046	0.10046
	n	10	10	10	10	10
	$\overline{X}$	0.10043	0.09924	0.09892	0.09969	0.09615
	s	$9.67\cdot10^{-5}$	$5.78\cdot10^{-4}$	$3.37\cdot10^{-4}$	$1.82\cdot10^{-4}$	$7.55\cdot10^{-4}$
	$s_{\overline{X}}$	$3.05\cdot10^{-5}$	$1.82\cdot10^{-4}$	$1.15\cdot10^{-4}$	$5.77\cdot10^{-5}$	$2.39\cdot10^{-4}$
	$\overline{X}_{P(99\%)}$	0.10043± 0.00010	0.09924± 0.00059	0.09892± 0.00037	0.09969± 0.00019	0.09615± 0.00078
	$t_{calc.}$	0.98	6.70	13.45	13.34	18.03
	$t_{tabl.}$	3.25	3.25	3.25	3.25	3.25
	$A = \overline{X} \pm t\cdot s_{\overline{X}}$	0.10033< <0.10046< <0.10053	$A > \overline{X} \pm t\cdot s_{\overline{X}}$	$A > \overline{X} \pm t\cdot s_{\overline{X}}$	$A > \overline{X} \pm t\cdot s_{\overline{X}}$	$A > \overline{X} \pm t\cdot s_{\overline{X}}$

I.: trans-$[Co(en)_2Cl_2]Cl$; II.: trans-$[Co(en)_2Br_2]Br$; III.: $[Co(en)_2(C_2O_4)]Cl$; IV.: $[Co(Py)_4Cl_2]Cl$; V.: $[Co(DH)_2(aniline)_2]Cl$
A = true value; n = number of measurements; $\overline{X}$ = average; s=standard deviation; t = Student distribution; $s_{\overline{X}}$ = standard dev. of mean; P = confidence limits

The best results were obtained by using trans-$[Co(en)_2Cl_2]Cl$ as precipitating agent in dil. alcoholic solution.

The dimethylglyoximine derivatives are much less suitable for this analytical determination because of the considerable solubility of the corresponding perchlorates, especially in dil. alcoholic media.

The solubility decreases in the order:

$$[Co(DH)_2(amine)_2]ClO_4 : amine : NH_3 > pyridine > aniline.$$

The solubility of the $[Co(en)_2Cl_2(ClO_4$ was determined gravimetrically after evaporation of an aliquot part of the saturated solution. The solubility of trans-$[Co(en)_2Cl_2]ClO_4$ at 20°C in water: $5.62 \cdot 10^{-3}$ *mole/l*, in 40% ethanol: $2.82 \cdot 10^{-3}$ *mole/l*, at 0°C in 40% ethanol was $9.84 \cdot 10^{-4}$ *mole/l*. The solubility of the other perchlorates used for the about mentioned purpose is greather, especially in diluted alcohol. As seen from Table 3, the gravimetric results with these cobalt(III)-amines, are smaller, also by using an excess of precipitating reagents.

From the oxoanions ReO_4^- and IO_4^- interfere the analytical procedure. The interference of 5—10 fold amount of ClO_3^-, BrO_3^-, IO_3^-, NO_2^-, NO_3^-, BO_3^-, MoO_4^-, WO_4^- is negligible.

Experimental. trans-$[Co(en)_2Br_2]Br$ and $[Co(en)_2(C_2O_4)]Cl$ were obtained from trans-$[Co(en)_2Cl_2]Cl$ by means of substitution reactions with HBr and $H_2C_2O_4$, respectively [15]. $[Co(Diox.H)_2(amine)_2]Cl$ (Diox.H_2 = dimethyglyoxime or heptoxime) were formed by air oxidation of the components in water or in dil. alcohol [12, 13].

$[Co(amine)_4X_2]ClO_4$ and $[Co(Diox.H)_2(amine)_2]ClO_4$

10 *mmoles* of the corresponding diacido-tetraamine-Co(III)-salt in 80—100 *ml* water (or in 40% alcohol, respectively) were treated with an exces of 2% $HClO_4$. The crystalline products formed were filtered off, washed with water and dried on air.

Analytical procedure. 25—150 *mg* ClO_4^- in 50 *ml* aqueous solution were treated with an excess of 1—2% cobalt (III)-amine salt in aqueous, or dil. alcoholic solution at room temperature up to the appearance of the dark colour of the reagent taken in excess. After a standing of 30—60 minutes, the precipitates formed were filtered off on a glass crucible (G_4), washed with water (dil, alcohol) and dried at 105—140°C.

The *i.r.* spectra were recorded in kalium bromide pollets with a UR 20 spectrophotometer (Carl Zeiss Jena).

The thermal measurements were carried out with a Derivatograph (MOM-Budapest). Sample weight 100 *mg*, heating rate 10°/*min*.

REFERENCES

1. O. Loeblich, O. Leimbach, Angew. Chem., **39,** 432 (1926).
2. V. K. Akimov, A. J. Busev, Zhur. analit. Khim., **26,** 956 (1971).
3. H. H. Willard, L. R. Perkins, Anal. Chem., **25,** 1634 (1953).
4. M. Siroki, V. Cesar, Croat. Chim. Acta, **49,** 408 (1977).
5. A. G. Fogg, C. Burghess, Talanta, **18,** 1175 (1971).
6. A. Bollinger, Z. analyt. Chem., **94,** 403 (1933).
7. A. G. Fogg, C. Burghess, D. T. Burns, Analyst (London), **96,** 854 (1971).
8. Masahiro Tsubouchi, Anal. chim. Acta, **54,** 143 (1971).
9. N. N. Gusakova, Zavod. lab., **46,** 22 (1980).
10. L. Johansson, Coord. Chem. Revs., **12,** 24 (1974).
11. R. Ripan, Cs. Várhelyi, E. Kékedy, Stud. Univ. Babeș-Bolyai, Chem., **10,** (1), 19 (1965).
12. R. Ripan, Cs. Várhelyi, J. Ürmösi, Studii și Cercetări Chim., Acad. RSR., Fil. Cluj, **14,** (2), 215 (1963).
13. J. Zsakó, Cs. Várhelyi, E. Kékedy, J. inorg. nuclear Chem., **28,** 2637 (1966).
14. J. Zsakó, J. Horák, Cs. Várhelyi, A. Benkö, Monatsh. Chem., **112,** 945 (1981).
15. A. Werner, Liebigs Ann. Chem., **386,** 1 (1912).

STUDIA UNIV. BABEŞ-BOLYAI, CHEMIA, XXXVI, 1—2, 1991

NEW TETRAACIDO-MERCURY(II)-DERIVATIVES AND THE GRAVIMETRIC DETERMINATION OF MERCURY WITH COBALT(III)-AMINES

FERENC MAKKAY*, CSABA VÁRHELYI* and EDIT KIS*

Received: 31.05.1991

ABSTRACT. A number of 40 new slightly soluble salts of $[HgI_4]^{2-}$ and $[Hg(SCN)_4]^{2-}$ with cobalt (III)-amine bases (hexamines, monoacido-pentamines and diacido-tetramines) were obtained and characterized. Some of the diacido--tetramine cobalt (III)-derivatives of these types were proved for the gravimetric determination of mercury.

Introduction. The tetraacido-mercuriates: $[HgX_4]^{2-}$ (X = Br, I, CN^-, NCS^-, NCS^- easily are formed in aqueous solutions of some mercury(II) salts ($HgCl_2$, $HgSO_4$, $Hg(NO_3)_2$, $Hg(ClO_4)_2$) in the presence of an excess of MX (M = Na, K, NH_4) [1].

In some cases the formation, to a certain extent, of $[HgX_3]^-$ was also demonstrated by means of physico-chemical measurements [2—4], (e.g. Raman spectra) and by preparative studies (e.g. isolation of $[Ni(NH_3)_n](HgI_3)_2$ (n = 4, 6) and of $[Co(NH_3)_5Cl](HgI_3)_2$ [5, 6].

In an excess of X^- the predominant form of the acido-complex in the system studied ($Hg^{2+} + nX^- \rightleftharpoons HgX^+$, HgX_2, HgX_3^-, HgX_4^{2-}) is $[HgX_4]^{2-}$.

Some metal(II, III) amine salts of the $[HgX_4]^{2-}$ anions were also isolated and proposed for analytical purposes.
(e.g. $[Cu(en)_2][HgI_4]$, ($[Cu(pn)_2][HgI_4]$, $[Cu(biguanide)_2][HgI_4]$ [7—11].

From the thiocyanato-derivatives $Zn[Hg(SCN)_4]$ [12, 13] and $Co[Hg(SCN)_4]$ [14] are suitable for gravimetric analysis.

In aqueous media sligthly soluble ammonium-, phosphonium-, and arsonium salts of $[HgI_4]^{2-}$ and $[Hg(SCN)_4]^{2-}$ also are formed easily. Some of these derivatives and especially the analogous combinations with organic dyes (soluble in organic apolar solvents) can be used for the spectrophotometric determination of mercury [15—23].

Results sand discussions. We have carried out a systematic preparative study on the formation of $[HgI_4]^{2-}$ and $[Hg(SCN)_4]^{2-}$ salts with cobalt(III)-amines of various types.

According to our observations, the majority of cobalt(III)-amine bases, without hydrophylic ligands (H_2O, NO_2, SO_3, OH, etc) in the inner coordination sphere, form easily sparingly soluble salts with the majority of hexamine-, monoacido-pentamine- and diacido-tetramine type cobalt(III)-amines in neutral and slightly acidic aqueous solutions.

A number of 40 new complex salts of the $[HgI_4]^{2-}$ and $[Hg(SCN)_4]^{2-}$-ions are characterized in Tables 1—3.

* *University Babeş—Bolyai, Dept. of Chemical Technology, 3400 Cluj-Napoca, Romania*

Table 1

1 Hexamine- and Monoacido-pentamine-cobalt (III) salts of $[HgI_4]^{2-}$ and $[Hg(SCN)_4]^{2-}$

Formula	Mol. wt. calcd.	Appearance		Analysis (%) Calcd.	Found
$[Co(NH_3)_6]_2 \cdot B_3$	1621.1	yellow microcryst.	Co	7.27	6.97
			Hg	37.12	36.95
$[Co(en)_3]_2 \cdot B_3$	1776.7	orange prisms (on stirring)	Co	6.63	6.92
			Hg	33.87	34.22
$[Co(en)_3]_2 \cdot A_3$	2602.7	yellow microcryst.	Co	4.52	4.33
			Hg	23.12	23.02
$[Co(NH_3)_5(NCS)] \cdot A$	910.4	orange prisms	Co	6.47	6.30
			Hg	22.03	21.61

A – $[HgI_4]^{2-}$; B – $[Hg(SCN)_4]^{2-}$; Yield: 85–90%

Table 2

cis-$[Co(en)_2X(amine)]^{2+}$ – salts of $[HgI_4]^{2-}$ and $[Hg(SCN)_4]^{2-}$

Formula	Mol. wt. calcd.	Appearance		Analysis (%) Calcd.	Found
$[Co(en)_2Cl(imidazole)] \cdot A$	990.7	light red dendrites	Co	5.95	6.10
			Hg	20.25	20.80
$[Co(en)_2Cl(imidazole)] \cdot B$	715.4	reddish-orange prisms	Co	8.23	8.57
			Hg	28.04	27.28
$[Co(en)_2Cl(pyridine)] \cdot A$	1001.7	brown needles	Co	5.88	6.00
			Hg	20.02	20.05
$[Co(en)_2Cl(pyridine)] \cdot B$	726.4	reddish irregular cryst.	Co	8.11	8.70
			Hg	27.61	27.36
$[Co(en)_2Cl(\beta\text{-picoline})] \cdot B$	740.5	reddish microcryst.	Co	7.96	7.41
			Hg	27.09	26.65
$[Co(en)_2Cl(\gamma\text{-picoline})] \cdot B$	740.5	reddish microcryst.	Co	7.96	7.80
			Hg	27.09	26.30
$[Co(en)_2Cl(aniline)] \cdot B$	740.5	reddish-violet microcryst.	Co	7.96	8.65
			Hg	27.09	27.56
$[Co(en)_2Cl(m\text{-toluidine})] \cdot B$	754.5	reddish-brown microcryst.	Co	7.81	8.30
			Hg	26.59	26.09
$[Co(en)_2Cl(m\text{-toluidine})] \cdot A$	1029.8	thin, brown plates	Co	5.72	6.08
			Hg	19.48	18.90
$[Co(en)_2Cl(benzylamine)] \cdot B$	754.5	red-violet microcryst.	Co	7.81	7.46
			Hg	26.59	26.10
$[Co(en)_2Cl(benzylamine)] \cdot A$	1029.8	reddish-violet irregular cryst.	Co	5.72	6.01
			Hg	19.48	19.02
$[Co(en)_2Cl(o\text{-anisidine})] \cdot B$	770.5	red-brown microcryst.	Co	7.67	7.88
			Hg	26.03	25.75
$[Co(en)_2Cl(o\text{-anisidine})] \cdot A$	1045.8	red-brown irregular cryst.	Co	5.63	5.32
			Hg	19.18	18.76
$[Co(en)_2Cl(m\text{-xylidine})] \cdot B$	768.5	red-brown irregular cryst.	Co	7.65	7.36
			Hg	26.10	25.85
$[Co(en)_2Cl(m\text{-xylidine})] \cdot A$	1043.8	red-brown irregular cryst.	Co	5.65	5.83
			Hg	19.22	19.86
$[Co(en)_2Br(\gamma\text{-picoline})] \cdot B$	784.9	reddish-brown microcryst.	Co	7.51	7.98
			Hg	25.56	24.95
$[Co(en)_2Br(\gamma\text{-picoline})] \cdot A$	1060.2	brown dendrites	Co	5.55	5.73
			Hg	19.94	20.14

Yield: 85–95%

Table 3

Diacido-tetramine-cobalt (III) — salts of $[HgI_4]^{2-}$ and $[Hg(SCN)_4]^{2-}$

Formula	Mol. wt. calcd.	Appearance		Analysis (%) Calcd.	Found
trans-$[Co(en)_2Cl_2]_2 \cdot A$	1208.34	dark green dendrites	Co	9.75	9.30
			Hg	16.60	16.35
$[Co(en)_3(C_2O_4)]_2 \cdot A$	1242.2	light red irregular cryst.	Co	9.48	8.97
			Hg	16.14	15.89
trans-$[Co(en)_2Br_2]_2 \cdot A$	1386.2	green-yellow short prisms	Co	8.50	8.31
			Hg	14.47	14.08
trans-$[Co(en)_2Br_2]_2 \cdot B$	1110.6	light green needles	Co	10.61	10.46
			Hg	18.06	17.77
trans-$[Co(pn)_2Cl_2]_2 \cdot A$	1264.4	green dendrites	Co	9.32	8.91
			Hg	15.86	15.31
trans-$[Co(pn)_2Cl_2]_2 \cdot B$	989.1	light green needles	Co	11.91	12.28
			Hg	20.28	20.73
$[Co(pyridine)_4Cl_2]_2 \cdot A$	1600.9	olive green microcryst.	Co	7.36	7.90
			Hg	12.53	13.10
$[Co(ec)(aniline)_2]_2 \cdot A$	1643	light brown dendrites	Co	7.17	6.74
			Hg	12.21	12.33
$[Co(ec)(p\text{-toluidine})_2]_2 \cdot A$	1699.1	yellow-brown plates	Co	6.94	6.66
			Hg	11.81	11.58
$[Co(ec)(\alpha\text{-naphtylamine})_2]_2 \cdot A$	1843.4	brown microcryst.	Co	6.39	6.15
			Hg	10.88	11.13
$[Co(ec)(\alpha\text{-naphtylamine})_2]_2 \cdot B$	1568.1	light brown prisms	Co	7.51	8.10
			Hg	12.79	12.05
$[Co(DH)_2(thiourea)_2]_2 \cdot A$	1591	dark brown microcryst.	Co	7.41	7.20
			Hg	12.61	13.13
$[Co(DH)_2(thiourea)_2]_2 \cdot B$	1315.7	sparkling yellow-brown plates	Co	8.95	8.47
			Hg	15.24	15.98
$[Co(DH)_2(m\text{-toluidine})_2]_2 \cdot A$	1715.3	yellow-brown dendrites	Co	6.87	6.38
			Hg	11.76	12.50
$[Co(DH)_2(o\text{-toluidine})_2]_2 \cdot A$	1715.3	brown needles	Co	6.87	7.10
$[Co(DH)_2(p\text{-toluidine})_2]_2 \cdot A$	1715.22	brown prisms	Co	6.87	6.99
$[Co(DH)_2(p\text{-toluidine})_2]_2 \cdot B$	1439.92	brown irregular cryst.	Co	8.18	8.45
			Hg	13.93	13.78
$[Co(DH)_2(aniline)_2]_2 \cdot A$	1659	light brown irreg. cryst.	Co	7.10	6.94
			Hg	12.09	11.86
$[Co(DH)_2(pyridine)_2]_2 \cdot A$	1603.0	light brown microcryst.	Co	7.35	7.15
			Hg	12.51	12.20

Yield: 80—98%; *ec* — $C_{12}H_{16}N_2O_4$; DH — $C_4H_7N_2O_2$

In the infrared spectra of some $[Hg(SCN)_4]^{2-}$ derivatives, e.g. $[Co(en)_2Cl_2]_2 \cdot [Hg(SCN)_4]$, $[Co(DH)_2(aniline)_2]_2[Hg(SCN)_4]$, $[Co(en)_2Cl(m\text{-toluidine})] \cdot [Hg(SCN)_4]$, the characteristic NCS^- frequencies: $\nu_{C=N}$, ν_{C-N} and the deformation (bending) δ_{NCS} appear at 2110—2100 (v.s.), 630—650 (s) and 410—420 (m—s) cm^{-1}. This phenomenon pleads for a Hg—SCN bonding through the sulphur atom in all the mentioned cases (thiocyanato-complexes) [24].

The thermal behaviour of some diacido-tetramine-cobalt(III)-salts of $[Hg(SCN)_4]^{2-}$ and $[HgI_4]^{2-}$ was studied by derivatography.

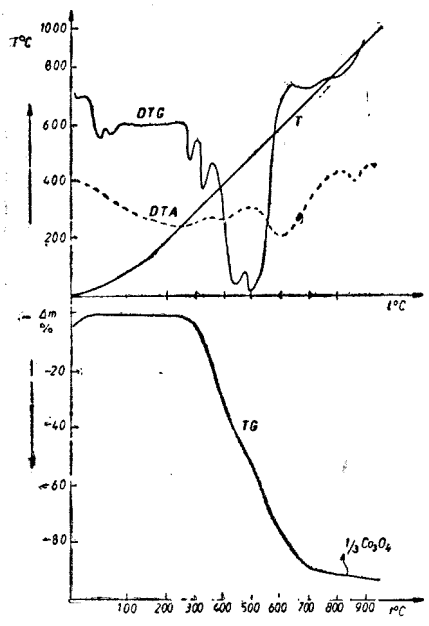

Fig. 1. Derivatogram of trans-$[Co(en)_2Cl_2]_2[HgI_4]$

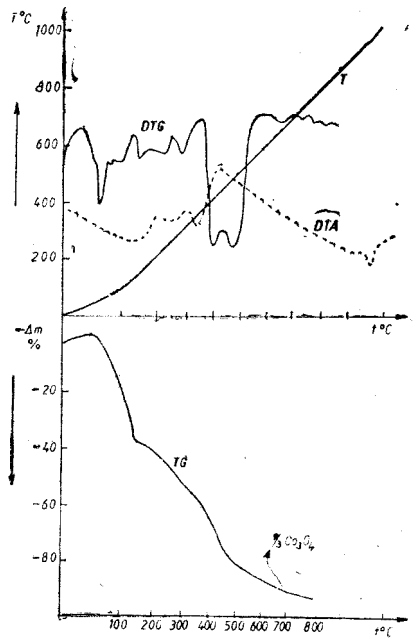

Fig. 2. Derivatogram of trans-$[Co(en)_2Cl_2]_2[Hg(SCN)_4]$

The derivatograms of the $[Co(en)_2Cl_2]_2[HgI_4]$ and $[Co(en)_2Cl_2]_2[Hg(SCN)_4]$ are presented in Figs. 1 and 2.

As shown, the tetraiodo-derivative presents a higher decomposition temperature as compared with the thiocyanato-complex. The weight loss begins at about 250 °C. The massive disintegration takes place between 260 and 650 °C without weight loss stop (failure of inflexion points or horizontal parts on the TG curve). The complicated succesive and parallel decomposition processes are demonstrated by the exo- and endothermal peaks on the DTA curve (exo: 280—330, 420—480, 780—810 °C and endo: 240—260, 380—410, 850 °C), and on the DTG curve at 280, 320, 430, 490 °C, respectively. In the case of the $[Hg(SCN)_4]^{2-}$-derivative, the thermal decomposition begins already at 80—100 °C. An inflexion point on the TG curve at 130—150 °C shows a non-stoechiometrical decomposition product. The main decomposition stages are demonstrated by the DTA peaks: endo: 120—140, 200—220, 330 °C; exo: 190, 280 and 400 °C and by the DTG ones: 80, 140, 220, 280, 380 and 460 °C, respectively. The residue at 800—900 °C is less, than the calculated Co_3O_4%, accordingly to the very fast decomposition and volatilization processes.

The thermal behaviour of the other $[HgI_4]^{2-}$ and $[Hg(SCN)_4]^{2-}$-salts with identical cations is analogous. The complicated decomposition processes are determined both by the nature of the complex cation and anion. The decompo-

sition begins at 160—240 °C in the case of the tetraiodo-derivatives and at 80—130 °C by the $[Hg(SCN)_4]^{2-}$-salts.

The thermal and chemical analyses show that all the obtained cobalt(III)-amine salts (Table 1—3) are anhydrous compounds.

Gravimetric determination of mercury with diacido-tetramine cobalt(III)-type complex salts

The cobalt(III)-amine derivatives characterized in this paper present, generally, a considerable thermal stability and a very low solubility in aqueous solutions in a wide *pH* range (*p*H 1—6) (approx. 10^{-4}—10^{-5} *mole/l*). Their chemical composition is constant. The salts appear in a well defined crystalline form, the precipitates are easily filtrable. The gravimetrical factors vary between 0.10—0.18 in the case of the diacido-tetramine salts and between 0.19—0.26 by the monoacido-pentamine ones.

The Hg^{2}-ion can be transformed easily in stable tetraacido-complexes and can be separated in this manner from the majority of the accompanying di- and tervalent metals.

The $[HgI_4]^{2-}$ is suitable for the determination of Hg in the presence of alcaline earth-, lanthanide and di- and tervalent transition metals ($3d^1$—$3d^{10}$). The determination of mercury as $[Hg(SCN)_4]^{2-}$ is interfered by the presence of Zn, Cd, Co and Cu ions, which form also slightly soluble $M[Hg(SCN)_4]$ salts. Therefore the tetraiodo-mercurates are more suitable for the above mentioned purpose having a higher thermal stability and selectivity.

To the Hg^{2+}-sample solutions, an excess of 1—2% KI or KCNS, in neutral or weak acidic aqueous solutions were added. The $[HgI_4]^{2-}$ or $[Hg(SCN)_4]^{2-}$ complexes were treated with an excess of cobalt(III)-amine salts. The crystalline products formed were filtered off, washed with water or dil. HCl and dried at the corresponding temperature. The analytical and statistical data are presented in Table 4.

Experimental. As starting compound for the synthesis of complexes with ethylenediamine, the trans-$[Co(en)_2Cl_2]Cl$ was used. The other derivatives were obtained by a series of substituiton reactions with HBr, $H_2C_2O_4$ and with organic amines, respectively [25]. The diacido-tetramine type complexes: $[Co(DH)_2(amine)_2]Cl$ and $[Co(ec)(amine)_2]Cl$ [26] form easily by air oxidation of the components ($CoCl_2$. DH_2 = dimethylglyoxime or ec. H_2 = a tetradentate Schiff's base: ethylenediimino-bis-acetylacetone) and organic amines ($pK_b = 8-12$) in aqueous or dil. alcoholic solutions.

Synthesis of cobalt(III)-amine salts of the $[HgI_4]^{2-}$ and $[Hg(SCN)_4]^{2-}$

10 *mmoles* of various cobalt (III)-amine complexes were dissolved in 80—100 *ml* water or dil. alcohol (20—40%), respectively, and treated with an excess of 1% $K_2[HgI_4]$ or $K_2[Hg(SCN)_4]$ in aqueous solution. After a standing of 30—40 minutes at room temperature, the crystalline precipitates formed were filtered off, washed with water and dried on air.

Analysis of the complex salts. The cobalt and mercury contents of the salts were determined complexometrically after destroying the samples (80—150 *mg*) with boiling conc. H_2SO_4 in the presence of some crystals of KNO_3. The solutions were diluted with water up to 250 *ml*. 100 *ml* of the sample solution was neutralized with urotropine up to $pH = 6$, and titrated with EDTA 0.01 *mole* in the presence of xylenolorange as indicator (sum of Hg + Co). In an other 100 *ml* sample the cobalt was determined complexometrically after neutralization with sodium acetate, in the presence of murexide as indicator and 2—3 *ml* ammonia solution. The mercury ions were sequestred with an excess of KI [27].

The derivatograms were recorded with a Derivatograph (MOM, Budapest, Hungary). Sample weight: 100±1 *mg*, heating rate: 10 °C/*min*.

Table 4

Analytical and statistical data on the gravimetric determination of mercury (as $[HgI_4]^{2-}$ or $[Hg(SCN)_4]^{2-}$ with cobalt (III)-amines

Experimental conditions		Determination form				
		I.	II.	III.	IV.	V.
Conc. of Hg^{2+} *mg*/50 *ml*		20—100	20—100	20—100	20—100	20—100
Precipitation conditions, *t*°C, time hr		20—25 2—3	20—25 2—3	20—25 2—3	20—25 2—3	20—25 2—3
Washing solution ($t = 0$ °C)		water	HCl 0.5%	HCl 0.5%	HCl 0.5%	HCl 0.5%
Drying conditions *t*°C, time hr		120—150 2—2.5	90 2—2.5	120 2—2.5	120 2—2.5	75—80 1—1.5
Gravimetrical factor		0.16602	0.14472	0.12514	0.11696	0.13933
Statistical data	*n*	8	8	8	8	8
	Ag	0.02002	0.02002	0.02002	0.02002	0.02002
	Digression	±0.4%	±0.6%	±0.6	±0.2%	±0.2%
	$\overline{X}$	0.02000	0.01998	0.01997	0.02000	0.02001
	s	$4.87 \cdot 10^{-5}$	$6.76 \cdot 10^{-4}$	$9.38 \cdot 10^{-5}$	$2.67 \cdot 10^{-5}$	$2.64 \cdot 10^{-5}$
	$s_{\overline{X}}$	$1.72 \cdot 10^{-5}$	$2.39 \cdot 10^{-4}$	$3.32 \cdot 10^{-5}$	$9.45 \cdot 10^{-6}$	$1.09 \cdot 10^{-5}$
	$\overline{X}_{P(99\%)}$	0.02000± 0,00006	0.01998± 0.00084	0.01997± 0.00012	0.02000± 0.00003	0.02001± 0.00004
	$t_{calc.}$	1,16	0.167	1.51	2.12	0.917
	$A \gtrless X \pm t \cdot s_{\overline{X}}$	0.01994< <0.02002< <0.02006	0.01914< <0.02002< <0.02086	0.01985< <0.02002< <0.02009	0.01997< <0.02002< <0.02003	0.01997< <0.02002< <0.02005
	Ag	0.10010	0.10010	0.10010	0.10010	0.10010
	Digression	±0.1%	±0.3%	±0.2%	±0.1%	±0.1%
	$\overline{X}$	0.10011	0.10003	0.10008	0.10009	0.10014
	s	$7.39 \cdot 10^{-5}$	$2.03 \cdot 10^{-4}$	$1.56 \cdot 10^{-4}$	$7.28 \cdot 10^{-5}$	$4.75 \cdot 10^{-5}$
	$s_{\overline{X}}$	$2.61 \cdot 10^{-5}$	$7.17 \cdot 10^{-5}$	$5.53 \cdot 10^{-5}$	$2.57 \cdot 10^{-5}$	$1.68 \cdot 10^{-5}$
	$\overline{X}_{P(99\%)}$	0.10011± 0.00009	0.10003± 0.00025	0.10008± 0.00019	0.10009± 0.00009	0.10014± 0.00006
	t_{calc}	0.383	0.976	0.362	0.389	2.38
	$t_{tabl.}$	3.50	3.50	3.50	3.50	3.50
	$A \gtrless X \pm t \cdot s_{\overline{X}}$	0.10002< <0.10010< <0.10020	0.09978< <0.10010< <0.10028	0.09989< <0.10010< <0.10027	0.10000< <0.10010< <0.10019	0.10008< <0.10010< <0.10020
Observation		—	—	fine precipitate, dif. to filt.		

I. trans-$[Co(en)_2Cl_2]_2[HgI_4]$; II. trans-$[Co(en)_2Br_2]_2[HgI_4]$; III. $[Co(DH)_2(pyridine)_2]_2[HgI_4]$; IV. $[Co(DH)_2(p\text{-toluidine})_2]_2 \cdot [HgI_4]$; V. $[Co(DH)_2(p\text{-toluidine})_2]_2[Hg(SCN)_4]$; A = true value; *n* = number of measurements; X = average; *s* = standard deviation; t = Student distribution; $s_{\overline{X}}$ = standard dev. of mean; P = confidence limits

The solubility of some mercury salts used for gravimetric analysis was determined gravimetrically after evaporation of an aliquot part of the saturated aqueous solution (50 *ml*) and dried at 100 °C. The solubility of some tetraiodo-mercuriates at 20 °C:

trans-$[Co(en)_2Cl_2]_2[HgI_4]$: $1.6 \cdot 10^{-4}$ *mole/l*;

$[Co(DH)_2(p\text{-toluidine})_2]_2[HgI_4]$: $2.4 \cdot 10^{-5}$ *mole/l*;

$[Co(DH)_2(p\text{-toluidine})_2]_2[Hg(SCN)_4]$: $1.9 \cdot 10^{-5}$ *mole/l*.

The infrared spectra were recorded in kalium bromide pellets with a UR 20-Spectrophotometer (Carl Zeiss Jena).

Analytical procedure for gravimetric determination of mercury.

20—100 *mg* Hg^{2+} (in form of $HgCl_2$, $HgSO_4$, $Hg(ClO_4)_2$ or $Hg(NO_3)_2$) in 50 *ml* aqueous solution were treated with an excess of KI or KSCN until the precipitated HgI_2 or $Hg(SCN)_2$ were dissolved again. Then 2% cobalt (III)-amine complexes(trans-$[Co(en)_2Cl_2]Cl$, $[Co(en)_2Br_2]Br$, $[Co(DH)_2$ k (p-toluidine)$_2]Cl$, $[Co(DH)_2(pyridine)_2]Cl$) were added in excess up to the appearance of the dark colour of the reagent (green . . ., brown) over the separated solid mass. After standing 30—45 minutes at 0 °C, the crystalline product is filtered off, washed with water or dil. HCl and dried at the corresponding temperature (Table 4).

As seen from Table 4, the most favorable forms for gravimetric purposes are the I, IV an·' V complexes (on the basis of solubility, statistical data and physical properties of the precipitates)d

REFERENCES

1. I. M. Kolthoff, P. J. Elving: *Treatise on Analytical Chemistry* Part II, Vol. **3**, p. 273 Interscience Publishers, New-York—London (1961).
2. F. Delwaulle, D. Wiemann, Compt. rend., **207**, 340 (1938).
3. A. Mondain-Montal, A. Paris, Compt. rend., **198**, 1154 (1934).
4. A. Rolfe, C. Sheppard, B. Woodward, Trans. Faraday Soc., **50**, 1275 (1954).
5. S. M. Jörgensen, J. prakt. Chem., /2/, **2**, 347 (1870).
6. F. Ephraim, A. Mosimann, Ber. dtsch. chem. Ges., **54**, 396 (1921).
7. C. Duval, Ng. D. Xuong, Anal. Chim. Acta, **5**, 494 (1981).
8. G. Spacu, G. Suciu, Z. analyt. Chem., **78**, 244 (1929).
9. G. Spacu, P. Spacu, Z. analyt. Chem., **89**, 187 (1932).
10. R. B. Sandin, E. T. Margolis, Ind. Eng. Chem. Anal. Ed., **7**, 293 (1935).
11. H. F. Walton, H. A. Smith, Anal. Chem., **28**, 406 (1956).
12. R. Cohn, Ber. dtsch. chem. Ges., **34**, 3502 (1901).
13. P. Wenger, C. Zimmermann, Helv. Chim. Acta, **14**, 718 (1931).
14. L. Lamure, Bull. Soc. chim. France, **1946**, 661.
15. H. B. Desai, R. K. Iyer, S. R. Kayasth., Radiochem. Radioanal. Lett., **41**, 299 (1979).
16. T. Braun, M. N. Abbas, Anal. Chim. Acta, **134**, 321 (1982).
17. P. Indrasenan, C. G. Nair, Ramachandran, Curr. Sci., **43**, 683 (1974).
18. W. S. Selig, Mikrochem. J., **35**, 321 (1987).
19. M. Malat, Z. analyt. Chem., **297**, 417 (1979).
20. A. T. Pilipenko, P. P. Kish, G. M. Vitenko, Ukr. Khim. Zhur., **40**, 850 (1974).
21. Sawaya Tsugo, Ishii Hajime, Odashima Tsugikatsu, Japan Analyst, **22**, 318 (1973).
22. T. V. Ramakrishna, G. Aravasnudan, M. Vijayakumar, Anal. Chim. Acta, **84**, 369 (1976).
23. K. De Anil, K. Pal Bata, Mikrochim. Acta II, **1979**, 201.
24. A. Sabatini, J. Bertini, Inorg. Chem., **4**, 959, 1665 (1965); **5**, 1025 (1966).
25. H. Meisenheimer, E. Kiderlen, Liebigs Ann. Chem., **438**, 217 (1924).
26. R. Ripan, Cs. Várhelyi, An. Nyesö, Z. anorg. Chem., **341**, 103 (1965).
27. J. Sajó: *Komplexometria*, Müszaki Könyvkiadó, Budapest, 3rd. Ed., p. 185 (1973).

STUDIA UNIV. BABEŞ-BOLYAI, CHEMIA, XXXVI, 1—2, 1991

COMPLEXOMETRIC TITRATIONS WITH TUNGSTEN ELECTRODE

E. HOPÎRTEAN and F. KORMOS*

ABSTRACT. The behaviour of the tungsten electrode as an indicator in the complexometric determination of some ions which form complexonates of high stability is presented. The potentiometric measurement of these ions is possible due to the fact that the metallic ions on the surface of the electrode are reduced at a lower valence state. There occurs a redox system whose potential is closely followed by the tungsten electrode. The validity of the results obtained in the potentiometric titrations has been checked out by spectrophotometric determinations.

Introduction. Either an adequate ion selective-electrode or a redox-electrode (in case that the redox system can be induced in the reaction medium) has been used as an indicator electrode in the potentiometric indication of the equivalence point in the field of complexometric titrations. The tungsten electrode is a solid electrochemical sensor, highly resistant even under nonfavourable conditions (high temperature, meltings, suspensions). [1]

The electrode has been widely used in the complexometric determination of Fe^{3+} in meltings, by potentiometric titration. [2].

This paper reports the behaviour of the tungsten electrode as an indicator electrode in the complexometric determination of some other ions like: Bi^{3+}, Cr^{3+}, Cu^{2+}, Fe^{3+}, Pb^{2+}, Ti^{4+}, UO_2^{2+}, VO^{2+}. These ions form complexonates (MZ) of high stability (K_{MZ}: $10^{18}-10^{20}$).

Experimental. The potentiometric titrations have been carried out on different levels of concentration ($10^{-2}-10^{-4}M$) in buffered media at $pH = 4{,}56$, at room temperature and versus the calomel reference electrode (S.C.E.). The stock solutions have been obtained by weighing.

Volumetric determinations, on basis of chemical indication have been performed simultaneously. An indigenous pH-meter (IAMC Otopeni of type pH-100) has been employed in the instrumental indication of the equivalence point.

The spectrophotometric determinations have been done on a Zeiss Jena spectrophotometer, in aqueous solutions of $10^{-2}-10^{-4}M$ concentration obtained from substances of p.a. purity.

Results and discussion. The results of the complexometric titrations are rendered in Table 1.

At the equivalence point it becomes apparent that the potential jumps are considerable in the titration of Cu^{2+}, Fe^{3+}, Mg^{2+}, Ti^{4+}, UO_2^{2+} VO^{2+} but nonsignificant in the titration of Cr^{3+}, Pb^{2+}, Bi^{3+}. Generally, the titrations can go up to the level of 10^{-3} M concentration. At lower concentrations the potential jump takes place at the equivalence point, but it is relatively small. However, in case of dosing VO^{2+}, Ti^{4+}, Mg^{2+}, the instrumental indication may reach the level of 10^{-4} M, as compared to the chemical indication that gives no result (as the potential jumps are above 55 mV at the equivalence point).

* *Institute of chemisty, 3400 Cluj-Napoca, România*

Table 1

Results of the potentiometric titrations

Cation	Conc. level (M)	Potentiometric titration $\Delta E_{\pm 5\%}$ at equiv. mV	Chemical titration Method, indicator	Conclusion
Cu^{2+}	10^{-2}	120	Direct titration murexid	+
	10^{-3}	82		+
	10^{-4}	56		+
Fe^{3+}	10^{-2}	140	Direct titration sulphosalycylic acid	+
	10^{-3}	67		+
	10^{-4}	45		+
Hg^{2+}	10^{-2}	135	Direct titration xylenolorange	+
	10^{-3}	84		+
	10^{-4}	55		−
Ti^{4+}	10^{-2}	140	Back-titration with $Bi(NO_3)_3$ xylenolorange	+
	10^{-3}	78		+
	10^{-4}	52		−
UO_2^{2+}	10^{-2}	98	Back-titration with $Th(NO_3)_4$ xylenolorange	−
	10^{-3}	55		+
	10^{-4}	−		+
VO^{2+}	10^{-2}	170	Back-titration with $MnSO_4$ erio T	+
	10^{-3}	86		+
	10^{-4}	55		−
Bi^{3+}	10^{-2}	40	Direct titration xylenolorange	−
	10^{-3}	25		+
	10^{-4}	−		+
Cr^{3+}	10^{-2}	58	Direct titration sulphosalycylic acid	+
	10^{-3}	30		+
	10^{-4}	−		+
Pb^{2+}	10^{-2}	35	Direct titration xylenolorange	+

The potentiometric measurement of these ions in the presence of tungsten electrode is possible due to the fact that metallic ions on the surface of the electrode are reduced to a lower valence state, according to the following reactions:

$$10Me^{2+} + 2W + 5H_2O \rightleftarrows 10Me^{+} + W_2O_5 + 10H^{+}$$

$$Me^{2+}: Cu^{2+},\ Hg^{2+}$$

$$6Me^{3+} + W + 3H_2O \rightleftarrows 6Me^{2+} + WO_3 + 6H^{+}$$

$$Me^{3+}: Fe^{3+}$$

$$6Me^{4+} + W + 3H_2O \rightleftarrows 6Me^{3+} + WO_3 + 6H^+$$

$$Me^{4+}: Ti^{4+},\ VO^{2+}$$

In terms of thermodynamics these reactions are fully acknowleged, because the standard potentials score corresponding values, according to Table 2.

Table 2

Standard redox potentials (3, 4)

Redox system	Standard potential, V
W_2O_5/W	$-0{,}440$
WO_3/W	$-0{,}010$
Hg^{2+}/Hg_2^{2+}	$+0{,}907$
Fe^{3+}/Fe^{2+}	$+0{,}771$
UO^{2+}/U^{4+}	$+0{,}360$
VO^{2+}/V^{3+}	$+0{,}337$
Cu^{2+}/Cu^{+}	$+0{,}153$
Ti^{4+}/Ti^{3+}	$+0{,}040$

As a result of these processes, there occurs a redox system in the reaction medium, whose potential is closely followed by the tungsten electrode. At the equivalence point, the potential decreases abruptly; this is explained by the complete engagement of this ion in the complexon solution Fig. 1.

These considerations lead us to the conclusion that the dosing of Cr^{3+} Pb^{2+}, Bi^{3+}, cannot be achieved complexometrically, by the potentiometric indication. Although these ions form complexonates of high stability, they cannot be submitted to the indication with tungsten electrode because they are not capable of shifting to lower valence states with corresponding standard potentials.

In order to establish the accuracy of the potentiometric titrations, the equivalence volumes (V_e) have been calculated according to Hahn-Weiler method. These results have been compared to those obtained by chemical indication. The results of this experiment are rendered in Table 3.

The results point out that the equivalence volumes approximate better the theoretic V_e (10 *ml*) obtained by instrumental indication. The validity of the results obtained in the potentiometric titrations has been checked out on some ions (Cu^{2+}, UO_2^{2+}, VO^{2+}) as well as by spectrophotometric determinations.

The diagram (fig. 2) of VO^{2+} dosing in the concentration range of 10^{-2}—$10^{-3}\,M$ is shown.

By examining the standard curve ($E = f(c)$, where E represents the extinction and c the concentration) established at $\lambda = 240$ *nm*, the concentration of $3.10^{-3}\,M$ is found for the unknown sample, 205 *mg/l* respectively, as compared to 200 *mg/l* found potentiometrically in the presence of tungsten electrode.

Finally we can state that the complexometric determination of these ions on tungsten electrode proves a highly effective method, more accurate and more rapid than the chemical indication.

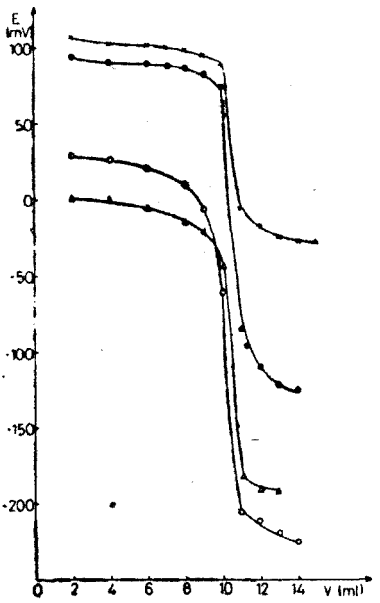

Fig. 1. Complexometric titration curves at 10^{-2}M concentration level: ▲—Ti^{4+}; ○—Cu^{2+}; ●—VO^{2+}; ✳ UO_2^{2+}.

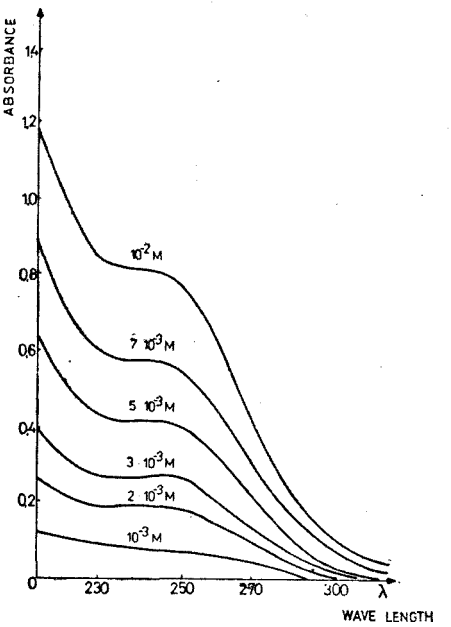

Fig. 2. Spectrophotometric calibration curves for the determination of VO^{2+}.

Table 3

Equivalence volume (V_e)

Cation	Conc. M	$V_{e,p}$ (ml)	σ(ml) ($10-V_{e,p}$)	$V_{e,ch}$ (ml)	σ(ml) ($10-V_{e,ch}$)
Cu^{2+}	10^{-2}	10,10	0,10	10,20	0,20
	10^{-3}	10,25	0,25	10,30	0,30
	10^{-4}	10,20	0,20	10,40	0,40
Fe^{3+}	10^{-2}	9,92	0,08	10,00	0,00
	10^{-3}	10,10	0,10	10,20	0,20
	10^{-4}	10,25	0,25	10,30	0,30
Hg^{2+}	10^{-2}	10,05	0,05	10,20	0,20
	10^{-3}	10,10	0,10	10,30	0,30
	10^{-4}	10,35	0,35	—	—
Ti^{4+}	10^{-2}	10,25	0,15	10,20	0,20
	10^{-3}	10,27	0,27	10,40	0,40
	10^{-4}	10,30	0,30	—	—
UO_2^{2+}	10^{-2}	10,25	0,25	10,40	0,40
	10^{-3}	10,05	0,05	10,40	0,30
	10^{-4}	—	—	—	—
VO^{2+}	10^{-2}	10,08	0,08	10,20	0,20
	10^{-3}	10,05	0,05	10,30	0,30
	10^{-4}	10,20	0,20	—	—

σ — accuracy

$V_{e,p}$ — at potentiometric indication

$V_{e,ch}$ — at chemical indication

REFERENCES

1. E. Hopîrtean, F. Kormos, Revista de chimie, **37**, 321 (1986).
2. K. N. Bagdasarov, V. A. Kimstach, L. G. Dokukina, T. F. Kovalenko, V. B. Ermakova, V. D. Chigiruitsev, Estetv. Nauki, Z., **12**, 18 (1980).
3. D. Dobos, *Electrochemical Data*, Elsevier Scientific Publishing Company Amsterdam — Oxford — New York, 1975.
4. Iu. Iu. Lurie, *Indreptar de chimie analitică*. Ed. tehnică Bucureşti, 1970.

STUDIA UNIV. BABEŞ-BOLYAI, CHEMIA, XXXVI, 1—2, 1991

AROMATIC SOLVENT INDUCED SHIFTS (ASIS) IN ^{1}H-NMR SPECTROSCOPY OF SOME 2,5-SUBSTITUTED 1,3-DIOXANES

SORIN MAGER*, ION GROSU*, MIHAI HORN*

Received: 15.02.1991

ABSTRACT. Some very conclusive examples of clear separation of superposed signals in the ^{1}H-NMR spectra of some monocyclic and spiranic 1,3-dioxanes, using the aromatic solvent induced shifts (ASIS), are presented.

As a continuation of our earlier work (1-4), several new 2, 5 substituted 1,3 -dioxanes were studied by means of 1H-NMR.

The synthesis were run starting from the 1, 3-diol *1* which was condensed with aldehydes and ketones. The use of cyclic ketones gave spiranic 1, 3-dioxanic structures *3* (5, 6).

The acetalysation of pentaerytritol 4 with aldehydes and ketones gave spiro-1,3-dioxanes namely 3,9 -substituted -2,4, 8, 10-tetraoxaspiro/5,5/undecanes *5* (7):

In many cases, because of the superposition of some signals in the NMR spectra, their interpretation was possible using the *ASIS* method. The use of an aromatic solvent C_6D_6 instead of the usual $CDCl_3$, by means of the produced shifting of signals, offers very clear cut examples in this field.

In the case of the conformational equilibrium $6 \rightleftharpoons 6'$ of the mobile 1,3-dioxanic structure *6* (the conformational free enthalpy difference between the CH_3- and the $-CH_2-COOCH_3$ substituents in the 2 position is too small to

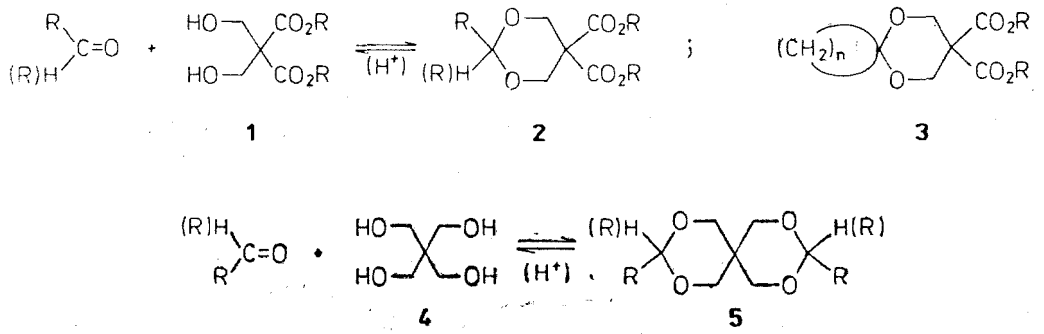

* *University Babeş-Bolyai Dept. of Organic Chemistry 3400 Cluj-Napoca România*

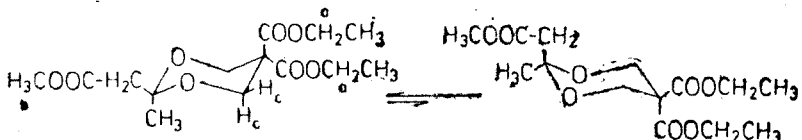

6 6'

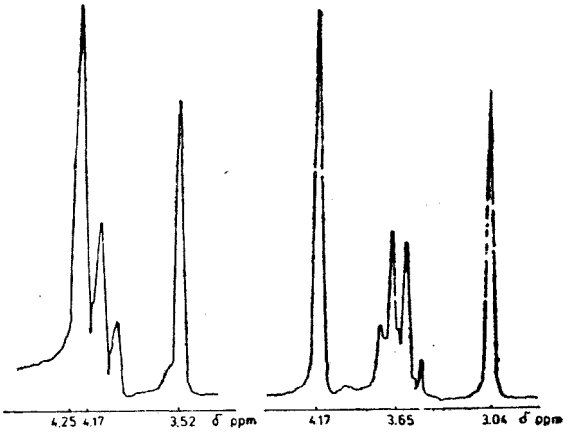

a b

Fig. 1. The fragment of the ^1H—NMR spectrum representing the protons *a*, *b* and *c* (of *6*) in $CDCl_3$ (Fig. 1a) and in C_6D_6 (Fig. 1b).

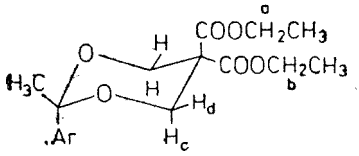

7-12

Ar = C_6H_5 (7); o-,m- and p-C_6H_4-NO_2 (8-10); α- and β-naphtyl (11;12)

generate anancomeric structure), the signal of the protons *c* is superposed on the signal (quartet) of the protons *a* in the spectrum run in $CDCl_3$ (fig. 1a).

$$6 \rightleftharpoons 6'$$

The use of C_6D_6 as solvent produces a significant shift of 0.52 *ppm* of the methylenic quartet and of 0.08 *ppm* of the mediated signal of the equatorial and axial protons (H_c) of the 1,3-dioxanic ring (Fig. 1b).

Concerning the fixed structures (*7—12*) obtained from aromatic ketones, $Ar = C_6H_5$ — (*7*); *o*-, *m*-, *p*-C_6H_4—NO_2 (*8—10*); α-, β-naphtyl (*11, 12*)

the importance of the ASIS experiments are very well demonstrated by the most significant cases illustrated by Fig. 2a, b and 3a, b and included in Table 1, which presents the chemical shifts of the protons *a* and *b* belonging to the axial respectively equatorial ethyl groups and of the axial (*Hc*) and equatorial (*Hd* protons linked to C^4 and C^6.

Table 1

Chemical shifts of protons *a-d* in compounds 7—12 showing the ASIS effect

Compound	Áryl group	Solvent	H_d	H_c	H_a	H_b
		$CDCl_3$	4.31	3.80	4.18	3.90
7	C_6H_5	C_6D_6	4.50	3.82	3.82	3.37
		Δ	0.19	0.02	0.36	0.53
		$CDCl_3$	4.25	3.56	4.10	3.86
8	o-$O_2N-C_6H_4-$	C_6D_6	4.50	3.75	3.75	3.37
		Δ	0.25	0.19	0.32	0.49
		$CDCl_3$	4.37	3.70	4.19	3.91
9	m-$O_2N-C_6H_4-$	C_6D_6	4.50	3.68	3.87	3.44
		Δ	0.13	0.02	0.32	0.47
		$CDCl_3$	4.32	3.70	4.16	3.90
10	p-$O_2N-C_6H_4-$	C_6D_6	4.45	3.60	3.82	3.42
		Δ	0.13	0.10	0.34	0.48
		$CDCl_3$	4.50	3.95	4.31	3.95
11	α-$C_{10}H_7$	C_6D_6	4.55	3.92	3.80	3.30
		Δ	0.05	0.03	0.51	0.65
		$CDCl_3$	4.50	3.95	4.30	3.97
12	β-$C_{10}H_7$	C_6D_6	4.65	4.00	3.87	3.37
		Δ	0.15	0.05	0.43	0.60

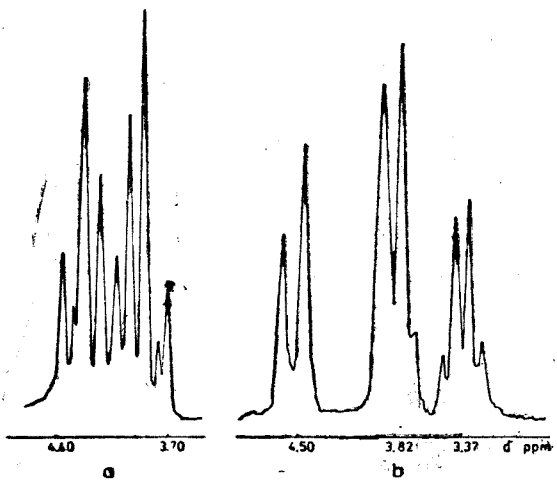

Fig. 2. The fragment of the ^1H-NMR spectrum representing protons *a—d* of compound *7* in $CDCl_3$ (Fig. 2a) and C_6D_6 (Fig. 2b).

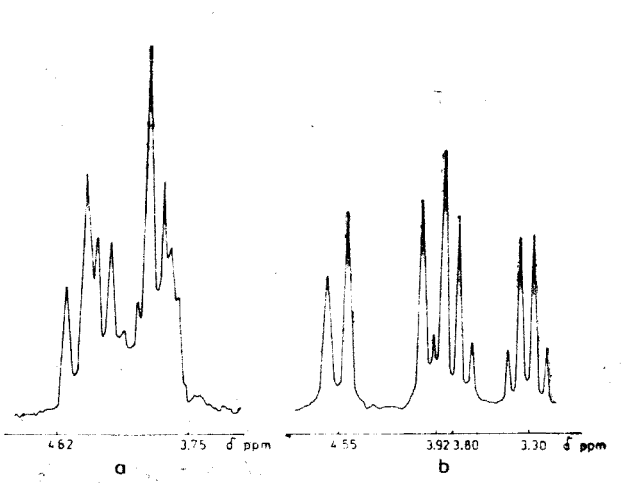

Fig. 3. The fragment of the ^1H-NMR spectrum representing protons *a—d* of compound *11* in $CDCl_3$ (Fig. 3a) and C_6D_6 (Fig. 3b).

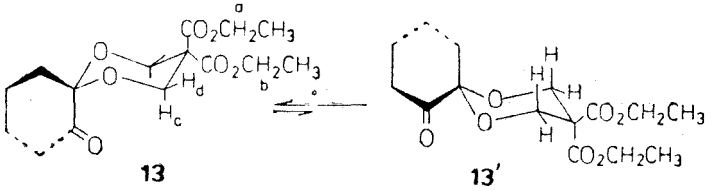

13 13'

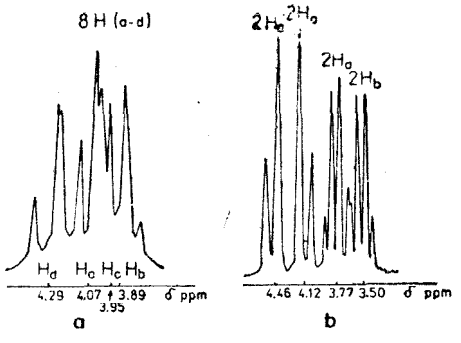

Fig. 4. The fragment of the ^1H—NMR spectrum representing protons *a*—*d* of compound *13* in $CDCl_3$ (Fig. 4a) and in C_6D_6 (Fig. 4b).

The condensation of the diol *1* with 1,2-cyclohexandione gave the anancomeric 1,3-dioxanic structure. *13*. The superposition of the two AX quartets

$$13 \rightleftharpoons 13'$$

(belonging to protons *c* and *d*) is also very well resolved using C_6D_6 instead of $CDCl_3$ as shown in Fig. 4a and b.

The anancomeric spiro-1,3-dioxanes (*14—20*) obtained from pentaerythritol with aldehydes or unsymmetrical ketones offers also very clear cut examples of the utility of the *ASIS* method.

14 R = CH_3; R′ = H
15 R = iC_3H_7; R′ = H
16 R = C_6H_5; R′ = H
17 R = C_2H_5; R′ = CH_3
18 R = iC_3H_7; R′ = CH_3
19 R = tC_4H_9; R′ = CH_3
20 R = CH_3; R′ = C_6H_5

Table 2 gives the chemical shifts and the Δδ values (differences between C_6D_6 and $CDCl_3$) for the dioxanes *14—20*.

In compound *16* the long range coupling between protons *Hc* and *He* may be easily observed using as solvent C_6D_6 instead of $CDCl_3$, as shown in Fig. 5a,b.

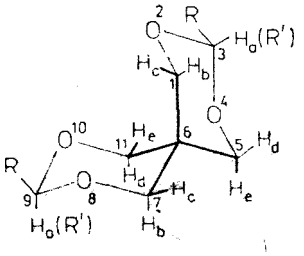

14 R=CH_3; R′=H **18** R=i-C_3H_7; R′=CH_3
15 R=i-C_3H_7; R′=H **19** R=t-C_4H_9; R′=CH_3
16 R=C_6H_5; R′=H **20** R=CH_3; R′=C_6H_5
17 R=C_6H_5; R′=CH_3

Table 2

Chemical shifts of protons *a-d* in compounds 14—20 showing the ASIS effect

Compound	C(3)/C(9)		Solvent	*H*	*H*	*H*	*H*	*H*
	R	*R'*						
14	CH_3	H	$CDCl_3$	4.60	3.56	4.56	3.45	3.58
			C_6D_6	4.12	3.07	4.58	2.64	2.97
				0.48	0.49	0.02	0.81	0.61
15	*i*-C_3H_7	H	$CDCl_3$	4.22	3.49	4.53	3.32	3.55
			C_6D_6	4.40	3.08	4.00	2.66	3.04
				0.18	0.41	0.06	0.66	0.51
16	C_6H_6	H	$CDCl_3$	5.41	3.79	4.84	3.59	3.80
			C_6D_6	5.20	3.33	4.95	2.92	3.25
				0.21	0.46	0.11	0.67	0.55
17	C_2H_5	CH_3	$CDCl_3$	1.28	3.71	3.78	3.60	3.60
			C_6D_6	1.10	3.49	3.67	3.24	3.31
				0.18	0.22	0.11	0.36	0.29
18	*i*-C_3H_7	CH_3	$CDCl_3$	1.21	3.70	3.86	3.53	3.53
			C_6D_6	1.02	3.47	3.88	3.19	3.27
				0.19	0.23	0.02	0.34	0.26
19	*t*-C_4H_9	CH_3	$CDCl_3$	1.26	3.64	4.27	3.48	3.27
			C_6D_6	1.02	3.39	4.41	2.99	2.87
				0.24	0.25	0.14	0.49	0.40
20	CH_3	C_6H_5	$CDCl_3$	1.50	3.61	4.44	3.21	3.13
			C_6D_6	1.46	3.53	4.58	2.93	2.65
				0.04	0.08	0.14	0.28	0.48

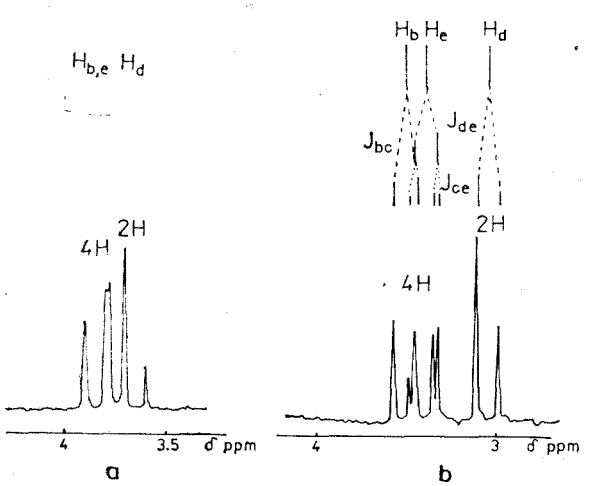

Fig. 5. The fragment of the $^1H-NMR^1$ spectrum representing protons *a*, *b* and *d* of compound *16* in $CDCl_3$ (Fig. 5a) and in C_6D_6 (Fig. 5b).

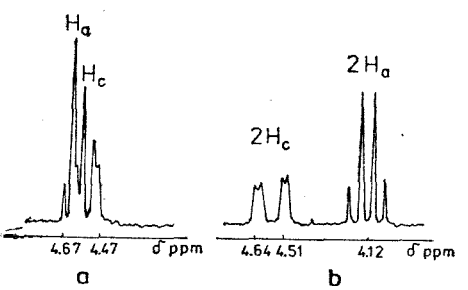

Fig. 6. The fragment of the ^1H-NMR spectrum of compound *14* for *Ha* and *Hc* in $CDCl_3$ (Fig. 6b).

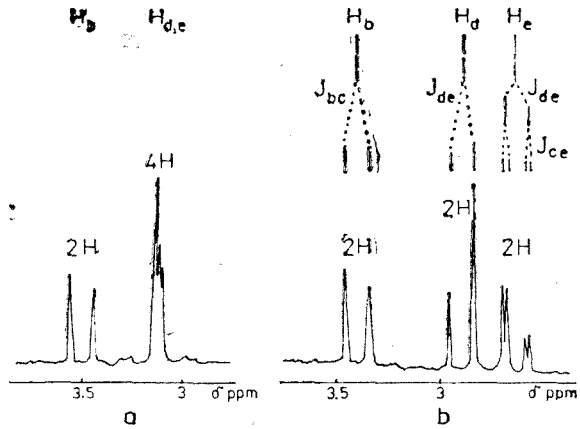

Fig. 7. The fragment of the ^{1}H—NMR spectrum of compound *20* for protons *Hd* and *He* in $CDCl_3$ (Fig, 7a) and C_6D_6 (Fig. 7b).

Other two striking examples are shown in Fig. 6 and Fig. 7. The superposed signals of protons *Ha* and *Hc* in compound *14* are very well resolved if one works in C_6D_6 (Fig. 6b) instead of $CDCl_3$ (Fig. 6a).

Concerning compound *20*, the difference between the equatorial (*Hd*) and axial (*He*) proton may be very well observed using C_6D_6 instead of $CDCl_3$ as shown in Fig. 7.

Experimental. The 1,3-Dioxanes were synthesized after the general procedure: the corresponding amounts of diols and aldehydes or ketones with catalytic amounts of *p*-toluenesulphonic acid were boiled in benzene. After the water completely removed, and the reaction product cooled, the solution was neutralized with sodium acetate and washed with water. The solvent was than removed and the compound[4] was purified by distillation or crystallisation..

The ^{1}H-NMR spectra were run with a —Bruker — SxP—4/100 apparatus with HMDS as internal standard using $CDCl_3$ and C_6D_6 as solvents.

REFERENCES

1. Binsch G., Eliel E. L. and Mager S., J. Org. Chem. **38,** 4079 (1973).
2. Mager S. and Eliel E. L., Rev. Roum. Chim. **18,** 1379 (1973).
3. Mager S. and Eliel E. L., Rev. Roum. Chim. **18,** 2097 (1973).
4. Mager S., Hopartean I., Horn M. and Grosu I., Stud. Univ. Babeş-Bolyai, Chem. **24,** 32 (1979).
5. Mager S. Ţăranu R., Horn M. and Mureşan M., Monatsh. Chem. **113,** 565 (1982).
6. Mager S., Horn M., Grosu I. and Bogdan M., Monatsh. Chem. **120,** 735 (1989).

STUDIA UNIV. BABEŞ-BOLYAI, CHEMIA, XXXVI, 1—2, 1991

SIMPOSIUM

„20 YEARS OF HIGH EDUCATION IN CHEMICAL ENGINEERING IN CLUJ-NAPOCA"

Between 19 and 22 september 1991, the Faculty of Chemistry and Industrial Chemistry of our University plaid host the jubilee Symposium „20 years of high education on Chemical Engineering in the university centre Cluj-Napoca".

Organized by the Department of Chemical Engineering to mark twenty years of research and teaching in Chemical Engineering in Cluj-Napoca, the Symposium have occasiones contacts, knowledges, acknowlegdes and profitable idea-changes between the chemical and chemical engineering schools, research centres and profile industrie of Romania. Proceedings were developed as plenary conferences (9), scientific communications on sections (119), posters (61) and round tables (2).

In programme were inscribed 191 papers of 316 authors.

The communications and the poster worRs were grupped in five Sections:

1. *Chemical Engineering (30 communications and 11 posters)*
2. *Chemistry and Technology of Oxide Materials (20 communications and 11 posters)*
3. *Chemistry and Inorganic Technology (20 communications and 12 posters)*
4. *Chemistry and Organic Technology (25 communications and 12 posters)*
5. *Analytical Chemistry, Physical Chemistry and Electrochemical Technologies (24 communications and 17 posters)*

A lot of these works are included in STUDIA number 1—2, 1991.

Plenary communications attacked problems of most actuality in chemical Research and the debates on the round table was refered to actual problems and of long-term concerning chemist engineer education and development of research in the chemical engineering field.

Symposium programme included some complementary manifestations like: opera show (W. A. Mozart), dyaporames in evening, meetings with graduate promotions of students and excursions in Cluj-Napoca (Botanic Garden, Old Centre, Museums) and on the Someş Valley (Tarniţa and Mărişelu).

Symposium was sponsorized by the Industrial Societies: CEROC S.A., IRIS S.A., SANEX S.A., TERAPIA. S.A. of Cluj-Napoca, CIMENTUL S.A. Turda and ELOR SRL Orăstie.

One of the conclusions of Symposium was the recognition of the Cluj chemical engineering education and its integration among the traditional schools (Bucuresti, Iasi, Timisoara) of Romania.

LIVIU LITERAT

STUDIA UNIV. BABEŞ-BOLYAI, CHEMIA, XXXVI, 1—2, 1991

BINDERS FOR GRINDING — STONES WITH HIGH HARDNESS

OLGA GOGU*, N. ZIMAN*, ADINA LATIA*

ABSTRACT. In the paper are presented experimentals concerning the obtaining of binders, based on modified borosilicate glass, agreeble as high-hardness grinding materials.

Introduction. Among the manifold utilisations of the grinding materials, abrasion is an important field, especially in the processing of the rolling coβ act bearings.

In order to carry out this operation under optimum conditions grinding stones are used. They are made from noble electrocorundum and of some binders which are used to ensure strength and high hardness, an absolutely indispensable requirement for the achievement of high precision grinding.

The studies performed in this field pointed out that good results are obtained by using binders which predominantly remain in the form of glass, after the firing process of the grinding stones. [1, 2, 3, 4, 5 and 6].

Experimental. Taking into account these facts, present paper deals with the problem of obtaining some grinding stones with the caracteristics mentioned above, by using a borosilicate glass as a binder and noble electrocorundum es an abrasive stuff. The influence of: refractory clay additions, firing temperature and pressing pressure have also been studied.

The raw materials used are: noble electrocorundum, Botesti refractory clay, borosilicate glass astes, synthetic. cryolite and monoaluminium phosphate.

The physico — chemical caracteristics of materials used are shown in Table 1 and 2.

Table 1

Noble electrocorundum granulometric composition.

Fraction [μm]	>80	>63	>50	>40	<40
%	39,8	21,4	8,8	6	24

Table 2

Borosilicate glass and Botesti clay chemical composition.

Oxides [%] / Raw materials	SiO_2	Al_2O_3	Fe_2O_3	CaO	MgO	Na_2O	K_2O	BaO	B_2O_3	TiO_2	P.C
Borosilicate glass	79,48	2,04	0,05	0,20	0,039	3,10	1,19	0,40	13,5	—	—
Botesti refractory clay	51,27	29,36	3,15	0,85	0,95	0,52	3,13	—	—	0,87	9,88

* *Technical University Timişoara; Dept of Chemical Engineering. 1900 Timişoara, Romania*

The aluminium monophosphate was used as a solution with $\rho = 1{,}61$ g/cm³.

The glass and clay were ground until a sieve residue of 1% was obtained on the 006 *mm* sieve for the glass and respectively a sieve residue of 1% on the 02 *mm* sieve for the clay.

A solution of aluminium monophosphate in proportion of 8—16% was added, in order to increase the binding power and provide optimum pressing condition. By pressing at 200 *daN/cm²*, and at 400 *da N/cm²* cylindrical samples with D = 34 *mm* and H = 19 *mm* and prisms of 130 × × 30 × 15 *mm* dimension were obtained. The samples were fired at 1160 °C and at 1250 °C, during a period of ten hours, being mantained for an hour at the maximum temperature.

The pastes were formed by maintaining the quantity of abrasive material and borosilicate glass constant, by changing the amount of the clay added and by modifing the firing temperature.

The pastes composition and their characteristics as a result of pressing and firing are shown in Table 3.

Table 3.

Pastes composition and their characteristics after pressing and firing.

Samples series	I			II		
Firing temperature [°C]	1160°			1250°		
Clay [%]	10	15	20	10	15	20
Glass + Cryolite [%]	15	15	15	15	15	15
Bending strenght, σ_i [*daN/cm²*]	578	684	706	580	596	580
Absorbtion capacity [%]	13,52	10,72	9,66	15,24	11,48	11,20
Apparent density [*g/cm³*]	2,42	2,50	2,50	2,28	2,53	2,49
Apparent porosity [%]	32,72	26,80	24,25	34,75	29,04	27,89
Hardness class	*R*	*T*	*T*	*R*	*T*	*T*

As it results from the facts presented above, by increasing the amount of the clay added, the bending strength is increased, the absorbtion capacity is decreased and hardness raises from class "hard" (*R*) to the class "very hard" (*T*).

The data presented in Table 3 also show that the temperature rise does not significantly modify the grinding stone characteristics.

The results obtained point out that the apparent density values lie mainly between 2.42—2.50 *g/cm³*. These values are higher than those found in literature for the grinding stones intended to fine grinding, for which are recommended values between 2.1—2.3 *g/cm³* [5].

In order to decrease the apparent density, two series of other samples were experimented; in one of them was investigated the variation of apparent density depending on the decrease of the amount of clay added, while in the other one, the quantity of borosilicate glass was reduced, and the amount of clay remained constant.

The firing was effected at 1160 °C. In these series of samples the influence of the pressing pressure was studied, though of less importance.

The pastes composition and the grinding stone characteristics are shown in Table 4.

As it results from the facts presented in the table above, for the first series (I), the decrease of the clay amount leads to the decrease of grinding stones apparent density to values within the limits requested for fine grin-

Table 4

The pastes' composition and their characteristics after firing.

Series	I				II			
Samples	1	2	3	4	1	2	3	4
Firing temperature [°C]	1160°							
Pressing pressure [daN/cm^2]	200		400		200		400	
Clay [%]	5	8	5	8	5	8	5	8
Glass + Cryolite [%]	15	15	15	15	11	11	11	11
Bending strenght [daN/cm^2]	485	473	566	559	485	493	502	556
Absorbtion capacity [%]	15,26	15,41	14,42	14,14	17,18	17,14	14,58	12,59
Apparent density [g/cm^3]	2,25	2,13	2,30	2,41	2,25	2,21	2,40	2,44
Apparent porosity [%]	34,26	32,82	33,21	34,18	38,66	37,88	34,99	30,72
Hardness class	*P*	*R*	*T*	*S*	*O*	*O*	*R—S*	*S*

ding. At the same time, a decrease of the strength and a change of the hardness class can be observed, most of the samples are now situated in class "hard". The modification of the pressing pressure brings about a slight increase in the values of both apparent density and strength.

The second series of samples (II), points out that the decrease of the glass amount causes similar effects as in the first series, with a marked decrease of the hardness class of grinding stones.

Conclusions. 1. The experimental researches pointed out the possibility of obtaining grinding stones from the hardness class "very hard", by using a binder consisting of 15% borosilicate glass wastes and an amount of 10—20% Botesti refractory clay. The grinding stones obtained presented higher apparent density values than the optimum ones as they are presented in literature. **2.** The decrease in the amount of clay up to 5—8% allowed to obtain grinding stones with characteristics close to those recommended in literature. **3.** The modification of the values of firing temperature and pressing pressure does not determine significant changes in the characteristics of the grinding stones obtained.

REFERENCES

1. Teoreanu I., Ciocea N., *Tehnologia produselor ceramice și refractare*, Ed. Tehnică, București 1985, p. 292.
2. Bakon A., Szklo i keramica, **Nr 28** (1), (1977), p. 303.
3. Wazniak K., Szklo i keramica, **Nr 29** (4), (1978), p. 102.
4. Knop L., Szklo i keramica, **Nr, 30** (3), (1979), p. 77.
5. Haupt D., Niebuhr M., Silikattechnik, **Nr, 4** (38), (1983), p. 118.
6. Branovskii V. A., Patent S.U. **Nr, 231346,** 29 April 1967.

STUDIA UNIV. BABEŞ-BOLYAI, CHEMIA, XXXVI, 1—2, 1991

MODELLING OF THE PRECIPITATE CALCIUM CARBONATE OBTENTION PROCESS

AL. SZÉP, M. D. BUCEVSCHI*, GH. MIHĂILĂ**

Recieved

ABSTRACT. The authors of the present article realised a modelling of the precipitate calcium-carbonate's obtaining. Based on their down results and those of the afferent technical literature, they searched the ,,reaction of double change between calcium-chloride and sodium-carbonate solutions. The three ir-dependent variables of the problem being: temperature; concentration of sodium-carbonate solution; and that of calcium-chloride, they studied four qualitative (dependent) variables: concentration of the calcium-carbonate-solution obtained, its density in bulk, sedimentation-speed ("number") and the *xH* of its 2% concentrated solution.

Using the "multiple regression" method, statistico-mathematical models were elaborated, describing the dependencies between the three independent- and four dependent (qualitative) variables. Imposing some restrictive conditions, resulted the optimal solution, confirmed later by repeated experimentals. The quality of the products obtained this way satisfies excessively the limits stipulated by the legal standards.

1. **Introduction.** The technical grade calcium carbonate is useful in many fields of economy. Besides classical ones, namely rubber industry, plastics, paper, cosmetics, farmaceutics and paints, in the last time, it is utilized in the new fields such as electrotechnics and machine construction [1, 2]. Both, new fields and the classical ones, request some restrictive conditions on chemical, physical and technological properties, i.e. bulk density, settling number, whiteness, fineness of grain, *pH* of the aqueous suspension etc.

Generally, the technical grade calcium carbonate can be obtained either by neutralization of the lime milk with carbon dioxide or by procedures based on a double exchange reaction between calcium salts and salts that contain the CO ion. During the manufacturing process, it crystallizes, besides the three stable crystalline forms, i.e. calcite, aragonite and waterite, in over 200 more or less stable varieties [1,4—7].

The obtention of calcium carbonate in one of its crystalline species, requested by user, is the main aim of the manufacture technology. Since the quality of the final product obtained by any known procedures is dependent on a great number of kinetical parameters, the technological regime establishing is usually preceded by a laboratory investigation as regards the influence of these parameters over its quality. Due to the great rate of transformation process, reaction — formation and growing of germs, the analytical modelling is very difficult, so that, the statistical one was necessary to be employed.

* *Politechnical Institute Jassy, Dept. of Chemical Engineering, 6600 Iaşi, Romania*
** *University ,,Al. I. Cuza" Dept. of Chemistry, 6600 Iaşi, Romania*

In order to find the optimal technological regime for obtention, by a double exchange procedure, of a final product with the properties requested by the user, in the present paper were carried out the following steps:

— establishing of kinetical parameters with significant influence overfinal product quality;

— establishing the quantitative and qualitative indexes;

— elaboration of the statistico-mathematical models describing the dependence of the product property on the kinetical parameters;

— finding the technological solution in a matrix from of the values of kinetical parameters that favour to obtain the product with requested qualitative indexes.

2. **Elaboration of the statistico-mathematical models.** To establish the independent variables of the system, from the great number of kinetical parameters influencing the quality of the final product, based on some previous investigations and the literature available data [4—11], we have considered as constant parameters the following: stirring intensity (560 *rot./min.*), simultaneous feed of the reactant phases, 0.4—0.6 *g* Na_2CO_3g/l excess, feed time (5 *min.*) and the process time (30 *min.*). Under these conditions, the variables of the system are as follows: temperature, concentration of calcium chloride solution and concentration of sodium carbonate solution. As qualitative indexes of the product, we have selected from several only 4, i.e. concentration of $CaCO_3$ ($CaCO_3$, %), bulk density (ρ_B, g/cm^3), settling number (S_N, %) and *pH* of its 2% suspension.

In order to elaborate the statistico-mathematical models which describe the dependences among the three variables and the four properties, the multiple regression has been employed. The great number of factors and the four simultaneous responses suggested us to employ a complet statistical modelling, consisting in elaboration of one experimental program followed by processing of the data by the *least squares* method.

Taking into account the three independent variables at the five levels considered, the data summarized in Table 1, have been obtained.

To carry out the programed experiments, we employed solutions of calcium chloride, obtained by dissolution and filtration of technical grade chloride and solutions of pure sodium carbonate. The experiments were carried out on a laboratory plant made up by a 1.5 *l* capacity reactor with mechanical stirring, 2 level thermostated bottles and a vacuum filtering device. For each experiments, the amounts of necessary reagents were measured and thermostated at oprating temperature. The solutions entered in the reactor with such a flowrate that feed duration was 5 minutes long. The thermostated reaction mass was stirred for 30 minutes, followed by solid separation by vacuum filtration, washed with distilled water to remove completly the chlorine ions and driedat 120°*C* for 3 *hours*. The dry product, after disintegration in an impact mill, was subjected to the laboratory tests, measuring besides the four indexes mentioned above, the bleaching degree and oversize pices on the0.063 μm screen. The results are also represented in Table 1.

Table 1

Experimental results

Run	$\bar{C}^{\circ}_{CaCl_2}$ g/l	$\bar{C}^{\circ}_{Na_2CO_3}$ g/l	Temperature, °C	Content of $CaCO_3$, %	*pH* of 2% suspension	Settling number after 5 *min.*, SN, %	Bulk density, $\rho\sigma$,	Bleaching degree, % %
1	70	5	35	97.092	9.80	41.0	0.8695	94.00
2	190	55	35	96.269	9.65	40.5	0.8695	91.00
3	70	145	35	95.631	9.94	42.5	0.7894	95.00
4	190	145	35	98.257	9.45	75.5	0.6060	91.50
5	70	55	65	96.277	9.80	38.0	0.8333	92.50
6	190	55	65	96.211	9.70	30.0	0.8695	92.65
7	70	145	65	96.311	9.95	45.0	0.8550	94.90
8	190	145	65	99.137	9.50	97.0	0.3921	95.50
9	10	100	50	96.311	10.0	56.0	0.5500	95.00
10	250	100	50	98.710	9.15	98.75	0.6238	95.2
11	130	10	50	96.935	9.65	50.0	0.5550	94.8
12	130	190	50	98.373	9.55	96.0	0.4938	95.6
13	130	100	20	98.507	9.60	98.0	0.6200	95.7
14	130	100	80	98.084	9.55	98.75	0.5839	95.7
15	130	100	50	98.657	9.60	96.0	0.4440	95.3
16	130	100	50	98.21	9.55	98.75	0.5550	95.4
17	130	100	50	98.565	9.55	95.0	0.4819	93.2
18	130	100	50	98.48	9.50	97.0	0.5550	95.7
19	130	100	50	98.257	9.50	99.5	0.5633	96.0
20	130	100	50	98.30	9.30	98.5	0.5759	95.7

The mathematical models proper to the four responses were found starting from a classical form of plynomial type, having the expression:

$$\hat{Y}_K = a_0^k + \sum_{g=1}^{n} a_i^k X_i + \sum_{i=1}^{n} a_{ij}^k X_i Y_i + \sum_{i=1}^{n} a_{ii}^k X_i^2 + \ldots$$

where $\hat{Y}_K$ is estimation of the Y_K property, K is the number of properties, n is the number of variables and a_0, a , a are the coefficients of the regression equation.

Statistico-mathematical processing of the experimental data has consisted in solving of the below matrix equation, based on a factorial program concretized by $NE = 2 + 2n + n_0$ [13]:

$$a^1_{(NE\S} = X_{(NE*NC)} * X^T_{(NE*NC)})^{-1} * X^T_{(NE*NC)} * Y_K$$

where, NC is the number of coefficients and NE is the number of experiments.

The found coefficients $a^1_{(NC)}$ provides a mathematical model characterized by a standard deviation of estimation SDE_1.

Having calculated the values of the Student's test for the $a^1_{(NC)}$ coefficients, diminishing of some terms is necessary, and their replacing with others, so that the vector of the new coefficients to provide a model characterized by $SDE_2 < SDE_1$.

The new terms can be found by iterative calculus making combinations of the powers at the level of general term $X_1^a \cdot X_2^b \cdot X_3^c$ with a, b and c, taking values from the [0, 1, 2, 3, 4[matrix [12].

At the same time, the number of coefficients was increased from its initial value NC to NC^*, respecting $NC \leqslant NE$.

Due to the octogonal feature of the $(X * X^T)$ matrix, when the variables take codified values for a, to obtain the minimum value of the SDE index, one was necessary to scalarize the variation range of variables in a such a manner that, indiferent of the structure of the attachable terms, $(X * X^T)$ does not lead to a singular matrix.

For a rapid finding of the coefficients of the new function, a program in the Basic language was elaborated and ruled on TIMS computer. The results of calculi are set out in Table 2.

To vizualize the form of functions, the dependences $\hat{Y} = f(X_2, X_3)X_1 = ct'$ have been ploted. For example, in Figure 1 is represented the two functions.

Table 2

Coefficients of the standard (1) and modified (2) regression equations

Functions / Terms	Y_1, % $CaCO_3$		Y_2, ϱ_b, g/cm^3		Y_3, S_N, %		Y_4, pH	
	1	2	1	2	1	2	1	2
O	98.2197	98.3846	0.5655	0.5291	91.0284	97.6875	9.5293	9.5787
X_1	0.585	0.585	−0.0289	−0.0289	10.125	9.1875	−0.1806	0.1275
X_2	0.3976	0.3976	−0.0576	−0.0176	12.6162	14.5833	−0.01937	0.01
X_3		0.009937	−0.1604	−0.01604		0.75	0.000625	0.000625
X_1^2	−0.3232	−0.2185	0.0326	0.01442	−8.2357	−5.0781	0.0334	0.01406
X_1X_2	0.7926	0.7926	−0.08131	−0.08131	11.6875	11.6875	−0.08625	−0.09625
X_1X_3			−0.03041	−0.03041			0.01125	
X_2^2		−0.1826	0.01697	−0.001195	−9.3295	−53,1718	0.03963	0.0203
X_2X_3			−0.01401				0.00125	
X_1^3			0.03636	0.01819			0.00125	
X_1^3						0.375		−0.02125
$X_1^3X_2^2$		−1.0813		0.2				0.1706
X_2^3						−0.7708		
$X_1X_2X_3$		−0.06962		−0.3946				
X_2^4						11.75		
X_3^4								−0.003749
COR	0.8763	0.973	0.6431	0.9064	0.7821	0.9893	0.8816	0.9593
SDE	0.733	0.3316	0.1632	0.0948	23.27	5.49	0.137	0.082

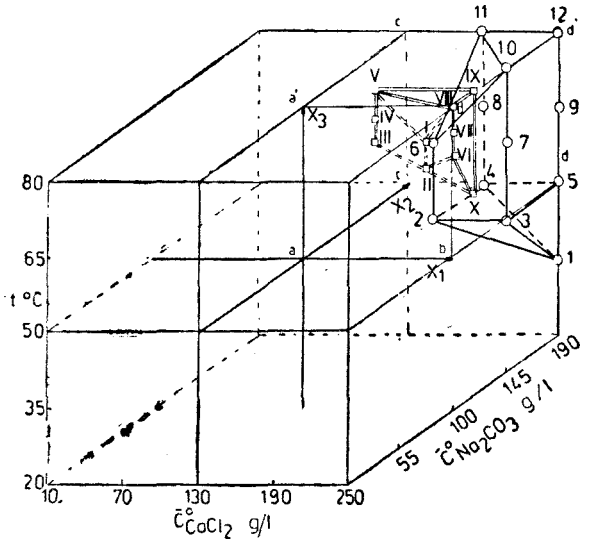

Fig. 1. Plot of the Y_3 function: **a** — standard; **b** — modified;

namely the standard one (*a*) and that with minimum SDE (*b*). It can be seen that the improved function is better adjusted around the experimental points, but it exhibits a large deviation at the range extremity.

3. **Technological solutions.** In order to establish the parameters that assure obtention of a final product with a desired quality, the equation systems formed by the 4×2 regression equations, with respect the following restrictive conditions: $\%CaCO_3 = 98 - 99$, $\rho_B < 0.45\ g/cm^3$, $S_N \leq 95\%$ and pH of its 2% suspension equal to 8.5—10, have been solved. Its solutions have been found using the iterative method, taking into account ten steps for each factor. The obtained results are represented in the experimental cube, Figure 2, in form of some bodies inside of the points 1—12, the case of classical model and I — *X*, for the improved model.

As can be seen from figure 2, the technological parameters found in this way are situated inside of the abcda'b'c'd' cube, i.e. at lower concentrations of $CaCl_2$ (146—250 *g/l*) and Na_2CO_3 (112—190 *g/l*), while the classical model gives the technological solutions in the range of higher concentrations of $CaCl_2$ (190—250 *g/l* and Na_2CO_3 (145—190 *g/l*). But, both models show that the operating temperature must be higher than 50°*C*.

In order to verify the veracity of the models, some replicate experiments were carried out under extreme conditions, given by point 12. The results set out in Table 3 show that the mathematical model developed, describes well enough the process under study, being useful for the determination of the kinetical parameters that control the obtention of calcium carbonate with a pre-established quality.

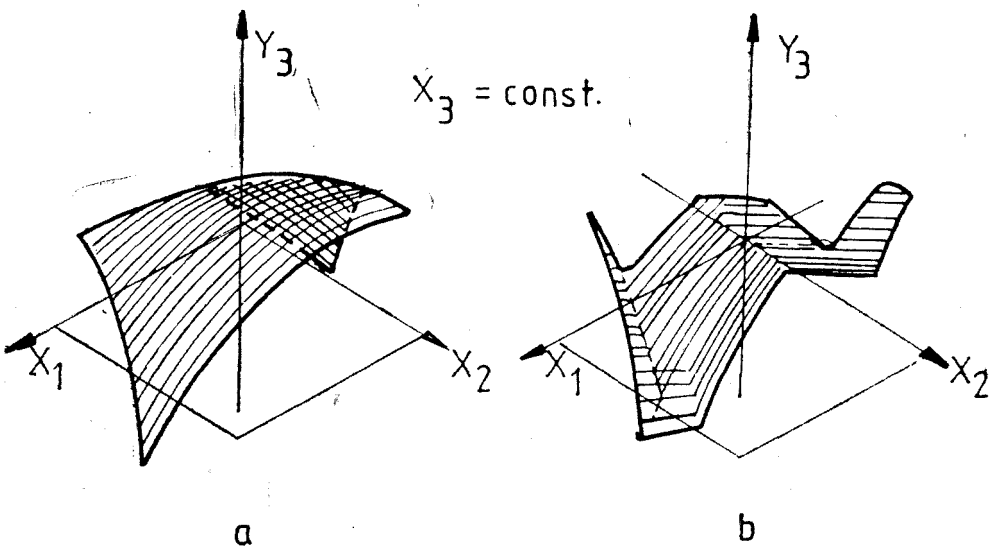

Fig. 2. The variation range of the parameters that satisfy simultaneously the restrictive quality conditions of the product.

Table 3

Comparative results

Product	% $CaCO_3$	ρ g/cm³	S, %	pH of 2% susp.	Bleaching degree, %
12+	98.475	0.3809	99.5	9.4	95.2
12++	98.917	0.3636	99.0	9.4	95.0
STAS 1083-76	97—99	0.45—0.47	90—95	8.5—9.5	92—97

4. **Conclusions.** The laboratory investigation of the calcium carbonate obtention by a double exchange procedure, using solutions of calcium chloride and sodium carbonate, allowed to establish the statistico-mathematical models that describes the dependences among the 3 process parameters and 4 properties of the final product. Their solving under restrictive conditions has given the technological solutions. Since these solutions were verified ulteriorly by replicate experiments, the veracity of the developed models was proved. The final product, obtained under conditions of the technological regime established, satisfies in abundence the quality indexes recorded in the actual standards.

REFERENCES

1. Dedek, J., *Le carbonate de chaux*, Librerie Universitaire, Leuven, 1966.
2. Chober, W., Ind. Miner., 1989, Nr. 265, p. 69.
3. Ludwig, G., Götlschalk, J., Silikattechnik, **39**, 347, 1988.
4. Rusznak, I., Kautschuk, **32**, 294, 1987.
5. Fekeev, A. A., Kniazeva, A. N., Khim. Prom., 1987, Nr. 4, p. 219.
6. Riabuha, A. A., Sîtnik, N. A., Gordienko, E. M., Abakumov, I. N., Zhur. Prikl. Khim., **58**, 647, 1985.
7. Miharcik, I. F., Filippova, F. I., Fesenko, N. M., Zhur. Prikl. Khim., **52**, 1111, 1979.
8. * * * Pat. Jap. 5307899/1973.
9. * * * Pat. Jap. 7901571/1984.
10. * * * Pat. Pol. 123041/1984.
11. * * * Pat. RO 96667/1987.
12. Derbişev, V. E., Vasiliev, P. M., Zhur. Prikl. Khim., **63**, 114, 1990.
13. Mihail, R., *Introducere în strategia experimentării, cu aplicaţii în tehnologia chimică*, Ed. ştiinţifică şi Enciclopedică, Bucureşti, 1976.

STUDIA UNIV. BABEŞ-BOLYAI, CHEMIA, XXXVI, 1—2, 1991

CARBON DIOXIDE ABSORPTION INTO PROMOTED POTASH SOLUTIONS

I. Enhancement Factor Determining

ILIE SIMINICEANU*

ABSTRACT. The absorption of carbon dioxide from gas mixtures into activated potassium carbonate-bicarbonate buffer solutions has been studied. The *enhancement factor* is defined as the ratio of absorption rate with and without chemical reaction. By assuming a pseudo-first order reaction and no gas-side resistance, the equation for the enhancement factor calculation, as a function of experimental data, has been derived. The method is numerically illustrated using the initial values of the absorption rate constant, obtained in the presence of eleven different promoters, at 298 K. The enhancement factor criterion is better than the relative reaction constant not only for the promoter selection but also for the absorption column design calculations.

1. **Introduction.** The removal of carbon dioxide from gas mixtures by liquid absorbents is an industrial process of both theoretical and practical importance. The applications and processes for removal of carbon dioxide ar extensively reviewed by Danckwerts and Sharma [1]. For economic reasons the absorbent must have a large capacity for carbon dioxide, be capable o regeneration by driving off carbon dioxide, and have a high specific absorption rate. The specific rate of absorption into physical solvents is generally much less than that into chemical absorbents. Potassium carbonate solutions are most commonly employed as chemical absorbent, especially for bulk CO_2 removal, becouse of their low cost, large capacity, ease of handling, and relative ease of regeneration. In particular, hot carbonate processes (Benfield, Carsol, Catacarb, Giammarco—Vetrocoke) are widely used, notably when decreased-pressure regeneration is practical, as in ammonia synthesis plants.

The reaction of carbon dioxide in carbonate solutions can be catalysed by a number of substances: amines, glycols, alcohols, glycine, arsenic oxide, amine borates [2, 3]. The main goal of the research works in this filed is to develop new promoters, more effective and less dangerous than those already known. The different catalysts are usually screened on the basis of the pseudo-first order relative rate constant (k^*/k). A new method for the promoter selection, based on the concept of *enhancemenet factor*, is proposed in this paper.

* *Polytechnical Institute Jassy, Dept. of Chemical Engineering, 6600 Iaşi, Romania*

2. **The mechanism of the process.** The chemical process of CO_2 absorption into potassium carbonate solutions may be represented by the following "characteristic equation"

$$[CO_2 + A'']_g + [K_2CO_3 + H_2O]_l \rightarrow [A'' + CO_2]_g + [K_2CO_3 + KHCO_3 + H_2O]_l \quad (1)$$

The overall process consists of a sequence of distinct steps: mass transfer of CO_2 from bulk gas to the interface, solvatization at the interface, mass transfer from phase boundary into bulk liquid, chemical reaction in the bulk liquid. The overall reaction taking place during CO_2 absorption in potassium carbonate solution is:

$$CO_2 + H_2O + K_2CO_3 = 2KHCO_3 \quad (2)$$

In an uncatalysed buffer solution the reaction (2) occurs in two steps:

$$K_2CO_3 + H_2O = KHCO_3 + KOH \quad (2.1)$$

$$CO_2 + KOH = KHCO_3 \quad (2.2)$$

the rate determining step being the reaction (2.2) becouse of the small hydroxyl ion-concentration (typically 10^{-3} to 10^{-} *mol/L*). The HO^- concentration is held almost constant by the buffer action of the carbonate-bicarbonate equilibrium. Concequently, the second order kinetic equation of the reaction (2.2):

$$r_{CO_2} = k_{OH} \cdot C_{CO_2} \cdot C_{HO}$$

may be written as a pseudo-first-order form:

$$r_{CO_2} = k \cdot C_{CO_2} \quad (3)$$

where, the pseudo-first-order constant k is the product: $k = k_{OH} \cdot C_{OH} \cdot$

Using the value of k_{OH} at 298 K given by Danckwerts(1), $k_{OH} = 10^4$ $L(mol\ s)^{-1}$, the rate constant k becomes: $k = k_{OH} \cdot C_{HO} = 10^{-1}$ to $10^1\ s^{-1}$.

In all aqueous solutions also takes place the slow hydration reaction

$$CO_2 + H_2O = HCO^{-3} + H^+ \quad (4)$$

At 298 K, the first-order rate constant of the reaction (4) is: $k_w = 10^{-2}\ s^{-1}$ [4].

As the value of k_w is usually much less than that of the pseudo-first-order rate constant k, and the "reaction" (4) is normally negligible in determining the rate of CO_2 absorption into alkaline solutions with $pH < 10$(3), the global rate of CO_2 consumption in the simultaneous reactions (2.2) and (4) is:

$$r_{CO_2} = (k_{OH} \cdot C_{HO} + k_w) \cdot C_{CO_2} = (k + k_w) \cdot C_{CO_2} = k \cdot C_{CO_2} \quad (5)$$

So, the most significant reaction in an uncetalysed potassium carbonat solution is the reaction (2.2) of dissolved CO_2 with hydroxyl ions formed from the available potassium carbonate:

$$CO_2 + HO^- = HCO_3^- \quad (2.2)$$

The modern commercial units usually employ a promoter which increases the rate of the reaction (2.2'), allowing a reduction in the size of the absorption equipment. Typical promoters reported in the literature include: potassium arsenite (Giammarco—Vetrocoke process), diethanolamine (Benfiled process), amine borates (Catacarb process).

The mechanism whereby carbonate-bicarbonate buffers could be catalyzed by small amounts of substances is not yet clearly explained. The best is to consider the promoter as a transfer agent of CO_2 from the interface to the bulk liquid. So, in an amine catalized solution, the reaction (2.2) takes place in two steps:

$$CO_2 + R_2NH \xrightarrow{k_{Am}} R_2NCOOH \qquad (2.2.\text{ a})$$

$$R_2NCOOH + HO^- = R_2NH + HCO_3^- \qquad (2.2.\text{ b})$$

$$CO_2 + HO^- \xrightarrow{\mu} HCO_3^- \qquad (2.2')$$

The ionic step (2.2. b) is faster than the step (2.2. a). The rate of the second-order reaction (2.2. a) is also fairly rapid, with a typical second-order rate constant $k_{Am} \sim 10^4\ L(mol\ s)^{-1}$ at 298 k [4]. Thus, even small amine concentrations ($\sim 0.1\ mol\ L^{-1}$ or 1% by volume) should provide sufficient free amine (say $10^{-2}\ mol\ L^{-1}$) to produce more rapid CO_2 absorption by reaction (2.2. a) than by the direct reaction (2.2), i.e.:

$$k^*/k = \frac{k_{Am} \cdot C_{Am}}{k_{OH} \cdot C_{HO^-}} = 10 \text{ to } 1\,000$$

The above disscution allows to consider a general first-order kinetic equation (5):

$$r_{CO_2} = k \cdot C_{CO_2} \qquad (5)$$

which may be applied in all the three different particular cases: Physical absorption in pure water (with $k = k_w$), chemical absorption by uncatalyzed carbonate-bicarbonate solutions (with $k = k^*$), and chemical absorption into promoted buffer solutions (with $k = k^*$).

The effect of promoters is usually measured by means of the relative reaction constant (k^*/k) as well as by the value of activation energy [3, 4]. Practically, is more important to evaluate the effect of promoters on the averall absorption rate, by means of the concept of *enhancement factor*. The following paragraph is concerned with the mathematical modelling of the process, leading to the definition of the enhancement factor.

3. **The enhancement factor equation.** By assuming a pseudo-first-order reaction and a negligible gasside resistance, the concentration profile at the interface is that illustrated in Fig. 1.

Let us consider an element of volume dV of thikness dX of the liquid phase. For a stagnant liquid-film, the Fick's low may be applied and the material balance of the element gives:

$$-D\left(\frac{dC_{CO_2}}{dX}\right) + r_{CO_2} \cdot dX = -D \cdot \left(\frac{dC_{CO_2}}{dX}\right)_{X+dX}$$

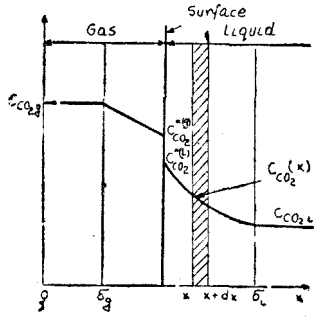

Fig. 1. Concentration profile at the interface under conditions of pseudo-first-order reaction.

Dividing by dX, with $dX \to 0$, the equation becomes:

$$D \cdot \left(\frac{d^2 C_{CO_2}}{dX^2}\right) + r_{CO_2} = 0$$

with the boundary conditions:

$$C_{CO_2} = C^e_{CO_2}, \text{ at } X = 0$$
$$C_{CO_2} = C_{CO_2}, \text{ at } X = \delta_L \tag{6}$$

According to the Whitman theory, the liquid-film thikness is:

$$\delta_L = D/k_L \tag{7}$$

where k_L is the mass transfer coefificient for CO_2 into distilled water (physical absorption). By substituting the equation (5) for r_{CO_2} into the equation (6), the differential equation (8) is obtained:

$$D \cdot \frac{d^2 C_{CO_2}}{dX^2} + k \cdot C_{CO_2} = 0 \tag{8}$$

with the general solution (9):

$$C_{CO_2} = C_1 \cdot e^{-rX} + C_2 \cdot e^{-rX} \tag{9}$$

where:

$$r = k/D \tag{10}$$

Using the boundary conditions, the constants C_1 and C_2 may be identified and the equation (9) becomes:

$$C_{CO_2} = \frac{C_{CO_2} \cdot \sin h[Xr] + C^*_{CO_2} \cdot \sin h[r(\delta_L - X)]}{\sin h[\delta_L r]} \tag{9'}$$

From (9') the concentration gradient is derived:

$$\frac{dC_{CO_2}}{dX} = \frac{r \cdot C_{CO_2} \cdot \cos h[rX] - r \cdot C^*_{CO_2} \cdot \cos h[r(\delta_L - X)]}{\sin h[\delta_L r]} \tag{11}$$

The amount of CO_2 crossing the interface, $-D \cdot \left(\frac{dC_{CO_2}}{dX}\right)_{X=0}$, is the actual rate of absorption per unit surface, or the effective absorption rate (r_{ef}). It may be derived by substituting $X = 0$ in the equation (11):

$$r_{ef} = -D\left(\frac{dC_{CO_2}}{dX}\right)_{X=0} = D \cdot \frac{r \cdot \cos h[\delta_L r]}{\sin h[\delta_L r]}\left(C^*_{CO_2} - \frac{C_{CO_2}}{\cos h[\delta_L r]}\right) \tag{12}$$

From (7) and (10) we obtain the dimensionless parameter Ha, called *Hatta number:*

$$\delta_L r = \frac{D}{k_L}\sqrt{\frac{k}{D}} = \frac{\sqrt{kD}}{k_L} = Ha \tag{13}$$

and the equation (12) becomes:

$$r_{ef} = \frac{k_L \cdot Ha}{\tan h[Ha]}\left(C^*_{CO_2} - \frac{C_{CO_2}}{\cos h[Ha]}\right) \tag{14}$$

The rate of physical absorption is given by:

$$r_{ab} = k_L(C^*_{CO_2} - C_{CO_2}) \tag{15}$$

The ratio r_{ef}/r_{ab} is a measure of the accelerating effect of the reaction on the absorption, named *enhancement factor* (Φ):

$$\Phi = \frac{r_{ef}}{r_{ba}} = \frac{Ha}{\tan h[Ha]}\left\{\frac{1 - \frac{C_{CO_2}/C^*_{CO_2}}{\cos h[Ha]}}{1 - \frac{C_{CO_2}}{C^*_{CO_2}}}\right\} \tag{16}$$

or:

$$\Phi = \frac{r_{ef}}{r_{ab}} = \frac{Ha}{\tanh[Ha]}\,1 - \varphi\left(\frac{\frac{\varphi}{\cos h\,[Ha]}}{1-\varphi}\right) \tag{16'}$$

where:

$$\varphi = \frac{C_{CO_2}}{C^*_{CO_2}} \tag{17}$$

Usually, $C_{CO_2} \ll C^*_{CO_2}$ ($\varphi \to 0$) and the enhancement factor is hence given by:

$$\Phi = \frac{r_{ef}}{r_{ab}} = \frac{Ha}{\tan h[Ha]} \tag{18}$$

According to the equations (13) and (18) the enhancement factor of the absorption by a first-order reaction, with no gas-side resistance, depends on the ratio of reaction rate constant (k) and the physical mass-transfer coefficient of CO_2 (k_L). Depending on the Hatta number, we may have three practical cases:

II. $Ha < 0.3$ (slow reaction), $Ha = \tan h\ Ha$, $\Phi = 1.0$. The reaction has no influence on the absorption rate and the kinetic equation becomes:

$$r_{ef} = r_{ab} = k_L(C^*_{CO_2} - C_{CO_2})$$

II. $0.3 < Ha < 5.0$ (fast reaction), $1.0 < \Phi < 5.0$. The kinetic equation has the general form (16')

III. $Ha > 5.0$ (instantaneous reaction), $\Phi = Ha > 5.0$. The reaction occurs in the liquid film ($C_{CO_2} = 0$) and the kinetic equation is:

$$r_{ef} = \Phi_L r_{bb} = Ha\ k\ (C^*_{CO_2} - C_{CO_2}) = k_L \cdot Ha \cdot C^*_{CO_2}$$

4. **Enhancement factor determining. Results.** The application of the equations (13) and (18) for the enghancement factor calculation needs the experimental values of D, k_L, and k. The values of D and k_L must be determined for physical absorption of CO_2 in pure water, at the industrial operating temperature. Table 1 presents the existing data for D and k_L of CO_2 in distilled water, at temperatures between 291 and 353 K/4, 5).

Table 1

Tnhe coefficients k_L and D in the carbon dioxide-water system

T, K	291	323	333	343	353
$10^4 \times k_L$, $m \cdot s^{-1}$	0.5	6.0	6.5	7.2	7.8
$10 \times D$, $m^2 s^{-1}$	1.0	1.85	2.25	2.65	3.17

Since these coefficients depend not only on the temperature but also on the viscosity and the density of the liquid, they must be corrected for the reacting solutions [3,4].

The[4]rate constant k depends on the temperature as well as on the chemical nature of the promotor. Table 2 presents the values of $k(k^*)$ obtained for a potash solution (20%) at 298 K activated with eleven different promoters at a concentration of 2.0% w/v. The rate constant has been evaluated from the experimental plots log ($p_{CO_2}/p^0_{CO_2}$) vs time of Gavarini [3], for contact time less than 300 s. In the two last columns of the Table 2 the computed values of the Hatta number as well as of the enhancement factor are presented. For all calculations the following corrected values of D and k_L have been employed: $D = 10^- m^2\ s^{-1}$, $k_L = 10^{-4}\ ms^{-1}$. The symbols of the promoters considered are: U(urea), GU(glucose), GL(ethylene glycol), MU(methylolurea), DEA (diethanolamine), NPA(neopentanolamine), DMNPA(dimethylneopentanolamine), GY(glicine), TEPA/CH_2O(tetraethylenpentamine-formaldehyde), TETA/CH_2O (triethylenetetramine-formaldehyde).

Table 2

Influence of the promoters on the enhancement factor

Nr.	System	k, s^{-1}	Ha	Φ
1.	H_2O	10^{-2}	0.0316	1.0000
2.	$H_2O + K_2CO_3$	6.67	0.8167	1.2130
3.	$H_2O + K_2CO_3 +$ U	10.67	1.0329	1.3327
4.	$H_2O + K_2CO_3 +$ GU	11.48	1.0714	1.3562
5.	$H_2O + K_2CO_3 +$ GL	12.99	1.1371	1.3979
6.	$H_2O + K_2CO_3 +$ MU	16.38	1.2785	1.4953
7.	$H_2O + K_2CO_3 +$ DEA	19.57	1.3990	1.5810
8.	$H_2O + K_2CO_3 +$ NPA	37.26	1.9309	1.8507
9.	$H_2O + K_2CO_3 +$ DMNPA	41.49	2.0369	1.9687
10.	$H_2O + K_2CO_3 + As_2O_3$	51.73	2.2744	2.3230
11.	$H_2O + K_2CO_3 +$ GY	71.27	2.6696	2.6954
12.	$H_2O + K_2CO_3 +$ TEPA/CH_2O	86.80	2.9470	2.9639
13.	$H_2O + K_2CO_3 +$ TETA/CH_2O	88.08	2.9667	2.9830

5. **Conclusions.** All the chemical systems in Table 2 are of the second type (fast reaction).

The most effective promoter in Table 2 (TETA/CH_2O), which increases the reaction rate with a factor of $13.2(k^*/k = 88.02/6.67 = 13.2)$, provides an enhancement factor $\Phi = 2.983$. This is equivalent to an increasing of the actual absorption rate of 2.983 times and to an identical reduction of the absorber volume.

The enhancement factor is a very practical concept in the R & D activities, devoted to the improvement of the existing plants. The method presented above can be applied for the evaluation and selection of the most suitable promoter in any other absorption process on a quantitative basis.

SYMBOLS

C_{CO_2}, $C^*_{CO_2}$ = concentration of carbon dioxide in the bulk liquid, and at the interface, respectively $mol \cdot m^{-3}$

cosh, sinh, tanh = hyperbolic functions
D = diffusizity of CO_2 in the liquid phase, $m^2 \cdot s^{-1}$
Ha = Hatta number, dimensionless
k_{OH} = 2nd-order rate constant of the reaction (2.2), $m^3 (mol \cdot s)^{-1}$
k_{Am} = 2nd-order rate constant of the reaction (2.2.a), $m^3 (mol \cdot s)^{-1}$
k_w = pseudo-first order rate constant of the hydration reaction (4), s^{-1}
k = pseudo-first order rate constant of the uncatalysed reaction (2.2), s
k^* = pseudo-first order rate constant of the catalyzed reaction, s^{-1}
k_L = physical mass-transfer coefficient of CO_2, $m \cdot s^{-1}$
r_{ab} = physical absorption rate, $mol (m^2 \cdot s)^{-1}$
r_{CO_2} = reaction rate, $mol (m^3 \cdot s)^{-1}$
r_{ef} = the effective chemical absorption rate, $mol (m^2 \cdot s)^{-1}$
X = distance from the interface, m
δ_L = liquid film thikness, m
Φ = enhancement factor, dimensionless

REFERENCES

1. Danckwerts P. V., Sharma, M. M., The Chemical Engineer, October, 1966, p. 244.
2. Leder F., Chem. Eng. Sci., 1971, 26, 9, p. 1381.
3. Giavarini C., Moresi M., Ing. Chim. Ital., 1981, 17, 3/4, p. 21.
4. Shrier A. L., Danckwerts P. V., I.E.C. Fundamentals, 1969, 8, 3, p. 415.
5. Leites I. L., Karpova Yu. G., *Spravochinik azotchika*, Moskow, Khimia, 1986.

STUDIA UNIV. BABEŞ-BOLYAI, CHEMIA, XXXVI, 1—2, 1991

MEDIUM'S *rH*-A POSSIBLE CRITERION FOR THE INTERPRETATION AND CHARACTERIZATION OF CORROSION PROCESSES

S. IVĂŞCANU, C. V. ZĂNOAGĂ*

ABSTRACT. The article deals with the phenomenon of corrosion in general, showing the advantages of using the „redox gradient-*rH*" instead of the "potential-*pH*" for expressing the corrosive characteristics of an aquaous solution.

Corrosion's dependence on factors like: solution's concentration, temperature, carbon-content (of steels) analysed, also showing some methods of protection of metals used in industry and at structural engineering.

The redox character of a given medium may be quantified both by the redox potential — *pH* pair of data or, — which is much more convenient — by the *rH* parameter.

Special mention must be, nevertheless, made of the caution with which this parameter should be applied, i.e., only in aqueous systems that actually represent the great majority of the cases of corrosion. In such systems, the *rH* parameter takes values ranging between 0 (extremely reducing) and 42.4 (extremely oxidative), the scale having a neutral point at 28.3.

It is generally known that, on the whole, metals corrosion may be considered as a redox heterogeneous reaction, in which — at the metalmedium interface — the metal is oxidized, while the medium is reduced [1]. In this respect, some facts interpreted in this manner may be ediying.

The existence of a redox mechanism on which electrochemical corrosion processes are based has been suggested by [2], who assigned — actually, quite naturally — an oxidative, respectively reductive character to the electrode reactions within corrosion micropiles.

By extension, corrosion may be considered as occurring when different regions of the same part, made of the same metal, are placed in a compositionally uniform electrolyte, yet at different temperatures; as, for the time being, the mechanism is not elucidated we should suggest extrapolation of the phenomenon observed within the biochemical domain; the optimum *rH* for the process is a function of temperature [3] (Fig. 1), which results in two different optimum values, and also in various differences as to the actual *rH* of the medium- in other words, a redox pile.

Within the same phenomenon, when employing copper, contacting a solution of copper sulfate, the cold part is dissolved while, on the warm portion, copper deposits occur [2], which is indicative of an inversely proportional $rH = f(t)$ dependence.

As generally known, redox phenomena are involved in a catalytic process, where the presence of redox systems such as Fe^{2+}/Fe^{3+} exercises a significant influence on the cathodic reaction, of oxygen reduction, through repeated reduc-

* *Politechnical Institute Jassy, Dept. of Chemical Engineering, 6600 Iaşi, Romania*
** *Institute of Biological Research Jassy, 6600 Iaşi, Romania*

tion and oxidation of the respective redox system [1]. Additional mention must be made, too, of the fact that oxygen consumption by wines- that is, their oxidation-, is catalyzed in the presence of Fe and/or Cu [4], which play the above-mentioned catalytic part.

Also, the medium's redox character influences considerably, intercrystalline corrosion of unoxidable steels, the weakly oxidative media facilitating this process in the case of steels with a high carbon content, while highly oxidative media play a similar role for steels with a low carbon content [1].

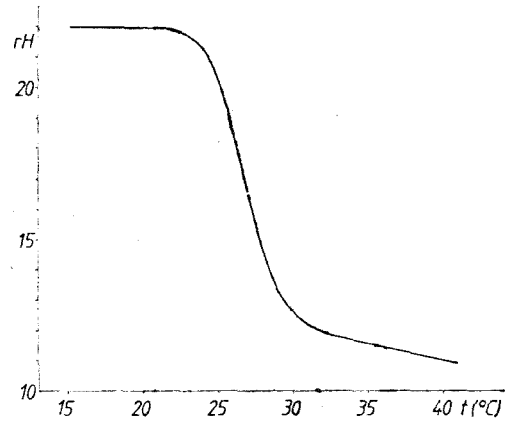

Fig. 1.

Certain amines, employed as absorption inhibitors, become active under cold conditions and inactive under warm conditions [2], which constitutes another reason supporting our demonstration, referring to the existence of a redox mechanism [5] — to be amply discussed in the following — on which their action is based.

The existence of a redox mechanism of electrochemical corrosion is also suggested by the fact that [2] reaching the Flade potential may be achieved, too, by, means of some oxidation agents, and only through anodic polarization with external current supply, which would create an oxidative medium around the metal to be protected. In such a situation, the pigments of anticorrosive grounds will turn the metal passive, due to their oxidative character, which is also the case of zinc chromate or lead minimum [1].

It is known that, in the case of corrosion anodic inhibitors, the nitrate forms corrosion compounds corresponding to higher valency states [2] in parallels with the obvious reverse part played by the nitrite [6], both substances being characterized by an inhibiting effect.

In other words, corrosion occurs within an interval ranging between OX (nitrate) and RED (nitrite) — therefore, an optium of the process is recorded between two inhibition regions, which suggests a Gauss dependence of corrosion's intensity on rH.

Unoxidative inhibitors are efficient only together with the dissolved oxygen [2], thus a new redox phenomenon occurs; more than that, cathodic inhibitors are inefficient in highly acid — therefore oxidative — [7] media [2]; at the same time, some substances play the role of inhibitor in high concentrations and for accelerator of corrosion, too, at low concentrations, while other behave reversely [2]. Such assertions lead to a certain similitude with substances, namely the $rH = f(c)$ spectrum (an exemple is given in Fig. 2 [8], within which various concentrations characterize certain rH values, inducing exactly opposite effects.

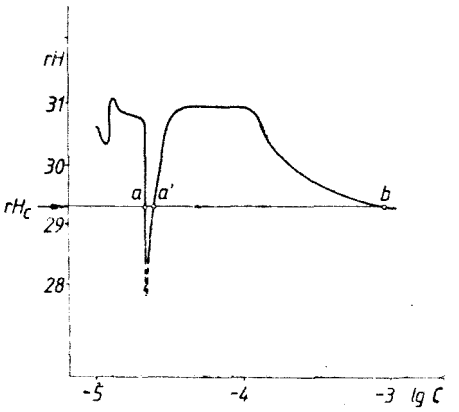

Fig. 2. The spectrum $rH = f(C)$ in the case of 2-chlor, 4-sulphom-amidofenoxyacetic acid, sodium salt. [8]: a certain value of $rH(rH_c)$ can be obtained in this case in three different concentrations (a, a', b).

Consequently, the mechanism is of a redox type, the more so that the molecular structure of the corrosion inhibitors represents an essential element in anticorrosive protecting action [2]; thus, the existence of some rH values' differentiated by concentrations may be discussed, as in the case of the above-mentioned bioactive substances.

Out of the main methods applied in anticorrosive protection, special mention is to be made of:

a) selection of the building material and of the treatments to be applied; b) application of protective layers; c) lowering of the corrosive medium's aggresiv eness; d) electrochemical protection; e) rational selection of the building type [1], direction a, c and d — i.e., the most important ones- involve exploitation of some redox phenomena.

The authors have checked experimentally the influence of the medium's character on corrosion phenomena, in several directions.

Thus, tests performed on the redox mechanism of the anticorrosive action exercised by aminic-type inhibitors, evidenced a Gauss-type dependence of inhibition on the medium's redox character, modulated by the inhibitor's presence (for example- cooper- see Fig. 3) [5].

Metal's corrosion, performed in a rH gradient, obtained by physical means, on employing a fedoxtron device [9], all interferences-except the redox one acting upon the process of corrosion being therefore excluded, evidenced both

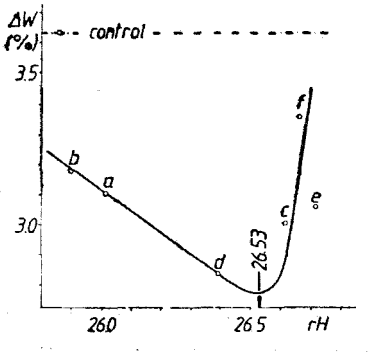

Fig. 3.

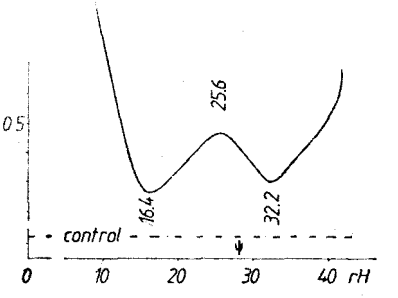

Fig. 4.

Consequently, corrosion occurs at several rH values of the medium, to which products including the metal in various oxidation stages are stable. For example, aluminium's corrosion, (Fig. 4) occurs at $rH < 7$, as a consequence of an $Al \rightarrow Al^-$ (hypothetical) type process, at an rH value of 25.6, following an $Al \rightarrow Al^+$ type process or, finally, at an extremely oxidative rH, following an $Al^+ \rightarrow Al^{3+}$ type process [10].

Resistance to corrosion is attained at an rH reducing value of 16.4 and at a relatively oxidative one (32.2), the latter being specific to natural media (such as water, soil, etc).

On studying plastics' corrosion in an rH gradient, surprising data have been obtained [11]. Thus, the weight variation of some tubes placed in a redoxtron device, in various rH regions (Fig. 5) recorded two peaks, at rH values of 17.5 and 35.0, respectively, which corresponded to the sensitivity zones of PVC and non-polymerized VC, respectively. The lowest of weight variation, i.e., maximum stability, are attained at an $rH \sim 30$, within the range of some usual values recorded in water or soil, as well as at an extreme rH value, which is nevertheless more rarely met.

Both the metal's stability and the nature of the corrosion products depend on both the electrode potential and on the pH of the aggressive medium [1], i.e. — on its rH. The metal/oxidation species equilibrium, plotted graphically as potential-pH diagrams (Pourbaix diagrams) may be interpreted as a function of rH.

Figure 6 represents a simplified Pourbaix diagram of the Fe/water system at 25° [1, 2]. Calculation of the rH-according to Clark's relation for the points plotted in the geometric centers of the diagram's domains (Fig. 7), representing corrosion (c), passivating and immunization (0), respectively, as a function of the rH obtained, leads to some interesting conclusions.

Thus, Fig. 7 represents a generalized case of Fe corrosion in rH gradient; the aspect of the dependence obtained previously on redoxtron (fig. 8) [10] being perfectly superposed on the 10 ... 42 rH domain presented in Fig. 7- More than that, of special interest is the likeness of the curves plotted in Figu. res 7 and 8 with the anodic polarization curve (Fig. 9), which confirms the role played by redox phenomena in metals' passivating.

The dependence of metals' stability on pH (Fig. 10 [12]) may be interpreted as a special case of our experiment on the redoxtron device. On knowing

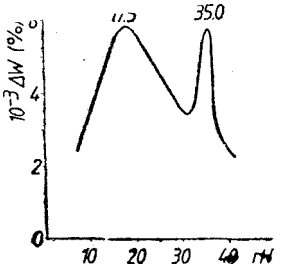

Fig. 5.

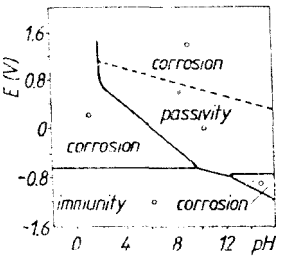

Fig. 6.

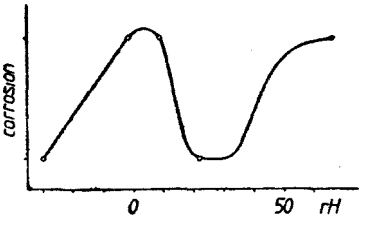

Fig. 7.

that the *pH* is, actually, a peculiar case of *rH*, contributing to *rH* formation in a 66% ratio, the plotted dynamics may be considered as the corrosion speed's dependence on *rH*, yet within an *rH* domain in which extreme values are excluded. Our data on corrosion in an *rH* gradient [9] complete- by the dotted line given in Fig. 10 — those from [2] (the continuous line).

Literature data support the idea that, in corrosion processes accompanied by hydrogen release, the solution's *pH* influences it by modifying the aspect of the hydrogen polarization curve (Fig. 11) [12]. Quite interesting, such modification occurs, too, when modifying the redox character of the corrosive medium [12], which demonstrates once more the specific character of *pH* within *rH* notion, actually the dependence of the reactions of electrochemical corrosion on the medium's redox character.

Pitting corrosion represents one of the most dangerous types of corrosion, both by the fact that it may rapidly penetrate the metallic piece and by its insufficient study and, consequently its predictability.

Pitting corrosion occurs mainly with passivated metals (on local destruction of the passivized layer), but also with chemically resistant steels [12]

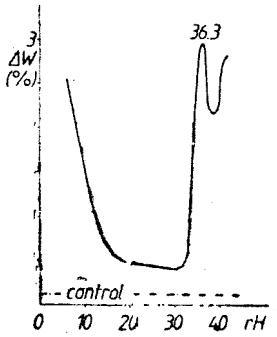

Fig. 8.

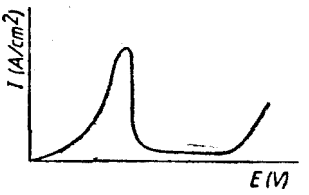

Fig. 9.

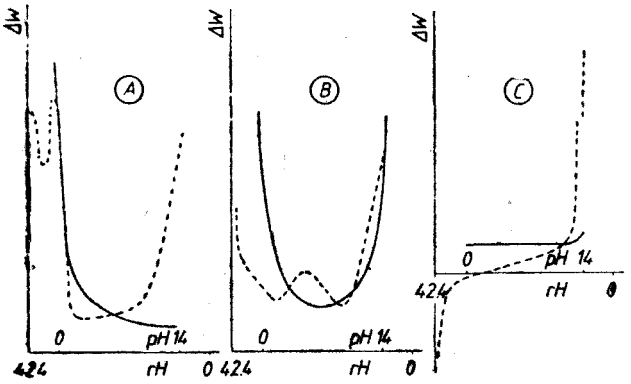

Fig. 10.

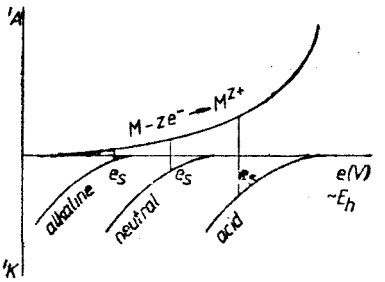

Fig. 11.

when the metal is contacted with aggresive substances, characterized by negative redox potentials (Table 1) [13] (which is a paradox, once knowing that the reduced—instable—form of the metal can be maintained only in a reducing medium). Such media usually contain chlorides, bromides or hypochlorites, corrosion being favoured by the presence of the cations of metals characterized by several oxidation states (such as Fe, Cu, Mg) [12].

Table 1

Substance	Eh (v)
Hypochloric acid	−1,63
$MgCl_2$	−0,91
$FeCl_3$	−0,77
$CuCl_2$	−0,57

Formation of pits (hollows) is accelerated by processes of cold mechanical processing of metals, as by the presence of some inclusions, microsegregations or precipitations on the metal's surface [12], inducing the apparition of a galvanic micropile that may record differeneces of potential of up to 0.5 ... 0.6 *V* [12]. As a matter of fact, one of the methods of preventing such phenomena is the fine processing of the metalic surface [12].

The mechanism of a pit development may be explained as a redox-determined process.

The defects on surface of some non-passivated yet chemically resistant metal (given in Fig. 12) are characterized by the existence of certain initial micro-pits.

At the metal-solution interface, an equilibrium state is observed — from a redox view-point —, between the metal's and the solution's redox potential. The metal being chemically resistant means that it has a redox potential higher to that characterizing the solution, yet these potentials are equal at their interface. The equilibrium is nevertheless attained only within the pit, and not on the smooth surface, directly exposed to the solution, too (a phenomenon also favoured by the known ratio — i.e., 2 : 3 [12] — between the pit's diameter and depth).

The metal-solution equilibration leads to maintaining a higher potentia of the metal at the bottom of the pit than on its (anode, cathode respectively) (Fig. 13), a galvanic micro-pile being thus formed. The thermodinamic condition for the existence of a corrosive process, namely that the cathode's equilibrium potential should exceed the anode's [12], is thus fulfilled.

The passivized metal represents a specific case. Passivation means that the metal is maintained at a higher artificial potential than of the solution's, while, with a discontinuity of the passive film, a pile as the one presented in Fig. 14 appears, the anode being thus dissolved.

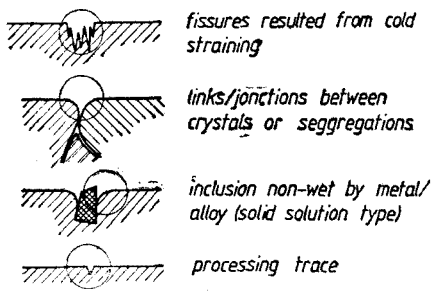

Fig. 12.

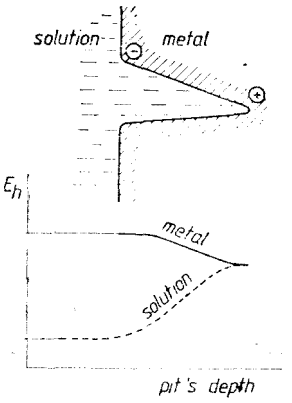

Fig. 13.

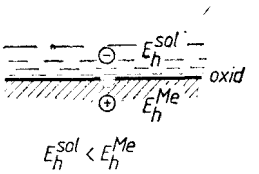

Fig. 14.

The difference of potential between the solution and the pit's bottom increases with the pit's depth, which means that corrosion process is intensified if, naturally, no insoluble corrosion products — to block the pit's lumen — appear. Attaining of a normal pit's size permits the free access of the solution into the pit, therefore, equilibration of the solution's and metal's potentials, which means stoppage of the corrosion process.

In its turn, chemical corrosion may be interpreted in a similar manner (i.e., as having a redox determinism) if considering the pile with solid electrolyte (the oxide separating a metalic from a gaseous electrode).

Although several other aspects involving redox phenomena are still to be studied, the conclusion one may draw is that they play, indeed, a significant part, which recommends them for application in the study of corrosion phenomena, both for testing materials in an *rH* gradient, in view of evidencing the stability regions of certain aggressive medium or for getting additional information upon the treatment of an aggressive medium, following the protection of a given material. To this last end, testing of corrosion inhibitors — as their capacity of redox modulation — is necessary. More than that, the examples we proposed have the advantage of a short duration of the experiment.

REFERENCES

1. Constantinescu, Maria, *Protecţia anticorosivă a metalelor*, Ed. Tehn., Bucureşti, 1979.
2. Oniciu, L., Ivăşcanu, Ş., Apostolescu, Maria, Schmidt, Eugenia, *Coroziunea metalelor. Aspecte fundamentale şi protecţia anticorozivă*, Ed. Şt. Encicl., Bucureşti, 1986.
3. Zănoagă, C. V., Tudose, I. G., Zănoagă, Mădălina, An. St. Univ. Iaşi, XXXIII, s. II a Biol., 1987, p. 95—6.
4. Ribereau-Gayon, J., Peynaud, E., Ribereau-Gayon, P., Sudraud, P. *Traité d'oenologie. Sciences et techniques du vin*, Tom 3, Ed. Dunod, 1976.

5. Zănoagă, C. V., Zănoagă, Mădălina, Paper to The 9th Symposium *Analythical chemistry and quality control*, Brăila, 18—19 May 1989.
6. Drimuș, I., Rev. Coroz., **1**, 1971, p. 47.
7. Zănoagă, C. V., Păun, Camelia, A 14-a sesiune de comunicări științifice. Rîmnicul Vîlcea, 13—15 oct. 1988. Caiet selectiv, sect. II, p. 54—58.
8. Zănoagă, C. V., Mem. sect. șt. Acad. Romane, ser. IV, **IX**, 1, 1986, p. 183—190.
9. Zănoagă, C. V., Păun, Camelia, Filipescu, T. T., Filipescu, Mihaela, Roumanian Patent 103.020.
10. Zănoagă, C. V., Filipescu, T. T., Filipescu, Mihaela, Paper to 10th Symposium: *Activitatea de cercetare din laboratoarele chimice, metalurgice și tehnologice în sprijinul calității și modernizării producției*, Brașov, 6—7 oct. 1988.
11. Zănoagă, C. V., Zănoagă, Mădălina, The 3rd National Congress of Chemistry, București 21—24 sept 1988, Abstracts, vol. **2**, p. 609.
12. Ivășcanu, Ș., Bandrabur, F., Apostolescu, Maria, *Principiile teoretice ale coroziunii metalelor*, Lito, Inst. Politehnic Iași, 1981.
13. Uhlig, H., *Korrozia metalov*, Iz.-vo Metal, Moskva, 1968

STUDIA UNIV. BABEŞ-BOLYAI, CHEMIA, XXXVI, 1—2, 1991

STEADY STATE SIMULATION OF A METHANOL TO HYDROCARBONS CONVERSION EXPERIMENTAL PLANT

TSAKIRIS, C.*, MARIA, G.*, IGNĂTESCU, G.*, MANOLIU, D.*, BOERU, R.*, NATU, N.*, POP, G.*, BOZGA, G**., MUNTEAN, O.**

ABSTRACT. A steady state model of a fluidized bed reactor-regenerator system for methanol conversion to hydrocarbons on a HZSM-5 mixed type (olefins and gasoline products) catalyst is used to simulate the main operating variables effects on the process performances. The model is written using a homogeneous structure hypotheses for the reactor and regenerator fluidized beds and a lumping stoichiometric model for the methanol conversion.

Introduction. The methanol conversion on zeolitic catalysis has become a new way of obtaining hydrocarbons from nonpetroleum sources. A large variety of zeolitic catalysts was prepared to selectively convert the methanol to gasoline, olefins or mixture of olefins and gasoline. A novel process for the straightforward conversion of methanol to gasoline over a ZSM-5 zeolite catalyst has been developed by Mobil Oil Co., commonly referred to as „Methanol to Gasoline" (MTG) process (L i e d e r m a n and others, 1978). In these processes crude methanol such as produced from synthesis gas in the comercially available technology is rapidly and almost quantitatively converted into hydrocarbon mixture. During the process, a slow catalyst deactivation by coke formation and deposition on catalyst inner surface is observed. The main effect of the catalyst deactivation is the change in the products selectivities (P o p and others, 1989). To ensure the continuous removing of the coke, the conversion process is conducted in fluidized bed reactor-regenerator unit. The scheme of such a pilot scale unit is shown in Fig. 1.

During operation, the methanol feed vapors are passed through the distributor and along with an inert diluent (N_2) and a recycle of gazeous products insures the fluidization of the catalyst bed. In the reactor bed, methanol is almost completely converted to a hydrocarbon-water mixture at temperatures in the range 430—470 °C. The methanol conversion being an exothermal process, the heat generated in the reactor is taken off by a cooling system.

The coke content of the catalyst, which amounts in the reactor to 0.7—1.0% (weight), is burnt in the regenerator with air at temperature of 550 to 600 °C.

The mathematical model of the reactor-regenerator unit. The mathematical model consists of the mass and heat balance equations for both reactor and regenerator, written in the hypothesis of perfect mixing of the gas phase and solid catalyst, and homogeneous structure of the bed, verified experimentally by values for the reacting temperature at 4 different heights of the fluid bed, that were almost equal and the small differencies without any tendence up or

* „ZECASIN" SA, 79611, Bucureşti, Romania
** Polytechnical Institute Bucharest, Dept. of Chemical Engineering, 79585 Bucureşti, Romania

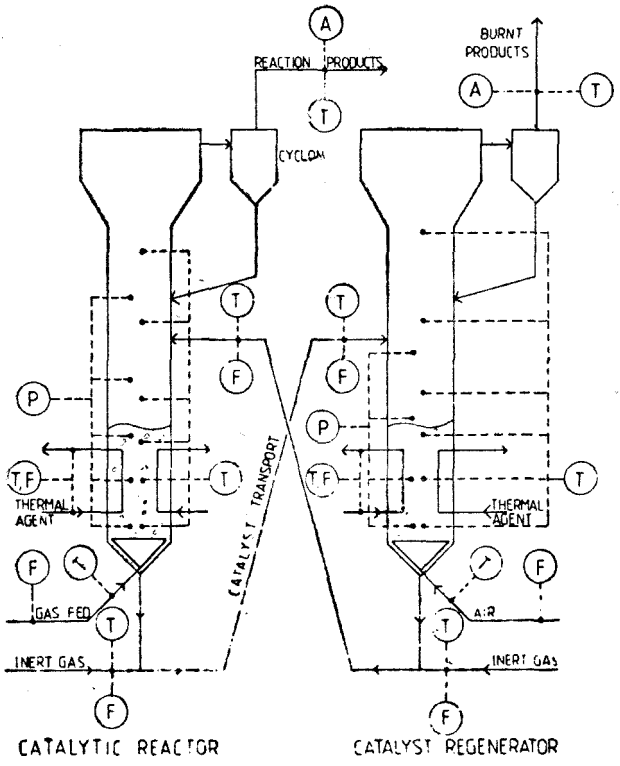

Fig. 1. The Pilot Plant Reactor-Regenerator Unit.

down. It has the advantage to be adequate for computing control of the process, being simpler than the Davidson-Harrison one.

The methanol conversion product contains a large number of hydrocarbons. To simplify the kinetic model, this was conventionally represented by class representatives (olefins, paraffins and aromates). The stoichiometry of the methanol conversion ZSM-5 mixt catalyst is globally described by the following reactions (ZECASIN S. A., 1983):

$$A \rightarrow : CH_2 + H_2O \qquad v_{r_1} = k_1 [A] \qquad (1a)$$

$$: CH_2 + A \rightarrow B + H_2O \qquad v_{r_2} = k_2 [: CH_2] [A] \qquad (1b)$$

$$: CH_2 + B \rightarrow B \qquad v_{r_3} = k_3 [: CH_2] [B] \qquad (1c)$$

$$B \rightarrow D + E \qquad v_{r_4} = k_4 [B] \qquad (1d)$$

A — methanol **B** — olefins D — paraffins **E** — aromates

For $[:CH_2]$ = constant, we find:

$$v_{rA} = k_1[A]\left(1 + \frac{1}{1 + \left(\frac{k_3}{k_2}\right)\frac{[B]}{[A]}}\right) \tag{2}$$

$$\text{and } v_{rB} = k_4[B] - \frac{k_1[A]}{1 + \left(\frac{k_3}{k_2}\right)\frac{[B]}{[A]}} \tag{3}$$

The kinetic constants were determined from a batch laboratory fluid bed reactor and are:

$$k_1 = \exp\left(43.9321 - \frac{28476}{T_R}\right) \quad s^{-1} \tag{4}$$

$$\frac{k_3}{k_2} = 0.47 \tag{5}$$

$$k_4 = \exp\left(4.32259 - \frac{5000}{T}\right) \quad s^{-1} \tag{6}$$

$\Delta H_{RA} = -1.177 \cdot 10^6$ J/kg of reacted methanol (7)

$\Delta H_{RB} = -5.887 \cdot 10^6$ J/kg of reacted olefins (8)

The species mass balance equations in the reactor have the general form:

$$D_{Mj0} - D_{Mj} = f \cdot V \cdot v_{rj} \qquad j = 1, 4 \tag{9}$$

The coke content of the catalyst in the reactor is computed from the empirical equation (ZECASIN A. S. 1983):

$$c = c' + \alpha + \beta t + \gamma t^2) \frac{D_{cat,\,0}}{D_{cat}} \tag{10}$$

where α, β, γ were found out for a given value of catalyst recirulcation rate, $D_{cat\ 0}$. The heat balance for the reactor and regenerator are taken of the same form:

$$Q_G = Q_T$$

where:

$$Q_T = D_{al}\ c_{p,\,al}(T_R - T_{al}) + D_{cat}c_{p.\,cat}(T_R - T_{cat}) + \sum_{i=1}^{3} K_{Ti}S_{Ti}(T_R - T_{Mi}) \tag{11}$$

$$Q_G = f \cdot v \sum_{j=A}^{B} [v_{nj}(-\Delta H_{Rj})] \quad \text{for the reactor} \tag{12a}$$

$$\text{and } Q_G = \frac{c - c'}{T_C} m_{cat}(-\Delta H_R) \quad \text{for the regenerator} \tag{12b}$$

The coke balance for the regenerator:

$$D_{cat}(c - c') = k \cdot y_{\infty} \cdot c' \cdot m_{cat} \tag{13}$$

$$k = 0.19 \cdot 10^9 \exp(-18989/T_{reg}) \ s^{-1} \tag{13a}$$

The cooling system consists of three segments: an external jacket, an internal tubes row immersed in the fluid bed and a thermostated jacket compensator for both cooling and heating purposes.

The global heat transfer coefficients are computed from the following equations:

$Nu = 0.664 \cdot Re^{1/2}Pr^{1/3}$ for air (F l o a r e a & S m i g e l s c h i, 1966) (14)

$$a(1 + Re \cdot \exp[(-0.44 \cdot H/d_t)(c_{pg}/c_{ps})] = h_w d_p/k_g[(1 - f_{mif})(c_{ps}\varrho_s/c_{pg}\varrho_g)]$$

for the fluid bed (Doraiswamy, 1984) (15)

The fluid bed parameters are estimated from the relations (Z E C A S I N, 1983), in order to find out te value for the f · v:

$$u = \frac{D_{vam} - u_{mf}A(1 - f_b)}{A \cdot f_b} \tag{16}$$

$$D_b = \frac{0.61}{H \cdot g^{0.2}}(u - u_{mf})^{0,4}\frac{(H + a_i)^{1.8} - a_i^{1.8}}{1.8} \tag{17}$$

$$f_b = \frac{u - u_{mf}}{u - u_{mf} + 0.711\sqrt{g \cdot D_b}} \tag{18}$$

$$H = H_0\frac{1 - f_0}{(1 - f_b)(1 - f_{mf})} \tag{19}$$

$$V = A \cdot H \tag{20}$$

$$f = f_b + f_{mf}(1 - f_b) \tag{21}$$

Reactor regenerator system steady state simulation. The main independent process variables for the reactor-regenerator system are: the reactor feed flow rate; methanol concentration in the feed; the feed temperature in the reactor fluid bed; the cooling air flow rates for the reactor and the regenerator; catalyst space time in the reactor (or catalyst recirculating flow rate between reactor and regenerator units); regenerating air feed rate and temperature. Using the mathematical model presented (eq. (9) to (17)), the effects of these operating variables on the product mixture composition (conversion process selectivities) and reaction temperature was investigated. To solve the simultaneous nonlinear equations of the model, a succesive iteration method was used, which proved good convergence characteristics.

Numerical example. The main characteristics of the system are presented in Table 1.

Results. In Fig. 2 to 4 are represented the effects of raw methanol liquid flow rate (at constant value of nitrogen flow rate) on the olefins yield, reacting temperature and methanol conversion. The olefins yield presents a minimum due to combined effects of increasing raw methanol feed rate on the total feed flow rate and methanol feed concentration.

From Fig. 4 it can be seen that practically a complete methanol conversion is obtained in all simulations.

Table 1

Operating and material constants

	Value (units)	
	Reactor	Regenerator
Fed flow rate	48.9 (*kg* methanol/*h*)	23 (Nm^3/h) air
Raw material and recycle/inert gas molal ratio	14.7/1	—
Fluid bed height	0.95 (*m*)	1.1 (*m*)
Catalyst recirculation flow rate	40 (*kg*/*h*)	
Catalyst particle density	1100 (kg/m^3)	
Minimum fluidization velocity	0.004 (*m*/*s*)	
Catalyst particle mean diameter	0.09 (*mm*)	
Fluid bed diameter	0.5 (*m*)	0.3 (*m*)
Reactor and ragenerator height	7 (*m*)	

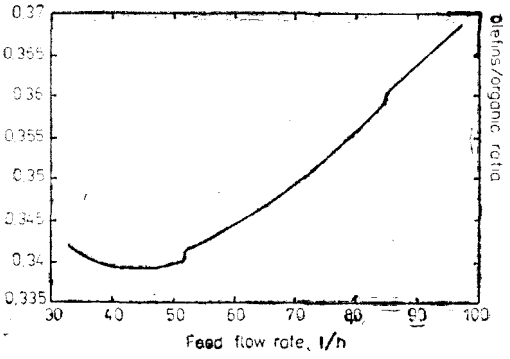

Fig. 2. Effects of raw methanol liquid flow rate (at constant value of nitrogen flow rate) on olefins yield.

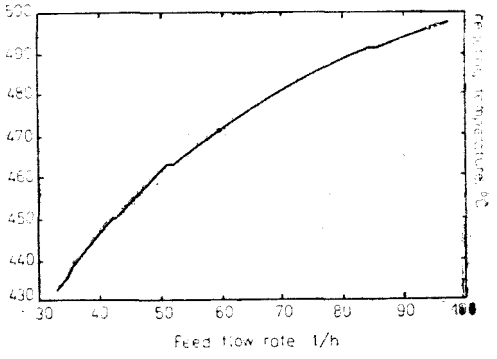

Fig. 3. Effects of raw methanol liquid flow rate (at constant value of nitrogen flow rate) on racting temperature.

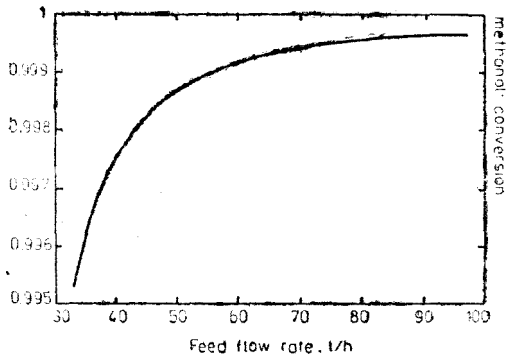

Fig. 4. Effects of raw methanol liquid flow rate (at constant value of nitrogen flow rate) on methanol conversion.

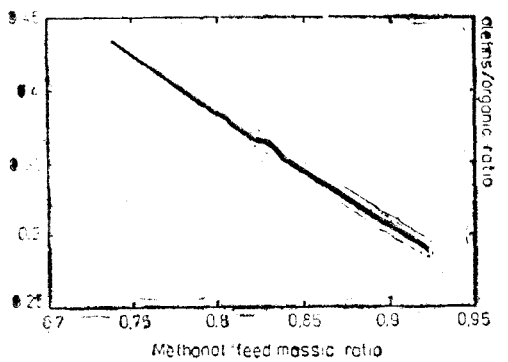

Fig. 5. Methanol feed concentration's effect on olefins yield.

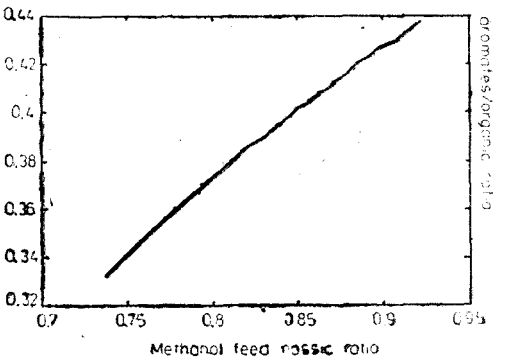

Fig. 6. Methanol feed concentration's effect on aromatics'yield.

Figures 5 to 8 present methanol feed concentration effects on the olefins yield, aromatics yield, methanol conversion and temperature of the catalyst. bed. The increase of methanol feed concentration in the operating range investigated brings to increasing the reaction temperature, higher olefins consumption rate, and consequently the increase of aromatics yield.

The effect of increasing cooling air rate in the reactor on the coke content of the catalyst is shown in Fig. 9. Due to decreasing effect on reacting temperature, the coke content has a decreasing tendence. The consequence of this phenomenon is a decreasing effect on the regenerating temperature and further a decrease of coke conversion in the regenerator (Fig. 10, 11).

The catalyst flow rate affects directly the reaction temperature, being fed at a lower temperature than the catalyst bed. The catalyst feeding temperature is also influenced by the catalyst flow through the amount of coke fed in the regenerator, and consequently the amount of heat generated (Fig. 12, 13).

Reactor total flow rate increasing involves greater amount of organic mass and an increasing production of olefins (Fig. 14, 15, 16).

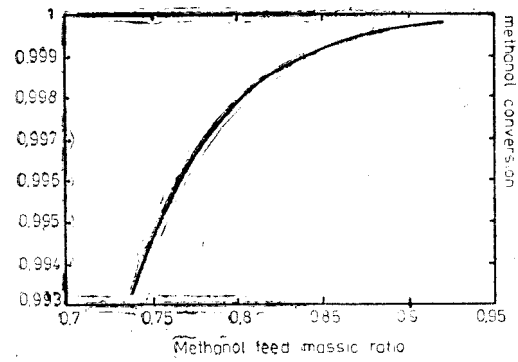

Fig. 7. Methanol feed concentration's effect on methanol conversion.

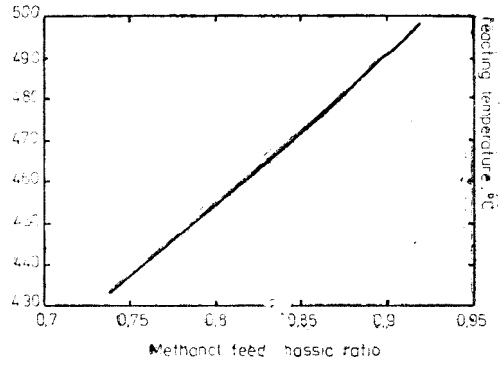

Fig. 8. Methanol feed concentration's effect on the temperature of catalyst bed.

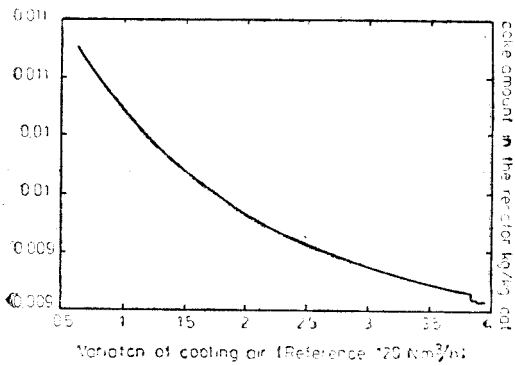

Fig. 9. The effect of the increasing of the cooking air rate in the reactor, on the coke content of the catalyst.

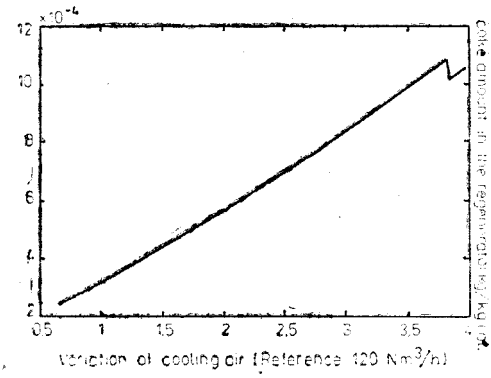

Fig. 10. The effect of the increasing of the cooking air rate on the regenerating temperature.

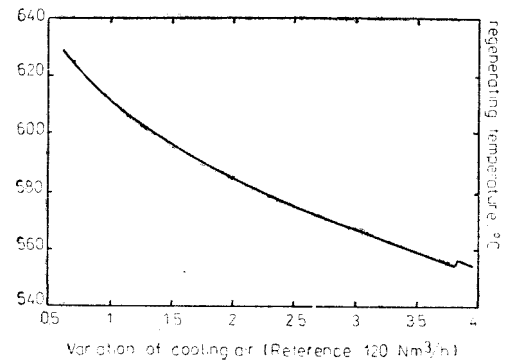

Fig. 11. The effect of the increasing of the cooking air rate on the decreassing of coke conversion in the regenerator.

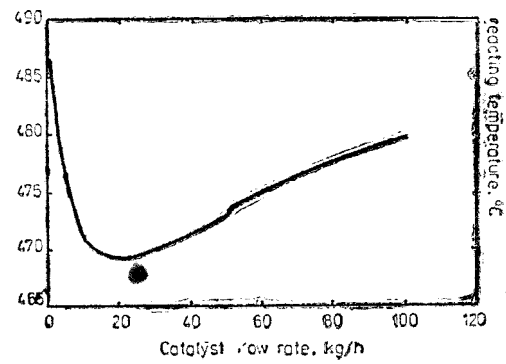

Fig. 12. The effects of the catalyst flow rate on the catalyst feeding temperature.

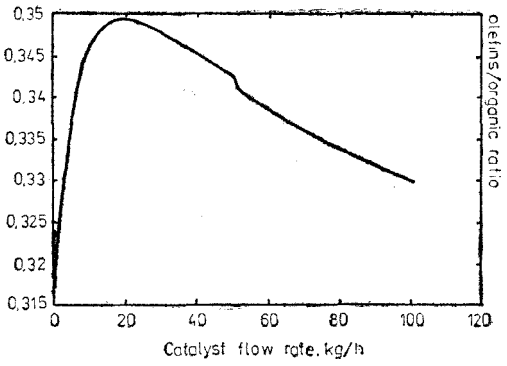

Fig. 13. The effects of the amount of coke in the regenerator (the amount of heat regenerated on the reaction temperature.

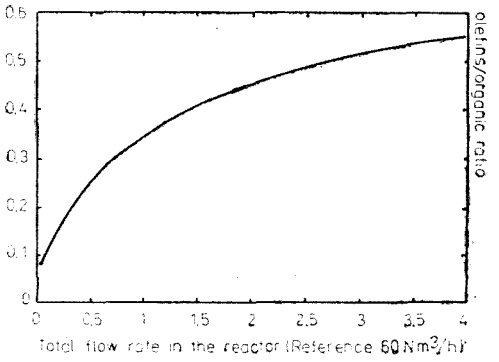

Fig. 14. Effect of the total flow rate increasing on the production of olefins.

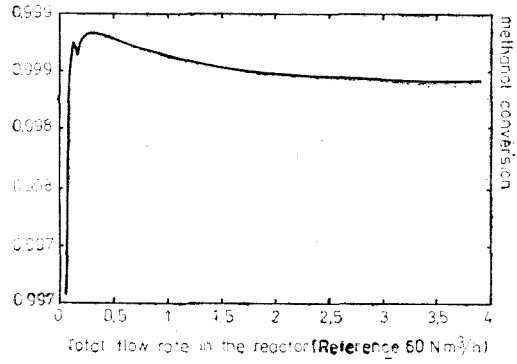

Fig. 15. Effects of the total flow rate on reacting temperature.

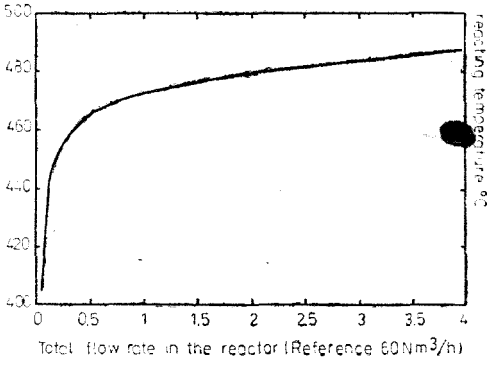

Fig. 16. Effects of the total flow rate on methanol conversion.

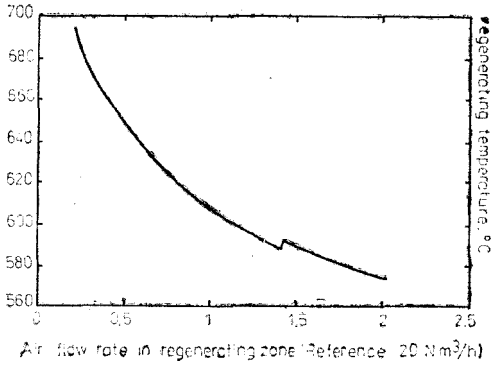

Fig. 17. Effects of the increasing of the air flow rate on regenerating temperature.

Increasing air flow rate in regenerating zone involves a decreasing regeneraton temperature, the additional heat due to burning coke intensification being smaller than the enthalpy necessary for incoming supplementary air (Fig. 17).

Discussion. A mathematical model for the reactor-regenerator system in steady state conditions was written considering the fluid bed being homogeneous. That is in agreement with experiment. Using criterial equations for heat transfer coefficients, the steady point obtained by solving the model equations is close to the practical one. The model allows to pracdict easily the effect of each operating variable on the state ones.

SYMBOLS

a — coefficient depending on Re number;
a_i — constant depending on the distributor of the fluidized agent, m;
c — coke amount in the reactor, kg coke/kg catalyst;
c' — coke amount in the regenerator, kg coke/kg catalyst;
c_{ai} — specific heat for raw material at feed temperature, $J/kg/grd$;
$c_{p,cat}$ — catalyst specific heat, $J/kg/hrd$;
c_{pg} — gas specific heat, $cal/g/grd$;
c_{ps} — solid specific heat, $cal/g/grd$;
D_{al} — liquid feed flow rate, l/h;
D_b — bulb diameter, m;
D_{cat} — catalyst flow rate, kg/s;
D_{Mi} — molar feed flow rate of component j;
D_{vam} — mixture volumetrically flow rate, m^3/a;
d_p — particle diameter, cm;
d_t — reactor diameter, cm;
f — gas fraction of the fluid bed;
f_{mf} — gas fraction at minimum fluidization;
f_b — bulb fraction şf thé fluid béd:
g — acceleration of gravity, m^2/s;
g_j — specie j concentration, $kmoles/kg$ product mixture;
H — fluid bed height, m;
h_w — fluid bed heat coefficient, $cal/(cm^2 \cdot s \cdot grd)$;
k — regeneration kinetic constant, s^{-1};
k_i — kinetic constant for reaction i, s^{-1};
k_g — gas heat conductivity, $cal/(cm \cdot s \cdot grd)$;
K_{Ti} — global heat transfer coefficients, $W/m^2/grd$;
m_{cat} — fluid bed catalyst mass, kg;
Nu — Nusselt number;
Pr — Prandtl numbr;
Q_G — generated heat in the fluid bed, W;
Q_T — transfered heat from the fluid bed, W;
Re — Reynolds number;
S_{Ti} — heat transfer surfaces, m^2;
t — reacting temperature, $°C$;
T_{ai} — feed temperature, K;
T_{cat} — catalyst feed temperature in the reactor, K;
T_{Mi} — mantle temperature, K;
T_R — reacting temperature, K;
T_{reg} — regeneration temperature, K;
u — gas velocity, m/s;
u_{mf} — gas velocity at minimum fluidization, m/s;
v — fluidized bed volume, m^3;
v_{ri} — reaction rate for component j, $kmoles/m^3/s$;
y_∞ — oxygen molar fraction in the regenerator fluid bed;

ΔH_R — regenerating heat, J/kg coke;
ΔH_{Rj} — mass reaction heat for component j, $J/kg\ j$;
ρ_g — gas density, g/cm^3;
ρ_s — solid (catalyst) density, g/cm^3;
T_c — residence time of the catalyst in the regenerator, s.

REFERENCES

1. Chang, C. D., Silvestri, A. J., (1977). *The Convesion of Methanol and Other O-Compounds to Hydrocarbons over Zeolite Catalysts*, Journal of Catalysis. **47,** 249—259.
2. Chang, C. D. (1978). *Process studies on the Conversion of Methanol to Gasoline*, IEC. PDD, **17,** 3, 255.
3. *Chemical engineer handbook* (1969) In Technic (Ed.), **2,** 1471—1863.
4. Doriuswamy, L. K., Sharma, M. M., (1984). In John Wiley & Sons (Ed.), *Heterogeneous reactions*, New-York.
5. Floarea, O., Smigelschi, O. (1966), In Technic (Ed.), *Applications for unit operations and equipment in chemical industry*, 147—150.
6. Iordache, O. (1982). In Politechnic Institute (Ed.), *Mathematical Methods in Chemical Engineering*, Bucharest.
7. Kaeding, W. W. (1980). *Production of chemicals from methanol*, Journal of Catalysis, **61,** 155—164.
8. Kramarz, J., Wyczesany, A. (1990). *Equilibrium restrictions in methanol-to-gasoline conversion*, Hungarian Journal of Industrial Chemistry Veszprém, **18,** 33—42.
9. Liederman, D., Jacob, S. M., Voltz, S. E., Wise, J. J. (1978). *Process variable effects in the Conversion of Methanol to Gasoline in a Fluid Bed Reactor*, Industrial Engineering Chemistry. Process Design and Development, **17,** 3, 340.
10. Mihail, R., Muntean, O. (1983). In Didactic and Pedagogic (Ed.), *Chemical Reactors*, Bucharest.
11. Pop, G., Musca, G., Pop, G., Herghelescu, D., Tomi, P. (1983). *Olefins on alumino-silicates catalytic synthesis domain researches IV. Methanol catalytic conversion on modified synthetic mordenites* Chemical Review, **34,** 4, 293—298, Bucharest.
12. Pop, G., Musca, G., Chirilă, E., Boeru, R., Niculae, G., Natu, N., Ignătescu, G., Straja, S. (1989). *Coke deposits formation and products selectivities for the MTF process in a fluidized bed reactor*, Chemical Engineering Science, **44,** 1, 49—52.
13. Ribeiro, F. R., Rodrigue, A. E., Rollmann, L. D., Naccache, C. (1984). In Martinus Nijhoff Publishers (Ed.), *Zeolites: Science and Technology*, The Hague (Netherlands).
14. „ZECASIN" S. A. (Chemical and Biochemical Energetics Institute Bucharest), *Division of Catalysis* (1983). Internal Technical Report.

STUDIA UNIV. BABEŞ-BOLYAI, CHEMIA, XXXVI, 1—2, 1991

L'ADSORPTION DES GAS EN RÉGIME NONSTATIONNAIRE

PINCOVSCHI E.,* REHNER H.*, UNTEA I.*, LATSOS TH.**

Résumé. On a établi un modèle théorique du processus d'adsorption des gas à pauvre concentration, permetant la représentation des courbes de saturation en système gas-adsorbant. La comparaison du modèle avec les dates expérimentales permete l'évaluation des caractéristiques cinétiques du processus.

Introduction. La pollution de l'atmosphere avec des polluants gaseux (SO_2, H_2S, N_xO_y, etc) exige des mesures de protection sévères. Etant donné le contenu assez faible de ces gas dans les melanges gaseux dégagés en atmosphère, l'adsorption en régime nonstationnaire représente, en ce cas, une méthode de depollution assez efficace. C'est pourquoi le moéle thèorique du processus établi dans le present ouvrage concerne, particulièrèment les gas dilués ($Y_0 < 0{,}005$).

Le modéle théorique. L'adsorption en régime nonstationnaire peut être caractérisée par les équations:

$$X = X(z, t) \text{ et } Y = Y(z, t) \tag{1–2}$$

ou X représente la concentration du gas dans l'adsorbant au moment t, a la distance z.

Y — la concentration du gas polluant en phase gaseuse au moment t a la distance z.

z — la distance parcurue des l'entrée du gas dans la couche adsorbante.

t — le temps.

La quantité du gas, d^2m adsorbée dans l'incrément dz, dans le temps dt peut être définie par les expressions qui suivent:

$$d^2m = V\left[Y - (Y + \frac{\partial Y}{\partial z}\, dz)\right] dt \tag{3}$$

$$d^2m = S\left[(X + \frac{\partial X}{\partial t}\, dt) - X\right] dz \tag{4}$$

$$d^2m = KS(X^* - X)dzdt \tag{5}$$

oú V représente le débit volumétrique du gas.

S — la section transversale de la couche.

K — le coefficient cinétique global

X^* — la concentration du gas dans l'adsorbant á l'équilibre, définie par l'éxpression:

$$X^* = aY \tag{6}$$

oú a représente la constante d'équilibre.

* *Polytechnical Institute Bucharest, Dept. of Chemical Engineering, 79585 Bucureşti, Romania*
** *L'Ecole Superieur de Larissa, Grece*

En considérant les équations (3), (5) et (6) on peut obtenir :

$$\frac{w_0}{K}\frac{\partial Y}{\partial z} = X - aY \tag{7}$$

où w_0 représente la vitesse fictive du gas qui traverse la couche, définie par l'expression :

$$w_0 = \frac{V}{S} \tag{8}$$

De même maniere on obtient, en considérant les relations (4), (5) et (6) :

$$\frac{1}{K}\frac{\partial X}{\partial t} = aY - X \tag{9}$$

En considérant les coordonnées adimensionales

$$\varphi = \frac{Kz}{w_0} \quad \text{et} \quad \tau = Kt \tag{10)—(11}$$

les expressions (7) et (8) deviennent :

$$\frac{\partial Y}{\partial \varphi} = X - aY \tag{12}$$

et

$$\frac{\partial X}{\partial \tau} = aY - X \tag{13}$$

En additionnant (12) et (13) on obtienne :

$$\frac{\partial Y}{\partial \varphi} + \frac{\partial X}{\partial \tau} = 0 \tag{14}$$

En derivant la relation (12) et tenant compte de l'expression (14) on résulte :

$$\frac{\partial^2 Y}{\partial \varphi \partial \tau} + \frac{\partial Y}{\partial \varphi} + a\frac{\partial Y}{\partial \tau} = 0 \tag{15}$$

En considerant les relation (13) et (14) on résulte :

$$\frac{\partial^2 X}{\partial \varphi \partial \tau} + \frac{\partial X}{\partial \varphi} + a\frac{\partial X}{\partial \tau} = 0 \tag{16}$$

Les écuations différentielles (15) et (16) doivent être résolues en considérant les condition d'unicité qui suivent :

Quand $z = 0$ $(\varphi = 0)$ à t variable :

$$Y = Y_0 \tag{17}$$

et

$$\frac{dX}{d\tau} = aY_0 - X \tag{18}$$

Quand $t = 0$ $(\tau = 0)$ à z variable :

$$X = X_0$$

et

$$\frac{dY}{d\varphi} = X_0 - aY \tag{19}$$

où X_0 représente la concentration au moment initial.

La solution générale de l'écuation (15) peut être exprimée par la relation :

$$\frac{X - aY_0}{X_0 - aY_0} = e^{-a\varphi-\tau} \sum_{m=0}^{\infty} \left[\frac{(a\varphi)^m}{m!} \sum_{n=0}^{m} \frac{\tau^n}{n!} \right] \tag{20}$$

De même manière la solution générale de l'écuation (16) peut être exprimée par la relation :

$$\frac{Y - X/a}{Y_0 - X_0/a} = 1 - e^{-a\psi-\tau} \sum_{m=0}^{\infty} \left[\frac{(a\varphi)^m}{m!} \sum_{n=0}^{m} \frac{\tau^n}{n!} \right] \tag{21}$$

Les écuations (20) et (21) peuvent évidentier les caractéristiques dinamiques des couches adsorbantes en régime nonstationnaire à condition que la constante d'équilibre a et la constante cinétiques K, contenues dans les relations (10)—(11), soient connues. La détermination de la constante d'équilibre a est présentée en [1]. La constante cinétique K peut être déterminée en connaissant (pour une vitesse donnée w_0) les valeurs t et z. Le probléme peut être résolu en déterminant expérimentalement la courbe de saturation et en la comparant avec la courbe de saturation théorique, obtenue par la représentation de l'équation (21).

Dates experimentales. Pour déterminer les courbes de saturation en régime nonstationnaire on a utilisé la methodologie présentée en [2] qui permete l'inregistration directe de la courbe $Y - t$. Figure 1 represente les courbes expérimentales de saturation du systeme CO_2-tamis moleculaire 13X obtenues par inrégistration directe dans l'intervale des concentrations initiales Y_0 comprises entre 0,022—0,0561. On peut utiliser ces courbes, pour calculer la zone de transfer de masse, z^0 [3].

La Figure 2 représente une famille des courbes de saturation théoriques obtenues par représentation de l'écuation (21) en coordonnées $\frac{Y - X_0/a}{Y_0 - X_0/a} - \lg \tau$ en considerant les valeurs $(a \cdot \varphi)$ entre 4 et 25.

Pour en faire une comparaison entre les courbes théoriques et celles déterminées expérimentalement on a représenté les dernières dans les mêmes coordonnées (Figure 3). Dans ce cas, étant donné que les déterminaisons expérimentales ont été effectuées en maintenant $X_0 = 0$, le thérme $X/a = 0$.

Discussions. La comparaison des courbes théoriques avec celles expérimentales (voir les figures 2 et 3) suggére la possibilité d'en calculer la valeur de la constante cinétique K, a condition qu'on réalise une superposition satisfaisante

[1] Ici on exprime Y en rapport — molaire

[2] La superposition est un peu „dénaturée" par l'existance d'un „temps mort" propre a l'instalation expérimentale

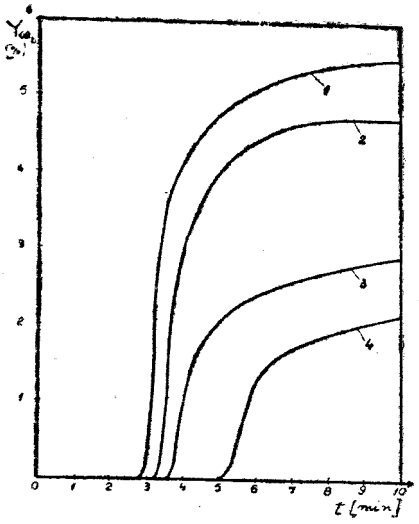

Fig. 1. Courbes expérimentales de saturation du systeme CO_2 — tamis moleculaire 13X. 1 — 5,6 CO_2
2 — 4,7% CO_2
3 — 3,0% CO_2
4 — 2,2% CO_2

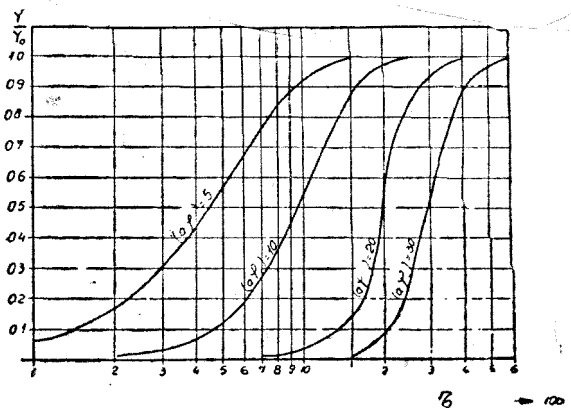

Fig. 2. Courbes théoriques de saturation.

entre les deux courbes (théorique et expérimentale)[2]. Dans l'affirmatif, on utilise l'écuation (10), d'où en résulte K, les autres valeurs de l'écuation (10) étant connues (φ en résulte directement de la figure 2; $z = z_0$ peut être calculé en utilisant les courbes de la figure 1 [3]; w_0 représente la vitesse du gas).

La méthode est tout a fait intuitive, permetant de mêtre en evidence, d'une maniere directe, les possibilités et les limites du model theorique élaboré. L'enrégistration directe des courbes de saturation en régime nonstationnaire, augmente la précision de la mèthode.

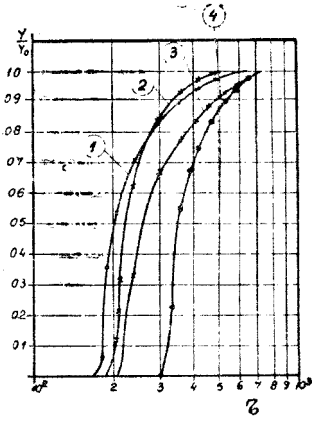

Fig. 3. Courbes expérimentales de saturation en coordonnées$_0$ Y/Y en fonction de ln τ

BIBLIOGRAPHIE

1. Pincovschi E., Rehner H., Untea I., Latsos Th., *Ibidem.*
2. Pincovschi E., Untea I., Rev. Chim., 1991 (sous presse).
3. Serpionova E. N., *L'adsorption industrielle des gas et des vapeurs*, Ed. Moscou, 1969 (russe).

STUDIA UNIV. BABEŞ-BOLYAI, CHEMIA, XXXVI, 1—2, 1991

L'ADSORPTION STATIQUE DES POLLUANTES POLAIRES EN UTILISANT DES TAMIS MOLECULAIRES NaX

PINCOVSCHI, E.*, REHNER, H.*, UNTEA, I.*, LATSOS, TH.**

Résumé. On a déterminé les isothèrmes d'adsorption des gas polaires SO_2, CO_2 and NH_3 dans l'interval des temperatures 25—80°C, en utilisant des tamis moleculaires NaX. On a utilisé les resultats expérimentals pour calculer la constante d'équilibre et la capacité d'adsorption en couche monomoleculaire aussi bien pour verifier l'application de la théorie du Polanyi au systhèmes étudiés.

Les tamis moleculaires NaX sont largement utilisés pour l'adsorption des gas, en particulier de faible et moyenne concentration. C'est pourquoi pour des expériences, le domaine des pressions partielles des gas a été choisi entre 0 et 120 *mm Hg*.

On a obtenu les dates d'adsorption en utilisant un appareil de construction special [1] permetant l'inrégistration directe de la variation de pression du gas durant l'adsorption, y comprie la pression d'équilibre.

Les isothérmes d'adsorbption sont représentées dans les figures 1—3. La forme générale des isothérmes corresponde à l'adsorption en couche monomolecu laire, conformement à l'écuation de l'isothèrme Langmuir [2]:

$$a = a_m \frac{Kp}{1 + Kp} \tag{1}$$

dans laquelle:

a répresénte la concentration d'équilibre dans l'adsorbant, en cm^3/g.

p — pression partielle du gas a l'équilibre, en *mm Hg*.

a — la capacité d'adsorption en couche monomoleculaire en cm^3/g.

K — la constante d'équilibre, en $mm\ Hg^{-1}$.

L'influence marquante de la temperature sur l'état d'équilibre dans le sys tème $NaX—CO_2$ (voir la Fig. 1) atteste le caractère préponderent physique de l'adsoption du dioxide de carbon; ce caractère devient moins pregnant dans le system $NaX—SO_2$ (voir la fig. 2). En ce qui concerne le systeme $NaX—NH_3$ (voir la fig. 3), le groupement étreint des isothèrmes 2, 3 et 4 indique le changement du caractère physique de l'adsoprtion en faveur de celui chimique au fur et à mesure que la temperature augmente.

La position relative, a diverses temperatures, des isothèrmes d'adsorption des systèmes étudiés indique l'accroissement du caractère chimique de l'adsorption en ordre $NaX—CO_2$, $NaX—NH_3$, $NaX—SO_2$, étant en concordance avec l'accroissement du caractère polaire des gas. Dans le même ordre baisse la constante d'équilibre (Tableau 1).

* *Polytechnical Institute Bucharest, Dept. of Industrial Equipments, 79585, Bucureşti, Romania*

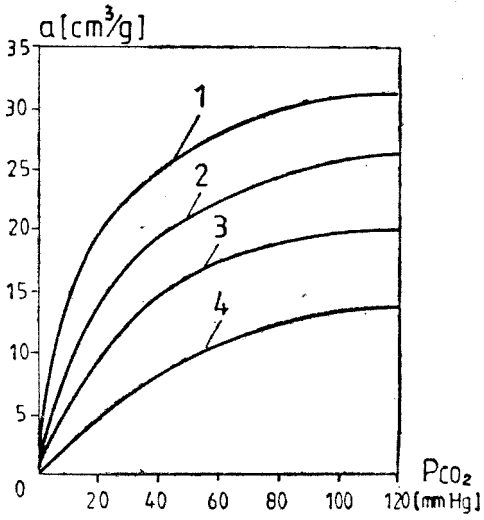

Fig. 1. La variation de la capacité d'adsorption a en fonction de pression partielle p_{CO_2}
1—25 °C ; *2*—40 °C ; *3*—60 °C ; *4*—80 °C.

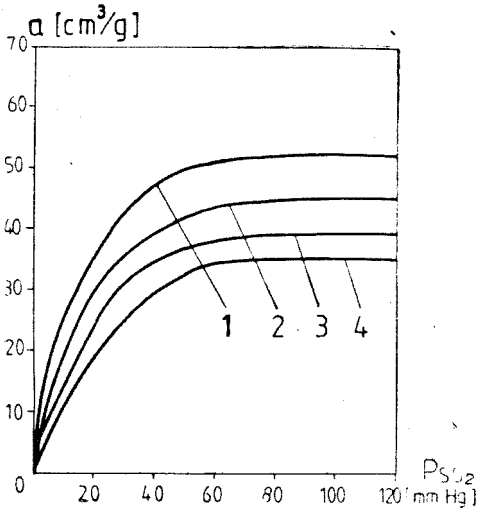

Fig. 2. La variation de la capacité d'adsorption a en fonction de pression partielle p_{SO_2}
1—25 °C ; *2*—40 °C ; *3*—60 °C ; 480— °C.

Tableau 1

La variation des paramètres K et a_m des systèmes NaX—CO_2, NaX—NH_3 et NaX—SO_2 a diverses temperatures.

Temp.	NaX—CO_2			NaX—NH_3			NaX—SO_2		
°C	a_m [cm³/g]	$K \cdot 10^{-2}$ [mm Hg^{-1}]	r coef. de corel.	a_m [cm³/g]	$K \cdot 10^{-2}$ [mm Hg^{-1}]	r coef de corel.	a [cm³/g]	$K \cdot 10^{-2}$ [mm Hg^{-1}]	r coef. de corel.
25	33,04	8,73	0,982	100,63	15,70	0,874	56,92	2,21	0,992
40	29,32	5,63	0,974	79,15	8,09	0,979	55,52	1,51	0,994
60	22,4	3,65	0,918	71,42	7,42	0,975	52,76	1,42	0,995
80	15,42	2,49	0,830	67,38	6,81	0,971	50.09	1,15	0,990

Pour vérifier l'invariabilité, avec le changement de la température, de la courbe caractéristique on a utilisé l'équation de Polanyi [3] :

$$\varepsilon = f(v) \tag{2}$$

dans laquelle :

ε represente le potentiel d'adsorption du système consideré.

v — le volume du gas adsorbé (considéré en phase liquide).

L'independence de temperature de la courbe caractéristique est exprimée par l'écuation :

$$\frac{d\varepsilon}{dT_{(v=et)}} = \text{constante} \tag{3}$$

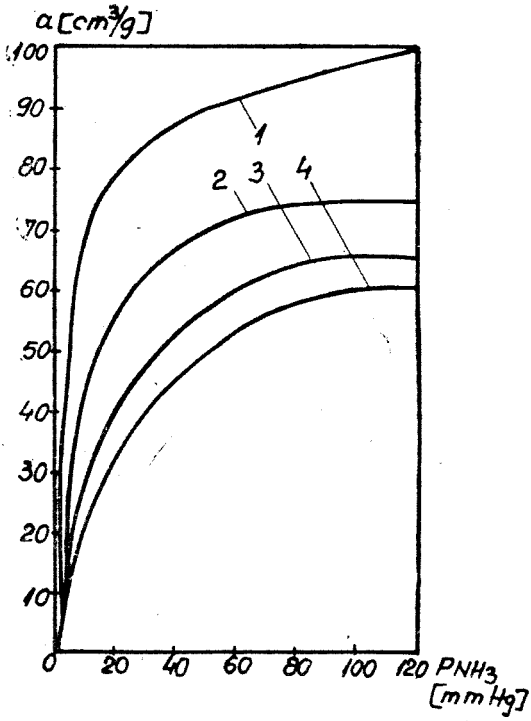

Fig. 3. La variation de la capacité d'adsorption a en fonction de pression partielle p_{NH_3}. 1—25 °C; 2—40 °C; 3—60 °C; 4—80 °C.

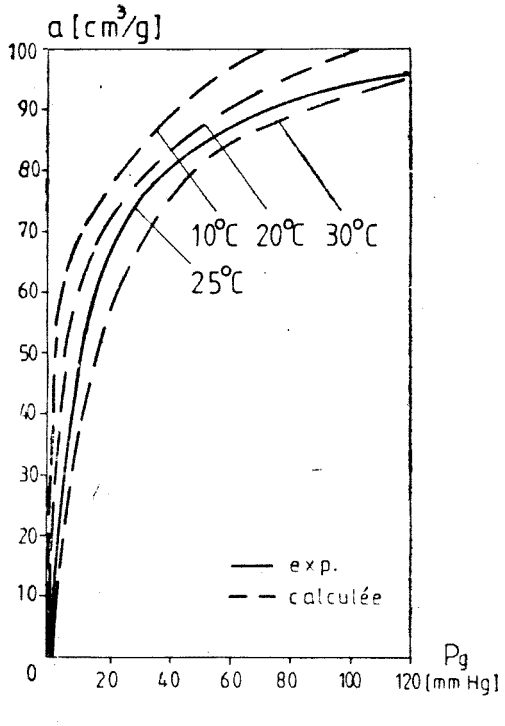

Fig. 4. La variation de la capacité d'adsorption a en fonction de pression partielle p_{NH_3}

Le potentiel d'adsorption ε est défini par l'équation:

$$\varepsilon = RT \ln \frac{p_s}{p} \tag{4}$$

dans laquelle p_s represente la pression de vapeur du gas liquefié à la temperature T; p — la pression partielle, correspondente au volume v du gas adsorbé. En considérant les équation (3) et (4) on peut écrire:

$$\varepsilon_{1(0)} = RT_0 \ln \frac{p_s(0)}{p_1(0)} = \varepsilon_{1(T)} = RT \ln \frac{p_s(T)}{p_{1(T)}}$$

$$\varepsilon_{2(0)} = RT_0 \ln \frac{p_{s(0)}}{p_{2(0)}} = \varepsilon_{2(T)} = RT \ln \frac{p_{s(T)}}{p_{2(T)}} \tag{5}$$

$$\varepsilon_{i(0)} = RT_0 \ln \frac{p_{s(0)}}{p_{i(0)}} = \varepsilon_{i(T)} = RT \ln \frac{p_{s(T)}}{p_{i(T)}}$$

où l'index 0 se rapporte à la temperature de référence T_0, c'est à dire à la temperature pour laquelle on connaît l'alure de l'isothèrme éxpérimentale.

A titre d'exemple on a utilisé les équations (5) pour détérminer les isothèrmes d'adsorption du systhème $NaX-NH_3$ aux temperature de 10°C, 20°C et 30°C, en utilisant les dates de l'isothèrme éxpérimentale à 25°C (figure 4). La position relative de ces isothèrme en rapport de l'isothèrme éxpérimentale à 25°C, indique que, en certaines limites[1], l'équation de Polanyi peut être utilisée pour caractériser les diverses systèmes gas-adsorbant [4].

Les isothèrmes détérminées expérimentalement dans le présent ouvrage peuvent être utilisées pour la calculation de la force motrice d'adsorbtion en régime stationnaires [5].

LITERATURE

1. Pincovschi E., Untea I., *Appareil pour la determination continue de la variation de pression*, Rev. Chim. (sous presse).
2. Langmuir I., Z. Anorg. Chem., 46, 1933, 719.
3. Polanyi, M., Trans. Faraday Soc., 28, 1933, 316.
4. Cruceanu M., Popovici E., Balbă N., Vlădescu L., Russu R., Vasile A., *Tamis moléculaires zeolitiques*, Ed. St. et Enciclop. Bucureşti, 1986 (roum).
5. Serpionova E. N., *L'adsorption industrielle des gas et des vapeurs*, Ed. Moscou, 1969 (russe)

[1] Au fur et à mesure que la tempèrature augumente, les ècuations (5) deviennent moins prècises pour les gases liquefiès.

STUDIA UNIV. BABEŞ-BOLYAI, CHEMIA, XXXVI, 1—2, 1991

RHEOLOGIC CONSTANTS OF CERTAIN BIOLOGIC MATERIALS

Gh. IORDACHE,* Gh. MENCINICOPSCHI, Gh. ENE**, TEODOR SIMA***

ABSTRACT. Rheograms (shearing stress depending on rheoslopes, $\tau - R$) for a biologic material mentioned in the paper, were drawn using a capillary viscosimeter. The constants, m and ν, were established from Ostwald — de Waele relation, necessary for projecting extruders for the materials under examination.

1. **Background.** The projection of screw-cylinder couple for a screw-extruder for plastic-state materilas (polymer materials, ceramic pastes, food pastes, etc.) could not be done without knowing the material features. There are many more mathematical models trying to mould different types of non-Newtonian material behaviour [1—8]. Among these, in view of the engineering calculations linear theories or theories liable to be linearized called specialists' attention on [2, 9, 10]. As for viscoelastic-type materials, Ostwald — de Waele empiric relation was quite often used [1—3, 11, 12]:

$$\tau = mR^{\nu} \tag{1}$$

where τ is the shearing stress; R is the rheoslope (shearing speed) m and ν are material constants. The relation is accepted due to the low number of constants to be determined and good results obtained practically by its application.

These constants can be determined from the rheogram taking the shearing stress as coordinates depending on the rheoslopes by means of the experimental determinations on capillary rheometer. [1, 13].

2. **The equipment used** In view of constant determination from the relation (1), there was used a capillary viscosimeter (Figure 1).

Capillary cylinder is shown in Figure 2. In the metal cylinder **1** the polytetrafluor-ethylene, barrel-shaped piston **2** runs lowering the limit of its friction with the cylinder wall. The material pressed by the piston is discharged by the capillary **3** having a cone-shaped inlet permitting the material input into the capillary. A polytetraflour-ethylene socket **4** was also put in view of friction lowering at the upper part. The geometric features of the capillary used during the experiments are shown in Table 1.

Table 1

No	Diameter, D *cm*	Length, L *cm*	L/D Ratio
1	0.6684	2.9964	4.482
2	0.4907	3.0148	6.143
3	0.506	2.0095	3.964

* *Polytechnical University Buchaest. Dept. of Jndustrial Equipment*
** *Institute for Food Chemistry, Bucureşti, Romania*

The geometric features of the capilalry have to be known accurately and that is why their measuring was done by optic means. From the capillary set, there were chosen those that permitted the determination accurately the material flow and in this case the L/D ratio does not require any alterations of the results [13, 14].

3. **Calculation elements.** The relations of shearing stress and rheoslopes calculations are [15, 16]

$$\tau = \frac{D \cdot \Delta p}{4L} \tag{2}$$

$$R = \frac{32 \cdot \delta_v}{\pi D^3} \tag{3}$$

where Δp is the pressure drop in the cylinder, daN/cm^2, Q_v is the material flow by capillary, cu cm/s.

The pressure drop of the material in the cylinder is given by the weight pressing.

$$\Delta p = \frac{G}{A_p} \tag{4}$$

where G is the weight pressing the piston, daN; A_p is the inner cross-sectional area, cm (inner diameter of the cylinder is 1.4 cm).

Gravimetric flow was measured by the material quantity within a certain range of time (time—checked). The volume flow was calculated by the material density determination ($\rho = 1.625\ g/cm^3$) according to the relation

$$Q_v = \frac{Q_G}{\rho} \tag{5}$$

4. **Material features.** The material subjected to the trials was composed of edible yeast micellium biomass, glucosisomerase biomass and biomass — compressed yeast (Saccharomyces cerevisiae).

The trials were developed at the room temperature (without thermo-regulation).

5. **Experimental results.** The pressures in the cylinder for the weights used are shown in Table 2.

Table

G, kg	1.698	2.648	3.748	4.798	5.748
Δp, daN/cm^2	1.1030	1.7201	2.4347	3.1168	3.7339

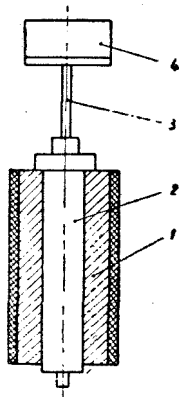

Fig. 1. Scheme ofthe capillary viscosimeter: 1 — thermostating body; 2 — capillary; 3 — piston; 4 — weights for material pressing.

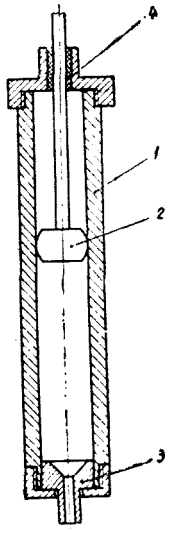

Fig. 2. Scheme 2 of the capillary cylinder: 1 — metal cylinder; 2 — barrel-shaped piston; 3 — capillary; 4 — polytetraf-luor-ethylene socket.

The results shown in Table 3 were obtained using the viscosimeter and the above-mentioned method.

Table 3

No	used Capillary (Table 1)	G, g	G_{enzime} g	t, e	Q_G, g/s	Q_v, cm^3/s
1		1698	1.1	90	0.01222	0.0075213
2	1	2648	2.6	30	0.08666	0.0533329
3		3748	9.3	8	1.1625	0.715384
4		1698	0.8	90	0.008888	0.005470
5		2648	1.0	30	0.03333	0.020512
6	2	3748	1.4	15	0.093333	0.057435
7		4798	2.4	10	0.2400	0.14769
8		5748	10.9	6	0.81666	1.117948
9		q698	1.5	10	0.036585	0.0022514
10	3	3748	5.7	15	0.3800	0.233846
01		4798	19.3	10	1.9300	1.187692

The results shown in Table 4 pointing out the shearing stress and the rheoslope were obtained using the relations (2) and (3) and the values enlisted in Tables 1, 2, 3.

Table 4

No	Q_v, cm^3/s	Δp, daN/cm^2	τ, daN/cm^2	$\mathcal{R}$ s^{-1}
1	0.0075213	1.1030	0.0615109	0.2565545
2	0.053324	1.72017	0.0959285	1.8192239
3	0.715384	2.43470	0.1357757	24.402279
4	0.00547003	1.1030	0.0448820	0.471565
5	0.0205126	1.72017	0.0699953	1.768369
6	0.0574357	2.43470	0.0990702	4.51456
7	0.1476923	3.11684	0.1268270	12.73238
8	1.117948	3.73396	0.1519386	96.37705
9	0.0022514	1.1030	0.0694349	1.770119
10	0.2338846	2.4347	0.1532667	18.38564
11	1.1187692	3.11684	0.1962080	93.37970

The results shown in Table 4 were used for drawing up the rheograms $\tau - R$ (Figure 3).

6. **Conclusions.** Studying the curves in Figure 3, we notice that the above-mentioned material, at low values of the rheoslope, behaves as a pseudoplas- tic liquid [17] (up to 20 s^{-1}).

At higher values of the rheoslope, its behaviour becomes linear.

The most complete result was obtained for the capillary having $L/D = = 6.143$.

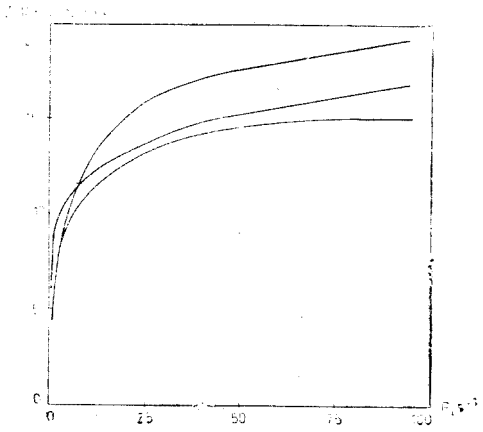

Fig. 3. The rheogram $\tau - \mathcal{R}$

7. **Determination of material constants.** In view of material con stant establishment, the obtained curves will be used (Figure 3).

The work rheoslopes in the screw extruder are located, in the case of the above-mentioned material, between 5 and 25 s^{-1} as shown in the Figure. The first part of the curves corresponds to a slow flow at a low pressure, that does not develop pressure necessary for the product to be pushed through the graining sieve (at the extruder). The rheoslope zone above 25 s^{-1} corresponds to a fast flow that does not allow the control over the graining process as high shearing stress above the critic values could appear resulting in material tearing out and, thus, a low quality product [18, 19].

Material constants in Ostwald — de Waele [relation (1)] remain unchanged except of some areas of the rheoslope.

In view ot the obtainment of the two constants, the relation (1) is logarithmed and thus:

$$\ln \tau = \ln m + \nu \ln \mathcal{R} \tag{6}$$

Using the two points on the curve the following can be written

$$\ln \tau_1 = \ln m + \nu \ln \mathcal{R}_1 \tag{7}$$

$$\ln \tau_2 = \ln m + \nu \ln \mathcal{R}_2 \tag{8}$$

The two relations are subtracted and thus

$$\ln \tau_2 - \ln \tau_1 = \nu(\ln R_2 - \ln \mathcal{R}_1) \tag{9}$$

or

$$\nu = \frac{\ln (\tau_2/\tau_1)}{\ln \mathcal{R}_2/\mathcal{R}_1} \tag{10}$$

The value of constant m is obtained by introducing the value of ν in the relation (7) or (8).

In our case, as for the three curves, the values shown in Table 5 are obtained on the area taken into account.

Table 5

L/D	τ_1 daN/cm^2	R_1 s^{-1}	τ_2 daN/cm^2	R_2 s^{-1}
4.482	0.109	5	0.137	25
6.143	0.105	5	0.140	25
3.964	0.130	5	0.168	25

If we apply the relations (10) and (11) to the data in Table 5, there were obtained the results shown is Table 6.

Table 6

L/D	m, $daN \cdot s/cm^2$	ν
4.482	0.086722	0.142057
6.143	0.078750	0.178747
3.964	0.100595	0.159328

8. **Final conclusions.** The determined constants enable the calculation of the main parameters (flow, working pressure, power demand) of the screw-cylinder couple of the screw extruder. Thus the material constants being known from Ostwald-de Waele relation enable the design of the active couple of this type of machine (including the strength calculation of this couple compounds).

REFERENCES

1. Skilland, A. H. P., *Non-Newtonian Flow and Heat Transfer*, John Wiley and Sons. Inc., New-York—London—Sidney, 1967, p. 52.
2. Middleman, S., *The Flow of Polymers*, John Wiley, New York—London—Sidney—Toronto, 1968.
3. Iordache, Gh., Materiale plastice, vol. **6**, nr. 5, 1969, p. 275.
4. Barrey, B. W., Grace, A. J., Rheologica Acta, vol. **10**, nr. 1, 1971, p. 113.
5. Cleman, B. D., Noll, W., Rev. Mod. Phys., vol. 33, 1961, p. 239.
6. Lodge, A. S., *Elastic Liquids*, Academic Press, London—New York, 1964, p. 231.
7. Harris, J., Rheologica Acta, vol. **11**, nr. 2, 1972, p. 145.
8. West, G. H., Rheologica Acta, vol. **9**, nr. 4, 1970, p. 554.
9. Oroveanu, T., *Mecanica fluidelor viscoase*, Ed. Academiei României, Bucureşti, 1967, p. 30.
10. Haraskoe, D., Reher, E. O., Plaste und Kautschuk, vol. **17**, nr. 5, 1970, p. 318.
11. Ly, B. P., Bellet, D., Bousquet, A., Rheologica Acta, vol. **14**, nr. 9, 1975, p. 783.
12. McKelvy, J. M., *Polymer Processing*, Ed. John Wiley and Sons Inc., New York—London, 1962, p. 32.
13. Van Wazer, J. R. Lyons, J. V., Kim, K., Collwel, R. F., *Viscosity and Flow Measurement*, Ed. John Wiley, New York—London, 1963, p. 15.
14. Iordache, Gh., Studii şi cercetări de chimie, tom. **19**, nr. 7, 1971 p. 797—810.
15. Iordache, Gh., *Materiale plastice*, vol. **7**, nr. 4, 1970, p. 172—178.
16. Iordache, Gh., *Materiale plastice*, vol. **8**, nr. 5, 1971, p. 256—261.
17. Renert, M., *Calculul şi construcţia utilajului chimic*, vol. **II**, Ed. Didactică şi Pedagogică, Bucureşti, 1971, p. 409.
18. Mihail, R., Goldenberg, N., *Prelucrarea materialelor plastice*, Ed. Tehnică, Bucureşti, 1963, p. 331.
19. Iordache, Gh., Buletinul IPB, tom. **XXXVI**, nr. 2, 1975, p. 35—40.

STUDIA UNIV. BABEŞ-BOLYAI, CHEMIA, XXXVI, 1—2, 1991

MONTE-CARLO SIMULATION OF SHORT-RANGE ORDER IN MONOATOMIC AMORPHOUS SEMICONDUCTORS

M. ANDRECUŢ*, I. BURDA*, C. ANDRECUŢ**

ABSTRACT. In this paper we propose an algorithm for generate clusters by using probabilistics methods of simulation (Monte-Carlo). The structure is random generated in a sequential process. At the each step we estimate the radial distribution function (RDF) of the new structure and we make a comparison with experimental RDF. Finally we prove that the sequence of calculated RDF is convergent to the experimental RDF. The proposed algorithm was applied to RDF of amorphous semiconductors (arsenium and germanium).

1. **Introduction.** The existence of short-range order in amorphous solids was proved by elastic scattering (diffraction) of X-rays and neutrons studies.

It was proposed by Bernal [1] three parameters for define the spacial distribution of atoms, they are: the mean number of neighbours of an atom, the mean distance of these atoms from a fixed atom and the fluctuation of this distance.

The structural model of Bernal is starting from the experimental information about structure contained in the radial distribution function wich results from the interpretation of diffraction images and which in essence is the expresion of finding two atoms at distance r from each other.

In this paper we shall give an algorithm for generate clusters by using probabilistics methods of simulation (Monte-Carlo), which finally seemes to be a good aproximation for experimental radial distribution function.

The proposed method of computation was applied to: amorphous arsenium and amorphous germanium.

2. **The radial distribution function (RDF).** Let us consider two concentric spheres with radii r and $r + \mathrm{d}r$ centratd on an atom. The volume of this spherical shell will be $\mathrm{d}F = 4\pi r^2\,\mathrm{d}r$ and the probability of finding one atom in this spherical shell is:

$$\mathrm{d}P(r) = 4\pi r^2 g(r)\mathrm{d}r/V \tag{1}$$

where V is the volume occupied by amorphous solid and $g(r)$ the radial distribution function, with the normalization condition given by:

$$\int_0^\infty g(r)\,4\pi r^2\,\mathrm{d}r/V = \int_0^\infty \mathrm{d}P(r) = 1 \tag{2}$$

If $\langle N(r, r + \mathrm{d}r\rangle$ is the mean number of atoms falling within the spherical shell and $\rho(r)$ the atomic density in the same spherical shell, then we have:

$$\rho(r) = \frac{\langle N(r, r + \mathrm{d}r\rangle}{\mathrm{d}V} : \langle N(r \cdot r + \mathrm{d}r\rangle = 4\pi r^2\rho(r)\,\mathrm{d}r \tag{3}$$

* *University Babeş—Bolyai, Dept. of Physics, 3400 Cluj-Napoca, Romania*

** *„CEROC" SA, 3400 Cluj-Napoca, Romania*

The radial distribution function defined by $f(r) = 4\pi r^2 \rho(r)$ respects the following normalization condition:

$$\int_0^\infty f(r)\,\mathrm{d}r = N - 1 \cong N \tag{4}$$

Using equation (2) and (4) results: $f(r) = 4\pi r^2 \rho_0 g(r)$ where $\rho_0 = N/V$ is the mean density.

The practical problem is to get from the experimental information the radial distribution function. This is done by a Fourier transformation of the angular distribution, $I(s)$, of the scattered X-ray intensity (or neutrons):

$$f(r) = 4\pi r^2 \rho(r) = 4\pi r^2 \rho_0 + 8\pi r \int_0^\infty s\,[I(s)\,F^{-2}(s)/N - 1] \sin(2\pi s r)\,\mathrm{d}s \tag{5}$$

where $F(s)$ is the scattering factor for one atom and $s = 2\sin(\theta)/\lambda$ (λ is the wave lenght of radiation).

3. **The Monte-Carlo simulation method.** Usualy the Monte-Carlo method is used like a multidimensional integration procedure in addition to calculus of thermodinamic properties of sistems [2].

Monte-Carlo method can also be used to obtain distribution function [2].

Let us consider the distance between two atoms as a random variable which has the distribution law done by the radial distribution function $f(r)$ normalized with:

$$N_0 = \int_0^{r_m} f(r)\mathrm{d}r \tag{6}$$

where r_m is the upper limit for experimental determination of RDF and N_0 the number of atoms from inside of sphere of radius r_m.
Consequently, the probability of finding an atom at distance:

$$r_1 \in [r, r + \Delta r] \subseteq [0, r_m]$$

will be given by:

$$p(r_1) = \int_r^{r+\Delta r} f(r)\,\mathrm{d}r/N_0 \tag{7}$$

The simulation will be made in a finite volume in wich the upper limit for distance r will be the maximum distance between two points of the volume.

The position of atoms will be generated in a sequential process and the random variable r will have a nonuniform distribution in accordance with $f(r)$.

For generate random numbers with a nonuniform distribution law, usually the Smirnov transformation is used, which states that: if the distribution law $\Phi(\xi)$ of a random variable ξ is done, then a sequence selection will be generate with $\xi = \Phi^{-1}(\alpha)$, where Φ^{-1} is the inverse of Φ and α is a random variable which has a uniform distribution on the interval $[0, 1]$.

Before to describe the algorithm we shall made some important observation.

Thus, in a cluster which has N atoms, for each atom we consider a radial distribution function which we shall note $f_i(r)$, $i = 1, \ldots, N$.

Because in the relation (3), $\langle N(r, r + dr)\rangle$ is the mean number of atoms situated in the spherical shell between distances r and $r + dr$, we shall use the mean value, $f_N(r)$ of function $f_i(r)$, $i = 1, \ldots, N$.

Finally we impose the aproximation of experimental RDF, $f_{exp}(r)$, with the sequence of function $\{f_N(r)\{$ where N tends to N_{max} which is the maximum number of atoms according to the volume V of simulation.

In the volume V there are atoms situated at frontiers with different RDF relative to experimental RDF and which will introduce distorsions in calculus of the mean function $f_N(r)$.

For to eliminate this size effect we do the multiplication of respective function with a weight function which is equal with $N_0/N'(r)$ where $N'(r)$ is the number of atoms from inside of the volume obtained through the intersection between the sphere with radius r_m centrated on the current atom and the volume V in which we do the simulation.

This compensation involve the same normalization constant for all functions $f_i(r)$, $i = 1, \ldots, N$.

In these conditions the algorithm has the following steps:

1) The function $f_{exp}(r)$ is transformated on the interval $[0, r_m]$ in a sequence of pairs:

$$(k\Delta r, f_{exp}(k\,\Delta r)),\ k = 1, \ldots, m,\ \Delta r = r_m/m \quad (m \text{ is fixed})$$

2) The limits of volume V are fixed (for example a cube with edge L).
3) The maximum number of atoms according to V is calculated (N_{max}).
4) The position of the first atom is random generated, the weight function according to it will be calculated, and we make $N = 1$.
5) The position of the atom $N + 1$ is random generated and it's weight function will be calculated.
6) For each $k = 1, \ldots, m$ the functions $f_i(k\Delta r)$, $i = 1 \ldots N + 1$, and the mean function $f_{N+1}(k\Delta r)$ are calculated.
7. At this step we shall made a comparison between $f_{N+1}(k\Delta r)$ and $f_{exp}(k\Delta r)$ if $(\exists)\ k \in \{1, 2, \ldots, m\{$ such that $f_{N+1}(k\Delta r) - f_{exp}(k\Delta r) > \delta$ (δ is fixed) then go to step 5)
8) The relative error in the aproximation of $f_{exp}(r)$ with $\{f_N(r)\{$ is calculated using:

$$\varepsilon_{N+1} = \frac{\int_0^{r_m} [f_{exp}(r) - f_{N+1}(r)]\, dr}{\int_0^{r_m} f_{exp}(r)\, dr}$$

9) If $\varepsilon_{N+1} < \varepsilon_m$ then go to step 5).
10) The variable N is transformated in $N + 1$ and if $N = N_{max}$ then STOP.
11) Contiune with step 5).

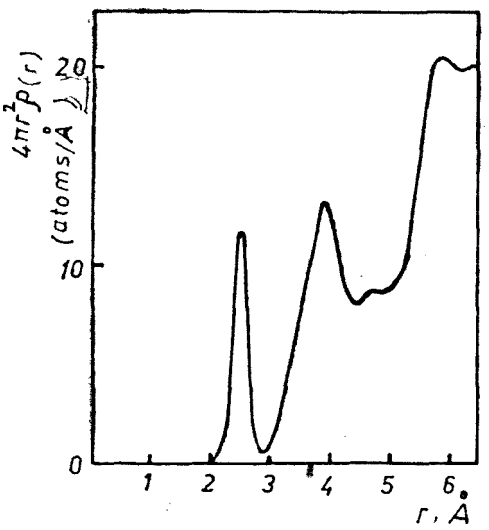

Fig. 1. RDF of amorphous As, experiment, after ref. 3.

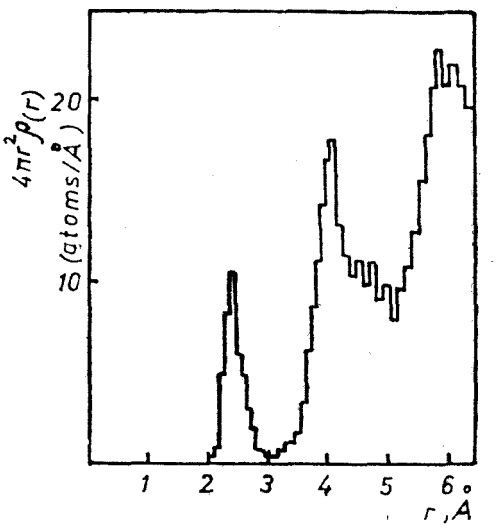

Fig. 2. Computer results for RDF of amorphous As.

About step 6), for calculus of N distribution functions the operation number must be $C_N^2 = N(N-1)/2$ because between N atoms exist C_N^2 distances. This is a problem which involves very much time for calculus.

By using an artifice of programming this bad point was eliminated, thus the number of operations was decreased to N and the time necesarry for calculus is only about few hours for clusters which contained hundreds of atoms (the program was running on an compatbile IBM—AT).

4. **Examples and conclusions.** For example let us take into consideration the cases of amorphous arsenium (a—As) Fig. 1, amorphous germanium (a—Ge) Fig. 3.

Figures 2 and 4 show the results of simulation in this cases.

The aproximation errors are:

— $\varepsilon = 7.5\%$ for a—As obtained with $N_{max} = 254$ atoms and after 525000 iterations.

— $\varepsilon = 7.75\%$ for a—Ge obtained with $N_{max} = 251$ atoms (510000 iterations)

These values for errors involve the conclusions that the described algorithm for Monte-Carlo simulation method is proper to generate structures for amorphous solids.

A better aproximation will be obtained if the volume V and implicit the number N_{max} of atoms will be increase but these will const in computer time.

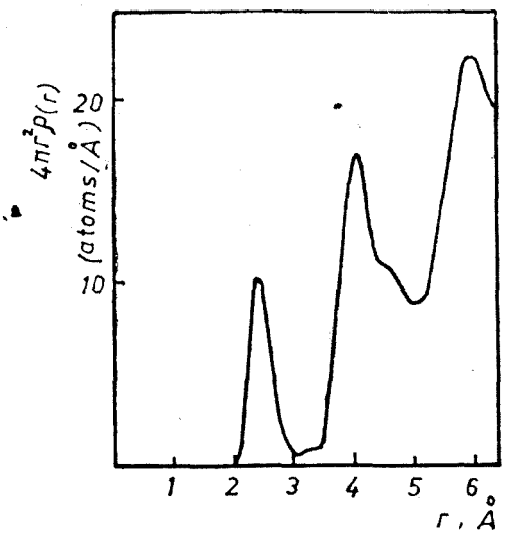

Fig. 3. RDF of amorphous Ge, experiment, after ref. 3.

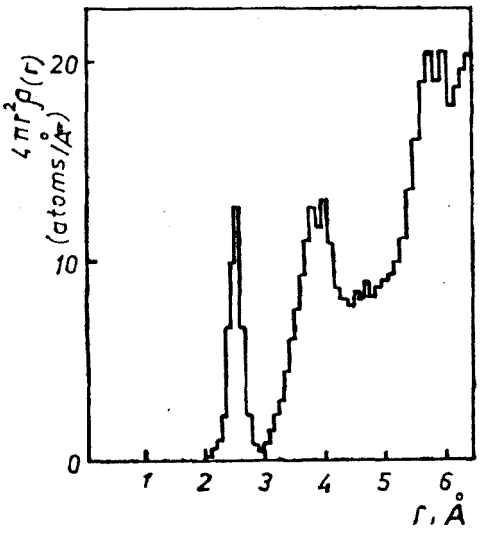

Fig. 4. Computer results for RDF of amorphous Ge.

REFERENCES

1. Bernal, J. D., Nature (London), **68,** 185, (1960).
2. Watts, R. O., McGee, I. J., *Liquid State Chemical Phisycs,* J. Wiley & Sons, 1976.
3. Grigorovici, R., J. Non-Cryst. Solids, **1,** 371, (1969).
4. Lannin, J. S., J. Non-Cryst. Solids., **97—98,** 203 (1987).
5. Brodsky, M. H., *Amorphous Semiconductors,* Springer-Verlag, 1979.

STUDIA UNIV. BABEŞ-BOLYAI, CHEMIA, XXXVI, 1—2, 1991

MODELLING AND SIMULATION OF THE UREA SYNTHESIS PROCESS AT EQUILIBRIUM

ILIE SIMINICEANU*, CORNELIU PETRILA*

ABSTRACT. A new thermodynamic model of the urea synthesis process has been proposed, based on two chemical reactions in the liquid phase:

$$CO_2 + 2NH_3 = NH_2COONH_4$$

$$NH_2COONH_4 = CO(NH_2)_2 + H_2O$$

and on three gas-liquid equilibria:

$$NH_{3(l)} = NH_3$$

$$CO_{2(g)} = CO_2$$

$$H_2O_{(l)} = H_2O$$

The mathematical model allows the prediction of the actual equilibrium liquid-phase composition (x_U, x_{Cb}, x_{CO_2}, x_{NH_3}, x_{H_2O}), the gas-phase composition calculation (y_{NH_3}, y_{CO_2}, y_{H_2O}), and the synthesis pressure evaluation (P), the only independent variables being the synthesis temperature (T) and the input molar ratios NH_3/CO_2 (a) and H_2O/CO_2 (b).

The model adequacy has been tested using our measurement on an industrial-scale synthesis column, as well as the laboratory equilibrium data of Piotroqwski and Szarawara. The simulation of the process has confirmed the capacity of the model to describe correctly the influence of the three parameters on the equilibrium composition and pressure in the following ranges: $t = 170-210\,°C$; $a = 2.0-6.0$; $b = 0.0-1.2$.

1. **Introduction.** Having major applications in agriculture as well as in industry, urea is produced in very large quantities. The world's production capacity was about 10 tons (44 × 10 tons N) in 1989 [1]. The existing commercial processes are all based on the urea synthesis from ammonia and carbon dioxide. Although the urea production capacity has been dramatically increased in the last three decades. the theoretical bases of the urea synthesis process are not yet clearly defined. This becouse the urea synthesis is one of the most difficult chemical processes.

● It is difficult, firstly, becouse of its complex stoichiometry implying the main reactions (1) and (2) in the liquid phase, the phase changes (3) to (5), as well as the side transformations (6) to (8) [2,3]:

$$CO_2 + 2NH_3 = NH_2COONH_4 \quad (1)$$

$$NH_2COONH_4 = (NH_2)_2CO + H_2O \quad (2)$$

$$CO_{2(l)} = CO_{2(g)} \quad \ldots\ldots \quad (3)$$

$$NH_{3(l)} = NH_{3(g)} \quad \ldots\ldots \quad (4)$$

$$H_2O_{(l)} = H_2O_{(g)} \quad \ldots\ldots \quad (5)$$

$$2(NH_2)_2CO = NH_3 + NH(CONH_2)_2 \quad (6)$$

$$(NH_2)_2CO = HNCO + NH_3 \quad (7)$$

$$(NH_2)_2CO_{(l)} = (NH_2)_2CO_{(g)} \quad (8)$$

* *Politechnical Institute Jassy, Dept. of Chemical Engineering, 6600 Iaşi, Romania*

● Secondly, the operating conditions are rather severe: pressure of 14.0 to 20.0 *MPa*, temperature of 453 to 473 *K*, and high concentrations ("melt"). As a result, both liquid and vapour phases deviate from ideality.

● In addition, the urea synthesis system has some peculiar properties: azeotropic points, extremal shape of the equalibrium conversion as a function of temperature, extremal dependence of equalibrim pressure on the excess of ammonia.

● Last, but not least, is the impossibility of direst determination of the actual liquid-phase composition at equilibrium. Being measurable only urea, water, ammonia and a "total" carbon dioxide, the following global reaction is usually considered:

$$CO_2 + 2NH_3 = (NH_2)_2CO + H_2O \tag{9}$$

The equation (9) could be regarded as the sum of (1) and (2) when the reaction (2) could be considered complete. Practically, the dehydration reaction (2) does not go to completion (the conversion per pass of the carbamate into urea usually varies from 60 to 75 per cent) and the unconverted carbamate must be decomposed and recycled to the synthesis. Consequently, the equation (9) does not describe the process correctly.

2. **Previous work.** The first method for the equilibrium liquid-phase composition determination of the urea system has been proposed by *Fréjacques*. By defining an equilibrium constant of the reaction (9):

$$K_x = \frac{x_u \cdot x_{H_2O}}{x_{CO_2} \cdot \cdot x_{NH_3}} \tag{10}$$

where in the molar fractions of the "fictitious" components are substituted as functions of the carbon dioxide conversion degree [4],

$$x_{CO_2} = \frac{1 - \eta_{CO_2}}{1 + a + b - \eta_{CO_2}} \; ; \qquad x_{NH_3} = \frac{a - 2\eta_{CO_2}}{1 + a + b - \eta_{exp}} \; ,$$

$$x_u = \frac{\eta_{CO_2}}{1 + a + b - \eta_{CO_2}} \; ; \qquad x_{H_2O} = \frac{b + \eta_{CO_2}}{1 + a + b - \eta_{CO_2}} \tag{11}$$

results:

$$K_x = \frac{\eta_{CO_2}(b + \eta_{CO_2})(1 + a + b - \eta_{CO_2})}{(1 - \eta_{CO_2})(a - 2\eta_{CO_2})^2} \tag{12}$$

where, a and b are the imput molar ratios:

$$a = n^0_{NH_3}/n^0_{CO_2}, \qquad b = n_0 H_2O/n^0_{CO} \tag{13}$$

Using the experimental values of K_x, Fréjacques has prepared a nomograph, based on the equation (12) [5]. This nomograph provides a means of evaluating the equilibrium yield of urea when the operating temperature and the feed molar ratios of reactants are known. But the theoretical yield obtained from this nomograph is always less than the actual yield calculated from industrial-scale

data [4]. That is why, although improved by other authors [6, 7], the semiempirical method of Fréjacques is not recommended today.

Another semiempirical method consists of the direct correlation of the equilibrium experimental data by regresion/8, 10, 11). The most important empirical equations are presented below.

● *Kucheryavyi* [3], using experimental data very similar to those of *Kawasumi* [9], has obtained the equation:

$$\eta_{CO_2} = 0.3428\,a - 0.0177\,a^2 - 0.293\,b + 0.03699\,ab - 0.7428 \times 10^{-3}\,at + 0.9129 \times 10^{-2}\,t - 0.53 \times 10^{-7}\,t^3 + 0.2293 \times 10^{-4}\,P - 1.121 \quad (14)$$

valid in the following ranges of parameters: $a = 2.0 - 6.0$, $b = 0.0 - 1.6$, $t = 170 - 230°C$, $P = 100 - 1.000$ atm.

● *Inoue, Kanai and Otsuka* [10] have proposed another regression equation based on their own experimental data:

$$\eta_{CO_2} = 0.2616\,a - 0.01945\,a^2 - 0.116\,b + 0.0382\,ab - 0.2732 \times 10^{-3}\,at + 1.64 \times 10^{-2}\,t - 1.394 \times 10^{-7}\,t^3 - 1.03 \times 10^{-3}\,bt - 1.869 \quad (15)$$

● *Piotrowski* [11] derived a new equation:

$$\eta_{CO_2} = 0.46365a - 0.018998\,a^2 - 0.2315\,b + 0.02988\,ab - 1.3294 \times 10^{-3}\,at + 1.1243 \times 10^{-2}\,t - 0.55339 \times 10^{-7}\,t^3 - 1.536 \quad (16)$$

based on laboratory measurements carried out in the following ranges of parameters: $a = 2.0 - 6.0$, $b = 0.0 - 1.2$, $t = 170 - 210°C$.

Table 1.

Table 1

Comparison of the semiempirical methods, under the operating conditions: $a = 3.947$ $b = 0.6418$ $t = 190°C$ $P = 20.0\,MPa$

Method	Nomograph		Regression equations			Actual Plant-scale
	Frejacques	Cook	(14)	(15)	(16)	
η	0.635	0.695	0.689	0.712	0.694	0.640

Table 1 presents the values of the carbon dioxide conversion at equilibrium resulting from the existing semiempirical models, for a commercial plant operated at $t = 190°C$, $P = 20.0\,MPa$, $a = 3.947$ and $b = 0.642$. The corresponding actual value of conversion is also presented, in the last column of the table. These results relieve that the industrialscale data are not consistent with the Fréjacques' nomograph. The other semiempirical models give numerical values that differ considerably from each other. In addition, they do not allow the prediction of the complete liquid-phase composition (with carbamate), and give no information on the gas-phase composition.

There are several attempts to describe the combined chemical and phase equilibria of the urea synthesis in the literature [12 15], too. Some of them

are formally correst [12, 15] but, becouse of their simplified assumptions (particularly concerning both phases of the system to be ideal), they do not permit a quantitative analysis of the urea synthesis process at equilibrium.

It is the aim of this paper to present a new thermodynamic model of the urea synthesis process. This model is theoretically substantiated by the recent progresses in the thermodynamics of non-ideal systems [16—18], and experimentally verified with the new experimental data [19, 20].

3. **The Model Development and Testing.** Whether the existing semiempirical model were based on the total liquid-phase reaction (9) alone, the new model assumes that the urea synthesis process is described by the reactions (1) and (2), and the phase changes (3) to (5). The side transformations (6) to (8) are negligible under normal operating conditions. As a result, the process proceeds in a two-phase gas-liquid system, the liquid phase being composed of ammonia, carbon dioxide, water, urea (U), and ammonium carbamate (Cb). The gas phase is composed of ammonia, carbon dioxide and water. Both phases are non-ideal mixtures. According to the phase rule, such system has three degrees of freedom and three independent variables can be arbitrary chosen. It was found that temperature and two concentration variables (a and b) are the most suitable [11, 16].

On the bases of the fundamental assumptions above, the mathematical model is composed of the following equations.

- The definitions of the equilibrium constants of the reactions (1) and (2):

$$K_1 = \frac{(\alpha - \beta)(1 + a + b - 2\alpha + \beta)^2}{(a - 2\alpha)^2(1 - \alpha)} \tag{17}$$

$$K_2 = \frac{\beta(b + \beta)}{(\alpha - \beta)(1 + a + b - 2\alpha + \beta)} \tag{18}$$

- The mole fractions related to the conversion degrees α and β and the molar ratios a and b:

$$x_{CO_2} = \frac{1 - \alpha}{1 + a + b - 2\alpha + \beta}\ ;\quad x_{NH_3} = \frac{a - 2\alpha}{1 + a + b - 2\alpha + \beta}\ ;\quad x_{H_2O} = \frac{b + \beta}{1 + a + b - 2\alpha + \beta} \tag{19}$$

$$x_u = \frac{\beta}{1 + a + b - 2\alpha + \beta}\ ;\qquad x_{cb} = \frac{\alpha - \beta}{1 + a + b - 2\alpha + \beta} \tag{20}$$

- The equations for the calculation of the equilibrium ocnstants as functions of temperature:

$$\text{Log } K_1 = 993.162/T - 2.444 \tag{21}$$

$$\text{Log } K_2 = -969.365/T + 2.768 \tag{22}$$

- The equations of the modified activity coefficients:

$$\gamma_{NH_3} = 4.7895 - 1.6679\, a - 7.2034 \times 10^{-3}\, at + 5.08 \times 10^{-1}\, a^2 + 1.5361 \times \times 10^{-5} at^2 - 3.4357 \times 10^{-2}\, a^3$$

$$\gamma_{CO_2} = 2.5702 - 2.9456 \times 10^{-2}t + 7.338 \times 10^{-5}t^2 + 1.4494 \times 10^{-1}b^2 + + 7.1914 \times 10^{-6}at^2 - 3.4036 \times 10^{-5}bt^2 - 2.3629 \times 10^{-4}a^2t + 3.3555 \times \times 10^{-3}\,abt + 2.9826 \times 10^{-3}a^3 - 8.4403 \times 10^{-2}a^2b$$

$$\gamma_{H_2O} = 55.509 - 0.44264\,t - 2.9217\,b + 4.617 \times 10^{-6}t^3 - 1.1077 \times \times 10^{-}\,at^2 + 9.5049 \times 10^{-5}bt^2$$

Starting from the equilibrium critetion in the transformations (3) to (5):

$$PY_if_i = p_ix_i\gamma_i^0$$

the modified activity coefficients have been defined as $\gamma_i^1 = \frac{\gamma_i^1}{f_i}$ (16)

- The equations of Claussius-Clapeyron type for the partial pressures p_i^0:

$$\mathrm{Ln}\ p^0_{NH_3} = -25.0698/T + 56.321\ \mathrm{Ln}T - 0.26246T + 1.7525 \times 10^{-4}T^2 - - 258.139 \qquad (26)$$

$$\mathrm{Ln}\ p^0_{CO_2} = -2370.26/T - 0.5913\ \mathrm{Ln}\ T - 1.1785 \times 10^{-2}T + 1.5977 \times \times 10^{-5}T^2 + 15.2721 \qquad (27)$$

$$\mathrm{Ln}\ p_{H_2O} = -5231.82/T - 6.1668 \times 10^{-2}\,\mathrm{Ln}\ T - 3.2907 \times 10^{-3}\,T + + 1.222 \times 10^{-6}\,T^2 + 13.1833 \qquad (28)$$

The coefficients of the equation (26) to (29) have been identified by regression, using the existing experimental data [17, 21].

- The total pressure equation:

$$P = \Sigma\, P_i^0x_i\gamma_i, \qquad i = CO_2,\ NH_3,\ H_2O \qquad (29)$$

- The mole fractions of the components in the gas-phase:

$$Y_{NH_3} = p^0_{NH_3}x_{NH_3}\gamma_{NH_3}/(\Sigma p_i^0x_i\gamma_i) \qquad (30)$$

$$Y_{CO_2} = p^0_{CO_2}x_{CO_2}\gamma_{CO_2}/(\Sigma p_i^0x_i\gamma_i) \qquad (31)$$

$$Y_{H_2O} = p^0_{H_2O}x_{H_2O}\gamma_{H_2O}/(\Sigma p_i^0x_i\gamma_i) \qquad (32)$$

The system (17) to (32) correlates the composition of the liquid phase (α, β), the composition of the gas sphase (Y_i) as well as the total pressure (P) as functions of the three independent variables: a, b, and t.

The equations (17) to (32) have been numerically solved by computer programming in PASCAL. The adequacy of the model has been tested by comparing the computed values of α, β, Y_i, P to those experimentally obtained by Piotrowski [4].

Table 2

Table 2

Model testing

Parameters			α		β		P, *MPa*		Y_{NH_3}		Y_{CO_2}	
t, °C	*a*	*b*	Ex.	Calc.	Ex.	Calc.	Ex.	Calc.	Ex.	Calc.	Ex.	Calc.
170	4.08	0.14	—	0.798	0.721	0.757	12.9	12.33	0.97	0.96	0.15	0.02
180	3.96	0.07	—	0.799	0.776	0.763	13.8	13.90	0.96	0.96	0.02	0.02
190	3.49	0.00	—	0.774	0.731	0.742	17.5	16.06	0.90	0.93	0.01	0.03
200	3.59	0.59	—	0.688	0.652	0.653	17.7	19.60	0.86	0.86	0.06	0.07
210	3.77	0.25	—	0.753	0.718	0.724	26.0	24.60	0.87	0.86	0.06	0.07

The data from Table 2 shows a good agreement between the computed and the experimental values. The most important deviations presents the mole fraction of carbon dioxide in the gas-phase (Y_{CO_2}) becouse of its low value.

4. **Process Simulation. Results.** The agreement between the com : ted data and the experimental values for a number of sets of parameters may be considered only a necessary condition, but not sufficient, for the validity of the model. It must be further tested the capacity of the model to simulate the influence of the parameters on the composition and total pressure according to the general lows of the thermodynamic equilibrium. The results of this simulation are partly presented in figures 1 to 3 : *Fig. 1, Fig. 2., Fig. 3.*

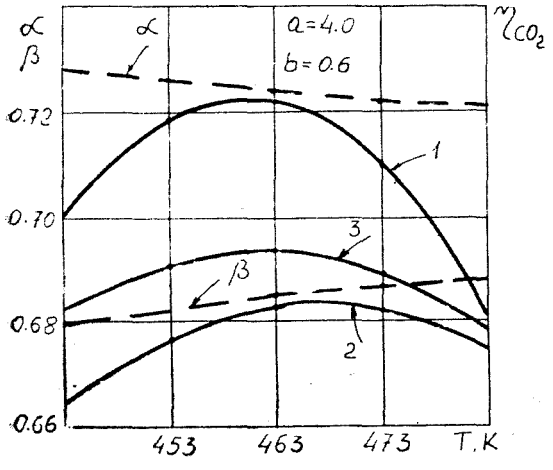

Fig. 1.a. Influence of the temperature on the conversion degrees α and β. The transformation degree η_{CO_2} computed by the regression equations of Otsuka (1), Kucheryavyi (2), and Piotrowski (3)

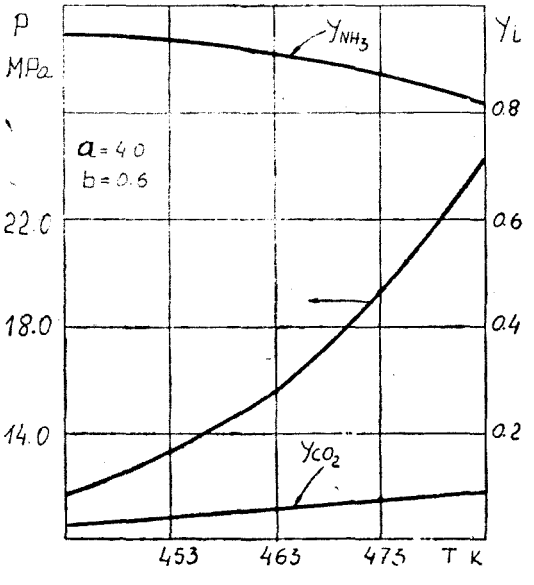

Fig. 1.b. Temperature dependence of the equilibrium pressure (*P*), and of the gas-phase composition (Y_{NH_3}, Y_{CO_2}).

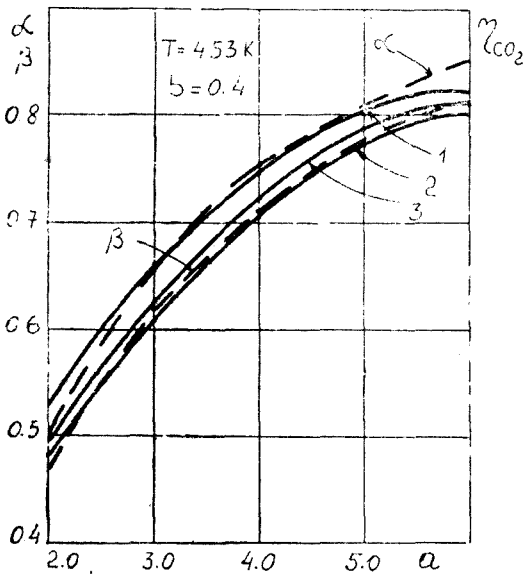

Fig. 2.a. Influence of the ammonia excess on the conversion degrees α and. The conversion η_{CO_2} computed by the equations of Otsuka (1), Kucheryavyi (2), and Piotrowski (3).

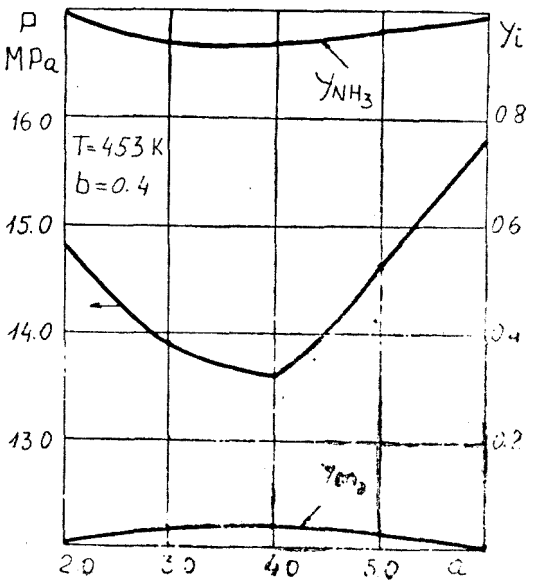

Fig. 2.b. Influence of the ammonia excess on the total pressure (P), as well as on the gas phase composition.

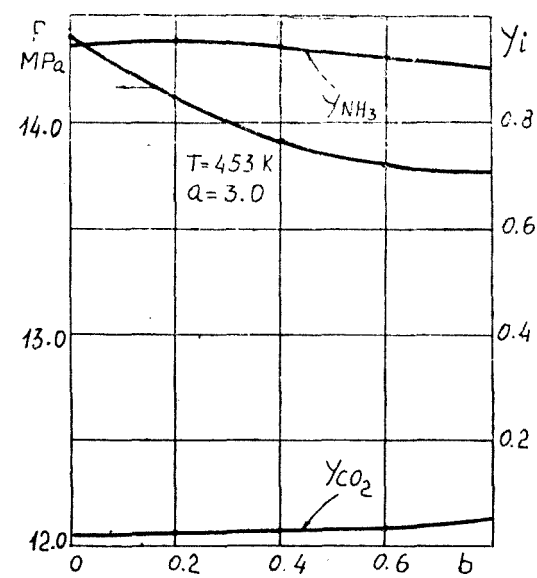

Fig. 3.a. Influence of the water excess on the conversions α and β. The conversion η_{CO_2} computed by the Otsuka (1), Kucheryavyi (2), and Piotrowski (3) equations.

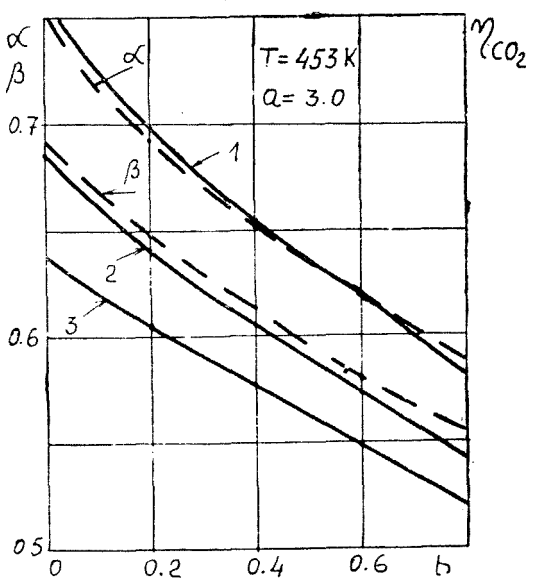

Fig. 3.b. Influence of the water excess on the total pressure (P) and gas phase composition.

The influence of the *temperature* on the dependent variables α, β P, Y_{NH_3} and Y_{CO_2}, for a given input composition ($a = 4.0$, $b = 0.6$) is represented in Fig. 1. The variations are qualitatively in agreement with Van't Hoff's rule: the equilibrium conversion in the exothermic reaction (1) is negatively influenced by the temperature. On the other hand, becouse of the inequality $\eta_{Cb} > \eta_{CO_2}$ the global conversion β monotonousely increases with the temperature, without any extreme point in the studied range. This is in contrast with the variations predicted by the regression equation (14) to (16). Maybe our model must be improved in order to increase sensibility of the two equilibrium constants in the temperature range 170—210°C. The other variables normally depend on the temperature: the total pressure increases with the temperature, while ammonia concentration in the gasphase decreases (Fig. 1.b.).

The influence of the *ammonia excess* is represented in Fig. 2. The two conversions continuously increase with the excess of ammonia. This is consistent with the law of mass action. Similar variation are predicted by the semiempirical equations (14) to (16). The equilibrium pressure has a minimum. The study of the curves $P - f(a)$ for other values of t and b has shown that the position of the minimum point (a_{min}) shifts with the increase of temperature and water excess to higher values of a. The curves $Y_{NH_3} - f(a)$ have an extreme shape, too, the position of the minimum point being almost the same.

The influence of the *excess of water* (b) is illustrated in Fig. 3. The predicted dependence of the conversions is still in agreement with the law of mass action. The effect of the excessive water on the equilibrium pressure is dependent on the values of the parameter a. For values $a < 2.0$, usually applied (n industry, the excess of water reduces the value of the equilibrium pressure as we can see in Fig. 3.b). The excess of water has a small influence on the composition of the gasphase.

á. Conclusions.

- The semiempirical methods, available in the literature, permit only the evaluation of a fictitious liquid-phase composition of the urea system at equilibrium.
- A new thermodynamic model of the urea synthesis process has been proposed in this paper, based on the two main reactions in liquid-phase and three gas-liquid equilibrium. The model can predict the complete composition of the two phases, as well as the total pressure, the only independent variables being the operating temperature and two input molar ratios.
- The new model complies with the experimental data as well as with the equilibrium thermodynamic laws.

SYMBOLS

a = molar ratio NH_3/CO_2 in the liquid phase
b = molar ratio H_2O/CO_2 in the liquid phase
Cb = ammonium carbamate
f_i = fugacity coefficient
K_1, K_2, K = approximate equilibrium constant of the reaction (1), (2), and (9) respectively
n_i^0 = mole number of component i, in the feed
P = total equilibrium pressure, MPa

p_i^0 = partial pressure of pure component
t = temperature, °C; T = absolute temperature, K
x_i = mole fraction of component i, in liquid phase
Y_i = mole fraction of component i, in gas phase
α = conversion degree of CO_2 in the reaction (1)
$\beta = \eta_{CO_2}$ = conversion degree of CO_2 in the global reaction
γ_i = the ratio γ_i''/f_i
η_{Cb} = conversion degree of the carbamate in the reaction (2)

REFERENCES

1. * * *, Informations Chimie, 302, 1989, p. 107.
2. Dürich, W., Chimie, **31**, 1977, p. 8.
3. Ruf A., Müller W., Buck A., Swiss. Chem., **6**, **9**, 1984, p. 129.
4. Calistru, C., Leonte C., Siminiceanu, I., Hagiu C., *Technology of Mineral Fertilizers*, Vol. **I**, Edit. Tehcn., Bucharest, 1984, p. 293.
5. Fréjacques M., Chimie et Ind., **60**, 1, 1948, p. 22.
6. Cook L., Hydrocarbon Processing, **45**, 2, 1966, p. 129.
7. Mavrovic I., Chem. Eng. Progress, **70**, 2, 1974, p. 69.
8. Kucheryavyi V. I., Gorlovski, D. M., Khim. Prom., **11**, 1969, p. 836.
9. Kawasumi S., Bull. Chem. Soc. Japan, **25**, 1952, p. 227, **26**, 1953, p. 218, **27**, 1954, p. 254.
10. Inoue S., Kanai K., Otsuka E., Bull. Chem. Soc. Japan, **45**, 1972, p. 1339.
11. Piotrowski J., Chem. Stosowana, **28**, 2, 1984, p. 239, **29**, 1—2, 1985, p. 41.
12. Lemkowitz S. M., de Cooker M., Van der Berg P. J., Appl. Chem. Biotechnol., **23**, 1973, p. 63.
13. Vicar S., Brit. Chem. Eng., **8**, **12**, 1963, p. 838.
14. Kucheryavyi, V. I., Zinoviev G., Khim. Prom., **5**, 1969, p. 354.
15. Efremova G. D., Leonteva G. G., Khim. Prom., **10**, 1962, p. 742.
16. Szaravara J., Gawdik, A., Chem. Eng. Sci., 1989, **44**, 7, p. 1489.
17. Sandler S. I., *Chemical & Engineering Thermodynamics*, Wiley, New York, 1989.
18. Siminiceanu I., *The Backgrounds of Inorg. Chem. Tech.*, I. P. Iași, 1987.
19. Piotrowski J., Doctor's Dissertation, Silesian Tech. Univ., 1976.
20. Szarawara J., Piotrowski J., Chem. Stosowana, **31**, 1, 1987, p. 73.
21. Reid R. C., Sherwood T. K., *The Properties of Gases and Liquids*, Mc Graw-Hill, New York, 1966.

STUDIA UNIV. BABEŞ-BOLYAI, CHEMIA, XXXVI, 1—2, 1991

THE STUDY OF THE TRANSALKYLATION REACTION BETWEEN TRIMETHYLBENZENE AND PHENOL

S. OPREA*, E. DUMITRIU*, V. HULEA*, A. MAREŞ*, I. RUSU*

ABSTRACT. A thermodynamic study of the transalkylation process between phenol and trimethylbenzenes was performed. The reaction was carried out in the presence of the SK-500 catalyst. A good connection between the theoretical results and the practical ones was estabilished. In both cases, the proportion of the ring alkylated products is superior to the oxygen atom alkylated products.

Introduction. The methylates derivatives of the phenol are compounds with wide applications in the process of obtaining some valuable organic products: insecticides, plastics, antiseptic substances, drugs, etc. The methyl-aryl-ethers are also very efficient additives for gasoline. The obtaining of these intermediate compounds is mainly based on the alkylation reaction of the phenol with methanol, in gaseous phase. In this idea the solid catalysts with acide-base properties are used, when ring [1—8] respectivelly oxygen atom [9—13] alkylated compounds are obtained.

The xylenes, especially the ortho- and para- isomers, are also very required compounds in the organic industry to produce synthetic fibres, plastics, resins, etc.

In this context we have proposed to study the reaction between phenol and trimethylbenzene, which can lead to the simultaneous obtaining of the cresols (respective anisole) and of the xylenes:

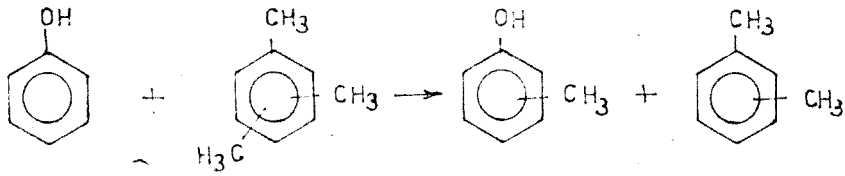

SCHEME I

In this paper the thermodynamic study of the process is done, and it is corelated with a series of experimental results, obtained by the realization of the above mentioned reaction in our laboratory.

* *Politechnical Institute Jassy, Dept. of Chemical Engineering, 6600 Iaşi, Romania*

Experimental part. The phenol and the trimethylbenzenes, high purity reagents, have been supplied by ALDRICH.

Catalysts

It was used the zeolite catalyst SK-500. It was delivered by VENTRON and the composition of the anhydrous SK-500 extrudate zeolite was: 65.0% SiO_2, 22.7% Al_2O_3, 1.6% Na_2O and 10.7% RE_2O_3 (by weight). The specific area was about 550 m^2/g.

The transalkylation reaction was tested on a pulse microreactor, coupled with a gas-liquid chromatograph, equiped with a column containing hexaphenylether 10% /Cromatron NAW-DMDS.

The thermodynamic calculus was carried out on the basis of our own programme, conceived in TURBO PASCAL for an IBM-PC consistent computer.

Results and discussions.

The chemical model. The basis of the thermodynamic study consists from the following set of reactions, considered to be illustrative for the general description of the studied process:

— the transalkylation trimethylbenzenes-phenol:

$$1,3,5\ TMB + F \xrightarrow{K1} mX + oC \qquad (1)$$

$$\xrightarrow{K2} mX + pC \qquad (2)$$

$$\xrightarrow{K3} mX + mC \qquad (3)$$

$$1,2,4\ TMB + F \xrightarrow{K4} mX + oC \qquad (4)$$

$$\xrightarrow{K5} mX + pC \qquad (5)$$

$$\xrightarrow{K6} mX + mC \qquad (6)$$

$$\xrightarrow{K7} oX + oC \qquad (7)$$

$$\xrightarrow{K8} oX + pC \qquad (8)$$

$$\xrightarrow{K9} oX + mC \qquad (9)$$

$$\xrightarrow{K10} pX + oC \qquad (10)$$

$$\xrightarrow{K11} pX + pC \qquad (11)$$

$$\xrightarrow{K12} pX + mC \qquad (12)$$

$$1,2,3\ \text{TMB} + \text{F} \xrightarrow{K13} \text{mX} + \text{oC} \qquad (13)$$

$$\xrightarrow{K14} \text{mX} + \text{pC} \qquad (14)$$

$$\xrightarrow{K15} \text{mX} + \text{mC} \qquad (15)$$

$$\xrightarrow{K16} \text{oX} + \text{oC} \qquad (16)$$

$$\xrightarrow{K17} \text{oX} + \text{pC} \qquad (17)$$

$$\xrightarrow{K18} \text{oX} + \text{mC} \qquad (18)$$

$$1,3,5\ \text{TMB} + \text{F} \xrightarrow{K19} \text{mX} + \text{A} \qquad (19)$$

$$1,2,4\ \text{TMB} + \text{F} \xrightarrow{K20} \text{oX} + \text{A} \qquad (20)$$

$$\xrightarrow{K21} \text{mX} + \text{A} \qquad (21)$$

$$\xrightarrow{K22} \text{pX} + \text{A} \qquad (22)$$

$$1,2,3\ \text{TMB} + \text{F} \xrightarrow{K23} \text{oX} + \text{A} \qquad (23)$$

$$\xrightarrow{K24} \text{mX} + \text{A} \qquad (24)$$

— the isomerization reactions:

$$1,3,5\ \text{TMB} \xrightarrow{K25} 1,2,4\ \text{TMB} \qquad (25)$$

$$\xrightarrow{K26} 1,2,3\ \text{TMB} \qquad (26)$$

$$1,2,4\ \text{TMB} \xrightarrow{K27} 1,2,3\ \text{TMB} \qquad (27)$$

$$\text{pX} \xrightarrow{K28} \text{mX} \qquad (28)$$

$$\text{pX} \xrightarrow{K29} \text{oX} \qquad (29)$$

$$mX \xrightarrow{K30} oX \qquad (30)$$

$$pC \xrightarrow{K31} mC \qquad (31)$$

$$pC \xrightarrow{K32} oC \qquad (32)$$

$$mC \xrightarrow{K33} oC \qquad (33)$$

$$A \xrightarrow{K34} oC \qquad (34)$$

$$A \xrightarrow{K35} mC \qquad (35)$$

$$A \xrightarrow{K36} pC \qquad (36)$$

— the disproportionation reactions:

$$2\ oX \xrightarrow{K37} T + 1,\ 2,\ 4\ TMB \qquad (37)$$

$$2\ oX \xrightarrow{K38} T + 1,\ 2,\ 3\ TMB \qquad (38)$$

$$2\ mX \xrightarrow{K39} T + 1,\ 3,\ 5\ TMB \qquad (39)$$

$$2\ mX \xrightarrow{K40} T + 1,\ 2,\ 4\ TMB \qquad (40)$$

$$2\ mX \xrightarrow{K41} T + 1,\ 2,\ 3\ TMB \qquad (41)$$

$$2\ pX \xrightarrow{K42} T + 1,\ 2,\ 4\ TMB \qquad (42)$$

We are also considering as possible other reactions too: the disproportionation of the toluene, the transalkylation trimethylbenzenes-anisole, the isomerization of the methyl-anisoles, the transalkylation cresols-trimethylbenzenes, demethylations, coking, etc. To accept these transformations, which have in fact a limited proportion in the considered process, it means to create major difficulties to the thermodynamic calculation of the composition.

The thermodynamic study. The calculus is based on the thermodynamic data offered by the literature, the proceedings being presented earlier [14].

For the temperature field ranged between 298K and 998K, the constants K1—K42, the composition and the conversions of the reacting substances according to the equilibrium state were determined.

In Table 1 the equilibrium constants values, considered only for few temperatures, are presented.

Table 1

The constants value at thermodynamic equilibrium

Ki	Temperature, K									
	298		448		598		798		998	
1	3.74		5.89		9.34		18.48		40.93	
2	0.3		0.71		1.35		3.01		7.23	
3	14.72		10.25		8.57		7.55		7.07	
4	2.29		2.99		4.59		10.62		34.23	
5	0.18		0.36		0.66		1.73		6.05	
6	9.02		5.2		4.21		4.34		5.91	
7	0.56		0.95		1.7		4.4		15.05	
8	0.04		0.11		0.24		0.71		2.65	
9	2.21		1.65		1.56		1.8		2.6	
10	0.91		1.29		2.01		4.6		14.46	
11	0.07		0.15		0.29		0.75		2.55	
12	3.6		2.24		1.85		1.88		2.49	
13	57.69		35.81		34.34		45.17		75.04	
14	4.69		4.36		4.96		7.36		13.26	
15	227.09		62.32		31.5		18.46		12.96	
16	14.14		11.39		12.71		18.73		32.99	
17	1.15		1.38		1.83		3.05		5.83	
18	55.69		19.82		11.66		7.65		5.7	
19	3.87	E−9	5.2	E−6	2.81	E−4	6.29	E−2	4.16	E−2
20	5.82	E−10	8.39	E−7	5.1	E−5	2.85	E−3	1.53	E−2
21	2.39	E−9	2.63	E−6	1.38	E−4	3.65	E−3	3.48	E−2
22	9.48	E−10	1.14	E−6	6.09	E−5	1.56	E−3	1.47	E−2
23	1.46	E−8	1	E−5	3.84	E−4	6.38	E−3	3.35	E−2
24	5.97	E−8	3.16	E−5	1.03	E−3	1.53	E−2	7.63	E−2
25	1.63		1.88		2.03		1.73		1.19	
26	6.48	E−2	0.12		0.27		0.4		0.54	
27	3.97	E−2	6.48	E−2	0.13		0.23		0.45	
28	2.5		2.35		2.27		2.3		2.36	
29	0.61		0.69		0.84		0.95		1.04	
30	0.24		0.29		0.37		0.41		0.43	
31	48.36		19.91		6.34		2.5		0.97	
32	12.28		8.99		6.91		6.13		5.65	
33	0.25		0.45		1.09		2.44		5.78	
34	9.65	E+8	6.54	E+6	3.31	E+4	2.93	E+3	9.82	E+2
35	3.79	E+9	1.44	E+7	3.03	E+4	1.19	E+3	1.69	E+2
36	7.85	E+7	7.27	E+5	4.78	E+3	4.78	E+2	1.73	E+2
37	10.74		7.17		5.26		3.54		2.19	
38	0.42		0.59		0.7		0.83		1	
39	0.39		0.36		0.35		0.35		0.35	
40	0.64		0.72		0.72		0.61		0.42	
41	2.56	E−2	6.06	E−2	9.66	E−2	0.14		0.19	
42	4.05		3.89		3.74		3.24		2.37	

Obs. E−a=10^{-a}

From the analysis of these data some remarks can be done:

(i) — the extreme value of the equilibrium constants are corresponding to the reactions in which is involved the anisole, product with an extremely low thermodynamic stability;

(ii) — the isomeric formes of the reaction products are characterized by various thermodynamic stabilities; on the background of isomerization reactions the equilibrium is displaced specially towards the formation of the next compounds: meta-xylene, meta-cresol and 1,2,4 trimethylbenzene;

(iii) — for a great part among the reactions, the value of the equilibrium constants is strongly influenced by the temperature.

On the basis of the equilibrium constants and of the preserving relations applied to the various molecular species, it was drawn out the next system of independent equations which allowed the calculation of the compositions to the thermodynamic equilibrium.

$$X1 + X2 + X3 + X4 + X5 + X6 + X7 + X8 + X9 + X10 + X11 + X12 = 1 \quad (I)$$

$$3(X2 + X3 + X4) + 2(X5 + X6 + X7) + X8 + X9 + X10 + X11 + X12 = 3X(0)2 \quad (II)$$

$$X1 + X8 + X9 + X10 + X11 = X(0)1 \quad (III)$$

$$K25 = X3/X2 \quad (IV)$$

$$K26 = X4/X2 \quad (V)$$

$$K28 = X5/X6 \quad (VI)$$

$$K29 = X7/X6 \quad (VII)$$

$$K31 = X8/X9 \quad (VIII)$$

$$K32 = X10/X9 \quad (IX)$$

$$K34 = X10/X11 \quad (X)$$

$$K3 = X5 * X8/X1 * X2 \quad (XI)$$

$$K39 = X12 * X2/X5 * X5 \quad (XII)$$

For $X(0)1 = X(0)2 = 0.5$ the results are presented in the Figures 1, 2 and 3. The effect of the temperature on the composition at equilibrium can be easily observed; it is also confirmed what we have specified above, about the distribution of the isomers on every class of compounds.

In Figure 1 are also reproduced the total conversions of the two reacting substances, according to the equilibrium state.

It must be emphasized the formation of the cresols in a very great proportion (over 1/3) in the final mixture; the distribution of the cresol isomers is strongly influenced by the temperature (Figure 3).

The fact that the second product of the transalkylation the xylenes are not formed in the same proportion as the cresols, is explained by the marked tendency of these ones to disproportion in toluene and trimethylbenzenes, fact easy to be ascertained from the presented figures.

A suggestion which is offered by this behaviour is that a trimethylbenzene excess vs. the phenol is necessary to obtain good results in the transalkylation reaction.

In Figure 1 we are also presenting the total conversions of the two reagents at the thermodynamic equilibrium state. It is ascertained that these

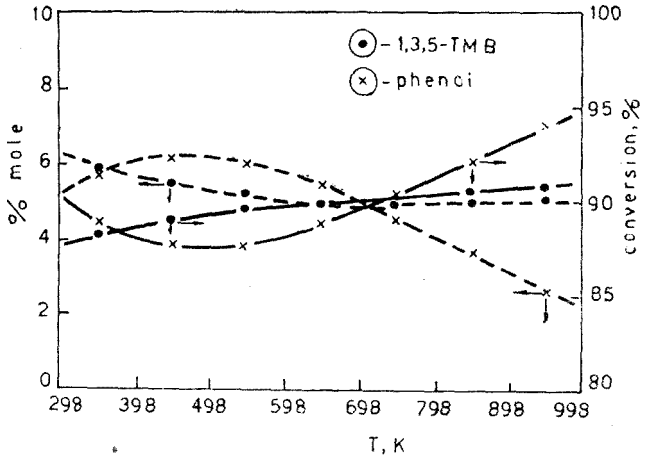

Fig 1. The temperature influence on the reagents conversions and concentrations at thermodynamic equilibrium.

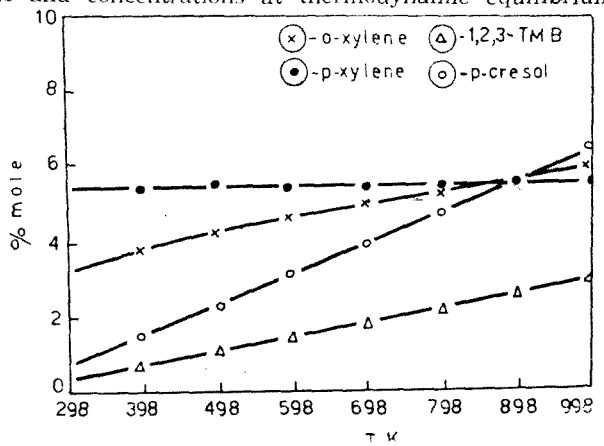

Fig. 2. Some products distribution in thermodynamic equilibrium conditions vs. temperature

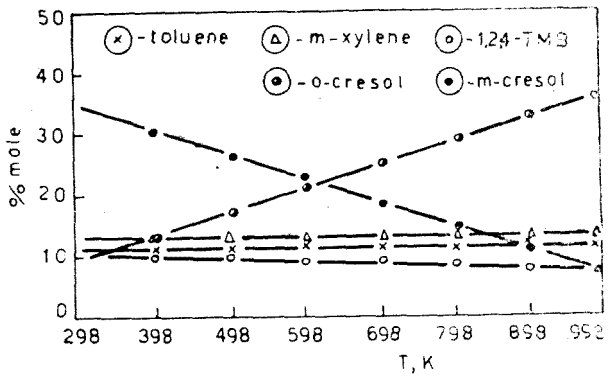

Fig. 3. The distribution of some products in thermodynamic equilibrium conditions vs. temperature

ones have high values (about 90%) for all the temperatures from the considered range.

In completion of this theroetical study we proposed ourselfs to test the transalkylation reaction between phenol and trimethylbenzenes in the presence of a synthetic zeolite. With this purpose it was used a faujasite, modified with elements from the rare earths family by ionic exchange.

By a preliminary programmed thermodesorbtion test of the ammonia, we have established that the acidity of this catalyst is 6.65 E20 acide centers/gr. of catalyst.

Two sets of experiences, phenol with 1, 3, 5-TMB and phenol with 1, 2, 4-TMB, were carried out. The obtained results of the two reactions are presented in Table 2.

Table 2

The product composition in the transalkylation reaction (% mol); $T = 675K$

the reaction	F+1,3,5 TMB	F+1,2,4 TMB	thermodynamic equilibrium
B	1.1	0.94	—
T	11.99	12.94	11
pX + mX	16.73	16.75	17.44
oX	6.59	6.1	4.84
1.3.5 TMB	4.97	3.18	4.93
1.2.4 TMB	7.49	9.06	9.6
1.2.3 TMB	1.09	1.01	1.6
F	18.52	14.54	5.16
A	0.29	0.56	0.01
oC	16.2	17.98	24
pC + mC	13.95	14.82	19.73
xylenols	1.02	2.09	—

The analysis of the experimental data and the comparison with the thermodynamic study results permit us to conclude:

(i) — in both reactions the products distribution is approaching much enough the theoretical data;

(ii) — the consumption rate of the 1, 3, 5-TMB in the isomerization reactions is higher than that one which correspond to the transalkylation reaction with phenol; this fact is indicated by different concentrations os the phenol, respective of the 1, 3, 5-TMB in the final mixture;

(iii) — the 1, 2, 4-TMB, which does not isomerize very much (see also the thermodynamic data), participes to the transalkylation with the phenol in a higher proportion than the 1, 3, 5-TMB isomer;

(iiii) — the proportion of the alkylated products of the phenol at the carbon atom (cresols) is much higher than the anisole one (product of alkylation at the oxygen atom).

The last observation is justified by the fact that the reactions were effected in the presence of a catalyst with acide properties, which favour the pro-

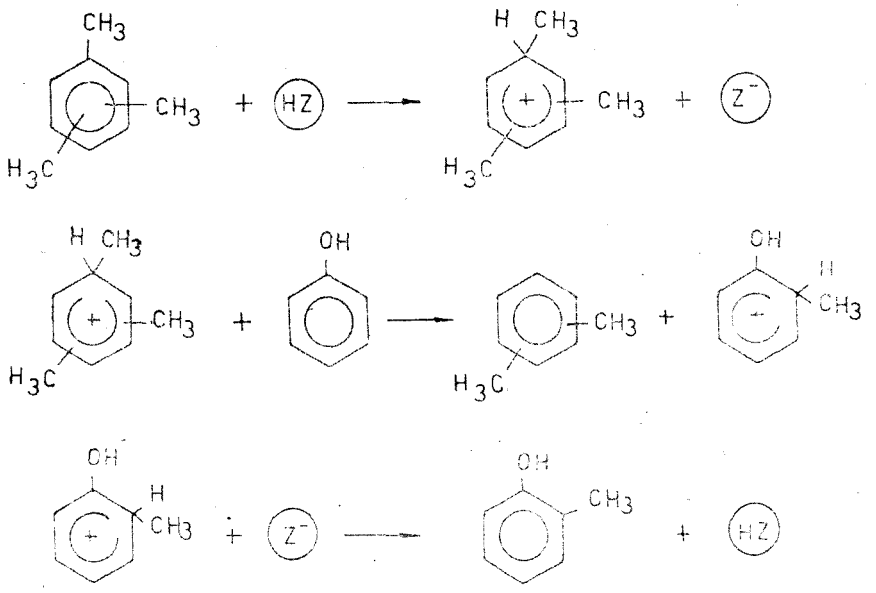

SCHEME II

cesses who are occuring by a carbocationic mechanism (electrophilic ring substitution).

In Scheme II, such a mechanism is presented in a simplified manner.

On the other hand, when we have a basic catalysis, the phenol alkylation to anisole takes place by a nucleophilic substitution mechanism.

In conclusion, it can be asserted, from a thermodynamic point of view, that the transalkylation reaction between trimethylbenzenes and phenol is possible, and the acide solid catalyst, as the synthetic zeolites, allow the practical achievement of the process. The composition of the final mixture obtained in the presence of the SK-500 catalyst is strongly approaching the results offered in the thermodynamic study; in both cases, the proportion of the alkylation products at the carbon atoms of the phenol being superior to the alkylation products at the oxygen atom.

SYMBOLS

T — toluene
pX — para xylene
mX — meta xylene
oX — ortho xylene
1, 3, 5 TMB — 1, 3, 5 trimethylbenzene
1, 2, 4 TMB — 1, 2, 4 trimethylbenzene
1, 2, 3 TMB — 1, 2, 3 trimethylbenzene
mC — meta cresol
pC — para cresol
oC — ortho cresol
F — phenol

A — anisole
Xi — molar fraction at equilibrium
X(0)i — molar fraction in feeding
X1 — phenol
X2 — 1, 3, 5 TMB
X3 — 1, 2, 4 TMB
X4 — 1, 2, 3 TMB
X5 — m xylene
X6 — p xylene
X7 — o cxylene
X8 — m cresol
X9 — p cresol
X10 — o cresol
X11 — anisole
X12 — toluene

REFERENCES

1. Kotanigawa T., Yamamoto M., Shimokawa K., Yoshida Y., Bull. Chem. Soc. Jpn., 1971, 44, 1961.
2. Fukuda Y., Nishizaki T., Tanabe K., Nippon Kaishi, 1972, 1754.
3. Tanabe K., Ishiya C., Matsuzaki, I., Ichikawa I., Hattori H., Bull. Chem. Soc. Jpn., 1972, 45, 47.
4. Hattori H., Shimazu K., Yoshii N., Tanabe K., Bull. Chem. Soc. Jpn., 1976, 49, 969.
5. Tanabe K., Nishizaki T., Proc. 6th Internat. Congr. Catal., London, 1976, The Chemica. Society, London, 1976, p. 363.
6. Nozaki F., Kimura I., Bull. Chem. Soc. Jpn., 1977, 50(3), 614.
7. Tanabe K., Shimazu K., Hattori H., Shimazu K., J. Catal., 1979, 57, 351
8. Kinka M., Karson, M. S., Ionesku, N. I., Kost. Kinet. Katal. Engl. Trans., 1985. 86, 1087.
9. Kannan S. V., Pillali C. N., Indian J. Chem., 1970, 8, 1144.
10. Namba S., Yashima T., Itaba Y., Hara N., „Catalysis by Zeolites", Elsevier, Amsterdam, 1980, p. 105.
11. Balsama S., Beltrame P., Beltrame P. L., Carniti P., Forni L., Zuretti G., Appl. Catal., 1984, 13, 161.
12. Esteban S., Marinas J. M., Martinez-Alcazar M. P., An. Quim., 1981, 77c, 218.
13. Campelo J. M., Garcia A., Luna D., Marinas J. M., Moreno M. S., Bull. Soc. Chim. Fr., 1988, 283.
14. Oprea S., Azzonez A., Dumitriu E., Constantinescu M., Bull. Soc. Chim Belg., 91(3), 289, 1983.

STUDIA UNIV. BABEŞ-BOLYAI, CHEMIA, XXXVI, 1—2, 1991

THE APPLICATION OF THE FLUIDIZED BED MODEL AT THE $(NH_4)_2SO_4$ DRYING.

ION BALASANIAN*

ABSTRACT. An analyse of the possibility of application fluidized bed reactors and the theory of macrokinetic and mathematical modelling of the drying process in view of the design of fluidized bed driers. The exemplification is done for the $(NH_4)_2SO_4$ drying. The obtained values are the same with the values of industrial driers. This confirm that the proposed model can be used in view of drier design.

The traditional calculation methods of the fluidized bed driers are based on approximated rules [1], on models who consider the mixing intensity [2], or are based on kinetic measurements in fluidized bed in laboratory conditions [2—6].

This scientific work tests the application of the reactor model in fluidized bed and the theory of macrokinetic and mathematical modelling of the drying process in view of the design of fluidized bed driers. The exepmlification is done for the $(NH_4)_2SO_4$ drying.

The analysed drier corresponds to the contact model of fluidized bed with solid feed, consisting of a mixture of different-size particles, without solid entrainment and it is shown in Fig. 1.

The mathematical model of the fluidized bed drier is obtained by passing from the mathematical model of the drying process at the grain level to the grain ensemble in conditions of solid flow in fluidized bed. This model considers the composition of the gaseous phase invariable and takes into consideration only the degree of water evaporation [7—9].

Since the solid flow in fluidized bed corresponds at the perfect mixing, and in the drying process it doesn't exist any change of the grain size it results; for fluidized beds without entreinment of solids, the distribution of the particles size in feed, in the bed and in the output current are the same. Thus we may con-

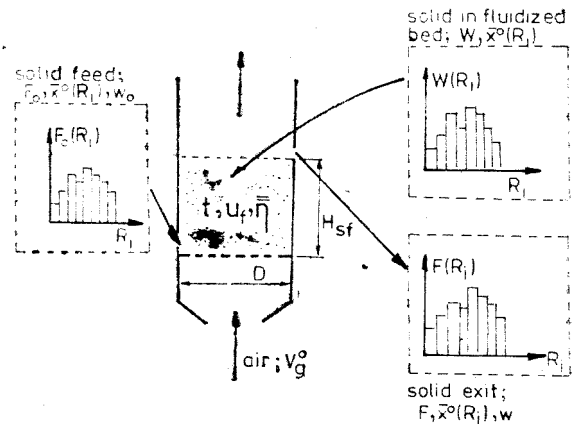

Fig. 1. The drier in fluidized bed without solid entrainment.

* *Polytechnical Institute Jassy, Dept. of Chemical Engineering, 6600 Iaşi, Romania*

sider that mean residence time of solids in bed is give by the Eq. (1).

$$\bar{\tau}_{[]s} = \bar{\tau}(R_i) = \frac{W}{F} \tag{1}$$

The residence time for the particles of R size in the drier being different, the mean degree of water evaporation is made by Eq. (2), where the age distribution at the solid exit of R size, for the perfect mixing flow of solids, results from the Eq. (3).

$$1 - \bar{\eta}(R_i) = \int_0^{\tau_0(Ri)} [1 - \eta_i(R_i)] E(\tau)\, d\tau \tag{2}$$

$$E(\tau) = \frac{1}{\bar{\tau}(R_i)} e^{-\tau/\bar{\tau}(R_i)} = \frac{1}{\tau_{[]s}} e^{-\tau/\tau_{[]s}} \tag{3}$$

Because the drier feed is made with particles of different sizes, corresponding to a particle size distribution, the total mean degree of water evaporation is made by Eq. (4).

$$1 - \bar{\eta}_i = \sum_{R_i = R\,min}^{R\,max} [1 - \eta_i(R_i)]\bar{x}_0(R_i) = \sum_{R_i = R\,min}^{Rmax} \left\{ \int_0^{\tau_0(Ri)} [1 - \eta_i(R_i)] \frac{1}{\bar{\tau}_{[]s}} e^{-\tau/\bar{\tau}_{[]s}} d\tau \right\} \bar{x}_0(R_i) \tag{4}$$

The determination of the mean residence time of the solids in fluidized bed, in view to realize a certain degree of water evaporation $\bar{\eta}_i = \eta_{H_2O}$, permits the calculation of technological dimensions of the drier. The diameter of the flow equation for the fluidizing velocity and the height from the relationship between a cantity of solids of the bed and his specific parameters:

$$H_{se} = \frac{W}{\frac{\pi}{4} D^2 \rho_s (1 - \varepsilon_{sf})} = \frac{4 F \tau_{[]s}}{\pi D^2 \rho_s (1 - \varepsilon_{sf})} \tag{5}$$

The determination of $\bar{\tau}_{[]s}$ through the solution of Eq. (4) requires a relatoinship, based on the macrokinetic and mathematical modelling of the drying process, between the degree of water evaporation for particles of R_i size and the drying time till at the equilibrum humidity of particles of R_i size.

The determination of $\bar{\tau}_{[]s}$ through the theory of macrokinetic and mathematical modelling of the drying process makes possible the use of the modern experimental technics and ask a smaller time unity and there are no problems at the translation of the experimental data for the industrial driers.

During the drying process of $(NH_4)_2SO_4$ in fluidized bed, the structural element is an unporous and wet crystal, enclosed by warm air. Since the fluidized bed represents a contact model characterized by great heat transfer coefficient at particle 7, 10, 11, in view of drying process modelling it's enough to be considered only the mass transfer and transformation processes. In accordance with that, the rate of drying process can be determinedted by the rate of elementary process of water evaporation on the grain surface or by elementary process of water vapour transfer from the grain surface in the drying medium.

The researches enter upon by author [12], point out the following fact: in specific hydrodynamic conditions of the fluidized bed the rate of $(NH_4)_2SO_4$ drying process is determinated by the rate of the humidity transfer from the grain surface in a gaseous phase, the matematical model being [6],

$$\eta(R_i) = \tau/\tau_0(R_i) \tag{6}$$

Figs. 2 and 3 show the agreement of the model with experimental data, again Fig. 4 shows the dependence of the drying time on at the equilibrium humidity at the particle size and gas velocity.

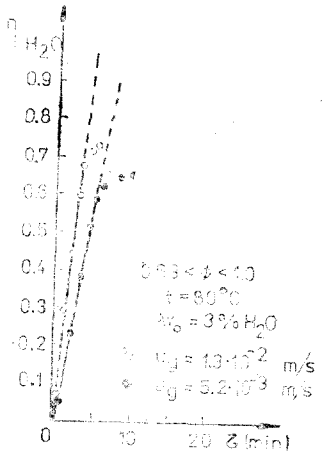

Fig. 2. The agreement of model with experimental date for $w_0 = 3\%$ H_2O, $dp = 0.815\ mm$ and $t = 80\,°C$

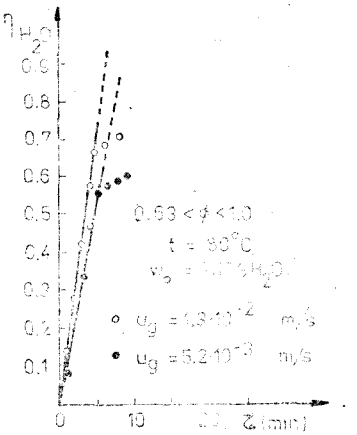

Fig. 3. The agreement of model with experimental data for $w_0 = 4.13\%$ H_2O, $dp = 0.815\ mm$ and $t = 80\,°C$

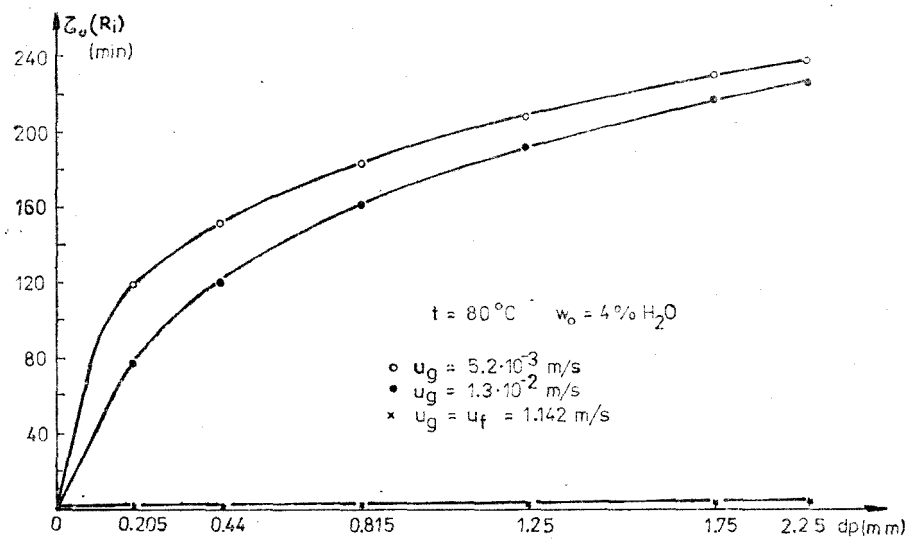

Fig. 4. The dependence of drying time till at the equilibrum humidity at particle size.

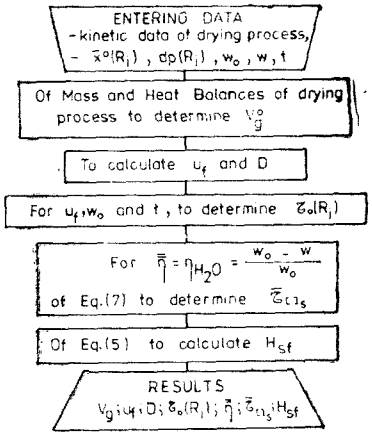

Fig. 5. The calculation algorithm of the fluidized bed drier.

Replacing the Eq. (6) in Eq. (4) and integrating, we are obtained [7—9],

$$1 - \eta = \sum_{Ri=R\,min}^{R\,max} \left\{ \frac{1}{2!} \left[\frac{\tau_0(R_i)}{\bar{\tau}_{[]s}} \right] - \frac{1}{3!} \left[\frac{\tau_0(R_i)}{\bar{\tau}_{[]s}} \right]^2 + \frac{1}{4!} \left[\frac{\tau_0(R_i)}{\bar{\tau}_{[]s}} \right]^3 \right\} \bar{x}^0(R_i) \qquad (7)$$

The system made by the Eqs. (1), (5), (6) and (7) makes possible the size determination of the fluidized bed drier. The calculation algorithm is reproduced in Fig. 5.

Using the data of [12], for drying the $(NH_4)_2SO_4$ from 4% H_2O to 0.14% H_2O, at the granulometric spectrum condition of Table 1, the application of the calculation algorithm conducts us to the following values for industrial drier;

— the temperature in drier, $t = 80°C$
— wet solid feed, $F_0 = 17\ t/h$
— drying air feed, $V_g^0 = 5.86\ Nm^3/s$
— fluidizing velocity, $u_f = 1.142\ m/s$
— weight of solids in the fluidized bed, $W = 2032\ kg$
— mean residence time of solids in the fluidized bed, $\bar{\tau}_{[]s} = 430\ s$
— height of the fluidized bed, $H_{sf} = 0.395\ m$

Table 1

The granulometric spectrum condition and the drying time till at the equilibrum humidity for fluidizing velocity and $t = 80°C$.

Granulometric Class	$x_0(R_i)$	$dp(mm)$	$\Sigma(R_i)$, (S) $U_f = 1142/s$ $t = 80°C$ $W_0 = 4\%\ U_2O$
$2.5 < Ø < 2{,}0$	0.032	2.25	130
$2.0 < Ø < 1.5$	0.025	1.75	125
$1.5 < Ø < 1.0$	0.019	1.25	107
$1.0 < Ø < 0.63$	0.532	0.815	94
$0.63 < Ø < 0.25$	0.387	0.44	73
$0125 < Ø < 0.16$	0.021	0.205	51

The obtained values are the same with values of the industrial drier. This shows that the fluidized bed model and the macrokinetic and mathematical modelling of the drying process can by used in view of drier design.

SYMBOLS

D — diameter of drier, m
dp — mean diameter of granulometric class, m
$E(\tau)$ — age distribution at solid exit,
$F_0, F_0(R_i)$ — wet solid feed and wet solid feed of R_i size, kg/s
$F, F(R_i)$ — solid exit and solid exit of R_i size, kg/s
H_{sf} — height of fluidized bed, m
t — temperature, $°C$
u_f — fluidizing velocity, m/s
u_g — gas velocity, m/s
V_g^0 — drying air feed, Nm^3/s
w, w — humidity of solid feed and humidity of solid exit,
$W, W(R_i)$ — weight of solid and weight of solid of R_i size in fluidized bed, kg
$\bar{x}_0(R_i)$ — mass fraction of solid of R_i size in granulometric spectrum
$\bar{\tau}_{[]s}, \bar{\bar{\tau}}(R_i)$ — mean residence time of solids and mean residence time of solids of R_i size in fluidized bed, s
$\bar{\eta}, \bar{\bar{\eta}}, \eta_{H_2O}$ — mean degree of water evaporation,
$\eta(R_i)$ — degree of water evaporation for solids of R_i size,
ρ_s — density of the solid, kg/m^3
ε_{sf} — porosity of fluidized bed,
$\tau_0(R_i)$ — drying time till at the equilibrum humidity for particle of R_i size, s

REFERENCES

1. Romankov, P. G., Raşkovskaia H. B. — *Suşca vo vîzveşennom sostoianii*, Izd. Himia, Leningrad 1979.
2. Strumillo C. — *Bazele teoriei şi tehnicii uscării*, Ed. Tehnică, Bucureşti, 1984.
3. Wornald D., Burnell E. M. W. — British Chem. Engng., vol. **16**, nr. 415, 1971, pp. 376.
4. Babenko V. E. — Him., Prom., — nr. **6**, 1974, pp. 353.
5. Kato K., Omura S., Taneda D. — Journal of The Chin. I. Ch. E. — vol. **14**, nr. 2, 1983, pp. 265.
6. Oigenblik A. A., Koriagin B. A., Sajin V. B., Solovieva I. V., Jiganova Z. M. — Him. Prom., nr. **11**, 1989, pp. 866.
7. Kunii D., Levenspiel O. — *Fluidization Engineering*, John Wiley and Sons, Inc., New York, 1969.
8. Levenspiel O. — *Chemical Reaction Engineering*, Second Edition, John Wiley and Sons, Inc., New York, 1972.
9. Grogoriu I., Balasanian I. — Rev. Chimie (Romania), vol. **28**, nr. 1, 1977, pp. 79; Idem, vol. 28, nr. 2, 1977, pp. 187.
10. Mihăilă C., Caluianu V., Marinescu M., Dănescu Al. — *Procese şi instalaţii industriale de uscare*, Ed. Tehnică Bucureşti, 1982.
11. Dăscălescu, A. — *Le séchage et ses aplications industrielles*, DUNOD Paris, 1969.
12. Balasanian I. — Rev. Chimie (Rumania), under printing.

STUDIA UNIV. BABEŞ-BOLYAI, CHEMIA, XXXVI, 1—2, 1991

POSSIBILITIES OF RECOVERY OF WASTE VANADIUM CATALYST

ROŞCA, I.*, FOCA, N.*, SUTIMAN, D.*

ABSTRACT. Two possibilities of recovering the waste vanadium catalyst, resulting from the oxidation of sulphur dioxide to sulphur trioxide, are described. By the first procedure the vanadium is extracted as vanadyl sulphate, the compounds of the vanadium (V) being previously reduced by oxalic acid then vanadium (IV) oxidized to vanadium (V) by hydrogen peroxide and vanadium pentaoxide separated by precipitation.

The second procedure consist in the vanadium extraction as sodium- or kalium-metavanadate, after the oxidation of the compounds of vanadium (IV) by sodium hypochlorite, followed by the separation of ammonium metavanadate by precipitation with ammonium chloride.

The first extraction is carried out at an acid pH and the second at a basic *pH*.

Introduction. Due to its remarkable properties, vanadium is largely used in industry both as metal and, especially, as compounds. Its recovery is particularly important since there are not natural sources of vanadium in our country.

In the present paper some possibilities of vanadium recovery from the waste catalyst used for oxidation of sulphur dioxide to sulphur trioxide in the industry of sulphuric acid are described.

Several procedures of exploitation of these catalysts are mentioned in literature [4 ... 13] which, however, cannot be applied at the industrial scale due to either corrosion (by using gaseous hydrogen chloride) or temperatures and pressures used as well as due to rather low recovery yields.

Experimental. The experiments were carried out with a waste catalyst of the wolffen type by the following composition: 2,02% V_2O_4, 2,24% V_2O_5, 2,5% Fe_2O_3, 3,92% Al_2O_3, 6,02% K_2O, 76,85% SiO_2, expressed as oxides.

The catalyst was ground in particles of size less than 1 *mm*.

The extraction was made in distilled water at an optimum solid-liquid ratio of 1 : 5 as determined experimentally.

The extractions were made in a sulphonation flask provided with termometer, stirrer and descending cooler for maintaining a constant level, with catalyst samples of 400 *g*.

Since in the waste catalyst, the vanadium is present in two oxidation states, V(IV) and V(V) in almost equal content, its extraction was followed both in its low oxidation state, as vanadyl sulphate stable in acid medium, and in its high oxidation state as sodium or kalium metavanadate, stable in basic medium.

1. Extraction of vanadium in acid medium

In acid solutions of $pH = 3$ the following equilibrium exists [3.]:

$$VO_2^+ + 2H^+ + 1e^- \rightleftharpoons VO^{2+} + H_2O \quad (1)$$

Based on this equilibrium the vanadium extraction is followed as vanadyl sulphate by shifting the equilibrium to the right.

The suspension of the catalyst in distilled water is brought to the temperature of 90 °C and maintained for 2,5 *h* when a part of vanadyl sulphate is solubilized based on the sulphuric acid for-

* *Politechnical Institute Jassy, Dept. of Chemical Engineering, 6600 Iaşi, Romania*

med from the sulphur trioxide from the initial catalytic mass. Then the compounds of vanadium V are reduced to vanadium IV and solubilized as vanadyl sulphate. Sulphuric acid and oxalic acid are added to the suspension. For the above mentioned catalyst amount 40 *ml* of 1 : 1 sulphuric acid solution and 1*g* oxalic acid as a 10% solution are used. The following reactions take place:

$$V_2O_5 + H_2C_2O_4 \rightarrow 2VO_2 + 2CO_2 + H_2O$$

$$VO_2 + H_2SO_4 \rightarrow VOSO_4 + H_2O$$

After the reducing agent addition the supsension is maintained for 4*h* at 90°C. In Fig. 1 the kinetics of solubilization of vanadyl sulphate from the catalytic mass are presented.

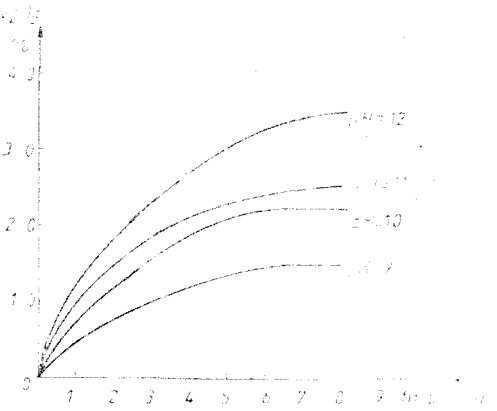

Fig. 1. Variation of concentration of vanadium tetraoxide in the liquid phase in time.

The vanadium was determined by titration with Mohr salt in the presence of diphenylamine [14].

After 7 hours from the extraction beginning, the solid part is separated by filtration. Due to the strong adsorption capacity of the catalytic support a part of the vanadyl sulphate is retained.

For this reason the solid mass is again taken with distilled water in the solid : liquid ratio of 1 : 3.

In Table 1, the contents of vanadium dioxide retained within the solid catalyst mass after every extraction are presented.

Table 1

Amount of vanadium tetraoxide retained within the solid mass after esch extraction.

Extraction	Semple 1 % V_2O_4	Sample 2 % V_2O_4	Sample 3 % V_2O_4
I	2,36	2,32	2,29
II	1,07	1,11	1,12
III	0,14	0,15	0,13
IV	0,14	0,12	0,12
V	0,13	0,11	0,12

The liquid phases from the extraction, practically the vanadium sulphate solutions, are processed together.

Since iron and aluminium compounds pass into solution together with vanadyl sulphate, they must be separated in order to prevent the impurification of the final product, and to increase the recovery yield.

Several method [15—17] may be applied for separation, but in this case the separation based on the *pH* differences at precipitation of iron and alluminium hydroxides toward the vanadium (V) compounds [18, 19] was prefered.

The vanadyl sulphate solution is oxidized with hydrogen peroxide at 50°C, and the *pH* increased by a 10% ammonium hydroxide solution.

At $pH = 1,5$ the precipitation of ferric hydroxide begins and at $pH = 2.0$ that of vanadium pentaoxide. After the separation of the solid phase containing vanadium pentaoxide and ferric hydroxide, it is treated with a 1% sodium hydroxide solution when the vanadium pentaxide only, is dissolved.

This can be again precipitated at $pH = 2$ as a pure product or at $pH = 7$ as ammonium metavanadate. The recovery yield varies between 78—82%.

II. Extraction of vanadium in basic medium. In this case, the extraction of vanadium in the oxidation state (V) as sodium or kalium metavanadate was followed.

Fisrtly, several oxidants were tested, namely: kalium dichromate, kalium permanganate and sodium hypochlorite.

As can be seen in Fig. 2, showing the variation of vanadium pentaoxide concentration in time for different oxidants, all of them can oxidate completely, the vanadium (IV) 2,5 hours. For economical reasons as well as due to the fact that the oxidation is favourized by the obtaining of singlet oxygen [20] the sodium hypochlorite was chosen. Then the optimum extraction *pH* was determined, 50—70 *ml* of sodium hypochlorite and a few *ml* of 10% sodium hydroxide solution are added to the catalyst suspension to initiate the oxidation process. When the oxidation is over a 10% sodium solution is added to obtain the desired *pH* value.

In fig. 3 the variation of vanadium pentaoxide concentration in the liquid phase at different *pH* values is depicted. The optimum *pH* value of 12 mustn't be exceeded due to the increase of silicon dioxide solubility resulting in a decrease of the extraction yield and difficulties of vanadium separation.

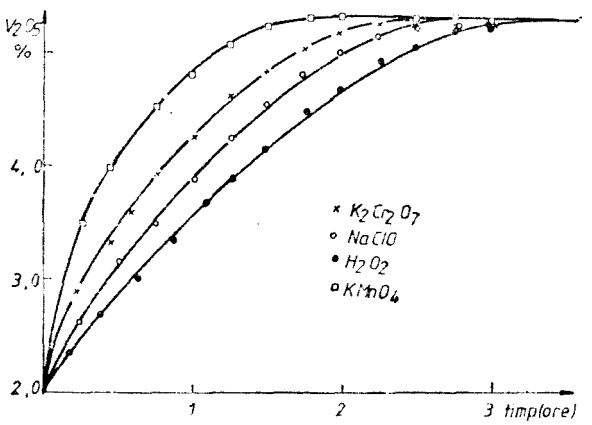

Fig. 2. Variation of concentration of vanadium pentaoxide in suspension in time for different oxidants.

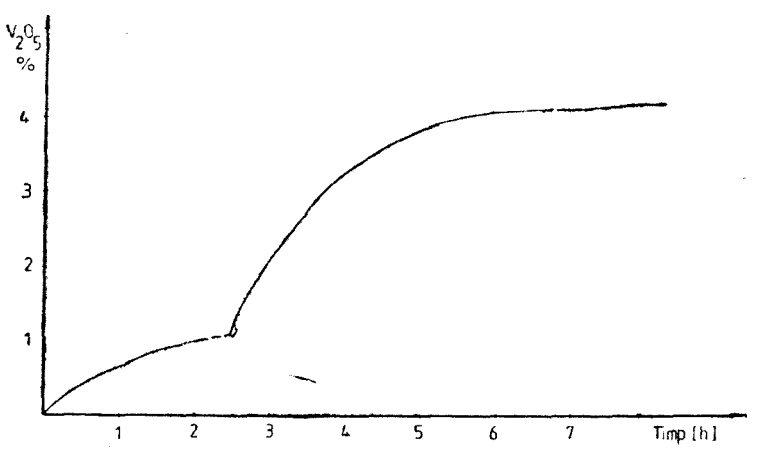

Fig. 3. Variation of concentration of vanadium pentaoxide in time at different *pH* value (sodium hypochlorite as oxidant).

The metavanadate solution obtained by the oxidation with hypochlorite at $pH = 12$ and 90 °C is separated from the solid catalyst mass after 7—8 hours of extraction. As in previous case a part of vanadium is retained on the catalytic support and must be taken again with distilled water at a solid : liquid ratio of 1 : 3 at 90 °C and the pH corrected. The contents of retained vanadium pentaoxide after each extraction are listed in Table 2.

Table 2

Amount of vanadium pentaoxide retained within the solid mass after each extraction

Extraction	Sample 1 % V_2O_5	Sample 2 % V_2O_5	Sample 3 % V_2O_5
I	3,397	3,471	3,352
II	2,202	2,181	2,271
III	0,782	0,801	0,753
IV	0,745	0,733	0,737
V	0,701	0,711	0,687

The liquid phase of the first extractions is processed as follows in order to obtain ammonium metavanadate: — it is brought at $pH = 8$ with a 1 : 1 nitric acid solution when the small amounts of extracted silicon dioxide precipitate.

— After the separation, the pH is brought to 6,5, an excess of solid ammonium chloride added under stirring, and cooling when the ammonium metavanadate precipitates.

The obtained amounts of ammonium metvanadate and the extraction yields are given in Table 3 and the ammonium metavanadate composition in Table 4.

Table 3

Amount of ammonium metavanadate obtained and recovery yield

Sample	I	II	III	IV	V
Amount of ammonium metavanadate	4,01	4,75	4,217	4,358	4,817
Recovery yield	65,2	76,3	68,4	70,5	77,3

Table 4

Composition of ammonium metavabnadate

Composition %	NH_4VO_3	Cl^-	SO_4^{2-}	Fe^{3+}	Na^+	K^+
	99,2	0,277	0,35	0,012	0,12	0,15

Conclusions. — The extraction in acid medium proceeds in higher yields than that in basic medium but the subsequent processing of the solution is more difficult.

— The maximum number of extractions is three in both cases, its increasing being not advantageous from economical point of view.

— The obtained products, both vanadium pentaoxide and ammonium metavanadate, can be used either for obtaining new catalytical mass, or directly, as a catalyst, in the adipic acid obtaining.

— The procedures are rather simple, without using high pressures and temperatures.

REFERENCES

1. C. Calistru, C. Leonte, *Tehnologia sărurilor anorganice*, Ed. did. și ped. București, 1972.
2. P. Pascal, *Nouveau traite de chimie minerale*, **XII**, Masson et Cie. Ed. Paris, 1958.
3. R. Ripan, I. Ceteanu, *Chimia metalelor*, **II**, Ed. tehnică, București, 1968.
4. A. Timinova, V. Ivașentev, Zh. Priel Khim, 52, 1, 1979, p. 26.
5. * * *, Patent RSR, 60167.
6. * * *, Patent RSR, 69754.
7. * * *, Patent RSR, 88425.
8. * * *, Patent RSR, 88435.
9. * * *, Patent RSR, 88436.
10. * * *, Patent RSR, 77275.
11. * * *, Patent RSR, 78284.
12. * * *, Patent RSR, 59759.
12. A. N. Vlevna, Khim Jud. 35(2)50, 1963.
14. C. Liteanu, *Chimie analitică și cantitativă*, Ed. did. și ped. București, 1969.
15. N. Babenko, A. Busev, Zh. Neorgan. Khim. **18**, 3, p. 715.
16. A. Denisovo, P. Sokin, *Izv. Vissih. Neebnii. Zavadeni tretnaia metalurghia*, **5**, 1971, p. 98.
17. O. Vicol. I. Berdan, Revista de chimie, **1**, 1986, p. 61.
18. I. Blok, *Chimie analitică calitativă*, Ed. tehnică, București, 1958.
19. S. Kopaci, L. Paidovschi, Zh. Neorgan. Khim., **16**, 2, 1971, p. 445.
20. I. Roșca, M. Palamaru, Zilele Academice Ieșene, 1987, p. 7.

STUDIA UNIV. BABEŞ-BOLYAI, CHEMIA, XXXVI, 1—2, 1991

ROMANIAN RESEARCH IN FILTRATION

OCTAVIAN FLOAREA*, MIHAELA MIHAI*

ABSTRACT. A very interesting review of Romanian researches in filtration was performed, specially is analised the optimization of the filtration. The optimization criterion and the method used for the estimation of the objective function are specific to tree filtration problem that is to be solved. The problem will be developed in this way: determination of the optimum filtration volume on existing filtration installation, and determination of optimal areas of a filtrer and the needed pressure difference.

Scientific works, published lately in Romanian journals reflect the researchers efforts for the determination of proper conditions of separation for a solid — liquid suspension as well as the choice of suitable equipment. The great variety of the suspension types in chemical industry directed the reseach to a synthesis of the practical experience in mathematical models. They describe the filtration behaviour of different suspension types. In [2], [4], [6] and [14], the filtration of the suspensions obtained from biosynthesis processes, the models based on the stochastic techniques in deep filtration, complex models for washing cakes process and special techniques for seleting a mathematical model and a proper separation technique for a certain suspension are presented.

The filtration of liquids from the synthesis of antibiotics of the solid biomass [2] is a difficult process for the following reasons: the complex composition of these substances, their fine granulometry, the compact character of the solid phase as well as a great viscosity and the nonnewtonian behaviour of the filtrate. They study the influence of the following: suspension temperature, the mass ratio between solid phase and liquid phase and additions of chemical aids to suspentions in the filtration process. In a common laboratory installation the filtration constants were measured. There were also determined the most favorable conditions of separation on laboratory and pilot installations (on a rotary vaccuum drum filter). The conclusions are interesting for the synthesis of the following antibiotics: tetracycline, oxytetracycline and penicilin.

O. Floarea and M. Mihai present in [14], filtration models from the chemical engineering literature and suggest the proper choice criterion for the best separation description and intensifying methods in the filtration process. They analysed two experimental data types obtained in a laboratory for filter different values of the pressure difference. The suspensions were: aqueous calcium carbonate and a polydispersion suspension of nickel salts in acid medium which contained high density fine particles mainly and colloids. They get interesting information about filtration mechanism in a process that took place on a precoated filtration support and about the criterion of choosing the best support.

* *Polytechnical Institute Bucharest, Dept. of Chemical Engineering, 79585 Bucureşti, Romania*

A deep filtration model based on stochastic techniques is presented by O. Iordache [4]. He considered that the separation of suspension particles in a porous layer is the result of the interaction of two main elementary processes: transport and reversible adsorption. The author used polystochastic mathematical models proper for these transfer phenomena. These models stated that the particles could be included in more stochastic processes. Passing from one process to another is given by a stochastic connection process. The bidimensional stochastic process that was studied was considered to be a markovian one. The comparison between experimental data presented by Mackrle and mathematical model predictions is satisfactory.

G. Jinescu and N. Dinu in [6] studied the washing cake phase. They presented the principal physical and mathematical models used for the cake washing phase. To select the best model for a certain cake washing they worked on an experimental installation.

Some articles, e.g. [5] and [7], study sizing methods for the main filter types. Thus, R. Zamfirescu, A. Niculescu and E. Dacin presented a mathematical model for a rotary vacuum drum filter sizing. This model is fitted for incompressible cake. It consists of the filtration equation written for a constant pressure difference. In addition to this equation mass balance equation was used too. Experimental observations on rotary vacuum drum filter on pilot and industrial installations revealed that hydraulic resistance of filtration support was going to change in time because of warping filtration support. The authors used an exponential relation to express the previous dependence. So they get the optimal thickness of the cake layer which corresponded to a maximum rotation number. When this number is achieved the filter is brought to a stop to clean the filtration cloth. The mathematical model presented above permits filter performances calculation which are: dry cake and filtrate flow in case that the geometry and operational parameters, process parameters are known.

A complete study was done by G. Jinescu and N. Dinu in [7], a paper which emphasizes their interest in high productive equipment. They suggest a mathematical model for a belt filter. For the filtration phase, the filtration model under constant pressure difference was used. The area and filtration time is a function of the geometrical sizes of the belt and of the belt velocity. The equations of material balance was also considered. For the cake washing they used a diffusional model; for draining phase, classical equations given by the chemical engineering literature were used.

Work [1] has an experimental character and suggests some manufacturing materials for a fitrable support which has a high restraining effect of submicfonic particles. The filtration support quality is appreciated as a function of irltration velocity, of the restraining effect of particles and of solid mass quantity

Works [3] and [8—13] reveal the usefulness of optimization techniques with a view to determing the filtration apparatus performances and their appropriate operation conditions. These works present more selection criteria of an economical and noneconomical nature and study the results critically. It is demonstrated that the filtration process is completely studied if we use optimization criteria based on economical principles.

Al. Woinaroschy mentioned in [3] how to establish the optimal number of filtration cycles for a determined quantity of suspension. The problem to solve is to find the equation for a filtration cycle. A cycle means the proper filtration process plus the cake washing and plus time of the auxiliary operations which is a function of the suspension volume and of the filtration cycle number. If this equation is derivative with filtration cycles number and equaled to zero, the optimal number filtration cycle will be obtained for a certain suspension. The problem solved that way is simple, but it is to be reconsidered because of the importance of the economical factors.

O. Floarea and M. Mihai [8—13] studied the optimization of the filtration on economical basis. The optimization problem is the following:

The mathematical model which describes the filtration of most suspension types us:

$$\tau_T = a'\Delta p^{s-1}\left(\frac{F}{A}\right)^2 + b'\Delta p^{s-1}\frac{F}{A} + Va\left(2a'\Delta p^{s-1}\frac{A}{F} + b'\Delta p^{s-1}\right)\frac{\eta_a}{\eta_l} + \tau_{us} + \tau_{aux}$$

$$\text{at } \Delta p = ct \tag{1}$$

In addition to equation (1) there are the material balance equations for the filtration process considering the filtrate free of the solid phase:

$$S = P + Fq_f \qquad \text{and} \qquad cS = (1 - u)P \tag{2}$$

The model contains seventeen variables. Such variables as ρ_f, c, a, b, s, η_a, η_l (constants) or u, Va τ_{aux}, τ_{us} (selected on empiric basis) are predicble. Thus the number of decision variabls will be: $d = 17-3-11 = 3$, that means three variables among the following ones: Δp, τ_p, F, S, P and A. The filtration area and optimal filtration conditions represent the extreme of the objective function that can be written:

$$opt\,(FO) = f(\Delta p,\ \tau_T,\ F,\ S,\ S,\ P,\ A) \tag{3}$$

One can replace S and P by:

$$S = \frac{Fq_f(1-u)}{1-u-c} \quad \text{and} \quad P = \frac{cF\rho_f}{1-u-c} \tag{4}$$

and from the equation (1) and the objective function is now:

$$opt(FO) = f(\Delta p,\ F,\ A) \tag{5}$$

Restrictions for the equation (5) are of operational and constructive nature:

$$p \leqslant p_{max} \text{ and } A \leqslant A_{max} \tag{6}$$

These restrictions appear because of the physical construction of the apparatus and of its material and energetic consuption.

The optimization criterion and the method used for the estimation of the objective function are specific to the filtration problem that is to be solved. The problem will be developed these ways:

1. **Determination of the optimum filtration volume on an existing filtration installation.** In experiments on a filtration installation we know the filtration are area and, sometimes, the difference pressure under which the filter operates.

In addition to this information we need to determine the optimal suspension volume in a filtration cycle. The optimization criterion used for this problem was the net profit *Ba*, *Ba* represents the difference between yearly installation achievements R and expenses C:

$$Ba = R - C \tag{7}$$

The achievments will be a function of the filtrate volume, if the filtrate is the main product, of the cake value or of both, if the cake and the filtrate are the goal. In order to simplify the equation, it is considered that the filtration volume is the main one and the achievements in this case are defined as:

$$R = C_F F \tag{8}$$

The expenses for a filtration cycle represent the cost of amortization, the running cost, the energy cost and the used materiales cost. The sum of all these costs is C the total cash cost:

$$C = C_{am} + C_{man} + C_{en} + C_{cons} \tag{9}$$

The amortization cost is then:

$$Cam = Cu * Ram \tag{10}$$

It is considered that the expenses for labour and maintenance are a percentage from the amortization cost. In Romania this percentaje is 0 = 40–90%.

The cost of the electric energy Cen is:

$$Cen = \Delta p * A * Gesp * cen * H * (\tau_T - \tau_{aux})/\tau_T \tag{11}$$

The electric energy consumption is difficult to be evaluated theoretically because the process takes place in unsteady state conditions in bi- or three-phase systems. The specific consumption of air *Gesp* used in the separation process, is determined experimentally. *Gesp* is a part of equation (11).

Ccons is a function of the cost of filtrate support:

$$Ccons = c_{csf} * A * cfiltr.a * H/\tau_T \tag{12}$$

The net profit is finally dependent only on F and Δp:

$$B_a = F_{cF} - c_1 F^2 \Delta p^{s-1} - c_2 F \Delta p^{s-1} - c_3 \Delta p^{s-1} - c_4 F^2 \Delta p^s - c_5 F \Delta p^s - c_6 \Delta p^s - c_7 F - c_8 \tag{13}$$

The maximum of function (13) represents the solution of the problem.

2. **Determination of optimal areas of a filtrer and the needed pressure difference.** In this case we want the best choice of the filtration areas and pressure difference; we decide upon the optimization criterion of the yearly total cash cost of separation process. The function (14) is obtained from (13) and expresses the dependence between the optimal criterion and the filtration area and pressure difference:

$$c_T = c_1 \Delta p^{s_2} A^{B-2} + c_2 \Delta p^{s-1} A^{\beta-1} + c_3 \Delta p^{s-1} A^{\beta} + c_4 A^3 + c_5 \Delta p^s A^{-1} + c_6 \Delta p^s + c_7 \Delta p^s A + c_8 \Delta p A + c_9 A \tag{14}$$

The cost of equipment Cu is connected with the filtration area as follows:

$$C_u = \alpha A^{\beta} \tag{15}$$

Constants α and β were determined for different equipment and material types by regression of the costs of the equipment made by Romanian factories as a function of area. The minimum of function [14] is the solution of the problem: filtration area and difference pressure when the cost of the process is minimum.

SYMBOLS

a', b' — specific resistance of cake filtration, support respectively
c — concentration of solid phase in suspension
csp — specific consuption of filtration material support
cen — price of energy
cf — price of filtrate
$cpinza$ — price of filtration support
H — total anual number of hours for an operating filter
P — cake
— index of cake compresibility
S — suspension
u — umidity
$V\,a$ — specific volume of washing water
τ_T — total time of filtration cycle
τ_{ns} — time of auxiliary operation, energy eating operations
a_{ux} — time of auxiliary operation, non energy eating operations
η_l — viscosity
ρ — density

REFERENCES

1. Meakin, O. C., — Chem. Rev. (Bucharest), 24, 1973, p. 879.
2. Moscovici, M., Nanescu, G., Ciobanu, I. — Chem. Rev. (Bucharest), 29, 1978, p. 55.
3. Woinarosky, Al. — Chem. Rev. (Bucharest), 31, 1980, p. 913.
4. Iordache, O. — Chem. Rev. (Bucharest), 32, 1981, p. 17.
5. Zamfirache, R., Niculaescu, A., Dacin, E. — Chem. Rev. (Bucharest), 33, 1982, p. 150.
6. Jinescu, G., Dinu, N. — Chem. Rev. (Bucharest), 36, 1985, p. 327.
7. Jinescu, G., Dinu, N. — Chem. Rev. (Bucharest), 37, 1986, p. 604.
8. Floarea, O., Mihai, M. — Chem. Rev. (Bucharest), 39, 1988, p. 419.
9. Floarea, O., Mihai M. — Chem. Rev. (Bucharest), 39, 1988, p. 593.
10. Floarea, O., Mihai, M. — Chem. Rev. (Bucharest), 39, 1988, p. 682.
11. Floarea, O., Mihai, M. — Chem. Rev. (Bucharest), 39, 1988, p. 1113.
12. Floarea, O., Mihai, M. — Chem. Rev. (Bucharest), 40, 1989, p. 49.
13. Floarea, O., Mihai, M. — Chem. Rev. (Bucharest), 40, 1989, p. 330.
14. Floarea, O., Mihai M., Sora, M., Kohn, D., Moraru, M. — Chem. Rev. (Bucharest), 42, 1991.

STUDIA UNIV. BABEŞ-BOLYAI, CHEMIA, XXXVI, 1—2, 1991

DER EINFLUSS VON PLASTIFIKATOREN AUF DIE EIGENSCHAFTEN DER ZEMENTPASTEN

MARIA GEORGESCU*, ANNEMARIE PURI*

ABSTRACT. The Effects of the Plasticizer Admixtures on the Properties of Cement-Pastes. The study analyses the flowing effect of four plastifiers: VIMO—11, FLUBET, LSC and DISAN, on cement-pastes: that prepared with Portland-cement, and that with a cement with 10% Si.

These plastifiers make possible the reducing of the W/C ratio, assuring the flowing of the cement-paste without adding water. Using these plasticizers we can obtain the same consistency of the paste, with a dosage of water equal to only 1/2 of that used for a simple paste (without admixtures).

1. **Einleitung.** Der Einsatz von Plastifikatoren bei der Herstellung von (Mörtel) Beton ermöglicht eine bedeutende Verbesserung ihrer Qualität, sowohl in frischem Zustand, als auch nach der Erhärtung. Die Wirkung der Plastifikatoren wird von ihrer Art und der zugesetzten Menge, im Zusammenhang mit der Natur des Zementes im Beton, bestimmt [1—6].

Die Plastifikatoren wirken an den Grenzflächen Fest-Flüssig-Gas, wobei sie sowohl die rheologischen Eigenschaften der Zementpasten (Mörtel oder Betone), als auch die Hydratation-Hydrolyse des Zementes und die Bildung der Erhärtungsstruktur beeinflussen, was sich günstig auf die mechanischen Eigenschaften der erhärteten Mörtel und Betone auswirkt.

In dieser Arbeit wurde der Einfluss von verschiedenartigen Plastifikatoren (mit verflüssigender Wirkung) auf die rheologischen Eigenschaften und das Erstarren von Zementpasten aus normalem Portlandzement, bzw. Zement mit ultrafeinem Si-Staub (silica fume), untersucht.

2. **Versuchsbedingungen und Ergebnisse.** Der in dieser Arbeit untersuchte Portlandzement, bzw. Portlandzement mit 10% Si-Staub hatte eine Mahlfeinheit von 2800—2900 cm^2/g Blaine. Als Plastifikatoren wurden Kalziumlignosulfonat (LSC), Disan, VIMC-11 und Flubet angewendet. Das LSC und Diesan waren pulverförmig, das VIMC-11 und Flubet lagen als 20%, bzw. 26% Lösungen in Wasser vor. Alle Plastifikatoren wurden im Bereich 0,1—2 Ma-% aktive Substanz dosiert.

Es wurde der Einfluß der Plastificatoren auf die, für Normalkonsistenz nötige Menge Anmachwasser, auf die Versteifung und die rheologischen Eigenschaften der Zementpasten, untersucht.

2.1. *Der Einfluß der Plastifikatoren auf die Konsistenz der Zementpasten.* Alle eingesetzten Plastifikatoren üben eine verflüssigende Wirkung auf die Zementpasten aus, was auf Grund ihrer dispergierenden Wirkung auf die Festkörperteilchen zu erwarten war. Die Diagramme au-s Bild 1 und 2 zeigen auch

* *Polytechnische Hochschule, 79585, Bukarest, Romania*

für kleine Zusatzmengen eine Reduzierung der W/Z-Werte, welche der Normalkonsistenz der Zemenet pasten entsprechen.

Für beide untersuchten Zementarten ist die verflüssigende Wirkung von VIMC-11 am bedeutendsten, es folgt abfallend Flubet, Disan und LSC.

Für Portlandzement ist die verflüssigende Wirkung und Zemendementsprechend die Reduzierung der W/Z—Werte der Pasten mit Normalkonsistenz auch bei kleinen Mengen Plastifikator sichtbar und ist für 0,5—0,9 Ma-% aktive Substanz (in Abhängigkeit von der Art des Plastifikators) am wirksamsten (s. Abb. 1). Die verflüssigende Wirkung von Disan und LSC ist etwas schwächer, so das bei gleichen oder sogar grösseren Zusatzmengen, die Reduzierung der W/Z—Werte für Normalkonsistenz nur ungefähr 20% beträgt, im Vergleich zu 30—33% bei VIMC-11 und Flubet.

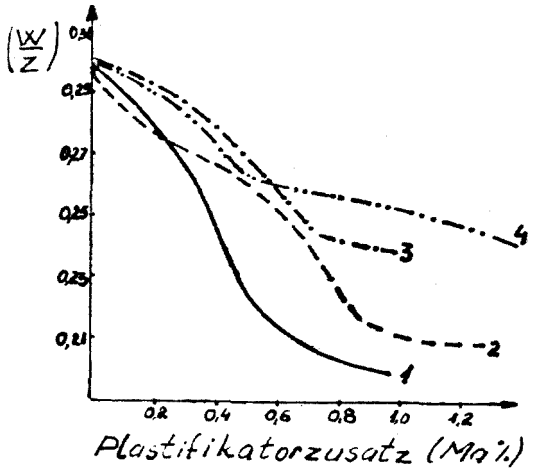

A b b. 1. Variation der W/Z — Werte der Portlandzementpasten mit Normalkonsistenz, als Funktion der Plastifikatormenge: *1* — VIMC-11; *2* — Flubet; *3* — Disan; *4* — LSC;

Bei dem Zement mit 10% ultrafeinem Si-Staub wird die verflüssigende Wirkung der Plastifikatoren nur bei mehr als 0,4—0,6 Ma-% aktive Substanz deutlich sichtbar und verstärkt sich bis zu ungefähr 1 Ma-% aktive Substanz bei VIMC-11 und Flubet, bzw. 1,7—2 Ma-% Zusatz bei Disan und LSC (Abb 2).

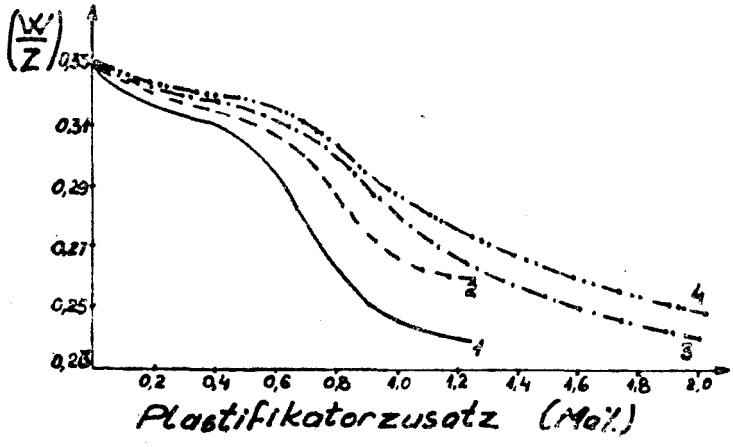

A b b. 2. ibidem 1, für (Portlandzement + 10% Si-Staub) Pasten

Das Vorhandensein von ultrafeinem Si-Staub im Zement vergrößert die Konsistenz der entsprechenden Zementpasten, so daß der W/Z-Wert von 0,30 (für Zement ohne Si-Staub) auf 0,32 (Zement mit 10% Si-Staub) gehoben werden muß, um Normalkonsistenz zu realisieren.

Die vom Si-Staub ausgelöste Reduzierung des Fließvermögens der Zementpasten wird von der besonders großen Feinheit dieses Materials bestimmt (200 cm^2/g spezifische Oberfläche BET) und macht dadurch den Einsatz von Plastifikatoren bei der Herstellung von Beton aus Zement mit Si-Staub, unerlässlich. Die optimalen Zusatzmengen der in dieser Arbeit untersuchten Plastifikatoren sind, im Allgemeinen, größer als bei Zement (ohne Si-Staub) und sind um so größer, je schwächer die Wirkung der Plastifikatoren ist.

2.2. *Der Einfluss der Plastifikatoren auf die rheologischen Eigenschaften der Zementpasten.* Die Ergebnisse der Viskositätsbestimmungen mit einem Rheotest-Viskosimeter, für Zementpasten mit $W/Z = 0{,}30$, bzw. Zement + Si-Staub Pasten mit $W/Z = 0{,}32$, sind in den Abb. 3—6 dargestellt. Bei den sehr aktiven Plastifikatoren VIMC-11 und Flubet, führen Zusätze von nur 0,1 Ma-% aktive Substanz zu einer ungefähr dreifachen Reduzierung der Viskosität der Zementpasten. Bei größeren Zusätzen sinkt die Viskosität nur noch schwach weiter. LSC und Disan haben eine weniger energische Wirkung auf das Fließvermögen der Zementpasten und bewirken nur bei 2—3 mal größeren Zusatzmengen eine vergleichbare Verflüssigung wie VIMC-11 und Flubet .

Die Verflüssigung der Zementpasten durch Plastifikatoren—Tenside mit Polargruppen in ihrer Struktur, ist das Resultat der Adsorbtion dieser Substant

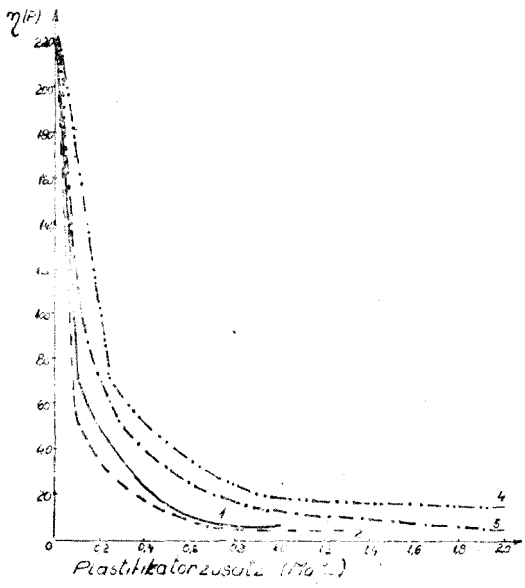

A b b. 3. Variation der Viskosität der Portlandzementpasten mit $W/Z = 0{,}3$, als Funktion der Plastifikatormenge: *1* — VIMC-11; *2* — Flubet; *3* — Disan; *4* — LSC;

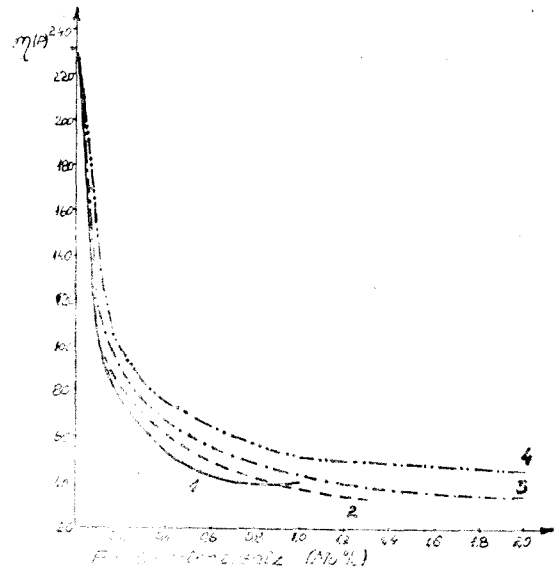

A b b. 4. ibidem 3, für (Portlandzement + 10% Si-Staub) Pasten.

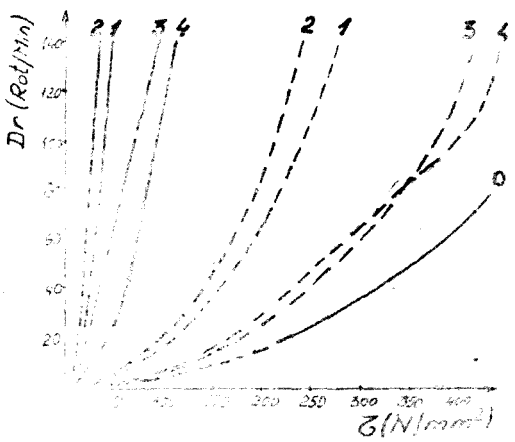

Abb. 5. Variation der Verformungsgeschwindigkeit als Funktion der Scherenspannung, für Portlandzementpasten mit $W/Z = 0{,}3$; *0* — ohne Plastifikator; *1* — mit VIMC-11; *2* — mit Flubet; *3* — mit Disan; *4* — mit LSC; —1,0% Zusatz, —0,1% Zusatz.

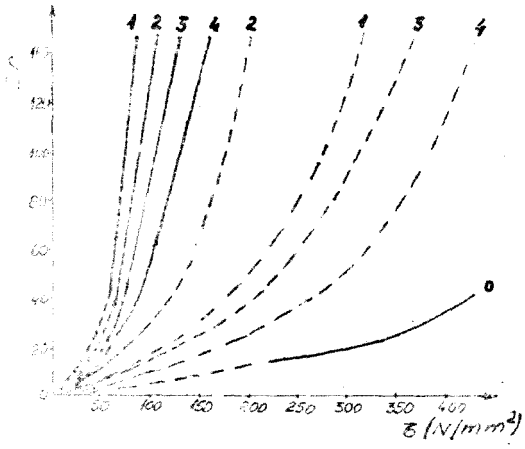

Abb. 6. ibidem 5, für (Portlandzement + 10% Si-Staub) Pasten, mit $W/Z = 0{,}32$.

zen auf der Oberfläche der Zementkörner, was die Mobilität der Zementteilchen verbessert und folglich das Fließvermögen der Zementpasten vergrößert. Die verschiedene Intensität der verflüssigenden Wirkung der untersuchten Plastifikatoren ist den Unterschied ihrer Strukturcharakteristiken, vor allem dem Anteil an Polargruppen, zuzuschreiben.

Die auch bei höheren W/Z-Werten größere Viskosität der Zementpasten mit Si-Staub wird durch Zusatz von Plastifikatoren verkleinert, bleibt aber auch bei optimalen Zusatzmengen ungefähr 2—3 mal größer im Vergleich mit derjenigen von Portlandzement pasten ohne Si-Staub.

Die Zugabe von Plastifikatoren in die Zementpasten führt zu wesentlichen Änderungen in der Verformungsgeschwindigkeit dieser Pasten, welche durch die Drehgeschwindigkeit des inneren, beweglichen Zylinders des Rheotest-Viskosimeters, gewertet wird. Für alle untersuchten Plastifikatoren zeigen die Rheogramme aus Bild 5 und 6, bei gleichbleibender Scherenspannung eine um so größere Verformungsgeschwindigkeit (*Dr*) der Zementpasten, je größer der Plastifikatorzusatz ist. Das ist durch die dispergierende Wirkung der Plastifikatoren auf die Zementteilchen, welche deren Mobilität verbessert, zu erklären.

Bei gleicher Scherenspannung ist die Verformungsgeschwindigkeit der Zement pasten mit Si-Staub, auch bei größeren W/Z-Werten, kleiner als diejenige der Zementpasten ohne Si-Staub, was den negativen Einfluß der sehr feinen Siliziumdioxidteilchen auf die rheologischen Eigenschaften der Zementpasten bestättigt. Obwohl die absoluten Werte bei den Zementpasten mit Si-Staub kleiner sind, ist die verflüssigende Wirkung der Plastifikatoren bedeutender als bei den normalen Zementpasten-s. den Unterschied zwischen den Kurven mit und ohne Plastifikator, besonders für 0,1 Ma-% Zusatz in Bild 5 und 6.

2.3. *Der Einfluß der Plastifikatoren auf das Erstarren der Zementpasten.* Die Plastifikatoren verzögern, im Allgemeinen, das Erstarren der Zementpasten. Diese Verzögerung ist eine Folge der Adsorbtion der Plastifikatoren, sowohl auf die Oberfläche der Zementkörner — was deren Hydratation-Hydrolyse verzögert, als auch der im ersten Stadium sich bildenden, gelartigen Hydratphasen — was zu einer Verzögerung der Polikondensationsvorgänge und der Strukturierung der Zementpaste führt.

Die von den Plastifikatoren bestimmte verzögernde Wirkung auf das Erstarren der Zementpasten muß im Zusammenhang mit den *W/Z*-Werten dieser Pasten analysiert werden.

Die Bestimmung der Abbindezeit für Zementpasten mit Normalkonsistenz hat eine Verzögerung des Abbindeanfangs — bei LSC und Disan für alle getesteten Zusatzmengen, bei VIMC-11 und Flubet nur für kleine Zusetzmengen (0,5 Ma-% aktive Substanz), gezeigt; größere Zusatzmengen bewirken, besonders bei VIMC-11, einen kürzeren Abbindeanfang — Abb. 7. Wenn man die für VIMC-11 und Flubet besonders kleinen W/Z-Werte für Normalkonsistenz in Betracht zieht, erscheint die verzögernde Wirkung dieser Plastifikatoren besonders ausgeprägt und ist durch die Bildung eines Adsorbtivfilms auf den Zementkörnern, welcher den Wasserzugang bedeutend erschwert und dementsprechend die Reaktion mit Wasser verzögert, zu erklären. Bei größeren Zusatzmengen (0,75—1,0 Ma-%) scheint die Wirkung der kleinen W/Z-Werte bedeutender als die verzögernde Wirkung der adsorbierten Plastifikatorfilme zu sein, demzufolge wird eine Verkürzung des Abbindeanfangs festgestellt (s. auch Abb. 1). Diese Befunde sind in gutem Einklang mit früheren Ergebnissen über die Wirkung von VIMC-11 und VIMC-22 auf Pasten aus Zement mit hohen Anfangsfestigkeiten, mit und ohne Flugasche [9].

Bei LSC und Disan, welche die W/Z-Werte für Normalkonsistenz weniger reduzieren, ist die verzögernde Wirkung auf den Abbindeanfang um so bedeutender, je größer die Zusatzmenge ist.

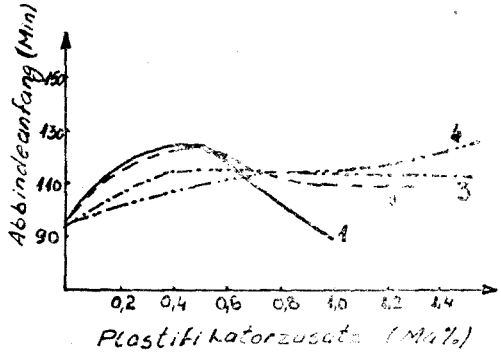

A b b. 7. Variation des Abbindeanfangs der Portlandzementpasten mit der Zusatzmenge Plastifikator *1* — VIMC-11 *2* — Flubet *3* — Disan *4* — LSC

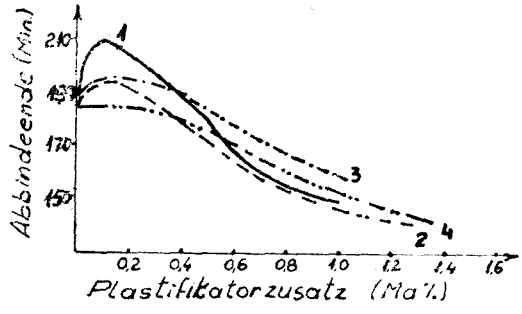

A b b. 8. Variation des Abbindeendes der Portlandzementpasten mit der Zusatzmenge Plastifikator *1* — VIMC-11 *2* — Flubet *3* — Disan *4* — LSC

Bei kleinen Zusatzmengen Plastifikatoren (0,1—0,25 Ma-% aktive Substanz) wird das Abbindeende in allen Fällen etwas verzögert, während bei größeren Zusatzmengen das Abbindeende um so früher stattfindet, je höher der Plastifikatorzusatz und je energischer dessen verflüssigende Wirkung sind (Abb. 8). Ein derartiges Verhalten wird durch die dispergierende Wirkung der Plastifikatoradsorbtion auf die anfangs gelartigen Hydratphasen im Zusammenhang mit der Reduzierung der W/Z-Werte der Zementpasten bewirkt.

3. **Schlußfolgerungen.** Die Versuchsergebnisse führen zu folgenden Schlußfolgerungen :

- Die Plastifikatoren VIMC-11, Flubet, LSC und Disan haben eine bedeutende, verflüssigende Wirkung auf die Zementpasten, sowohl aus einfachem Portlandzement, als auch aus Zement mit 10% ultrafeinem Si-Staub ; die verflüssigende Wirkung verstärkt sich in der Reihe LSC—Disan—Flubet—VIMC-11 und führt zu einer bedeutenden Reduzierung der, für Normalkonsistenz notwendigen W/Z-Werte. Bei den Zementpasten mit 10% ultrafeinem Si-Staub werden etwas größere Plastifikatorzusätze benötigt, um verflüssigende Wirkung zu erzielen, als bei normalen Zementpasten.

- Die Plastifikatoren verbessern, bei gleichbleibendem Wassergehalt, das Fliessvermögen der untersuchten Zementpasten.

- Die Abbindezeit der Zementpasten wird von den Plastifikatoren diskontinuirlich beeinflußt, was durch die gleichzeitige Wirkung der reduzierten W/Z-Werte der Pasten mit Normalkonsistenz zu erklären ist.

LITERATUR

1. V. Moldovan, — *Aditivi în betoane*, Ed. Tehnică, Bucureşti, 1978.
2. V. Moldovan, D. Tatu — Materiale de Construcţii, **9**, (3), 119, 1979.
3. I. Teoreanu — Materiale de Construcţii, **10**, (1), 31, 1980.
4. I. Ionescu, — Materiale de Construcţii, **10**, (1), 41, 1980.
5. G. Popescu, u.a. — Materiale de Construcţii, **10**, (1), 37, 1980.
6. I. Teoreanu u.a. — *Durabilitatea betonului*, Editura Tehnică, Bucureşti, ET 1982.
7. H. Ukikawa — 8th Congr. on the Chem. of Cem., Rio de Janeiro 1986, vol. **I**, S. 249.
8. T. Managialiardi, A. E. Paolini — Cem. and Concr. Res. **18**, (3), 351, 1988.
9. M. Georgescu, A. Puri — Materiale de Construcţii, **12**, (2), 63, 1982.

STUDIA UNIV. BABEŞ-BOLYAI, CHEMIA, XXXVI, 1—2, 1991

NEUE GENERATIONEN FEUERFESTER BETON — ADDITIVIERTER BETON MIT GERINGEM TONERDEZEMENT — GEHALT. ERHÄRTUNGSMECHANISMEN

ION TEOREANU*, NICOLAE ANGELESCU**

ABSTRACT. New Genérations of Fire-Proof Concretes. Effects of Admixtures upon their Hardening. The authors studied the properties of four new fire-proof concretes, depending on W/C Ratio, dosage of water, and of different plastifiers: CrO_3, and organic ones: LSC and VIMC-22; that of cement and aggregats. Their strenght's variation with the increasing of temperature, and durability was also analysed.

1. Einleitung.

Das Betrachten von Beton im Allgemeinen, von feuerfestem Beton im Besonderen, als Komposit-materialien, bestehend aus einer kontinuirlichen Phase — der zementierenden Matrix, welche die Zuschlagstoffe, als diskontinuirliche Phase, enthalt, mit dem Ausbilden von Grenzflächen, liefert eigentlich die Grundelemente zu der Evolution der Anschauung über den Aufbau und bzw die Technologie dieser Erzeugnisse, welche zu spektakulären Änderungen ihrer Eigenschaften und somit ihrer Nutzungsperformanzen führen.

Die mechanische Festigkeit, als entscheidende Eigenschaft für den strukturellen Beständigkeisgrad, hat für, aus körnigen Systemen hergestellte Erzeugnisse um so größere Werte, je größer die Zwischenkorn Kohäsion ist. Unter diesen Umständen erfüllt der hydraulische Zement im feuerfesten Beton eine komplementäre Rolle, folglich kann sein Anteil reduziert werden.

Die Reduzienung des Anteils an hydraulichem Zement — Tonerdezement, im feuerfesten Beton, hat folgende positive Auswirkungen:

— die Anmachwassermenge wird reduziert, was sich direkt auf die Porosität des Betons auswirkt;

— die mechanischen Festigkeitsverluste des Betons im kritischen Temperaturbereich werden vermindert;

— die pyroskopischen Eigenschaften des Betons verden verbessert, vor axem seine Feuerfestigkeit.

Auf diese Art sind neue Generationen feuerfeste Betone — mit geringem oder sehr geringem Zementanteil, entstanden [1—22]. Die besonderen Eigenschaften dieser Betone haben ihr Anwächsen in der Palette der gebrannten und nichtgebrannten feuerfesten Materialien bestimmt. In den entwickelten Ländern bilden die nichtgebrannten, nichtgeformten feuerfesten Materialien, zu welchen auch die Betone gehören, 40—50% der verwendeten feuerfesten Materialien, wobei der feuerfeste Beton ungefähr 50% der nichtgeformten feuerfes-

* *Polytechnische Hochschule, 79585, Bukarest, Romania*
** *Forschungsinstitut für Metallurgie, Bukarest, Romania*

ten Materialien ausmacht. In der neuen Betongeneration mit geringem oder sehr geringem Tonerdezementanteil, dienen als spezifische Komponente, neben den feuerfesten Zuschlagstoffen, komplexe Bindemittelmischungen, dispergierende und verflüssigende Additive, ultradispergierte Mineralpulver. Auf diese Art werden die positiven Folgen der Reduzierung des hydraulischen Zementanteils besser gewertet, und zwar weil gleichzeitig die Kohäsionskräfte der Matrix mit den Zuschlagstoffen nicht vermindert und die rheologischen Eigenschaften und das Verarbeitungsverhalten bedeutend verbessert werden. Die Konvergenz der Wirkungen welche die Kompositionsänderungen der neuen feuerfesten Betongenerationen hervorrufen, konnte nur auf Grund der Erhärtungsmechanismen erzielt werden.

2. Der Einfluß der Komponenten des feuerfesten Betons auf seine Eigenschaften.

Die Dauerhaftigkeit und die Höchstleistungen des feuerfesten Betons sind von der Natur und den Eigenschaften seiner beiden Makrophasen — der Matrix und des Zuschlagstoffes, sowie von der Kompatibilität zwischen Matrix und Zuschlagstoff und dem Matrix/Zuschlagstoff Wert, abhängig.

2.1. **Der Einfluß der Matrix.** Bei der Generation der gewöhnlichen, herkömmlichen Betone, welche mit einem verhältnismäßig großen Anteil Tonerdezement zubereitet werden, bildet die Bindemittelmatrix den „schwachen Teil" des Betons. Diese Matrix macht den Beton hochporös, führt zu bedeutenden Festigkeitsabnahmen im kritischen Temperaturbereich und zu geringeren Feuerfestigkeiten. Darum werden bei kleineren Matrix/Zuschlagstoff Werten, also einem kleineren Tonerdezementanteil, diese Unzulänglichkeiten reduziert. Die Verkleinerung des Matrix/Zuschlagstoff Werts durch die Reduzierung des Tonerdezementanteils, ohne andere zusätzliche Maßnahmen führt aber gleichzeitig zu einer Verminderung der Kohäsionskrräfte zwischen der Matrix und den Zuschlagstoffen, also zu kleineren Betonfestigkeiten. Um des zu vermeiden muß in erster Reihe die Zusammensetzung des Systems beeinflußt werden und zwar sowohl durch die Qualität der Matrix (Porosität, Volumenbeständigkeit, eigene mechanische Festigkeit) als vor allem durch die Natur und den Wert ihrer Grenzflächen mit den Zuschlagstoffen.

2.1.1. *Der Einfluß des Zementes.* Um unter normalen Bedingungen entsprechend zu erhärten werden die herkömmlichen feuerfesten Betone mit einem Tonerdezementantail von 15—30% zubereitet; der hydratisierte Zement entwickelt Neubildungen, welche durch Verkettung die Struktur des Betons verfestigen und ihm entsprechenden mechanische Festigkeiten bei normalen Erhätungsbedingungen verleihen.

Der große Zementanteil setzt eine große Menge Wasser voraus, welche eine gute Verarbeitbarkeit und einen entsprachenden Ablauf der Hydrations, vorgänge sichert. Im Vergleich damit ist bei den Betonen der neuen Generationmit einem kleinen oder sehr kleinen Zementgehalt, der Wasseranteil 2—3 mal kleiner — Abb. 1 [12]; das erklärt die bedeutend kleinere Porosität dieser Betone, mit günstigen Auswirkungen auf ihre Nutzungsperformanzen.

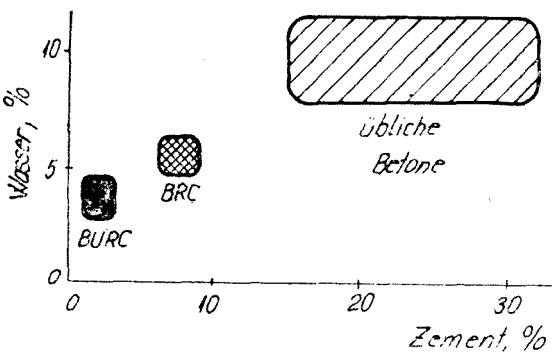

A b b. 1. Wechselbeziehungen zwischen Zementgehalt und Wasserbedarf bei der Zubereitung von feuerfesten. Beton BRC — Beton mit reduziertem Zementgehalt BURC — Beton mit ultrareduziertem Zementgehalt

Der große Anteil an hydratisierten Neubildungen in dem Gefuge der gewöhnlichen feuerfesten Betone erklärt gleichzeitig den Festigkeitsverlust im kritischen Temperaturbereich, als Folge der Dehydratation dieser Hydratphasen — Abb. 2 [4].

Da der Zement (die zementierende Matrix) den Flußmittelanteil des Betons darstellt, ist auch die dritte, bei gewöhnlichen Betonen auftretende Unzulänglichkeit verständlich — eine kleinere Feuerfestigkeit bei anwachsendem Zementanteil — Abb. 3 [21].

Eine große Fähigkeit der Bindemittelmatrix die Zuschlagstoffe zu leimen und entsprechende Matrix-Zuschlagstoff Kohänsionskräfte zu entwickeln — sowohl bei normalen, als auch bei Nutzungstemperaturen, unter Anwendung eines kleinen Tonerdezementanteils (hydrauliches Bindemittel), können durch Einsatz von dispergierend — verflüssingenden Additivstoffen, von Trägern von chemischen (nichthydraulischen) oder keramischen Bindungen oder von hoch-

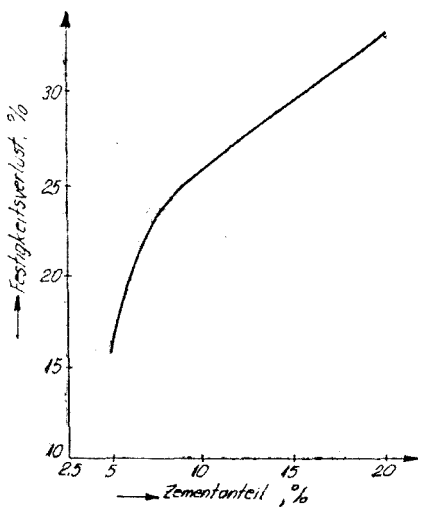

A b b. 2. Variation der Festigkeitsverluste der feuerfeste Betone aus Tabulartonerde (maximale Körnung 3,36 *mm*) und Tonerdezement, im kritischen Temperaturbereich, als Funktion des Zementgehaltes.

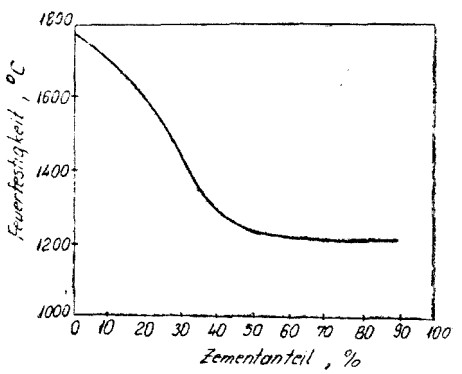

A b b. 3. Die Wirkung des Zementgehaltes auf die Refraktarität eines Betons aus Zuschlagst off mit 42% Al_2O_3 und Tonerdezement.

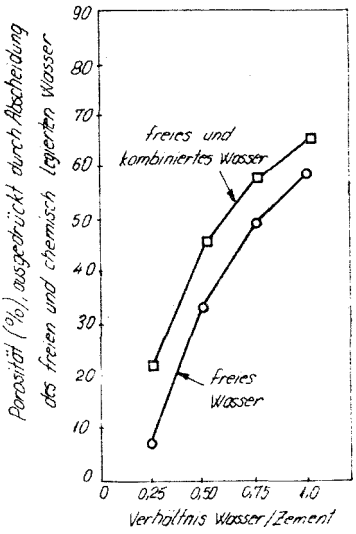

A b b. 4. Die Wirkung des W/Z — Wertes auf die Porosität der Tonerdezementpasten, durch die Entferung des freien und chemisch gebundenen Wassers ausgedrückt.

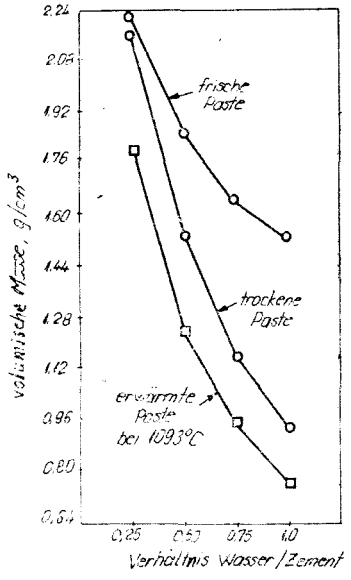

A b b. 5. Die Wirkung des W/Z — Wertes auf die Volumenmasse der Tonerdezementpasten.

dispersen Mineralzusatzstoffen zum frischen Beton, erreicht werden. Eine anf diese Art entstandene Zementierende Matrix wird hochwertigere Eigenschaften haben.

2.1.2. *Der Einfluß des Anmachwassers.* Die Menge des Anmachwassers ist gewöhnlich größer als genau für die Hydratations — Konversions — Vorgänge benötigt wird. Der Wasserüberfluß liegt im Beton als freies Wasser vor, welchsen der Betonporosität beiträgt (beim Erwärmen hat die Ausscheidung des chemisch gebundenen Wassers die gleichen Folgen) — Abb. 4; entsprechend ist auch die Dichtigkeit des Betons beeinflusst — Abb. 5 [8]. Eine Gesammt-darstellung dieser Phänomene zeigt Abb. 6, in welchen der gleichzeitige Einfluß des Wasseranteils — al a W/Z — Wert ausgendnickt, auf den Volumenanteil der Matrix im Beton bzw auf die Raumdichte der Matrix, dargestellt ist [8]; der Anteil der Matrix mit einer progressiv kleineren Raumdichte wächst mit dem Anwachsen des W/Z — Wer-

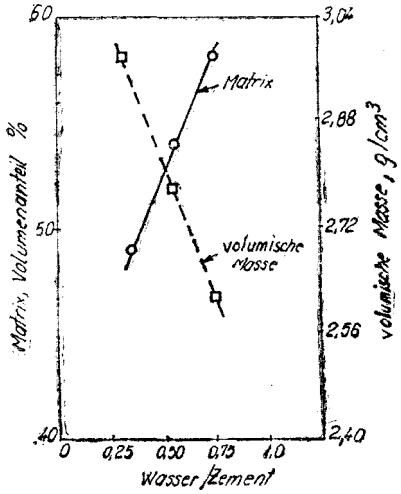

A b b. 6. Die Wirkung des W/Z — Wertes auf die Volumenmasse und den Matrix/Zuschlagstoff — Wert für einen Beton mit Tabulartonerde.

tes. Um hochwertige Betone zu erhalten muß folglich der Wasseranteil bei niedrigen Werten gehalten werden.

Die Reduzierung des Matrixanteils im Beton wird simultan durch die Reduzierung des Zementanteils und des W/Z — Wertes erreicht. Obwohl die Reduzierung des Zementanteils den Wassergehalt des Betons verkleinert, kommt es doch zu größeren W/Z — Werten um eine gute Verarbeitbarkeit des Betons zu sichern. Um gute rheologische Eigenschaften und demzufolge ein e gute Verarbeitbarkeit bei möglichst kleinen W/Z — Werten zu erzielen ist die Anwendung wasserreduzierenden Additivstoffen mit dispergierend — verflüssigender oder superverflüssigender Wirkung unerlässlich. Eine noch bedeutendere Verdichtung der Matrix kann durch gleichzeitige Anwendung von verflüssingenden oder superverflüssigenden Additivstoffen mit hochdispersen Mineralzusatzstoffen und energischen Verdichtungsmethoden erreicht werden.

2.1.3. *Der Einfluß der Additive und Zusatzstoffe.* Aus der vorgehenden Analyse der quantitativen und qualitativen Einflußgrößen auf die Bindemittelmatrix und demzufolge auf die Performanzen der feuerfesten Betone, entsteht für einfache Zuschlagstoff-Tonerdezement-Wasser Systeme ein Widerspruch: es besteht eine antagonische Beziehung zwischen der Notwendigkeit den Anteil Bindemittelmatrix im Beton zu reduzieren um ein möglichst hochwertiges Nutzungsverhalten zu erzielen (was Strukturbeständigkeit und Eigenschaften, sowie Feuerfestigkeit anbelangt) und der Notwendigkeit möglichst große (entsprechende) mechanische Festigkeiten, einschließlich bei normaler Temperatur, zu entwickeln, Dieser Widerspruch kann — wie schon vorausgesagt wurde, durch Anwendung von dispergierend — verflüssingenden und superverflüssigen den Additivstoffen oder/und nichthydraulischen Zusatzstoffen welche Träger von Zementtierenden Bindungen sind oder von hochdispersen, reaktiven besonders Kieselgur — oder Tonerde-haltigen-Zusatzstoffen, gelöst werden.

Eine, der Dichte des Betons möglichst nahe Raumdichte setzt nicht nur eine entsprechende Auswahl der Körnung des feuerfesten Zuschlagstoffes, Sondern auch einen möglichst hohen Volumen/Raum-Wert (ε), als Folge der Zementhydratation voraus, welcher eine möglichst hohe Kompaktität und eine möglichst große Kohäsion an den Grenzflächen Zuschlagstoff-Matrix (hydratisierte Neubildungen) sichert. Der Einsatz von dispergierend — verflüssigenden oder superverflüssigenden Additivstoffen ermöglicht die Verwirklichung dieser Notwendigkeit. Durch ihre dispergierende Wiskung ermöglichen sie eine größere Beweglichkeit und demzufolge das Ausbilden von nahen Koagulationsstrukturen der hydratisierten Neubildungen des Zementes, auf welchen sich später kompakte, homogene, widerstandfähige Kristallisations-Polykondensations Strukturen aus bilden. Die deflokulierende, die Koaleszenz der, bei der Zementhydratation enstandenen Neubildungen, zerstörende Wirkung, führt außer dem Anwachsen der Kompaktität und Homogenität — als Folge der Evolution der Strukturierung und der Charakteristiken der Strukturen welche bei der Zementhydratation entstehen zu einer Reduzierung des Anmachwassers und folglich, der Porosität, wodurch die Matrix auch auf diesen Weg kompakter und dementsprechend widerstandsfähiger wird.

Der große Dispersionsgrad, welchen solche Additivstoffe bestimmen, führt zu einem bedeutenden Anwachsen der Grenzflächen Zuschlagstoff-Matrix was das Anwachsen der Kohösionskrafte erklärt; für den gleichen Zementanteil im Beton, erhält man eine um so größere Festigkeitszunahme, je stärker die dispegierende Wirkung der eingesetzten Additivistoffe ist (s. Abb. 7 zusammen mit Tabelle 1).

Die gleichen Wirkungen können mit Zusatzstoffen, welche Träger von nicht hydraulischen, Zementierenden Bindungen sind, erzielt werden, hauptsächlich Träger von Fosfatbindungen. Diese können gleichzeitig die rheologischen Eigenschaften des frischen Betons sowie auch die Morphologie und den Dispersionsgrad der im Erhärtungsprozess entstandenen Neubildungen beeinflussen, mit positiven Folgen für die Nutzungsperformanzen der Betone, bei einer sogar drastischen Reduzierung des Tonerdezement-Anteils im Beton.

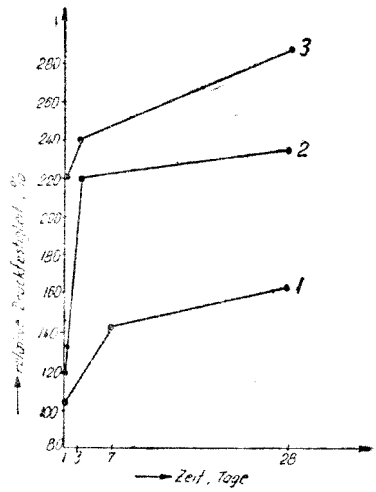

Abb. 7. Der Einfluß von organischen Additivstoffen (bei optimalem Mengenanteil) auf die relative Druckfestigkeit der feuerfesten Betone mit (12,5%) Tonerdezement und Tabulartonerde als Zuschlagstoff (maximale Körnung 3,36 *mm*) *1* — Vergleichsbeton (ohne Additiv) *2* — Beton mit LSC *3* — Beton mit VIMC-22

Die Kompaktität von feuerfestem Beton kann durch Einsatz von hochdispersen Mineralpulvern, welche die Kapilarien zwischen den Zementteilchen ausfüllen, noch erhöht werden. Man erhält simultan mit einer größeren Kompaktität, eine bedeutend bessere Strukturbeständigkeit des Betons unter Nutzungsbedingungen.

Im Vergleich mit einem Korind-onbeton mit 8% Tonerdezement entwickelt ein feuerfester Beton in welchem die Hälfte des Zementes durch ultrafeines

Tabelle 1

Spezifische Oberfläche BET des mit und ohne Additivstoffen hydratatisierten Zementes

Geprüfte Probe	Additiv Zement	Spezifische Oberflache BET, m^2/g
3 Tage hydratisierter Tonerdezement	0	2,524
Tonerdezement + Naftalenformaldehyd Verflüssiger (VIMC 22), 3 Tage hydratisiert	0,004	5,666
Tonerdezement + Kalziumlignosulfonat (LSC), 3 Tage hydratisiert	0,001	3,094
Tonerdezement + Natriumtripolifosfat (TSF), 3 Tage hydratisiert	0,01	3,438
Tonerdezement + Chromsäure-anhydrid (CrO_3), 3 Tage hydratisiert	0,001	3,477

Kieselgurpulzer ersetzt ist, sowohl bei normalen, als auch bei mittleren (200 ... 900°C) und erhöhten (> 900° ..., maximale Anwendungstemperatur) Temperaturen, bessere mechanische Eigenschaften [20]. Der Einsatz von hochdispersem Kieselgurpulver an Stelle von Tonerdezement führt bei dem oben erwähnten Beton auch zu einer Anmachwasserreduzierung von ungefähr 35—40%, mit einer drastischen Reduzierung de Porosität und entsprechend, der Permeabilität; die Gaspermeabilität ist in diesem Fall mehr als fünf mal kleiner. Die Strukturbeständigkeit des Betons im kritischen Temperaturbereich ist ebenfalls bedeutend besser; bei dem feuerfesten Beton mit hochdispersem Kieselgurpulver treten praktisck keine Festigkeitsverluste in den oben genannten Temperaturbereichen auf.

Die Natur und die Menge der verwendeten ultrafeinen Pulver werden erster Reihe von der Art zu projectierenden Betons bestimmt, die Kompatibiltät der Pulver mit den Zuschlagstoffen muß gesichert sein; gleichzeitig muß auch die Fähigkeit der hochdispersen Pulver, mit den anderen Betonkompo nenten bei der Nutzungstemperatur zu reagieren, sowie die Art der Gasat mosphäre wecher der Beton ausgesetzt ist, berucksichtigt werden.

Die Festigkeitszunahme bei der teilweisen Ersetzung des Tonerdezementetes mit hochdispersen Mineralpulvern wird — als Folge ihrer besonders hohen spezifischen Oberfläche, nicht nur durch eine höhere strukturelle Kompaktität der Matrix, sondern auch durch die intergranulären Kohäsionskräfte welche sich entwickeln, sowie auch das Entstehen von vielartigen keramischen Bindungen bei bedeutend niedrige-ren Temperaturen als bei Betonen ohne Mineralpulver und um so mehr als bei gewöhnlichen, herkömmlichen feuerfesten Betonen bewirkt. Dieser letzte Umstand ist auch der hauptsächliche Grund für die strukturelle Beständigkeit des Betons im kritischen Temperaturbereich, gefolgt von einer späteren Festigkeitszunahme auf keramischer Basis wobei sich, in Gegenwart von hochdisperser Tonerde oder Kieselgur, in Beton mit kleinem Zementanteil — Anortit und mit sehr kleinem Zementanteil — Mulit, bildet.

2.2. **Der Einfluß der Zuschlagstoffe.** Der Zuschalgstoff ist der Hauptkomponents des Betons und bestimmend für dessen Feuerfestigkeit. Demzufolge steht die Betonqualität in direker Beziehung mit der chemisch-mineralogischen Zusammensetzung, der mechanischen Festigkeit, der Porosität (Volumenmasse), der Volumenbeständigkeit, der Feuerfestigkeit und der Fähigkeit der Zuschlagstoffe mit der Bindemittelmatrix und dem Arbeitsmedium zu reagieren. Von diesem Gesichtspunkt aus müssen die Zuschlagstoffe bessere technische Nutzungseigenschaften haben als die Bindemittelmatrix. Bei kompositioneller Kompatibilität mit der Bindemittelmatrix und dem Arbeitsmedium, bei höherer Feuerfestigkeit als die Nutzungstemperatur und guter Volumenbeständigkeit, sind geschmolzene oder durch fortgeschritene Sinterung ezeugte feuerfeste Zuschlagstoffe vorzuziehen, deren offene Porosität 5% nicht überschreitet und deren Volumenmasse sich dem Dichtewert nähert; derartige Zuschlagstoffe haben auch große mechanische Festigkeiten, welcke aber in erster Reihe von ihrer chemischmineralogischen Zusammensetzung abhängig sind.

Bei der Projektierung von feuerfestem Beton mit großer Kompaktität — was für die Erzielung von, den Nutzungsbediengungen entsprechenden termot

mechanischen Eigenschaften unerläßlich ist, ist die Körnung der Zuschlagstoffe ein bestimmender Faktor, Die Körnung der Zuschlagstoffe ist integral durch den Anteil der verschiedenen Elementarsorten aus welchen der Zuschlagstoff besteht, und durch die maximale Korngröße, bestimmt. Eine fortlaufende Körnung, welche einer Parabelverteilung (der Art Fuller, Bolomey, Feret, Litzow) entspricht, ermöglicht eine maximale kompaktität des Betons mit einem kleinen Matrixanteil. In Wirklichkeit ist der Bindemittelmatri bedarf auch von fer maximalen Größe des Zuschlagstoffes abhängig, und zwar ist er um so kleiner, je größer die maximale Dimension des Zuschlogstoffes ist; es wird festgestellt daß das tatsächliche Volumen des freien Raumes zwischen den Körnern eines Totalzuschlangstoffes umgekehrt proportionell mit der Größe $\sqrt[n]{D}$ ist (in welcher D die größte Dimension des Zuschlagstoffes ist und $3 < mm < 6$) — S. [22]; das Anwachsen der maximalen Dimension der Zuschlogkörner ist von den Ausmessungen der feuerfesten Ausmauerung aus Beton, begrenzt. Der größere Bedarf an Bindemittelmatrix bei Zuschlagstoffen mit kleineren Dimensionen des Größtkornes ist nicht nur eine Folge des größeren Leerraumes zwischen den Körnern sondern auch der größeren spezifischen Oberfläche des Zuschlagstoffes und folglich der Notwendigkeit daß die Bindemittelmatrix den Zuschlagstoff bedeckt, daß viele Grenzflächen Zuschlagstoff-Matrix geschaffen werden. Außerdem ist auch zu beachten, daß beim Anwachsen des Anteils an sehr feiner Körnung im Zuschlagstoff, die intergranulären Repulsionskraäfte zunehmen; das führt zu einem größeren Bedarf an Bindemittelbrei für das Entstehen von suplimentären Kohäsions-kräften um die Repulsionskräfte zu annulieren und um Anziehungskräfte zu entwickeln welche dem erhärtenden System entsprechende mechanische Festigkeiten sichern. Abb. 8 zeigt eine komplexe Korrelation zwischen der maximalen Dimension des Zuschlagkorns und dem Anteil an Bindemittelmatrix im Beton, bzw. Abb. 8 seiner Volumenmasse [8].

3. Erhärtungsmechanismen bei feuerfesten Betonen mit kleinen Tonerdezementgehalt, bei Anwendung von komplexen Bindemittelgmischen

Due feuerfesten Betone mit komplexen Bindemittelmischungen sind zur Zeit die sich vor allem durchsetzende Lösung bei der Herstelliung der neuen Generationen derartiger Materialien. Die komplexen Bindemittelmischungen enthalten, außer Tonerdezement, verschiedene Anteile an Stoffen welche Träger andersartiger (nichthydraulischer) Zementierened-er Bindungen sind; gewöhnlich sind es, wie schon gezeigt wurde, fosfatische Bindungen; so

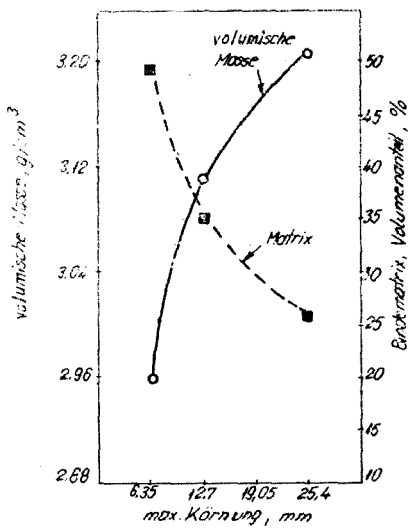

A b b. 8. Wechselbeziehungen zwischen de-Körnung des Zuschlagstoffes, dem Matrixanteil und der Volumenmasse der feuer rfesten Betone.

zum Beispiel eignet sich Tripolyfosfat sowohl als Träger von Fosfatbindungen, als auch als Dispersant.

In größeren Mengen wirkt Natriumtripolyfosfat (TFS) hauptsächlich als Bindemittel, neben dem Tonerdezement. Für die allergünstigsten TFS-Anteille erhält man einen bedeutenden Festigkeitszuwachs, selbst wenn der Tonerdezementanteil bedeutend kleiner als bei einem Vergleichsbeton ist (12,5% Tonerdezement). Obwohl bei kleinen Tripolyfosfatanteilen der Beitrag an Zementierenden Bindungen vernachlässigbar klein ist, wird ebenfalls eine postivie Wirkungfestgestelit; diese ist, in Abhängigkeit vom Zementanteil, für TFS/Zement — Werte von 0,01 ... 0,02, am bedeutendsten — wie aus der graphischen Darstellung in Abb. 9 hervorgeht [19]; ein derartiges Verhalten wird haupsächtlich durch die dispergierende Wirkung des TFS erklärt (s. Tabelle 1).

Aus Abb. 9 sind, für die Betone mit Tonerdezement und TFS, zwei verschiedene Kompositionsgebiete ersichtlich, in welchen der TFS — Gehalt positive Wirkung auf die Ausbildung von widerstandsfähigen Erhärtungsstrukturen der Bindemittelmatrix im feuerfesten Beton hat; in diesen Gebieten ist der vorwiegende Mechanismus nach welchem das TFS wirkt, verschieden: im Gebiet (I) wirkt seine dispergierende Wirkung auf des Bindemittelsystem und in (II) die Entwicklung von Fosfatbindungen. Zwischen diesen beiden Gebieten, für zwischenliegende TFS/Zement — Werte, ist der Beitrag der Fosfatbindungen zu der Erhärtung des Systems weniger bedeutend und die dispergierende Wirkung des TFS kann seine verzogernde Wirkung auf die Tonerdezementhidratation und seine hemmende Wirkung auf die Ausbildung von Kristallisationsstrukturen, nicht ausgleichen (s. [19]). In Abhängigkeit von dem Tonerdezementanteil im feuerfesten Beton, folgt für die Gebiete in welchen das Vorhadensein von TFS positiv wirkt daß bei kleinem Tonerdezementanteil kauptsächlich die zementierende Rolle des TFS von Interesse ist, wahrend in den Betonen mit größerem Zementgehalt die dispergierende Wirkung des TFS besser verwertet wird (Abb. 9).

Zu gleichen Schlußfolgerungen führen auch die Informationen welche bei Anwendung von Chromsäureanhydrid als Träger von zementierenden Bindungen, neben Tonerdezement, bei der Zubereitung von feuerfesten Betonen, erhalten wurden (s. Abb. 10, im Zusammenhang mit den Daten aus Tabelle 1 und den Diffraktometeranalysen [19].

Die oberflächenaktiven Additivstoffe, welche nicht Träger von zementierenden Bindungen sind, wirken verflussigend — dispergierend bei sehr kleinen Additiv/Tonerdezement — Werten, von nur 0,001 ... 0,0045 (s. Tabelle 1 für die dispergierende Wirkung von LSC und VIMC 22, wobei die Wirkung von VIMC 22 besonders intensiv ist, was durch die bedeutend größeren, mechanischen Festigkeiten zum Ausdruck kommt). Der konjugierte Einsatz, neben Tonerdezement, von einem zementierende Bindungen tragenden Zusatzstoff, in einem Mengenanteil bei welchem sein zementierender Beitrag bedeutend ist, und einem verflüssigend — dispergierenden Additiv führt zu einer konvergenten Wirkung, nach parallelen, eigenen, unabhängigen Mechanismen, mit positiven Folgen für die Entwicklung der Struktur und der Struktureigenschaf-

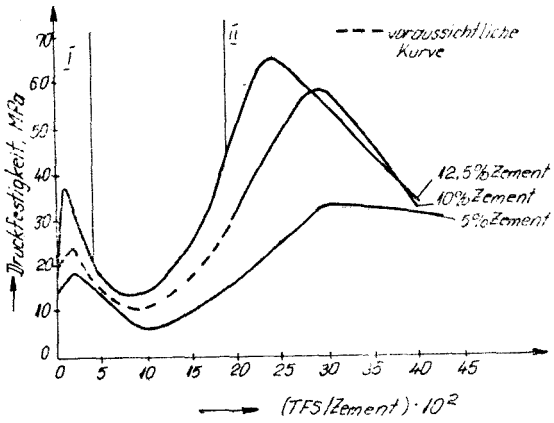

A b b. 9. Variation der Druckfestigkeit der 3 Tage frei gehärteten und bei 110°C getrockneten feuerfesten Betone mit verschiedenem Tonerdezementanteil, als Funktion ihres TFS — Gehaltes. *I* — kleinen TFS — -Zuzätzen entsprechendes Gebiet, mit dispergierender Wirkung *II* — verhlätnismaßig großen TFS-Zusätzen entsprechendes Gebiet, bei einer hauptsachlich zementierenden (fosfatischen) Wirkung.

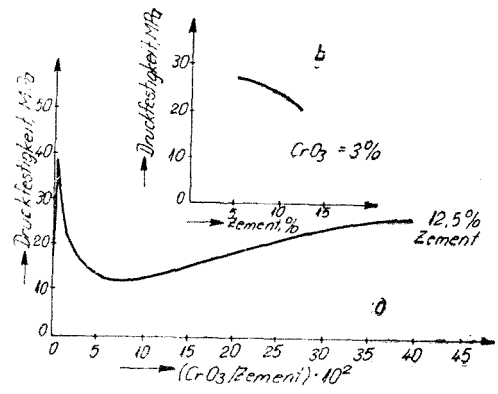

A b b. 10. Variation der Druckfestigkeit der 3 Tagefrei gehärteten und bei 110°C getrockneten feuerfesten Betone, als Funktion ihres CrO_3 — Gehaltes, Bzw. Tonerdezementgehaltes: *a* — Abhängigkeit der Druckfestigkeit von Beton mit 12,5% Tonerdezementanteil, vom CrO_3— Gehalt; b — Abhängigkeit der Druckfestigkeit von Beton mit 3% CrO_3, vom Tonerdezementgehalt.

ten des Betons — der zementierenden Matrix und der Grenzflächen Matrix — Zuschlagstoff.

4. Allgemeine und vergleichende Charakterisierung der feuerfesten Betone der verschiedenen Generationen

Das Anwendungsfed der gewöhnlichen, feuerfesten Betone ist obiektiv begrenzt, im Vergleich mit demjeningen der geformten, gebrannten feuerfesten Steine. Die ökono-mischen und technologischen Vorteile, welche die Anwendung der feuerfesten Betone mit sich bringt, haben die Herstellung von Erzeugnissen dieser Art, mit Eigenschaften welche denjeningen der geformten, gebrannten, feuerfesten Steine wenigstens gleichwertig sind, notwendigerweise gefördert. Das ist der Grund für das Auftreten, in den letzten zwei Jahrzehnten, von Betonen mit reduziertem Tonerdezement — Anteil (BRC) und, in letzter Zeit, von Betonen mit ultrareduziertem Zementanteil (BURC); die Herstellung dieser letzen Kategorie Beton war von dem besonders hohen Niveau der Nutzungsperformanzen der Brennagregate für moderne Technologienbestimmt, deren hohe Ansprűche an die feuerfeste Ausmauerung von den feuerfesten Betonen mit reduziertem Zementgehalt nicht erfűllt werden konnten.

Gegenwärting sing folglich drei vershiedene Generationen feuerfeste Betone bekannt:

— traditionelle Betone (mit 15—30% Tonerdezement), als feuerfeste Betone der ersten Generation bekannt;

— feuerfeste Betone mit reduziertem Zementgehalt (5—12,5% Tonerdezement) — der II — Generation angehőrend;

— feuerfeste Betone mit sehr reduziertem Zementgehalt (unter 5% Tonerdezement) — der III. Generation angehörend

Diese Erzeugnisse unterscheiden sich in ihren grundlegenden Eigenschaften — sowohl was die Zusammensetzung, als auch die Anwendung, anbelangt, wie aus Tabelle 2 [12] hervorgeht. Als Folge devon sind auch ihre Nutzungsgebiste streng begrenzt.

Tabelle 2

Charakteristiken der feuerfesten Betone

Charakteristik	Herkömmlicher feuerfester Beton	Feuerfester Beton mit reduziertem Zementgehalt	Feuerfester Beton mit ultrareduziertem Zement-gehalt	Feuerfeste Steine
CaO-Gehalt (%)	6,5—8	1—3	~0,6	~0,3
Durckfestigkeit von bei 1250°C gebrannten Proben, *MPa*	35—65	55—120	100—120	~60
Offene Porosität in. bei 1200°C gebrannten Proben	26—28	16—18	~12	~21

5. Anwendung der feuerfesten Betone mit reduziertem und ultrareduziertem Tonerdezement

Das Anwachsen des Zuschlagstoff/Matrix Wertes im feuerfesten Beton, sowie auch die Sicherung von hochwertigen mechanisch — strukturellen Charakteristiken der Matrix, einschließlich einer hohen strukturellen Stabilität, führen bei Reduzierung des Tonerdezementgehaltes, zu hohen Nutzungsperformanzen des gesamten Systems. Auf diese Art sind die thermomechanischen Eigenschaften und das Verhalten im Nutzungsmedium der Betone mit reduziertem und ultrareduziertem Zementgehalt, bedeutend verbessert.

Bei der Anwendung von Zuschlagstoffen mit bestimmten chemisch-mineralogischen Zusammensetzungen ist die Dauerhoftigkeit dieser Betone und ihre Nutzungstemperatur größer. Nachdem die Anderungen in der Bindemittelmatrix bis zu 1000—1200°C unbedeutend sind — Abb. 11 [13], was zu einer

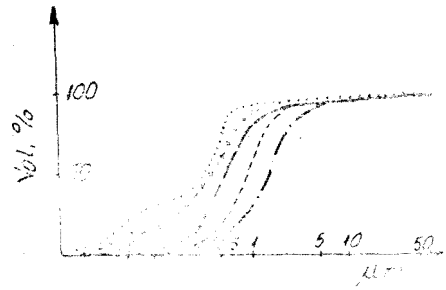

Abb. 11. Kumulative Porosität von, auf verschiedene Temperaturen erhitztem, feuerfestem Beton mit reduziertem Zementgehalt:

... 110°C; — — — 1500 C° (5stunden);
*** 1000°C (5 stunden); —.—.—.— 1600°C (5 stunden)
— 1200 C (5 stunden).

bedeutenden Strukturstabilität in dem für gewöhnliche Betone kritischen Temperaturbereich führt, kann der Anwendungsbereich der Betone mit reduziertem und ultrareduziertem Zementgehalt, unter gewissen Bedingungen, auch auf das Gebiet verhältnismaßig niedriger Temperaturen ausgedehnt werden.

Die feuerfesten Betone mit reduziertem und ultrareduziertem Zementanteil werden, mit hervorragenden Ergebnissen hauptsächlich in der Eisen — und Buntmetallmetallurgie angewandt Einige dieser Betonarten finden Anwendung bei: der Ausmauerung von Hochöfen (Oberschacht, Hochofengicht, Abgasführung, Hochofenrast, Gußeisenrinnen, Winderhitzer und Warmluftführung); Elektroöfen für die Stahlherstellung (die Delta-Zone oder das ganze Gewölbe des Flammenbogenofens, Ausmauerung der Induktionsöfen mit Kanal oder Tiegel, Ausmauerung der Stahlgießrinnen); Instalationen für die Vakuumbehandlung von Stahl (Herstellung der Immersionsröhren); Installationen für die kontinuirliche Stahlgießung (Ausmauern der Verteiler); Herstellung des Einblasrohrs der Gase und Pulver in, der Tiegelmetallurgie spezifische Installationen; Ausmauerung der Stahlgieß-und Transportpfannen, sowie der Aufprallplatte bei den Walzwerköfen; Karusselöfen; Salzschmelzeöfen Guß — und Transporttiegel für Guß eisen, Kupfer, Aluminium oder Kupfer — und Aluminiumlegierungen; Herstellung von Brennersteinen für einige ofenarten; Ausmauerung der Ofen für Wärmebenhandlung, der tiefen Öfen; Ausmauerung der Schmelzöfen für Aluminium und Aluminiumliegierungen, für Kupfer und Kupferliegierungen u.s.w.

In der chemischen und petrochemischen Industrie werden die Betone mit geringem Zementgehalt erfolgreich eingesetzt bei der Ausmauerung des primären und sekundären Reformers und der Abhitzekessel der Ammoniakindustrie, bei der Ausmauerung der Schweferlkiesofen in der Schwefelsäureindustrie, der Veräscherer der Rezipienten und Reaktoren der Zyklone und katalytischen Übergangslinien der Installationen für katalytisches Kracken des Erdöls, Ausmauerung der Brennerkegel u.s.w.

Die Silikat-und feuerfeste Steinindustrie ist ein potentieller Anwender von Beton mit reduziertem Zementgehalt, für die Ausmauerung der Förderwagen, verschiedener Zonen des Tunnelofens, der Rund-und Zick-Zack-Ofen. Solche Betone werden bei der Ausmauerung von Wärmetauschern und gewisserZonen der Drehöfen der Zementindustrie, oder der Schachtöfen der Kal-kindustrie, eingesetzt.

Beton mit reduziertem Zementgehalt kann auch auf anderen Gebieten angewendet werden: bei der Ausmauerung der Koksöfen der Dampfkessel der Elektizitätszentralen, der Rollbahnen für den Abund Äflug von Überschallflug zeugen u.s.w.

6. **Schlußfolgerungen.** Die Herstellung der aufeinanderfolgenden Generationen feuerfester Betone hat eine Überlagerung der Wirkungen der Reduzie-rung des Zementgehaltes und der zusätzlichen Anwendung von zementierenden, nicht hydraulische Bindungen tragenden Zusatzstroffer, von verflüssigend-dispergierenden Additivstoffen und von ultradispersen Mineralstoffen auf die Struktur der Bindemittelmatrix und die Beziehung Zuschlagstoff-Matrix, verfolgt. Auf diese Art entstehen qualitative, wesentliche Mutationen welche den feuerfesten

Betonen der letzten Generationen ein bedeutendes Anwachsen der Strukturbeständigkeit zusichern, eine bedeutende Verbesserung ihrer mechanisch — strukturellen Eigenschaften — insbesondere der thermomechanischen, sowie ein hochwertigeres Verhalten im Nutzungsmedium und eine bedeutend größere Dauerhäftigkeit. Demzufolge wurden die Anwendungsbereiche der feuerfesten Betone bedeutend erweitert und für die verschiedenen Generationen genau umgrenzt, im Verhältnis zu den Nutzungsbedingungen der feuerfesten Ausmauerungen der rennaggregate. Der Anwerndungsbereich der feuerfesten Betone der II. Generation (mit reduziertem Zementanteil) entspricht demjeningen der geformten, gebrannten feuerfesten Steine — mit allen verfahrenstechnischen Vorteilen welche die Anwendung von Beton mit sich bringt. Die feuerfesten Betone der III. Generation (mit ultrareduziertem Zementanteil) können, bei einer bemerkenswerten Dauerhaftigkeit, unter viel härteren Temperatur-und Mediumbedingungen, eingesetzt werden.

LITERATUR

1. Prost, L. — L'industrie Ceramique nr. **661**, 279 (1973).
2. Teoreanu, I., Angelescu, N. — Materiale de Construcţii, **10** (4), 195 (1980).
3. Teoreanu, I., Angelescu, N. — XIII Siliconf, vol. **II** — Sect. B, 183, Budapest, 1981.
4. Angelescu, N. — *Beton mit reduziertem Zementgehalt.* Dissertation, Polytechnische Hochschule Bukarest, 1983.
5. Teoreanu, I., Angelescu, N. — Matreiale de Construcţii **16** (4), 240 (1986).
6. Teoreanu, I., Angelescu, N. — IX Conf. on Refract. Concr., 231 Karlovy-Vary, 1986.
7. Moeck, M. — Zement, Kalk, Gips **38** (2), 91 (1985).
8. Lankard, D. R. and collab. — Refract. Journal nr. **1**, 6 (1986).
9. Kawasaki, S. — Taikabutsu Overseas **6** (1), 34 (1986).
10. Routschka, G., Majdic, A. — Sprechsaal **119** (3), 164 (1986); **119** (9), 677 (1986).
11. Chastant, M. — Rev. de Metallurgie **83** (10), 719 (1986).
12. Moreau, J. P. — Interceram **37**, nr. special de refractaires — Aachen Proceed., 8 (1988).
13. Avis R., Chavand, B., Randal, P. — Interceram **37**, nr. special de refractairs — Aachen Proceed., 33 (1987).
14. Hawecker, M., Robert, S. — Silikattechnik **38** (4), 137 (1987).
15. Angelescu, N. — Materialy Ogniotrwale nr. **4**, 93 (1989).
16. Teoreanu, I., Angelescu, N. — Verre **1** (2), 160 (1987).
17. Nagai, B. — Taikabutsu Overseas **9** (1), 2 (1989).
18. Eguchi, T. and collab. — Taikabutsu Overseas **9** (1), 10 (1989).
19. Teoreanu, I., Angelescu, N. — Die Arbeit befindet sich in Druck, Anterceram.
20. Shikano, H. and collab. — Taikabutsu Refract. **41** (8), 437 (1989).
21. Teoreanu, I., Angelescu, N. — Interceram **34** (5), 49 (1985).
22. Lapouyade, P. and collab. — *Traite pratique sur l'utilisations des produits refractaires.* Ed. H. Vial, Dourdan, 1986.
23. Steel, G. — Refract. Journal nr. 3, 74 (1985).
24. Venuat, M. — Rev. Mat. Constr. nr. 629, 59 (1968).

STUDIA UNIV. BABEŞ-BOLYAI, CHEMIA, XXXVI, 1—2, 1991

TECHNOLOGY AND LINE FOR COMPLEX PROCESSING OF PLANTS

VICTOR KASZTL*, IOAN MARINESCU**

ABSTRACT. These last years, the utilization of plants in the pharmaceutical industry is increasingly spread in the world. This paper sets forth a new original technology for complex processing of plants into finished products of varions forms. At the same time, there are shown the processing equipment and plants of our own design, which carry out the proposed technology.

1. **Introduction.** Since the oldest times, the man used the vegetal products from nature to his own advantage. He noticed that some of them act on the organism. Thus, the utilization of the preparations obtained by processing the vegetal products is known for thousands of years.

The first purified and stable pharmaceutical forms obtained from vegetal or animal raw materials, the first biosynthesis medicines that met the conditions of reducing the volume in which there are the active substances, and of long preservation, are tinctures and extracts.

Over four centuries old as officinal products, tinctures and extracts are at the same time the first pharmaceutical forms obtained on a large scale about two centuries ago, the first medicines the presence of which became possible everywhere and at any time.

2. **Research Objective** In the course of reascarch there were analyzed and developed more technologies of extraction, filtration, concentration, aroma and solvent recovery, as well as of processing tinctures and extracts with a view of getting high-quality products under new forms of presentation. Since there is enough information about some operations within the technology developed, the operations that contribute to getting products of high quality and under new presentation forms were dealt with in a larger extent. Thus, the concentration of the fluid extracts with flavour and solvent recovery, as well as the granulation technologies of some products based on plant extracts, were particularly studied.

The aim was that the new technology should satisfy the following requirements : to process a wide range of plants ; to provide a high degree of extraction ; to provide a high degree of flavour and solvent recovery ; high output- to be able to elaborate the finished products in a new fine form that should contain the active principles and the accompanying compounds required, qualitatively undamaged providing at the same time a guarantee period as long as possible ; to provide the hygienic-sanitary conditions throughout the process.

* *I.C.P.I.A.F.- S.A., 3400 Cluj-Napoca, Romania*
** *I.C.C.F., 3400 Cluj-Napoca, Romania*

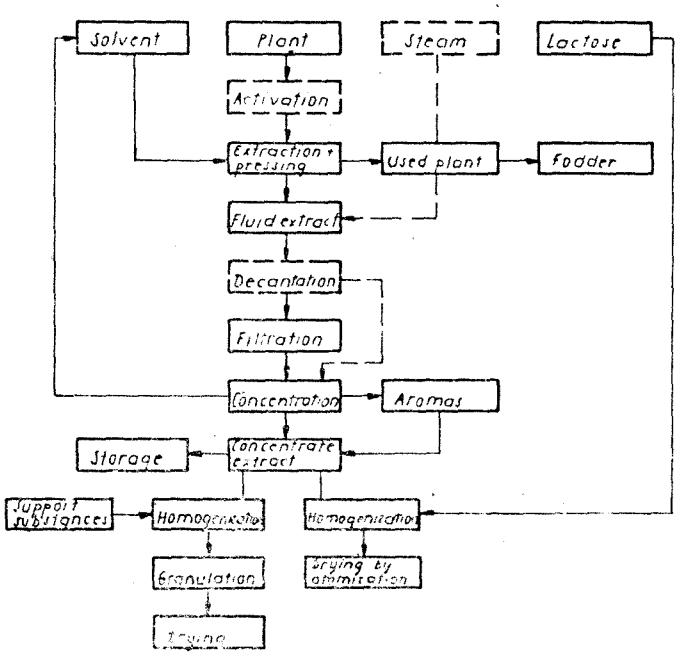

Fig. 1. Floww sheet for the processing of plants.

3. **Processing Technology and Line.** After analyzing the demands of the market in the field of medicinal and aromatic plants, as well as the results obtained in the course of research, it was worked out the processing technology shown in Fig. 1:

The operations marked by a dotted line are performed only under certain circumstances and at certain plants. The complex processing line is modularly shown in Fig. 2. Under the form shown, the processing line is able to carry out the operations presented in Fig. 1, less the solvent recovery by using steam.

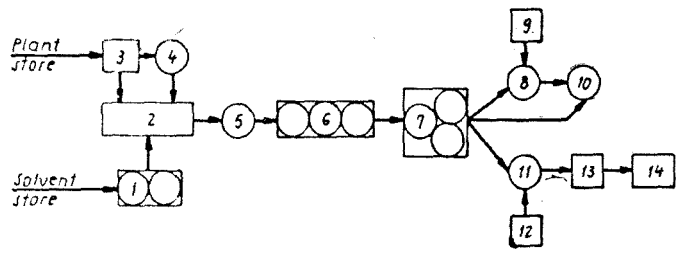

Fig. 2. Basic diagram of the line for the complex processing of plants. 1 — solvent tank, 2 — Continuous extractor, 3 — plant hopper, 4 — activating vessel, 5 — transfer pump, 6 — filter, 7 — concentrating instalation 8 — homogenizer, — 9 lactose tank, 10 — atomization dryer, 11 — blender, 12 — excipient tank, 13 — granulating aggregate, 14 — dryer.

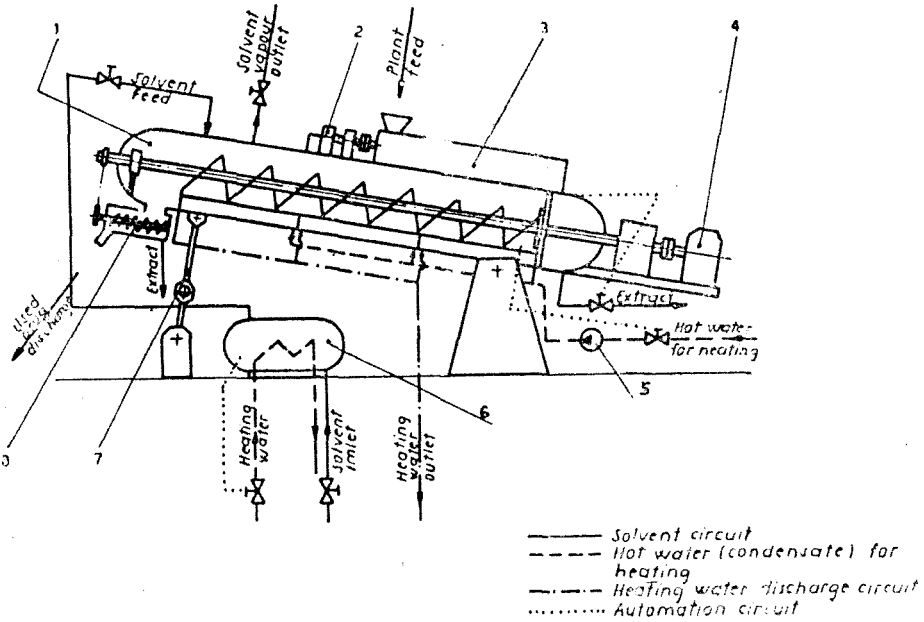

Fig. 3. Modular diagram of continuous extracting line: 1 — extractor with conveyer screw, 2 — proportioner driving mechanism, 3 — proportionr, 4 — conveyer driving mechanism, 5 — heating water pump, 6 — solvent heater, 7 — inclining mechanisms, 8 — press for used plant.

The plant enters the process in dry and crushed state. Activation is meant to introduce the solvent at the intercellular level, the operation being made especially on the root plants.

Extraction is carried out by a modern, continuous, counterflow method, the machine-feed being made with the aid of two scrollershafts. The line shown schematically in Fig. 3 ensures the extraction of a very wide variety of plants with high output and a high degree of exhaustion of drug. At the same time, by the press (8), from the spent drug it can be recovered about 50 ÷ 60% from the extract left in the plant structure. The high extraction parameters are obtained by providing more possibilities of monitoring the process variables such as: extracting temperature and solvent temperature, time of contact between the drug and the solvent by controlling the spedd of the scroller-shaft solvent flow, and the inclination of the extractor body. The extracting and solvent temperatures are automatically controlled.

Filtration of extracts and tinctures is carried out by means of a machine which works on a new principle and which allows to perform the process continuously.

The simplest diagram of such a line is given in Fig. 4.

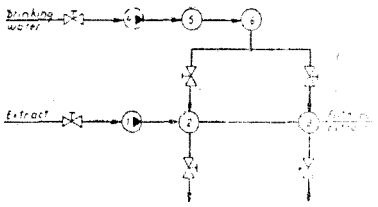

Fig. 4. Basic diagram of filtering line: 1 — pump for product, 2 — coarse filter for product, 3 3 — fine filter for product, 4 — water pump, 5 — coarse filter for water, 6 — fine filter for water.

Filtration is made in two stages in order to extend the period of clogging up. Constructionally, the filters are made so, that on clogging up, by interrupting the product circuit, the filter elements should be cleared by washing with water under pressure, flowing in a direction opposite to that of the product. The washing operation takes $1 \div 2$ minutes and the filtering operation can be immediately resumed after that.

Filtering fineness is adopted by using cylindrical filter elements of stainless steel gauze with mesh size ranging from 2 to 500 μm. The method makes possible the elimination of cold decantation of the products. For the extracts that do not require filtration, only a cold sedimentation and decantation are made.

The concentration of extracts, recovery of solvents (is most cases ethyl alcohol), and separation of aromas are carried out in a machine of our own design, with high energetic efficiency. Concentration of extracts is made at $40 \div 45$°C by vacuum evaporation in a falling film shell and tube evaporator. Vacuum is created by a water ring pump. The aroma and solvent recovery is performed in a column for rectification with plates, cooled by a refrigerating unit. The line carries out the automatically pre-set concentration by using a process refractometer.

The processing line also includes units wich enable the extracts to be processed into verious forms. Thus, to extend the shelf-life of the product, the extracts can be brought into the form of powder.

For this purpose, it is used an atomization drying machine equipped with a centrifugal atomizer. In this way, powders with size of $50 \div 100$ um and maximum humidity of 5% are obtained. Besides powders, in the course of investigations, a family of new products, the instant granulates were also obtained from the extract by impregnating some support substances (sugar, lactose,etc) with concentrated extracts. To get the mass of granulates it is used a mixer with two Z-shaped arms which rotate at different speeds. Granulation is carried out on a granulator with two cylinders which rotate at different speeds. One of the cylinders is provided with holes corresponding to the granule size, on the side surface and the other is grooved with a view of carrying the material away.

The granulates are dried in drying cabinest with forced circulation of air and possibility of regulating the drying temperature depending on the nature of the support substance. It is also taken into account, that the drying temperature should not exceed the value at which the deterioration of the active principles in the extracts takes place. After drying, the granules are sized by means of a swinging sieve.

4. **Conclusions.** The form of the complex processing line shown is the result of our own laboratory experiments and of using the experience of some well-known producers.

By using the technology described, high quality products were successfully obtained due to the non-deterioration of the active principles contained by plants and due to the possibility of recovering and reducing aromas.

After having developed the complex processing line follows a second stage of research i.e., to determine the optimum operating parameters of the aggregates and equipment. At the same time, the line will make possible the accomplisment of some products other than those obtained during the first stage of research. The determination of the optimum operating parameters of the plants and units is facilitated by the fact that the machines were designed so that they should allow the regulation of parameters within a very wide range. During the second stage of research, is also contemplated the execution of the line recovering the solvents from plants resulted from extraction, by entrainment with steam.

In a subsequent stage, taking into account the high level of automation of the line, the realization of the computer-assisted control of the process is foreseen.

REFERENCES

1. Ionescu Stoian P., Savopol E., *Extracte farmaceutice vegetale*, Ed. Medicală, Bucureşti, 1977.
2. Popescu, H., *Medicamente de sinteză şi extracţie*, Ed. Dacia, Cluj-Napoca, 1985.
3. Laza A., Racz G., ş.a., *Plante medicinale şi aromatice*, Ed. Ceres, Bucureşti, 1975.
4. Boeru Gh., Puzdrea D., *Tehnologia uleiurilor vegetale*, Ed. Tehnică.
5. Răşenescu I., *Operaţii şi utilaje în industria alimentară*, vol. **II**, Ed. Tehnică, Bucureşti, 1972.
6. Dăscălescu, A., *Uscarea şi aplicaţiile ei industriale*, Ed. Tehnică, Bucureşti, 1964.
7. Segal H., ş.a., *Maşini de ridicat şi transportat*, Ed. Tehnică, Bucureşti, 1960.
8. * * * *Farmacopeea romană*, ed. IX, Ed. Med. Bucureşti, 1976.
9. * * * *Tehnică farmaceutică*, E.D.P., Bucureşti, 1974.

RECENZII

Proceedings of the Sixth International Symposium on Instrumental Planar Chromatography, Interlaken, Switzerland, April 23 — 26, 1991, Edited by H. Traitler, O.I. Voroshilova and R.E. Kaiser; Published by the Institute for Cromatography, Bad Durkheim, Germany.

The volume contains 49 articles presented at this Symposium.

The gratest par of these articles are about quantitative densitometric measurements of various mixtures of compounds.

Another group of articles is about mobile and stationary phases optimisation problem and development of techniques.

We must observe the articles concerning qualitative determination by coupling TLC or HPTLC with UV—VIS and FTIR Spectrometry and MS — MS.

The articles of this volume are valuable materials and there are of great interest for all scientists searching Planar Cromatography.

This Symposium takes place biannually in Europe, brings together specialists of Planar Cromatography; the articles show the actual stage of this field. The next Symposium will take place in 1993 at Brighton, Sussex, **U.K.**

S. GOCAN

Tiparul executat la Imprimeria „ARDEALUL" Cluj, C-da 11

În cel de al XXXVI-lea an (1991) *Studia Universitatis Babeş-Bolyai* apare în următoarele serii:

matematică (trimestrial)
fizică (semestrial)
chimie (semestrial)
geologie (semestrial)
geografie (semestrial)
biologie (semestrial)
filosofie (semestrial)
sociologie-politologie (semestrial)
psihologie-pedagogie (semestrial)
ştiinţe economice (semestrial)
ştiinţe juridice (semestrial)
istorie (semestrial)
filologie (trimestrial)

In the XXXVI-th year of its publication (1991) *Studia Universitatis Babeş-Bolyai* is issued in the following series:

mathematics (quarterly)
physics (semesterily)
chemistry (semesterily)
geology (semesterily)
geography (semesterily)
biology (semesterily)
philosophy (semesterily)
sociology-politology (semesterily)
psychology-pedagogy (semesterily)
economic sciences (semesterily)
juridical sciences (semesterily)
history (semesterily)
philology (quarterly)

Dans sa XXXVI-e année (1991) *Studia Universitatis Babeş-Bolyai* paraît dans les séries suivantes:

mathématiques (trimestriellement)
physique (semestriellement)
chimie (semestriellement)
géologie (semestriellement)
géographie (semestriellement)
biologie (semestriellement)
philosohpie (semestriellement)
sociologie-politologie (semestriellement)
psychologie-pédagogie (semestriellement)
sciences économiques (semestriellement)
sciences juridiques (semestriellement)
histoire (semestriellement)
philologie (trimestriellement)